

# Functional Polymer Gels based on Oligomer Fluids

Zur Erlangung des akademischen Grades eines  
DOKTORS DER NATURWISSENSCHAFTEN

(Dr. rer. nat.)

von der KIT-Fakultät für Chemie und Biowissenschaften  
des Karlsruher Instituts für Technologie (KIT)

genehmigte

DISSERTATION

von

M. Sc. Zhenwu Wang

1. Referent: Prof. Dr. Pavel A. Levkin

2. Referent: Prof. Dr. Patrick Théato

Tag der mündlichen Prüfung: 13.12.2022



## Acknowledgement

During the past years of my doctoral studies, I obtained tremendous help and support. Many people made my time at KIT and Deutschland and built an unforgettable and special experience during the past years. I would like to express my deep appreciation to my dear family, colleagues, and friends, who helped me to reach my destination.

First of all and at most, I would like to thank my father, my mother, my girlfriend, my sister, my brother-in-law, and my cute nephew for the unreserved and comprehensive support during my doctoral study. I am always allowed to get relaxed from my family while meeting some challenges during my work. Although my parents know nothing about my research, they still gave me great encouragement and confidence unconditionally when I was frustrated with my projects. The gratitude particularly goes to my girlfriend. Her optimism, love, and wisdom empowered me to finish my PhD work.

I would like to express my deepest appreciation to Prof. Dr. Pavel Levkin for accepting me as a PhD candidate. Working with Pavel has been a tremendous experience. I still remember the first interview with Pavel, where he asked me the question “How do you understand and deal with pressure?”. My answer was “I regard the pressure as motivation”. I hope I fulfilled this sentence well in the past years. In the last three years, I saw his passion for work, which had a great impact on me and urged me not to slack off. I think it is the best course I gained in the last three years, hardworking, hardworking, and hardworking. Thank you very much, Pavel!

This adventure would never be possible without the help of my colleagues. You are all excellent and I learned a lot from all of you. Shuai, Changming, Zheqin, Haijun, Ye, Wenxi, Yanxi, and Johannes, thank you for your warm heart to help me adapt to the new environment when I was first in the lab. My appreciation also goes to Saeid, Anna, Shraddha, Alisa, Janne, Maria, Max, Julius, Max, Qianyu, Yaqi, Lutong, Weiyi, Sida, Junning, Xiaotao, Dorothea, Razan, Maryam, Joaquin, Carola, Jovana, Charlotte for offering me a friendly working environment. All the time I spent with you was nice and inspirational.

## Acknowledgement

---

I would like to express my particular appreciation to Yelda. Thanks for your warm help and caring for that stupid and ignorant Zhenwu. Without your support, I am unable to get into my lab work and life in Deutschland well. I know I can't thank you enough.

Much work in this thesis was finished using the facilities of Institute of Nanotechnology, Institute of Organic Chemistry, Institute of Chemical Technology and Polymer Chemistry, and Institute of Biological Interfaces IBG-2 at KIT. I would like to thank all my collaborators there, especially Prof. Patrick Théato, Prof. Wenzel Wolfgang, Prof. Jasmin Aghassi-Hagmann, Prof. Manfred Wilhelm, Prof. Shan-Hui Hsu, Prof. Chia-Ching Chou, Dr. Stephan L. Grage, Maxi Hoffmann, Dr. Xiaowei Feng, Dr. Gabriel Cadilha Marques, Dr. Matthias Heck, Dr. Modan Liu, Dr. Elaheh Sedghamiz, Yu-Cheng Lai, Ya-Tang Chiang, Hongrong, Wenwu, and Kai. You are all excellent and I learned a lot from all of you. Also, hearty appreciation to the guys in INT and KIT for the Saturday basketball games, which is really nice and interesting to play with you.

I want to thank my TAC members, including Prof. Jasmin Aghassi-Hagmann, Prof. Véronique Orian-Rousseau, Dr. Gerardo Hernandez Sosa, and of course Pavel. Thanks so much for your constructive advices during my doctoral studying.

Last but not least, I am very grateful to the China Scholarship Council. Without the scholarship supporting overseas PhD studies, I would never finish my PhD abroad without livelihood pressure. Now I am happy and honored to be back in China and make my contribution to my country.

## Abstract

Polymer gels, such as hydrogels, consisting of cross-linked polymer chains and small molecule solvents, have been widely used in biomedical applications, flexible electronics, and soft machines due to the similarity of their mechanical properties to those of soft biological tissues. Polymer network design and its contribution to the properties of such materials have been extensively studied. However, the infused solvents, which would strongly influence the internal structure of gels, are rarely studied. This thesis aims to provide a series of solvent strategies for fabricating functional polymer gels.

In chapter 1, a general introduction to functional polymer gels based on different solvents is provided, covering various choices of solvents for polymer gels and functions derived from the solvent strategies. For the choices of solvents, the fabrication methods and the latest developments of the polymer gels based on various solvents were summarized, including organic solvents, ionic liquids, deep eutectic solvents, and polymer fluids. Then, the functions derived from the solvent strategies were discussed, containing slippery performance, freezing resistance or thermal stability, superior mechanical properties, and electrical performance.

In chapter 3.1, a gel system based on poly(ethylene glycol) (PEG) used as the solvent was demonstrated. The critical influence of the solvent nature on the mechanical properties and performance of polymer gels was investigated. A physically cross-linked copolymer of 2-hydroxyethyl methacrylate and acrylic acid was selected as the elastic polymer network. Compared to the corresponding hydrogel or ethylene glycol based gel, the PEGgel demonstrates exceptional physical properties, such as high stretchability and toughness, rapid self-healing, and long-term stability under ambient conditions. Depending on the molecular weight and fraction of PEG, the tensile strength of PEGgels varied from 0.22 MPa to 41.3 MPa, fracture strain from 12% to 4340%, modulus from 0.08 MPa to 352 MPa, and toughness from 2.9 MJ m<sup>-3</sup> to 56.2 MJ m<sup>-3</sup>. The obtained polymer gels can be used to fabricate a self-healing pneumatic actuator by 3D printing. The enhanced mechanical properties of the PEGgel system could be extended to other polymer networks (both chemically and physically cross-linked).

In chapter 3.2, ions were introduced into the solvent system to fabricate ionic PEGgel. The incorporation of ions into PEG simultaneously enhanced the strength and toughness of the polymer gels. The typical ionic PEGgel is composed of in-situ formed physically cross-linked poly(2-hydroxyethyl methacrylate) networks and PEG, demonstrating high conductivity ( $0.04 \text{ S m}^{-1}$ ), excellent electrochemical stability ( $> 60,000$  cycles), ultra-stretchability (up to 1400%), high toughness ( $7.16 \text{ MJ m}^{-3}$ ), fast self-healing property enabling restoration of ionic conductivity within seconds, as well as no solvent leakage. Several applications of ionic PEGgel were demonstrated as (a) flexible sensors for strain or temperature sensing, (b) skin electrodes for recording electrocardiograms, and (c) a tough and sensing material for pneumatic artificial muscles.

In chapter 3.3, *in-situ* phase separation was studied in the PEGgel system based on a mixture of PEG and polypropylene glycol (PPG) as the solvent. The phase-separated polymer gels were fabricated by directly polymerizing 2-hydroxyethyl methacrylate in a mixture of PEG and PPG. The polymerized elastic networks present distinct solubility in PEG (highly soluble) and PPG (poorly soluble due to the existing methyl on the main chain), resulting in a macroscopically homogeneous covalent network with *in-situ* phase separation. The resulting phase-separated gel demonstrates high strength (8.0 MPa), favorable fracture strain (430%), and large toughness ( $17.0 \text{ J m}^{-3}$ ). The separated phases endow the polymer gel with shape memory property, which can be used for various soft machines combined with 3D printability. Then, ions were incorporated into PEG/PPG solvent to achieve hierarchical interactions in polymer gels ranging from the ionic interactions (nano-level) to phase separation (micro-level). Such a hierarchical structure further enhanced the strength and toughness of polymer gels, showing high fracture strength (12.2 MPa) and fracture energy ( $54 \text{ kJ m}^{-2}$ ).

In the end, the outlook on the challenges that must be faced toward developing functional polymer gels is provided. To speed up the development of polymer gels in various fields, we need to optimize both the network design and the solvent strategies. Advances on only one side are not enough to solve all the challenges.

## Zusammenfassung

Polymergele, wie beispielsweise Hydrogele, die aus vernetzten Polymerketten und niedermolekularen Lösungsmitteln bestehen, wurden aufgrund der Ähnlichkeit ihrer mechanischen Eigenschaften mit denen von weichen biologischen Geweben weit verbreitet in biomedizinischen Anwendungen, flexibler Elektronik und weichen Maschinen verwendet. Das Design von Polymernetzwerken und sein Beitrag zu den Eigenschaften solcher Materialien wurden ausgiebig untersucht. Die infundierten Lösungsmittel, die die innere Struktur von Gelen stark beeinflussen würden, werden jedoch selten untersucht. Ziel dieser Dissertation ist es, eine Reihe von Lösungsmittelstrategien zur Herstellung funktioneller Polymergele bereitzustellen.

In Kapitel 1 wird eine allgemeine Einführung in funktionelle Polymergele basierend auf verschiedenen Lösungsmitteln gegeben, die die verschiedenen Wahlmöglichkeiten von Lösungsmitteln für Polymergele und von den Lösungsmittelstrategien abgeleitete Funktionen abdeckt. Für die Auswahl der Lösungsmittel wurden die Herstellungsmethoden und die neuesten Entwicklungen der Polymergele auf Basis verschiedener Lösungsmittel zusammengefasst, darunter organische Lösungsmittel, ionische Flüssigkeiten, tiefeutektische Lösungsmittel und Polymerflüssigkeiten. Dann wurden die aus den Lösungsmittelstrategien abgeleiteten Funktionen diskutiert, darunter rutschige Oberflächen, Gefrierbeständigkeit oder thermische Stabilität, überlegene mechanische Eigenschaften und elektrische Leistung.

In Kapitel 3.1 wurde ein Polymergelsystem auf Basis von Poly(ethylenglykol) (PEG) als Flüssigphase demonstriert. Der kritische Einfluss der Lösungsmittelnatur auf die mechanischen Eigenschaften und die Leistung von weichen Polymergelen wurde untersucht. Als elastisches Polymernetzwerk wurde ein physikalisch vernetztes Copolymer aus 2-Hydroxyethylmethacrylat und Acrylsäure gewählt. Verglichen mit dem entsprechenden Gel auf Hydrogel- oder Ethylenglykolbasis weist das PEGgel außergewöhnliche physikalische Eigenschaften auf, wie z. B. hohe Dehnbarkeit und Zähigkeit, schnelle Selbstheilung und Langzeitstabilität unter Umgebungsbedingungen. Je nach Molekulargewicht und PEG-Anteil variierte die Zugfestigkeit von PEGgelen von 0,22 MPa bis 41,3 MPa, die Bruchdehnung von 12 % bis 4336 %, der Elastizitätsmodul von 0,08 MPa bis 352 MPa und die Zähigkeit von 2,89 MJ m<sup>-3</sup> bis 56,23 MJ m<sup>-3</sup>. Die erhaltenen Polymergele können zur

Herstellung eines selbstheilenden pneumatischen Aktuators durch 3D-Druck verwendet werden. Die verbesserten mechanischen Eigenschaften des PEGgel-Systems könnten auf andere Polymernetzwerke (sowohl chemisch als auch physikalisch vernetzt) ausgedehnt werden.

In Kapitel 3.2 wurden Ionen in das Lösungsmittelsystem eingeführt, um ionisches PEGgel herzustellen. Der Einbau von Ionen in PEG erhöht gleichzeitig die Festigkeit und Zähigkeit der Polymergele. Das typische ionische PEGgel besteht aus in situ gebildeten, physikalisch vernetzten Poly(2-hydroxyethylmethacrylat)-Netzwerken und PEG und weist eine hohe Leitfähigkeit ( $0,04 \text{ S m}^{-1}$ ), eine ausgezeichnete elektrochemische Stabilität ( $> 60.000$  Zyklen), eine extreme Dehnbarkeit (bis zu 1400 %), hohe Zähigkeit ( $7,16 \text{ MJ m}^{-3}$ ), schnelle Selbstheilungseigenschaft, die eine Wiederherstellung der Ionenleitfähigkeit innerhalb von Sekunden ermöglicht, sowie keine Lösungsmittelleckage auf. Mehrere Anwendungen von ionischem PEGgel wurden als (a) flexible Sensoren zur Dehnungs- oder Temperaturmessung, (b) Hautelektroden zur Aufzeichnung von Elektrokardiogrammen und (c) als robustes und sensorisches Material für pneumatische künstliche Muskeln demonstriert.

In Kapitel 3.3 wurde eine In-situ-Phasentrennung im PEGgel-System unter Verwendung der Mischung aus PEG und Polypropylenglykol (PPG) als Lösungsmittel gebildet. Die phasenetrennten Polymergele wurden durch direktes Polymerisieren von 2-Hydroxyethylmethacrylat in einer Mischung aus PEG und PPG hergestellt. Die polymerisierten elastischen Netzwerke weisen eine unterschiedliche Löslichkeit in PEG (hochlöslich) und PPG (schwach löslich aufgrund des vorhandenen Methyls in der Hauptkette) auf, was zu einem makroskopisch homogenen kovalenten Netzwerk mit in-situ-Phasentrennung führt. Das resultierende phasenetrennte gel zeigt eine hohe Festigkeit (8,0 MPa), eine günstige Bruchdehnung (430 %) und eine große Zähigkeit ( $17,0 \text{ J m}^{-3}$ ). Die getrennten Phasen verleihen dem Polymergel eine Formgedächtniseigenschaft, die für verschiedene weiche Maschinen in Kombination mit 3D-Druckfähigkeit verwendet werden kann. Dann wurden Ionen in das PEG/PPG-Lösungsmittel eingebaut, um eine hierarchische Verbesserung in Polymergelen zu erreichen, die von den ionischen Wechselwirkungen (Nanoebene) bis zur Phasentrennung (Mikroebene) reicht. Eine solche hierarchische Struktur verbesserte die Festigkeit und Zähigkeit von Polymergelen weiter und zeigte eine hohe Bruchfestigkeit (12,2 MPa) und Bruchenergie ( $54 \text{ kJ m}^{-2}$ ).



Abschließend wurde ein Ausblick auf die Herausforderungen gegeben, denen man sich bei der Entwicklung funktioneller Polymergele stellen muss. Um die Entwicklung von Polymergelen in verschiedenen Bereichen zu beschleunigen, müssen wir sowohl das Netzwerkdesign als auch die Lösungsmittelstrategien optimieren. Fortschritte auf nur einer Seite reichen nicht aus, um alle Herausforderungen zu lösen.

# Table of Contents

<b>Acknowledgement</b> .....	III
<b>Abstract</b> .....	V
<b>Zusammenfassung</b> .....	VII
1 Introduction .....	13
1.1 Choices of Functional Solvents for Functional Polymer gels.....	13
1.1.1 Organic Solvents .....	13
1.1.2 Ionic Liquids (ILs).....	21
1.1.3 Deep Eutectic Solvents.....	25
1.1.4 Polymer Fluids.....	32
1.2 Functions Derived from Solvents .....	35
1.2.1 Slippery Performance .....	35
1.2.2 Freezing Resistance or Thermal Stability.....	38
1.2.3 Superior Mechanical Properties .....	41
1.2.4 Electrical Performance .....	44
2 Work Objectives.....	48
3 Results and Discussion .....	50
3.1 PEGgel.....	50
3.1.1 Abstract.....	50
3.1.2 Introduction .....	51
3.1.3 Results and Discussion .....	53
3.1.4 Materials and Methods .....	72
3.1.5 Supporting Information .....	76

## Table of Contents

---

3.2	Ionic PEGgel.....	95
3.2.1	Abstract.....	95
3.2.2	Introduction .....	96
3.2.3	Result and Discussion.....	98
3.2.4	Materials and Methods .....	113
3.2.5	Supporting Information .....	117
3.3	Phase-separated PEGgel .....	137
3.3.1	Abstract.....	137
3.3.2	Introduction .....	137
3.3.3	Result and Discussion.....	139
3.3.4	Materials and Methods .....	148
3.3.5	Supporting Information .....	150
4	Conclusions and Outlook .....	154
4.1	Conclusions.....	154
4.2	Outlook .....	156
5	Appendix .....	158
5.1	List of Figures .....	158
5.2	List of Tables .....	165
5.3	List of Abbreviations .....	166
5.4	Curriculum Vitae .....	167
5.5	Publications and Conference Contributions .....	168
6	Literature .....	170



**Figure 1.** A picture of a jellyfish swimming taken at Musée océanographique de Monaco. Jellyfish, the oldest multi-organ animal group in nature, contains more than 95% of water as solvent in the body. They can move, sense, and grow up based on such a completely soft gel-like system. What do we need to create artificial soft functional machines similar to jellyfish?

# 1 Introduction

## 1.1 Choices of Functional Solvents for Functional Polymer gels

### 1.1.1 Organic Solvents

An organogel is generally considered as a class of gel composed of a liquid organic phase within a cross-linked three-dimensional network. The formation of organogels can be considered as a fabrication of cross-linked polymer networks in organic solvents (Table 1). Depending on the fundamental gelation process, organogels can be mainly divided into three types (**Figure 2**): 1) self-assembly of polymer chains, 2) chemical cross-linking of polymer chains, 3) polymerization of polymer monomers and 4) polymer bulks swelled by organic solvents.

#### 1.1.1.1 *Self-Assembly of Polymer Chains*

This type mainly depends on the physically cross-linked network, which is highly related to the concentration of polymers. Most of the driving forces for the self-assembly of polymer chains are reversible interactions, such as hydrogen bonds, van der Waals forces,  $\pi$ -stacking, coordination interactions, hydrophobic interactions, and electrostatic.<sup>1,2</sup> Via these interactions, the aggregation of polymer chains occurs spontaneously, thereby forming the cross-linked networks. This gelation mechanism is usually decided by the concentration of the polymer chains, equal to the density of interactions between polymer chains.<sup>3</sup> A typical self-assembled gelation of block-polymer of polyethylene glycol and hexamethylene diisocyanate (HDI) based polyurethanes (PEG-HDI) in 1,3-propanediol was reported.<sup>4</sup> The synthesized PEG-HDI initially appeared as a suspension in 1,3-propanediol, but on heating to 24°C, it appeared as a solution. An optically homogeneous white gel is obtained when the clear solution is cooled. The gelation of the PEG-HDI was caused by phase separation of the HDI and PEG components in 1,3-propanediol, as well as hydrogen bonding between amino groups and hydroxyls on each HDI unit. Normally, the self-assembly gelation is influenced not only by the intrinsic nature of chemical components of gels such as the compatibility, solubility profile, and even the chirality of the cross-linkers in the organic solvent but also by the external driving condition including temperature, agitation modes, and the cooling rate.<sup>5</sup>

### 1.1.1.2 *Chemical Cross-linking of Polymer Chains*

Self-assembled organogels are mainly based on physical cross-linking, which requires strong physical interactions between polymer chains. To speed up the gelation process, chemical crosslinkers or curing agents are added to connect free polymer chains with covalent bonds through the polymerization or curing reaction.<sup>6</sup> The activation of chemical groups on the polymer chains can be triggered by external energy, such as temperature, pH, light, and even ion concentration. Compared to self-assembled organogels, these organogels with covalently cross-linked polymer networks are usually more stable on swelling and mechanical behavior. For example, the popular and commercial silicone (Sylgard® 184) can be mixed with various organic solvents for preparing covalently cross-linked organogels.<sup>7</sup> Organic solvents include toluene, *n*-hexane, *n*-octane, isooctane, *n*-dodecane, *n*-5-tetradecane, and *n*-hexadecane. It was found that the volume percentage of organic solvent influences the properties of obtained organogels a lot. When the volume percentage of all organic solvents (Volume of solvent to Volume of polymers) is over 1200%, the corresponding organogels become untransparent, showing phase separations. Due to the low silicone polymers available for polymer network formation, gel networks cannot be connected, becoming discontinuous. Thus, the ratio between solvents and polymers still plays an important role in gelation, although the driven force for cross-linked network is strong.

### 1.1.1.3 *Polymer Bulks Swollen with Organic Solvents*

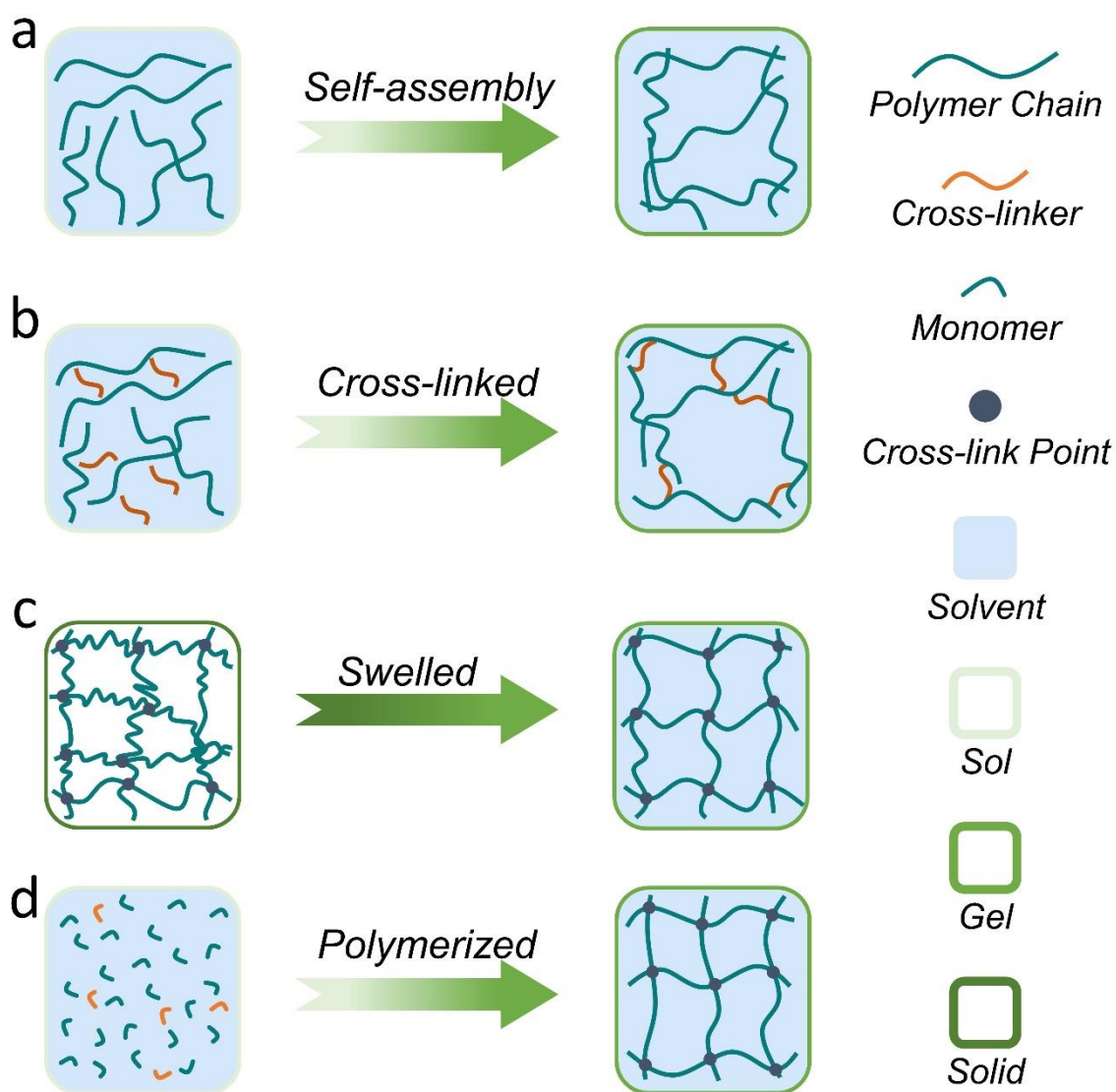
The cross-linked polymer bulks, swelling in a good organic solvent with high compatibility for the polymers, can form a uniform organogel. Due to the penetration of organic solvents into the polymer networks, swollen polymer bulks exhibit liquid-like properties,<sup>8</sup> definitely called organogels. In general, polymer networks' swelling ability depends on the swelling solvents' compatibility with the network. For example, a commercial poly(dimethylsiloxane), owning the cross-linked networks, can be directly transferred into an organogel by swelling in crude oil until the solvent is balanced.<sup>9</sup> The interaction between a solvent and the cross-linked polymer network can be quantified as

$$D_C^S = kT/6\pi\eta_S\xi_H.$$

The  $D_C^S$  is a co-diffusion coefficient related to the degree of expansion of the cross-linked network,  $k$  is the Boltzmann constant,  $T$  is the swelling temperature,  $\eta_S$  is the viscosity of the corresponding solvents, and  $\xi_H$  can be regarded as the polymer chain length between adjacent crosslinks.<sup>10,11</sup> With the help of this equation, the swelling ratio of the obtained organogels can be tuned by the molecular weight of the swelling solvents and the cross-linking density of poly(dimethylsiloxane).

### 1.1.1.4 *Polymerization of Monomers*

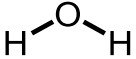
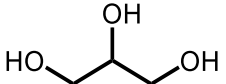
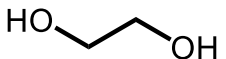
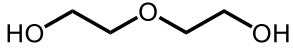
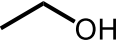
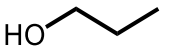
The two strategies discussed above are top-down methods, while polymerization of monomers in organic solvents is a bottom-up approach. The monomers are dissolved in organic solvents with initiators uniformly. After the polymerization of monomers, the organic solvents are trapped within the cross-linked polymer networks, forming polymer gels. The pre-polymerization solution is usually liquid, which can be shaped into the different molds or 3D printed directly. A free-radically polymerization of monomers can produce a cross-linked polymer network in organic solvents with or without cross-linkers. Free-radical polymerization is an efficient and popular method, rapidly forming cross-linked networks. These organogels are remarkably stable due to the strong and uniform covalent networks. According to the application environment of organogels, many initiation types can be chosen, such as visible or UV light, heat, and redox.



**Figure 2.** Schematic illustration of gelation mechanism of organogels. (a) Polymer chains self-assemble into physically cross-linked organogels. (b) Cross-linkers connect polymer chains to form chemically cross-linked organogels. (c) Solvents swell cross-linked bulk polymers to prepare organogels. (d) Monomer solutions are polymerized to form organogels.

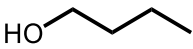
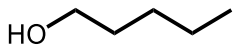
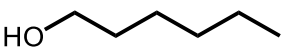
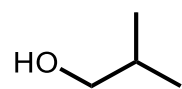
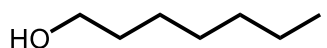
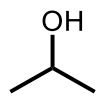
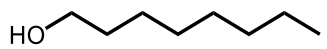
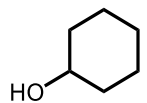


**Table 1.** Common small molecule solvents for **organogels**

Solvent	Chemical Formula	Boiling point (°C)	Melting point (°C)	Refractive Index at 20°C	Density at 20°C (g/mL)	Viscosity at 20°C (mPa·s)	Water Solubility (g/100g)	Relative Polarity
Water		100	0	1.333	0.998	1.00	Miscible	1
Glycerol		290	17.8	1.467	1.261	11.10	Miscible	0.812
Ethylene glycol		197	-13	1.439	1.115	16.10	Miscible	0.79
Diethylene glycol		245	-10	1.447	1.118	35.70	Miscible	0.713
Ethanol		78.5	-114.1	1.362	0.789	1.04	Miscible	0.654
1-Propanol		97	-126	1.387	0.803	1.96	Miscible	0.617

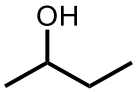
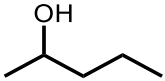
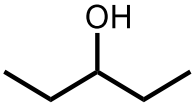

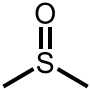
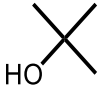
## 1.Introduction

---

1-Butanol		117.6	-89.5	1.399	0.81	3.00	7.7	0.586
1-Pentanol		138	-78.2	1.409	0.814	3.51	2.2	0.568
1-Hexanol		158	-46.7	1.416	0.814	4.59	0.59	0.559
<i>i</i> -Butanol		107.9	-108.2	1.396	0.803	3.95	8.5	0.552
1-Heptanol		176.4	-35	1.422	0.819	5.97	0.17	0.549
2-Propanol		82.4	-88.5	1.377	0.785	2.37	Miscible	0.546
1-Octanol		194.4	-15	1.428	0.827	7.59	0.096	0.537
Cyclohexanol		161.1	25.2	1.465	0.962	41.07	4.2	0.509

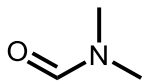
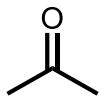
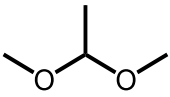

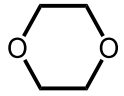
## 1.Introduction

---

2-Butanol		99.5	-114.7	1.397	0.808	2.95	18.1	0.506
2-Pentanol		119	-50	1.406	0.81	3.47	4.5	0.488
3-Pentanol		115.3	-8	1.410	0.821	8.13	5.1	0.463
Acetonitrile		81.6	-46	1.344	0.786	0.38	Miscible	0.46
Dimethyl sulfoxide  (DMSO)		189	18.4	1.479	1.092	2.00	Miscible	0.444
<i>t</i> -Butyl alcohol		82.2	25.5	1.387	0.786	3.38	Miscible	0.389

## 1.Introduction

---

Dimethylformami de (DMF)		153	-61	1.431	0.944	0.92	Miscible	0.386
Acetone		56.2	-94.3	1.359	0.786	0.30	Miscible	0.355
Dimethoxy ethane		85	-58	1.380	0.868	1.10	Miscible	0.231
Tetrahydrofuran (THF)		66	-108.4	1.407	0.886	0.48	30	0.207
Dioxane		101.1	11.8	1.422	1.033	1.20	Miscible	0.164

---

### 1.1.2 Ionic Liquids (ILs)

Ionic liquids (ILs) are salts, normally defined as compounds composed of ions with a melting point below 100°C.<sup>12,13</sup> Current ILs mainly consist of cations (such as pyridinium, imidazolium, quaternary ammonium, and quaternary phosphonium) and anions (such as halogen, triflate, tetrafluoroborate, and hexafluorophosphate) (Table 2).<sup>14</sup> In 1914, Paul Walden first reported ethyl ammonium nitrate as IL.<sup>15</sup> In the following century, ILs emerged into a major scientific area due to their admirable properties, including virtually no vapor pressure, non-flammability, high thermal stability, relatively low viscosity, wide liquid temperature range, high ionic conductivity, and broad electrochemical window.<sup>16-18</sup> These unique properties of ionic liquids and the prospect that they can be tailored or custom-designed to meet specific requirements make them all the more interesting.<sup>19,20</sup>

Depending on the nature of the cations and anions and the intermolecular interactions between ions, ILs demonstrate interesting solvation properties.<sup>20</sup> For example, ILs can dissolve various substances, including polar or nonpolar organic compounds,<sup>21</sup> metal elements,<sup>22</sup> metal salts,<sup>23</sup> proteins, and even some natural polymers (e.g., cellulose,<sup>24</sup> lignin,<sup>25,26</sup> and directly wood<sup>27</sup>). Their powerful solvating ability to different substances may originate from the heterostructure of IL, which own both polar and non-polar domains.<sup>28</sup> Regardless of polar or non-polar organic solutes, they can find relatively affinity domains in IL and segregate into them. In detail, non-polar compounds will be distributed in non-polar domains, while polar molecules will reside in charged networks, forming extensive hydrogen-bonding interactions with charged moieties.<sup>29</sup> Such strong solvating ability makes ILs a new generation of solvents for synthesis,<sup>30</sup> catalyzes,<sup>31</sup> and separation.<sup>32</sup>

For polymer science, ILs have been used in free-radical polymerization processes as green media.<sup>33</sup> The application of ILs in polymer gel came naturally due to the various properties of ILs mentioned above.<sup>34</sup> Depending on the high ionic conductivity ( $10^{-4}$  to  $8.10^{-2}$  S cm<sup>-1</sup> at room temperature) and the wide electrochemical potential window (up to 5.7 V between Pt electrodes), ILs have been widely used by electrochemists for a long time, especially in the solid electrolytes.<sup>35</sup> There are two normal approaches to fabricating polymer gels based on ILs (Figure 3): 1) mixing a polymer and ILs directly or with a co-solvent,<sup>36</sup> 2) in situ polymerization of monomers in ILs.<sup>37</sup> In the former method, the key point comes to the miscibility between the IL and the polymer. Many polymers have been reportedly swollen

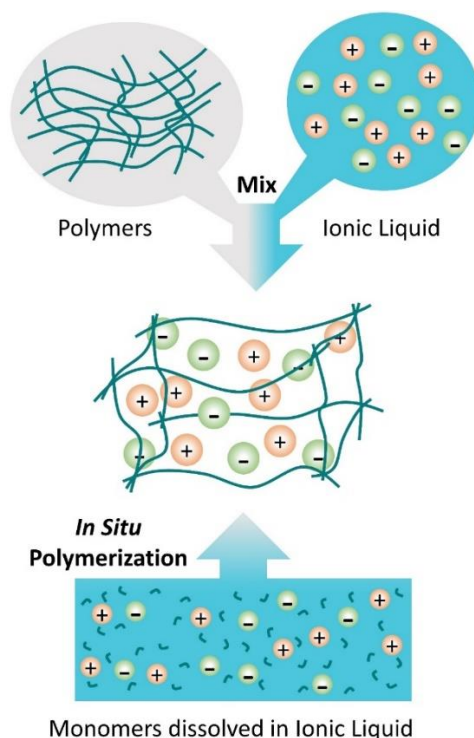
in ILs, such as poly(methyl methacrylate) with imidazolium salts,<sup>38</sup> cellulose with triazolium salts,<sup>39</sup> polyurethane-polybutadiene elastomer, polydimethylsiloxane and polyvinylidene fluoride with imidazolium salts.<sup>36</sup> In these cases, ILs can be considered plasticizers, lowering the glass transition temperature of corresponding polymers, thus providing flexibility. The second method mainly depends on the good solubility of many monomers in ILs. The vinyl monomers were carried out for in situ polymerization in ILs to form polymer networks in a gel.<sup>40</sup> In situ free radical polymerization of the compatible vinyl monomers in ILs usually yields transparent and highly conductive polymer gel with appropriate network design. Like conventional polymer gels based on water or organic solvents, the IL gels are comprised of polymer networks and ILs. However, the IL gels are distinctly discriminated from conventional polymer gels in terms of nonvolatility and high thermal stability of the liquids incorporated in the network polymers.

Herein, this section presented some typical IL gels reported recently to demonstrate their interesting properties and potential applications. Soft electrolyte materials based on non-volatile IL gels are emerging as promising candidates for use in flexible electronics. Suffering from poor mechanical properties, such as high stiffness, limited stretchability, and low toughness, most existing IL gels cannot meet the practical requirements of flexible electronics. Thus, poly(ethyl acrylate) was used as elastomer networks combined IL (i.e., 1-ethyl-3-methylimidazolium bis(trifluoromethylsulfonyl)imide, [C<sub>2</sub>mim][NTf<sub>2</sub>]) through hydrogen bonds (Figure 4a). Anions [NTf<sub>2</sub>] play a major role in the molecular interactions between ILs and elastomers. The obtained IL gels exhibited high transparency (95% for visible light), ultra-stretchability (up to 5000%), and large toughness (around 4.7 kJ m<sup>-2</sup>).<sup>40</sup>

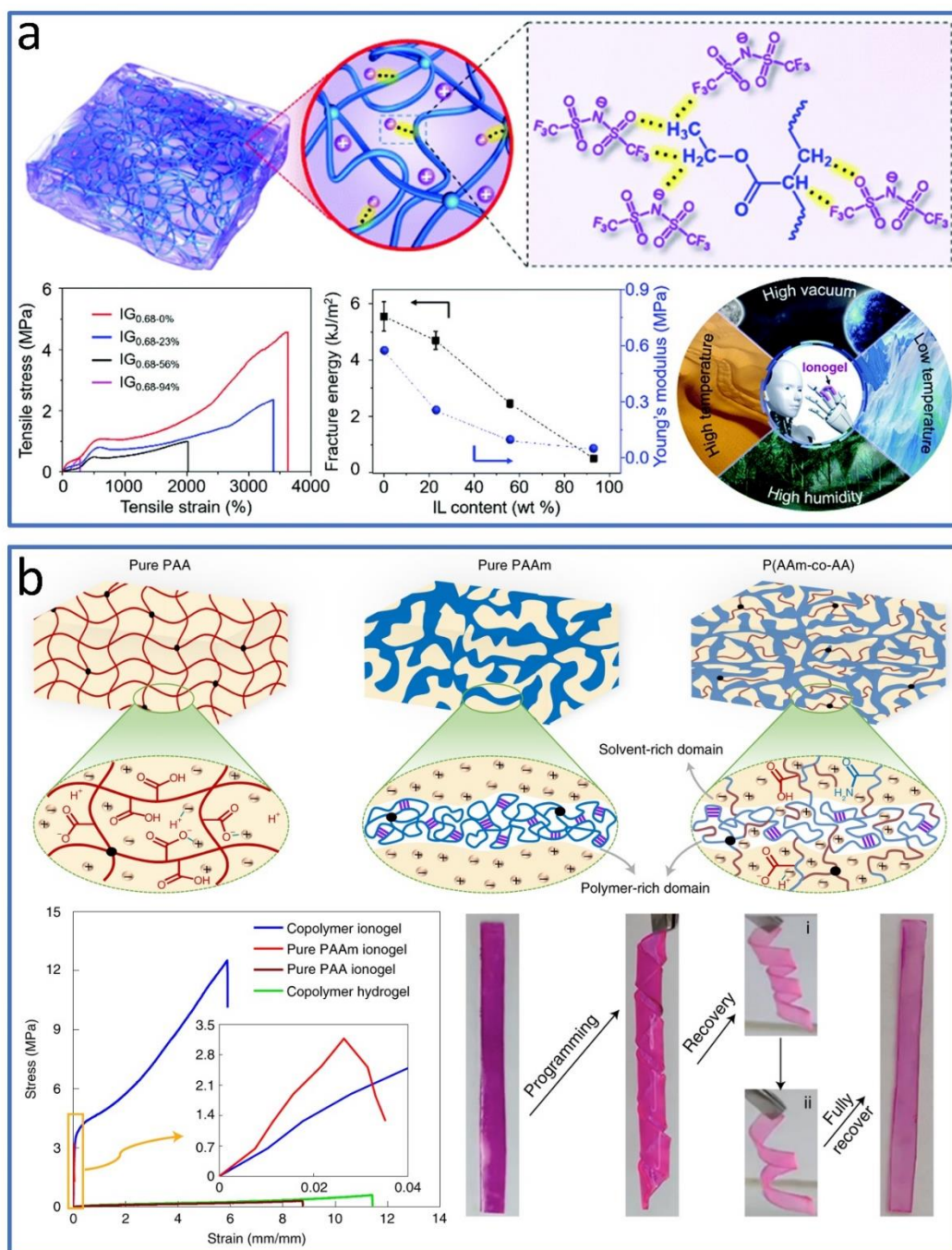
Additionally, the obtained gels presented good thermal stability, wide voltage window, and humidity resistance due to the introduction of ILs. The IL gels can be used directly for serving as a high-performance strain sensor that can work under sharp environmental conditions, such as 99% relative humidity, high vacuum conditions ( $6 \times 10^{-4}$  Pa), and low (-70 °C) and high (100°C) temperatures.<sup>41</sup> For further improving the mechanical properties of IL gels, in situ phase separation of polymer networks was introduced into IL gels. As shown in Figure 4b, two common monomers with distinct solubility of the corresponding polymers in an ionic liquid are randomly copolymerized.<sup>42</sup> In detail, the random copolymerization of acrylamide and acrylic acid in 1-ethyl-3-methylimidazolium ethyl sulfate results in an isotropic IL gel that forms in situ separated phase domains. As a result of the solvent

separation between polymer networks, highly solvated polymer networks contain few hydrogen bonds, presenting soft and stretchable gels.

Conversely, poorly solvated polymer networks own fewer solvents and lose the nature of a gel, often exhibiting stiff and brittle. In this case, polyacrylic acid serves as highly solvated networks, forming solvent-rich domains with few hydrogen bonds. Moreover, polyacrylamide is a poorly solvated network, becoming a polymer-rich domain with many hydrogen bonds. The IL gels are toughened by the polymer-rich phase with hydrogen bonds, which dissipates energy during deformation efficiently. These IL gels exhibit large fracture strength (12.6 MPa), high fracture energy ( $\sim 24 \text{ kJ m}^{-2}$ ), and considerable stretchability ( $\sim 600\%$  strain). Based on this phase separation in polymer networks, the IL gels have shape-memory properties, showing the potential application in soft actuators. This one-step method to form tough IL gels with in situ phase separation can be applied to other monomers and ionic liquids, such as acrylic acid with 2-hydroxyethyl methacrylate or 2-hydroxyethyl acrylate in 1-ethyl-3-methylimidazolium ethyl sulfate, and the same polymers in 1-ethyl-3-methylimidazolium tetrafluoroborate.



**Figure 3.** Strategies to fabricate IL gels. a) Top-down strategy to fabricate IL gels by mixing polymers and ILs. b) Bottom-up strategy to fabrication of IL gels based on the polymerization of monomers in ILs.





**Table 2.** Some common examples of cations and anions used in the formation of corresponding ionic liquid and thereby admirable properties, and changes of water miscibility with anion type.

Cations		<b>Property:</b>
<b>Ionic Liquid</b>		
	<b>Anions</b> 	

### 1.1.3 Deep Eutectic Solvents

Deep eutectic solvents (DESs) were first found in the 1:2 mole fraction combination of powdered choline chloride ((2-hydroxyethyl)-trimethylammonium chloride) with crystalline urea.<sup>43</sup> In this case, the melting points of choline chloride and crystalline urea are about 302°C and 133°C, respectively. At the same time, the mixture is a liquid at room temperature (melting point of the mixture at eutectic composition,  $T_{Eutectic} = 12\text{ }^{\circ}\text{C}$ ). Further studies found that this abnormally deep melting point depression relies on the eutectic composition of certain hydrogen bond donors and acceptors.<sup>44-46</sup> Deep eutectic mixtures melt at low enough temperatures to make novel liquids economically accessible as solvents or electrolytes for new and existing applications.<sup>47</sup>

Generally, DESs were introduced as a subclass of ILs and an alternative to ILs to overcome the drawbacks of ILs.<sup>48</sup> There are some general characteristics between DESs and ILs, including low vapor pressures, high thermal stabilities, low volatility, and adjustable

polarity.<sup>49</sup> However, ILs are expensive, often non-biodegradable, and have high toxicities, whereas DESs are typically inexpensive, biodegradable, nontoxic, and easier to prepare.<sup>49,50</sup> For example, choline, the most common hydrogen bond acceptor, is a constituent of vitamin B, and is currently produced on a megaton per annum basis as a nutritional supplement for livestock, making for a cheap, plentiful, nontoxic. Then, the corresponding popular hydrogen bond donor can use urea, which is environmentally friendly and is commonly used in fertilizers.<sup>51,52</sup>

The majority of DESs that have been prepared and studied thus far are traditionally classified as Type I-V, summarized in Table 3. Type III attracts tremendous research interest among these types due to its wide choices and great potential applications. A constituent of Type III DESs used in previous studies were roughly listed (Table 4). By adjusting the molar ratio and types of hydrogen bond acceptors and donors, the physical and chemical properties of DES can be tuned to meet a wide range of applications. This section focuses on the applications of DESs in polymer gels. For the other fundamentals and applications, the recent reviews about EDSs are highly recommend.<sup>47,51,53</sup> Based on the good conductivity and excellent stability of DESs, the eutectogel owns a wide range of applications in energy materials and flexible devices.<sup>54,55</sup> To clarify and inspire the eutectogel design, the following part mainly claimed the preparation of the eutectogel.

**Table 3.** General Formula for the Classification of DESs.<sup>47</sup>

<b>Type</b>	<b>Composition</b>
Type I	a quaternary ammonium salt and a metal chloride
Type II	a quaternary ammonium salt and a metal chloride hydrate
Type III	a quaternary ammonium salt and a hydrogen bond donor (typically an organic molecular component such as an amide, carboxylic acid, or polyol)
Type IV	a metal chloride hydrate and hydrogen bond donor
Type V	a relatively new class composed of only non-ionic, molecular hydrogen bond acceptors and donors.

Due to the wide presence of hydrogen bonding sites in the molecular structure of DESs, water can be miscible with most of DESs.<sup>56,57</sup> Thus, the most common and easy method to fabricate eutectogel is immersing prepared hydrogel in a DES for solvent replacement.<sup>58</sup> Thus, prepared sulfonated lignin-Fe<sup>3+</sup> hydrogel was engaged in the choline chloride and urea for 12 h for solvent replacement (Figure 5a). The obtained eutectogel can maintain mechanical flexibility and electrical stability at extremely low temperatures (-80 °C). Another approach to fabricating eutectogels is the polymerization of the gel network in DESs directly (Figure 5b). In the case of homogeneous polymerization of monomers dissolved in DES, the first step is to assess their miscibility. Due to the high density of hydrogen bonds and the ionic nature of DES, acrylic acid and methacrylic acid are the most studied monomers for free radical polymerization.<sup>59</sup> The acrylic acid can be dissolved and polymerized in different DESs to make eutectogel by a one-pot method. The ubiquitous hydrogen bonds of poly acrylic acid and DESs can effectively dissipate separation energy during the deformation of the eutectogel, which presents higher toughness than the corresponding hydrogel with the same polymer network.<sup>60</sup>

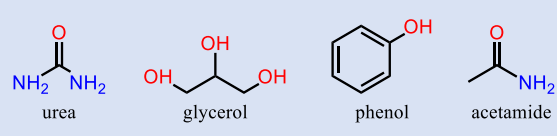
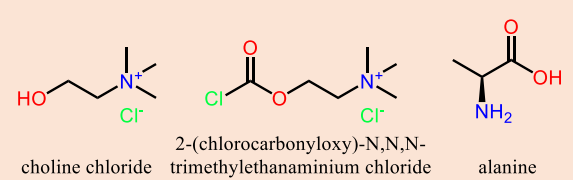
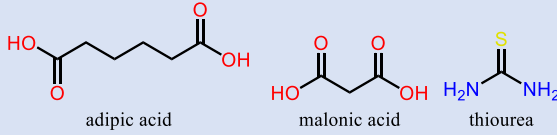
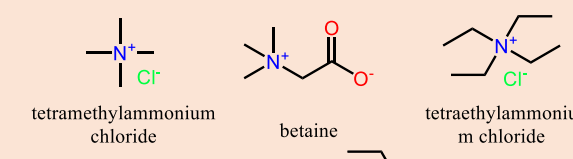
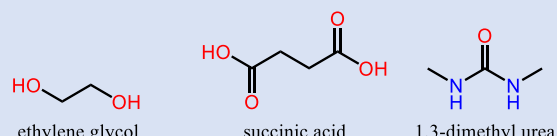
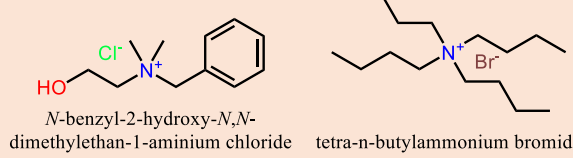
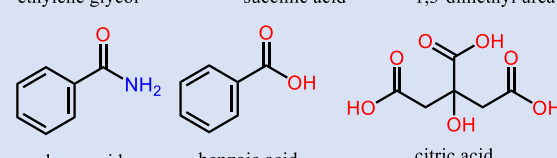
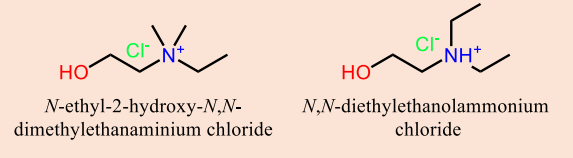
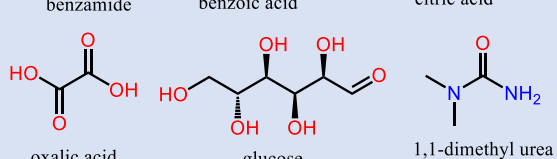
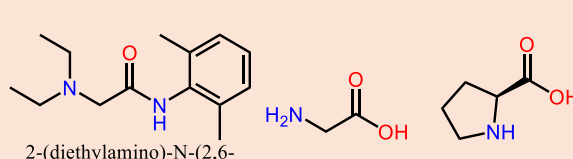
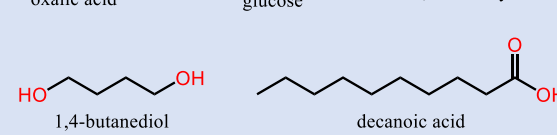
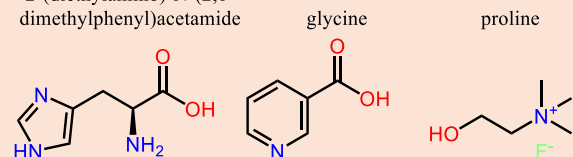
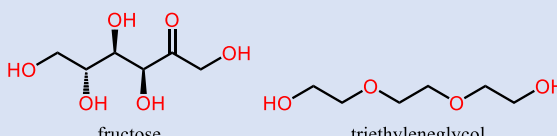
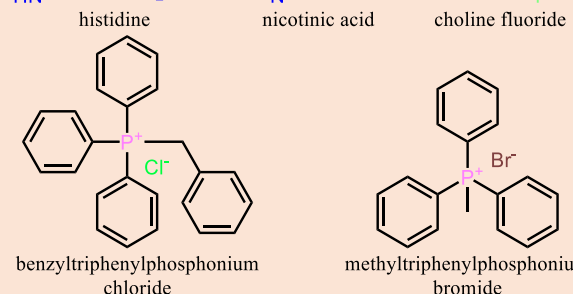
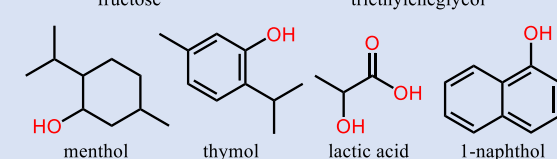
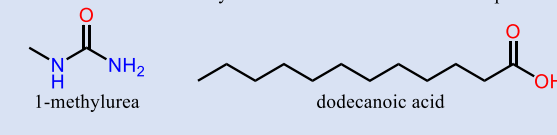
Indeed, some popular acrylates can serve as a part of DES by themselves (e.g., acrylic acid can play the role of hydrogen bond donor, and HEMA can be the hydrogen bond acceptor).<sup>53,56,61,62</sup> For example, acrylic acid and choline chloride were chosen as the hydrogen bond donor and acceptor, respectively. After mixing at 90°C for around 4 hours, a transparent and polymerizable DES liquid was obtained. Then, with a small amount of photoinitiator and cross-linker, the polymerizable DES liquid can be quickly cured into a eutectogel under UV light.<sup>61</sup> The obtained eutectogel presented favorable ionic conductivity (0.2 S/m) and transparency (81%), however, limited mechanical properties. By changing the hydrogen bond acceptor into tetramethylammonium chloride, the corresponding eutectogel can be stretched into over 3600%, whose strength and toughness were up to 31.2 MPa and 615 MJ m<sup>-3</sup>, respectively (Figure 5c).<sup>63</sup> Copolymerization of two polymerizable deep eutectic solvent monomers is another way to modify the performance of eutectogel.<sup>64</sup> Acrylic amide/choline chloride and maleic acid/choline chloride were copolymerized together to prepare supermolecular network eutectogel (Figure 6a), showing high transparency (an average transmittance of 95.1%), intrinsically ionic conductivity (0.04 S/m), and fast self-healing property (within 2 s) without any other external stimuli with efficiency up to 94%.

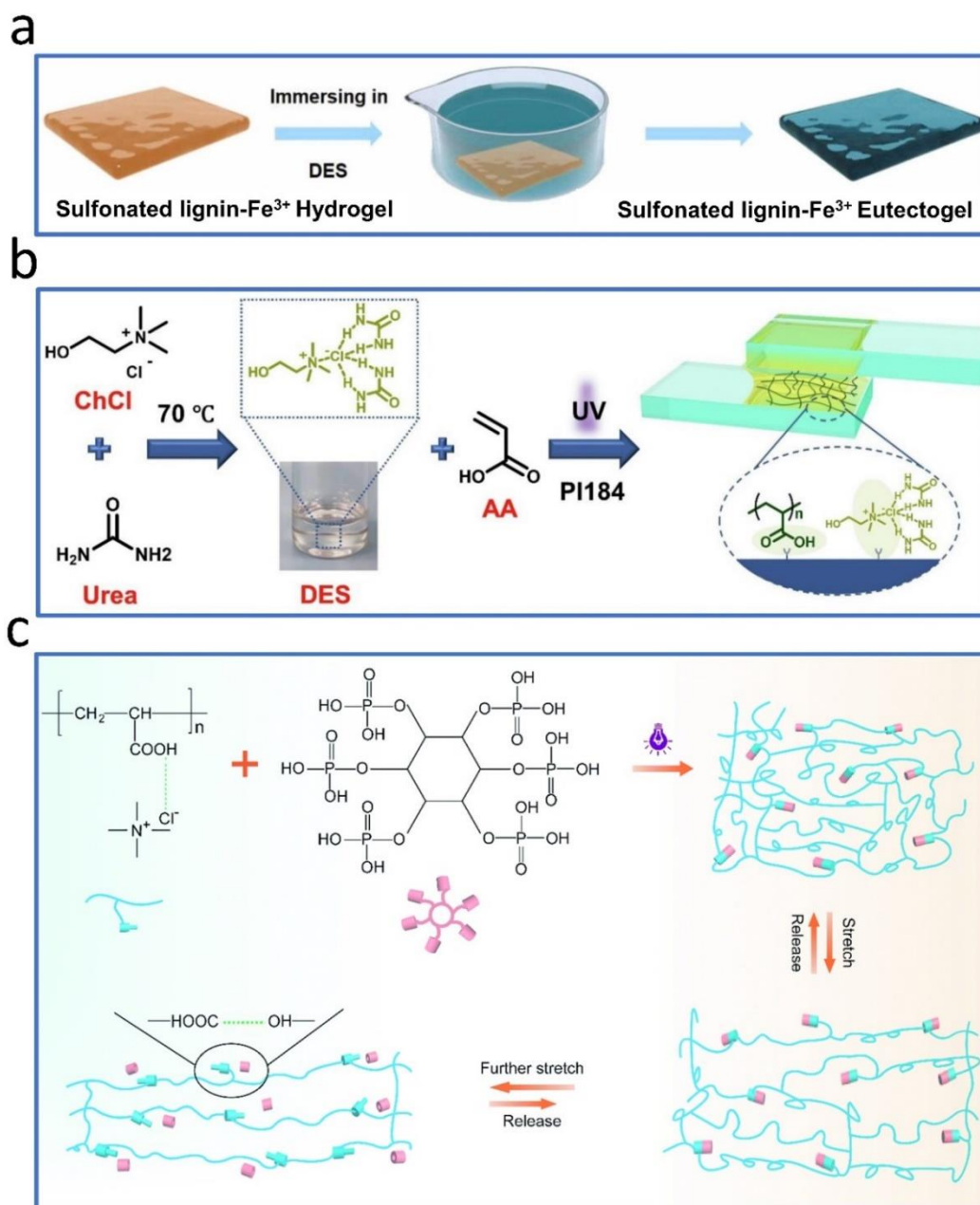
Besides selecting hydrogen bond donors and acceptors, the popular gel network design is also important in eutectogel fabrication.<sup>62</sup> A self-assembled cellulose nanocrystal skeleton was embedded in a polymerized DES matrix to constitute a eutectogel (Figure 6b). In this case, acrylic acid, choline chloride, and phytic acid were selected as hydrogen bond donors, acceptors, and small-molecule regulators. The assembly process is accomplished through executing the elaborate strategy, including glucose-assisted self-assembly of cellulose nanocrystals, diffusion-induced penetration of monomers, and in situ photoinitiated polymerization. The strong interfacial interactions between cellulose nanocrystals assembled in the skeleton and poly DES matrix were based on the hydrogen-bond interactions between carboxyl groups of acrylic acid, phosphate groups of phytic acid, and hydroxyl groups of choline chloride and cellulose nanocrystals. The flexible intrinsic conducting poly DES matrix, embedded cholesteric cellulose nanocrystal skeleton, and multiple interfacial hydrogen bonding networks endow the resulted eutectogel with favorable mechanical properties and excellent self-healing ability.

As shown above, most eutectogels usually have good thermal stability, favorable conductivity, and moderate mechanical properties. However, many challenges remain to be addressed, such as a balance between high strength and high conductivity, poor weather resistance, and limited choices of green monomers or polymers. Overall, eutectogels have great potential as a new generation of functional polymer gels and are in their infancy. More research is needed in the future to explore novel designs and exotic applications of eutectogels.

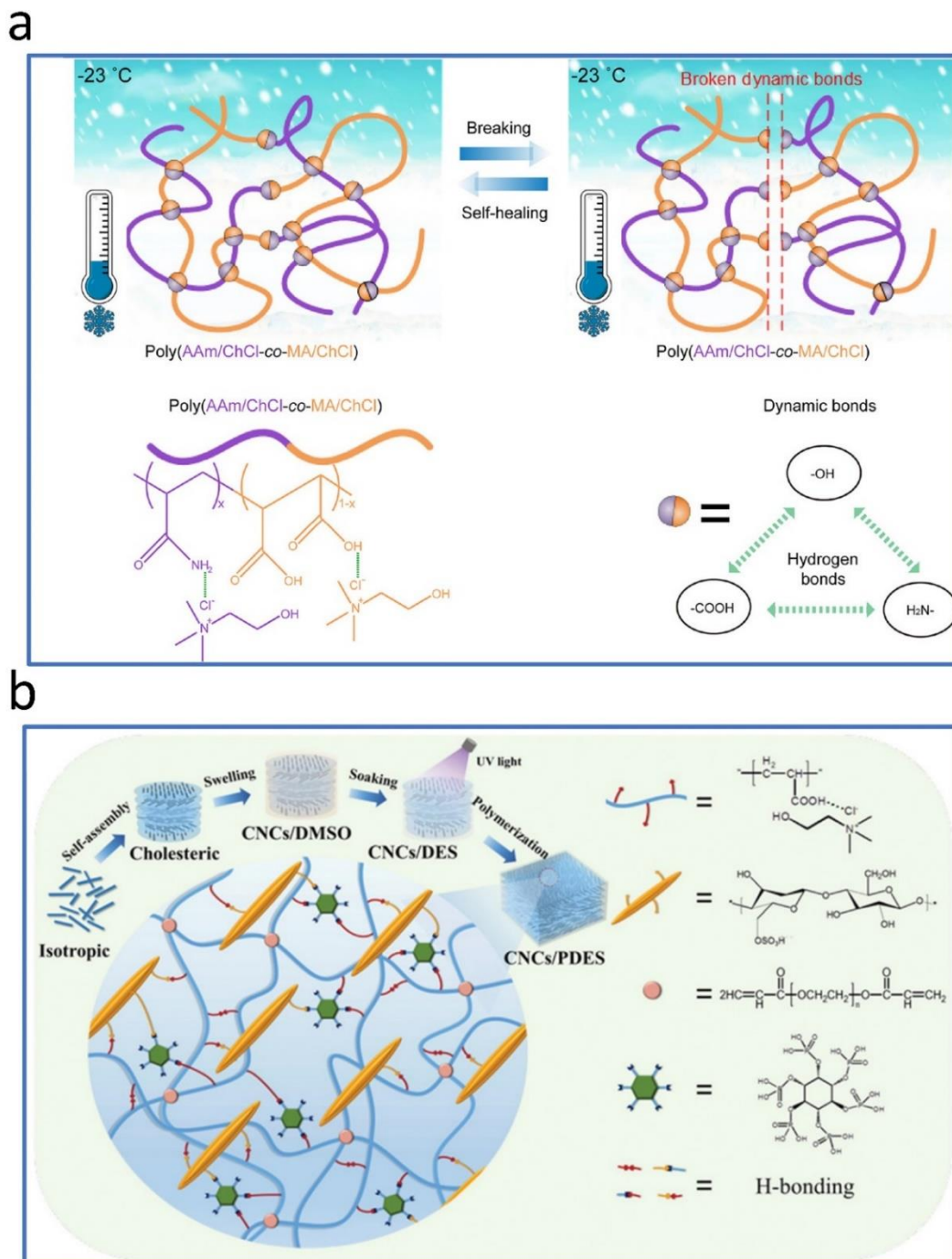
# 1. Introduction

**Table 4.** Representative sampling of common constituents of Type III DESs used in previous studies.<sup>51</sup>

Hydrogen Bond Donors	Hydrogen Bond Acceptors
 <p>urea, glycerol, phenol, acetamide</p>	 <p>choline chloride, 2-(chlorocarbonyloxy)-N,N,N-trimethylethanaminium chloride, alanine</p>
 <p>adipic acid, malonic acid, thiourea</p>	 <p>tetramethylammonium chloride, betaine, tetraethylammonium chloride</p>
 <p>ethylene glycol, succinic acid, 1,3-dimethyl urea</p>	 <p><i>N</i>-benzyl-2-hydroxy-<i>N,N</i>-dimethylethan-1-aminium chloride, tetra-<i>n</i>-butylammonium bromide</p>
 <p>benzamide, benzoic acid, citric acid</p>	 <p><i>N</i>-ethyl-2-hydroxy-<i>N,N</i>-dimethylethanaminium chloride, <i>N,N</i>-diethylethanolammonium chloride</p>
 <p>oxalic acid, glucose, 1,1-dimethyl urea</p>	 <p>2-(diethylamino)-<i>N</i>-(2,6-dimethylphenyl)acetamide, glycine, proline</p>
 <p>1,4-butanediol, decanoic acid</p>	 <p>histidine, nicotinic acid, choline fluoride</p>
 <p>fructose, triethyleneglycol</p>	 <p>benzyltriphenylphosphonium chloride, methyltriphenylphosphonium bromide</p>
 <p>menthol, thymol, lactic acid, 1-naphthol</p>	
 <p>1-methylurea, dodecanoic acid</p>	



**Figure 5.** a) Schematic illustration of the fabrication of Sulfonated lignin-Fe<sup>3+</sup>-DES eutectogel from hydrogel by the method of solvent replacement.<sup>58</sup> b) Scheme illustration of the preparation of PAA gel in the presence of DES.<sup>59</sup> c) Schematic illustration of the strong, tough, and ultra-stretchable eutectogel based on tetramethylammonium chloride and acrylic acid.<sup>63</sup>



**Figure 6.** a) Schematic illustration of eutectogel based on copolymer of acrylic amide/choline chloride and maleic acid/choline chloride polymerizable DES.<sup>64</sup> b) Schematic illustration for the preparation of cellulose nanocrystals/poly DES in situ composites and network of dynamic interfacial hydrogen bonds.<sup>62</sup>

### 1.1.4 Polymer Fluids

Polymer fluids are an old fashion spawned from the increasing regulatory pressure on the use and disposal of volatile organic compounds (VOCs).<sup>65,66</sup> As a non-hazardous alternative, polymer fluids were developed to be widely used as a solvent and phase-transfer catalyst in biotechnology and medicine.<sup>67</sup> Of course, solvent issues are vitally important for polymer gels' continued and sustainable development. More importantly, solvents play a decisive role in maintaining and improving the preparation and performance of polymer gels.

In principle, polymer fluids as solvents can be achieved in some polymers with low melting temperatures (below room temperature) or lots of oligomers. Currently, some commonly used polymer fluids are polyethylene glycol (PEG,  $M_n < 1000 \text{ g mol}^{-1}$ ), polypropylene glycol (PPG,  $M_n < 4000 \text{ g mol}^{-1}$ ), and poly tetrahydrofuran (PTHF,  $M_n < 6000 \text{ g mol}^{-1}$ ). Due to the low molecular weight and plenty of weak hydrogen bond sites, they exhibit low viscosity and good solvability. Compared to the small molecular solvents mentioned above, polymer fluids own negligible solvent evaporation and leakage, which is crucial to the performance, stability, and reliability of the obtained polymer gels.

For the polymer fluids as solvents, there is always a controversy between the polymer blends<sup>68</sup> and polymer gels based on polymer fluids.<sup>69</sup> To be clear, this part only discuss the system was built networks in polymer fluids from down to top directly, rather than mixing the existing polymer fluids and polymer networks. Compared to the blend systems, polymer gels based on polymer fluids have advantages in the diversity of the polymer monomers, regulation of interactions within polymer networks, and processing. Due to the strong interactions between polymer chains (e.g., hydrogen bonds, electrostatic interactions, and entanglements),<sup>70</sup> the existing polymers in blend systems usually need external organic solvents to mix with oligomers uniformly.<sup>71</sup> Thus, the shaping or processing of blend systems always involves fellow steps for removing organic solvents,<sup>72</sup> which lead to the molding stability of the obtained samples and unnecessary environmental concerns.

However, the polymer fluids, used as green solvents in various fields already,<sup>66</sup> can dissolve different monomers with corresponding initiators easily and uniformly. Based on this feature, the prepared mixture can be poured into multiple molds to achieve one-time molding or even shaping complex structures through 3D printing technology. Furthermore, all polymer network design strategies, developed and applied in other solvent systems, are accessible in



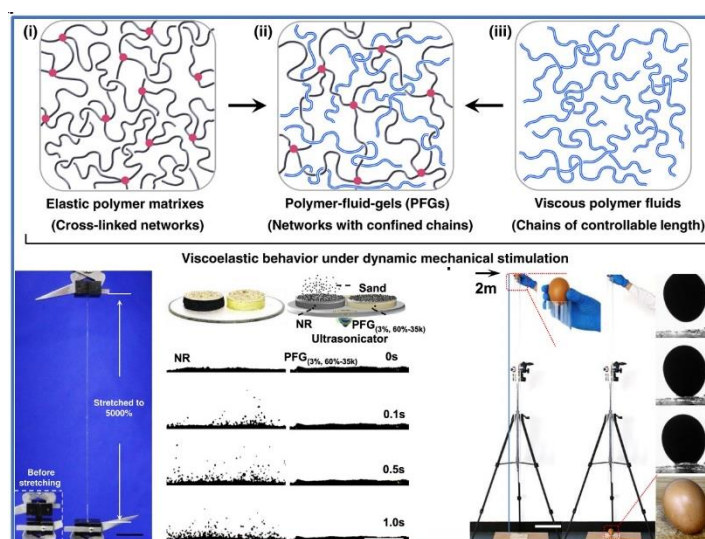
the polymer fluid systems. This feature guarantees the strong innovation ability and high-performance scalability of the polymer gels. In another word, there is an extremely wide window to tune the performance of polymer gels based on polymer fluids, even if no changes are allowed in the choice of polymer monomers. This section will introduce several examples based on polymer fluids demonstrating the advantages of this system.

PEG is a liquid oligomer at room temperature ( $M_w < 600 \text{ g mol}^{-1}$ ),<sup>73</sup> widely used in biotechnology and medicine,<sup>65</sup> and was already approved for internal consumption by the US FDA.<sup>66</sup> Previously, it was demonstrated that PEG could provide strong hydrogen bonding in blends with polymers possessing hydroxy groups via ether bonds on the main chain.<sup>70,72</sup> Thus, our group indicates that PEG can serve as a functional solvent, swell a polymer network, and provide non-covalent multivalent interactions.<sup>69</sup> Compared with small molecular solvents, PEG provides more polymer chain entanglement because of its polymer nature for dissipation of energy during deformation. Also, the hydrogen bonds solidified by covalently linked polymer chains consolidate the polymer network more effectively than those relatively disconnected hydrogen bonds in a small molecular solvent gel system (**Figure 7a**). These interactions between the PEG and polymer network lead to several important properties of the produced material, such as rapid self-healing, high toughness, and 3D printability. Thus, the copolymer of hydroxyethyl methacrylate and acrylic acid (P(HEMA-*co*-AAc)), both widely used in biomedical applications, was selected as a mold to prepare PEGgel. Via adjusting the PEG fraction and its molecular weight, the obtained PEGgel exhibits tunable mechanical properties over a large range: tensile strength from 0.22 MPa to 41.3 MPa, fracture strain from 12% to 4336%, modulus from 0.08 MPa to 352 MPa, and toughness from 2.89 MJ m<sup>-3</sup> to 56.23 MJ m<sup>-3</sup>.

Besides the tuneable mechanical properties of polymer fluid systems, high energy-dissipation between networks and flows in polymer gels is another research hotspot. To dissipate energy effectively, biological damping tissues, like dolphin skin, use a synergistic network design by introducing viscous fluids into dense elastic fiber networks. The elastic fiber network eliminates vibrations caused by the water impact by moving viscous liquid in and out when the skin vibrates under water pressure. Inspired by this facile biological mechanism, polymer fluids were introduced into the elastic network for modulating energy dissipation (**Figure 7b**). A polymer-fluid-gels was manufactured by infusing viscous polymer fluids into the elastic networks, showing high energy-dissipation property (loss

factor  $> 0.5$ ) over a broad frequency range ( $10^{-2}$ - $10^8$  Hz).<sup>74</sup> Poly (*n*-butyl acrylate) ( $M_w = 35,000$  g mol<sup>-1</sup>) with a low  $T_g$  (around  $-56$  °C) was selected as polymer fluids, serving as the dissipative medium by repeating back and forth under the applied stress. For excellent compatibility, *n*-butyl acrylate was chosen as the monomer, dissolved in poly (*n*-butyl acrylate) fluid with a chemical cross-linker and photoinitiator. After free-radical polymerization, a cross-linked and elastic poly (*n*-butyl acrylate) network was formed in poly (*n*-butyl acrylate) fluids, achieving a uniform gel with the flow state and the high-elastic state. With such high compatibility and favorable intermolecular van der Waals forces in fluids and networks, the obtained gels can reduce vibration strength by 90% and impact force up to 85%.

So far, polymer gels based on polymer fluids are an emerging research field. Although using polymer fluid as solvents sometimes overlaps with the previous polymer blending research, it is an independent field for developing novel polymer gels with advanced functions via solvent strategies. Besides the polymer fluids mentioned above, many commercial and useful polymer fluids behave as a liquid at room temperatures, such as polyethylene glycol dimethyl ether, polypropylene glycol dimethyl ether, polypropylene glycol diacetate, polybutylene glycol diacetate, polytetramethylene ether glycol diacetate, poly dimethyl siloxane, and perfluoropolyether. Compared with the normal PEG, these fluids have different hydrophobicity and higher stability, which may bring more unpredictable and admirable performance.



**Figure 7.** Schematic structure of high energy-dissipation polymer-fluid-gels (PFGs) design.<sup>74</sup>

### 1.2 Functions Derived from Solvents

In the last section, the methods to fabricate polymer gels based on different solvents were summarized and discussed. This section focuses on the specific properties derived from solvents, such as slippery properties, freezing resistance or thermal stability, electrical performance, and electrical performance.

#### 1.2.1 Slippery Performance

Surface interactions are limiting in almost any liquid handling or encounter scenario.<sup>75</sup> For example, they create drag in the transport system, trigger blood clotting, and promote aircraft icing.<sup>76</sup> Inspired by the Nepenthes, a slippery liquid-infused porous surface was invented,<sup>77</sup> which showed almost perfect slipperiness toward pure liquids (such as various organic solvents and water), mixture solutions (such as blood, crude, and ketchup), a variety of bacteria and algae, and even some solid materials (such as ice, dust, and insects).<sup>75,78,79</sup> These liquid-infused surfaces always involve the leakage of infused liquid, which harshly destroy the slippery function. Here, the polymer gels are composed of sufficient solvents and crosslinked polymer networks, showing high liquid retention capacity. Due to strong interactions between molecules and polymers, liquid molecules are tightly trapped within crosslinked polymer networks. These materials combine liquid and solid properties and are the ideal substrates for liquid impregnation.<sup>80</sup> Hydrophobicity or hydrophilicity of polymer gels is mainly decided by the nature of solvents. Hydrogels and organogels formed from hydrophilic and oleophilic networks with water or organic solvent, respectively. Thus, the hydrogel is hydrophilic, and the organogels with hydrophobic solvents are hydrophobic or oleophilic. The polymer gel surfaces present repulsion to other liquids that are immiscible with the solvents in the gels.<sup>81</sup>

Inspired by the underwater superoleophobic property of fish scales, hydrogel-based self-cleaning surfaces have been successfully fabricated.<sup>82</sup> Due to the water entrapped in the micro/nanostructured hydrogel, this hydrogel-based surface repels immiscible oil. The hydrogel coating can be applied onto porous stainless-steel mesh to prepare superhydrophobic and underwater superoleophobic surfaces.<sup>83</sup> By combining rough nanostructured hydrogel coatings with microscale porous metal substrates, the modified mesh can selectively and effectively separate water from oil/water mixtures including

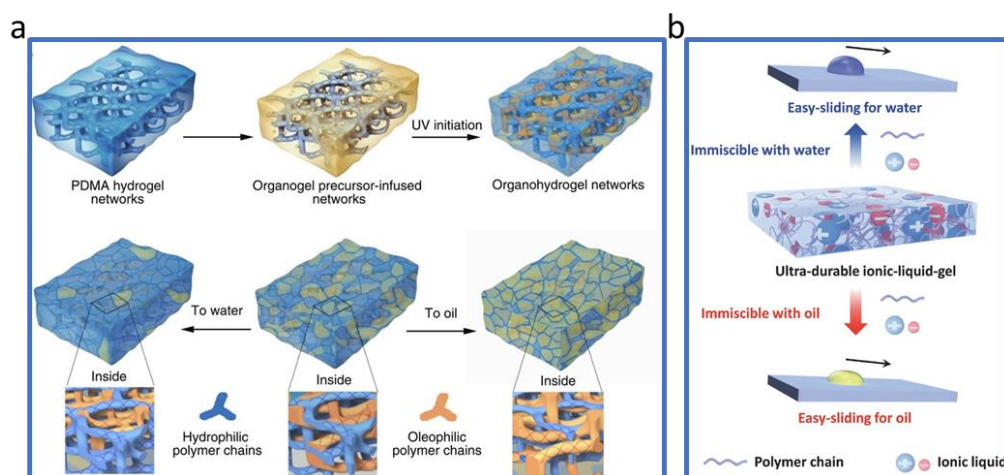
vegetable oil, gasoline, diesel, and crude oil/water mixtures. The designed underwater superoleophobic interfaces prevent oil contamination of coated mesh during separation. This facilitates oil and material recovery. Compared with traditional hydrophobic and oleophilic materials, this new type of mesh material has an entirely opposite wettability, thereby eliminating the limitations of easy scaling and difficult recycling. Using wettability in next-generation oil/water separator design is a facile strategy with great potential. Besides the hydrogels, organogel-based slippery surfaces with excellent self-cleaning properties were also developed.<sup>84</sup> In detail, a thin layer (about 30 nm) of poly(butyl methacrylate-co-lauryl methacrylate) was first built on the silanized substrate. Then, this thin polymer film was immersed in silicon oil and swollen into thicker organogels (about 110 nm). Due to the crosslinked networks, the organogels could hold the silicon oil, providing slippery functions. Such an organogel surface allows water droplets to slide easily and remove dust when inclined. This approach can be applied onto various common industrial metals, such as aluminium, copper, and iron.<sup>85</sup> Besides the hydrogels and organogels with only water or organic solvent, organohydrogels based on a mixture of water and organic solvents were developed, combining the features of hydrogels and organogels.<sup>86</sup> The organohydrogel was prepared via *in situ* polymerizations of hydrophobic polymer (copolymer of lauryl methacrylate and *n*-butyl methacrylate) within a cross-linked hydrophilic network (poly dimethyl acrylamide) swollen with amphiphilic solvents. Organohydrogels can adopt a wide range of surface structures and network structures due to the interpenetrating heterogeneous networks. For example, the organohydrogel equilibrated in water is superoleophobic, behaving like a hydrogel. When immersed in oil, the organohydrogel is superhydrophobic, present like an organogel.

In addition to static lubricating properties, responsive or dynamic lubricating surfaces were developed by introducing responsive gel onto the substrates.<sup>87</sup> There are many potential stimuli, including but not limited to temperature, mechanical stimuli, electric field, magnetic field, pH, and light. The organogels swollen by *n*-paraffin were developed and capable of switching water adhesion in response to thermo-stimulus.<sup>88</sup> Inside, the solvent, *n*-paraffin (*n*-tetracosane, *n*-heptadecane), owns the phase change property upon temperature variety. At room temperature below  $T_m$  of *n*-paraffin, micro-phase separation of paraffin formed in the organogel and induced rough surfaces, which show a high water contact angle hysteresis

of  $\approx 50.2^\circ$ . When the temperature is above  $T_m$ , homogeneous organogel is obtained, exhibiting low-adhesion to water drops with a low water contact angle hysteresis of  $1.9^\circ$ .

Polymer gel based on ionic liquid was used on the surface to pursue the long-term stability of the gel-based surfaces vital for practical applications.<sup>89</sup> The ionic liquid gel was fabricated with 1-octyl-3-methylimidazolium tetrafluoroborate and poly(methyl methacrylate), both immiscible with water. The strong interaction between the polymer chains and the ionic liquid provides a stable liquid-like surface. The ionic liquid gels maintain hydrophobic properties even after thousands of liquid drops were launched at the same spot. The problems of solvent evaporation in hydrogel and some organogels can be addressed due to the negligible volatility of the ionic liquids. The practical experiments show that the critical sliding angle of water droplets on the surface of the prepared ionic liquid gels remains below  $5^\circ$  after exposure to air for more than 240 days, which is the same as that of fresh ones.

As discussed above, polymer gel-based functional surfaces with superb wettability and exceptional stability have the potential to address the challenges of various applications. However, current gel-based surfaces are far from practical applications compared to natural surfaces. Some essential features, such as biological compatibility, durability, and self-healing ability, need much effort to realize. There are many opportunities to address these key problems with novel gel designs, especially solvent strategies, which will greatly benefit our healthcare and everyday life in the near future.



**Figure 8.** Slippery surfaces based on polymer gels with solvent strategies. a) Schematic illustration of the preparation and reconfiguration of hetero network organohydrogels.<sup>86</sup> b) Rational design of ionic liquid gel surfaces with easy-sliding and ultradurable features.<sup>89</sup>

### 1.2.2 Freezing Resistance or Thermal Stability

With emerging developments of polymer gel-based devices and machines in the last decade, the solvent leakage or evaporation of gels in harsh environments has become a critical challenge.<sup>90</sup> For practical application, weight loss and further performance drop are unacceptable.<sup>91</sup> For example, hydrogels use water as the solvent, easily evaporating at room temperature and even freezing below 0 °C. With the evaporation of water, the hydrogel loses its flexibility at first and declination in other admirable properties, such as optical property, electrical property, adhesion, slippery property, and self-healing property. For these polymer gels based on volatile solvents especially hydrogels, there are several strategies to achieve non-drying and/or anti-freezing, such as elastomer hybrids, salt addition in solvents, solvent displacement, and multiple solvent mixture. This section mainly focuses on the fellow three methods based on solvent strategies.

#### 1.2.2.1 *Salt Addition in Solvents*

This strategy is mainly developed for improving the anti-dehydration of hydrogels. Many organisms can tolerate cold conditions in nature. For example, peeping frogs and rainbow fish have evolved ways to survive under extremely cold conditions by generating and cumulating salts or alcohol in their tissues. The abnormal freezing resistance stems from the collinearity of high-concentration solutions, which inhibit the formation of intracellular ice crystals.<sup>92</sup> This freezing point drop also causes seawater (a mixture of salts in the water) to remain liquid at sub-zero temperatures. In industry, salts are often used for anti-icing due to their ability to lower the melting point of aqueous solutions. Freezing and boiling points are collinear properties of solutions, depending on the concentration of dissolved substances.<sup>93</sup> To achieve the anti-dehydration of hydrogels, common and highly water-soluble salts, such as LiCl, NaCl, KCl, CaCl<sub>2</sub>, ZnCl<sub>2</sub>, and their mixtures, have been added into the water phase.<sup>94</sup>

To compare the effects of different salts, Suo group used polyacrylamide hydrogels as a model and dissolved different salts into the hydrogels.<sup>90</sup> The influence of both salt types and concentration on the anti-dehydration capacities as well as the mechanical and electrical properties of hydrogels, were demonstrated. As for improving the anti-dehydration capacity of the polyacrylamide hydrogel, NaCl is less effective, while lithium chloride, potassium

acetate, and magnesium chloride are effective at different levels. With increasing concentration of all three salts, the overall performances of the obtained hydrogels are enhanced. Particularly, lithium chloride is proved to be the most effective salt for anti-dehydration. With dissolving 12 mol/L of lithium chloride, the hydrogel can retain over 70% of the water in an environment with 10% relative humidity. In addition to the excellent anti-dehydration capacity, the hydrogels with lithium chloride also show a low freezing point of  $-80\text{ }^{\circ}\text{C}$ , good ionic conductivity (10 S/m), and high fracture strain (over 2000%).

The method of directly dissolving salts in the preparation solution can be extended to other hydrogel networks. The typical tough hydrogel, polyacrylamide-alginate double network, was selected and equilibrated with aqueous solutions of calcium chloride.<sup>93</sup> The influences of salt concentration on mechanical properties were demonstrated. The hydrogel without  $\text{CaCl}_2$  owns the highest strength and stretchability at room temperature compared to the hydrogels with 10 and 30 wt%  $\text{CaCl}_2$ . After decreasing the temperature to  $-15\text{ }^{\circ}\text{C}$ , the hydrogel without  $\text{CaCl}_2$  becomes brittle and stiff, while the hydrogels with 10 and 30 wt%  $\text{CaCl}_2$  maintain their stretchability under  $-30$  and  $-50\text{ }^{\circ}\text{C}$ , respectively. The elastic modulus and strength of all hydrogels increase with the decreasing temperature. This hardening effect mainly results from the increasing ice crystals in the hydrogels. Similarly to nanocomposites made of polymer, these ice crystals stiffen the gel while allowing for large deformations through shear yielding. In a word, the hydrogels with 30 wt%  $\text{CaCl}_2$  maintain flexible at  $-57\text{ }^{\circ}\text{C}$ , and can be stretched over 400% with a high fracture toughness of  $5000\text{ J m}^{-2}$ .

### 1.2.2.2 *Solvent Displacement*

This method is based on the solvent displacement of the pre-prepared hydrogel.<sup>95</sup> Due to the fluid nature of solvents in polymer gels, the pre-fabricated polymer gels can be directly immersed in another solvent (miscible with the original solvent) for solvent displacement. In practical, tough Ca-alginate/polyacrylamide hydrogels were immersed in the cryoprotectant solutions, such as glycol, glycerol, sorbitol, or mixtures of these components.<sup>96</sup> Cryoprotectant solutions have been widely used in biological experiments to protect living samples from freezing damage at low temperatures, as their inhibitory behavior hinders the ice crystallization of water molecules. This method is simple and avoids any aggregation or synthesis of polymer networks.

Furthermore, the anti-dehydration and anti-freeze properties of the obtained polymer gels can be tuned by changing the degree of solvent displacement or by choosing the various cryoprotectant. During the immersing process, water molecules between the hydrogel networks are replaced by the ubiquitous cryoprotectant molecules around them. After solvent displacement, the original hydrogels with high water content become organohydrogels based on cryoprotectant, showing significantly increased drying and freezing tolerance. For example, glycerol was selected as a model.<sup>97</sup> The volume and weight of hydrogels decreased at the first hour of immersion. Notably, the gel is still transparent at room temperature after solvent displacement of 6 hours. The obtained polymer gel can maintain flexible at -45 °C. By changing the choices of cryoprotectant, the frozen temperature of polymer gels can be decreased to -50 and -70 °C with sorbitol and glycerol, respectively.

### 1.2.2.3 *Multiple Solvent Mixtures*

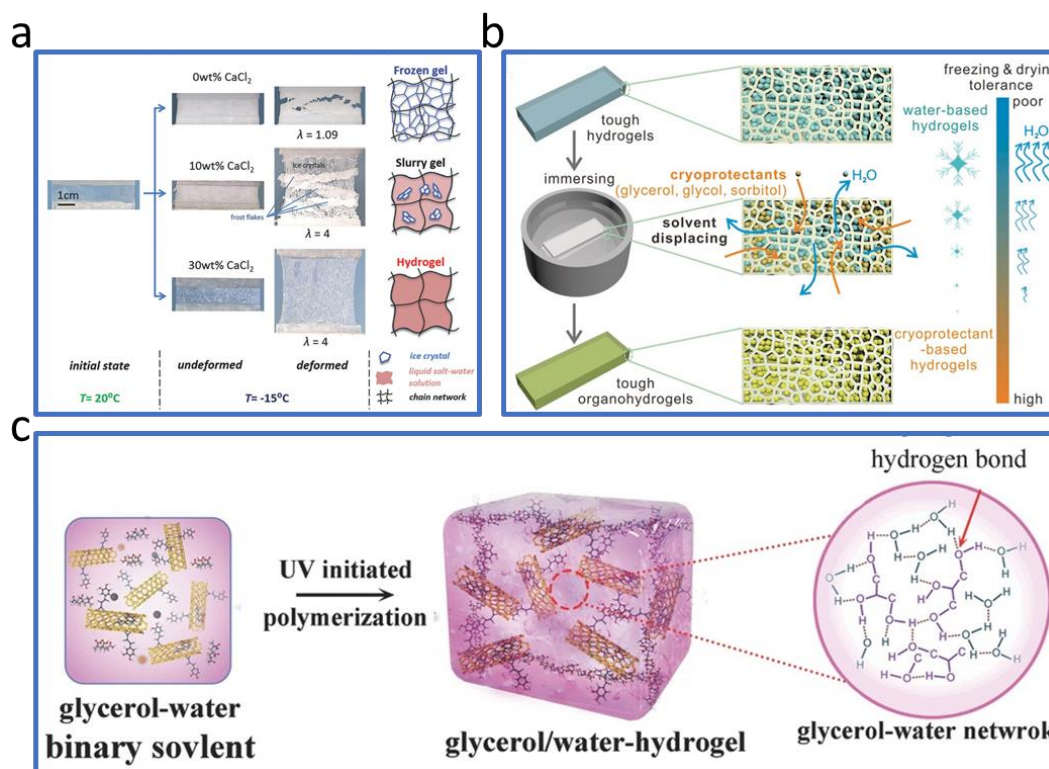
Organic solvents with lower melting points than water or higher vapor pressure are also suitable for use as functional compounds. The polymer gels based on a mixture of organic solvents and water are usually called organohydrogels. Alcohols such as methanol, ethanol, and ethylene glycol have been the basis of normal antifreezes since their commercialization in the 1920s. The most common water-based antifreeze used for cooling electronics is a mixture of water and ethylene glycol or propylene glycol. Ethylene glycol has a long history of use, especially in the automotive industry. The water/ethylene glycol binary solvent was introduced into polymer gel as a dispersion medium in 2017.<sup>98</sup> Depending on the anti-freezing of this binary solvent, the fabricated polymer gels maintain flexibility in the temperature range from -55 to 45 °C. In this case, PVA was selected as the main polymer network, which forms abundant hydrogen bonds with solvent molecules. These hydrogen bonds induce the crystallization of PVA, improving the polymer gels' mechanical strength.

In addition, water/glycerol was also used to prepare polymer gels with outstanding anti-freezing and anti-dehydration.<sup>99</sup> Covalently cross-linked copolymer of acrylic acid and acrylic acid was chosen as polymer network and formed in this solvent mixture via in situ polymerization. Polydopamine-decorated carbon nanotubes were dispersed uniformly in pre-polymerization solution, serving as conductive fillers and dynamic cross-linkers between polymer networks. The obtained polymer gels show large stretchability (700%),



## 1. Introduction

high toughness ( $2300 \text{ J m}^{-2}$ ), and strong tissue adhesiveness (60 kPa). Importantly, the water/glycerol solvent system provides the polymer gels with superior anti-freezing and anti-dehydration performance to maintain all the above properties in the temperature range from  $-20$  to  $60 \text{ }^{\circ}\text{C}$  with a long period of storage (30 days).



**Figure 9.** Anti-freezing and anti-hydration polymer gels based on functional solvent strategies. a) Salt addition in solvents for anti-freezing hydrogel.<sup>100</sup> b) Solvent displacement for the fabrication of tough organohydrogels.<sup>97</sup> c) solvent mixture for the fabrication of hydrogel with long-lasting moisture and extreme temperature tolerance.<sup>101</sup>

### 1.2.3 Superior Mechanical Properties

Sufficient mechanical properties that no longer need to be emphasized are crucial to various applications of polymer gels. In the pursuit of superior mechanical properties, most pioneering works in the field of polymer gels have been focused on the chemical nature and polymer network architectures and their interactions,<sup>102</sup> such as ideal polymer networks,<sup>103-105</sup> interpenetrating polymer networks,<sup>106-108</sup> nano/micro composite polymer networks,<sup>109,110</sup> and hierarchically structured polymer networks.<sup>111,112</sup> The solvents, which occupy more than half the weight or volume in polymer gels, can greatly affect the behaviors or structures of

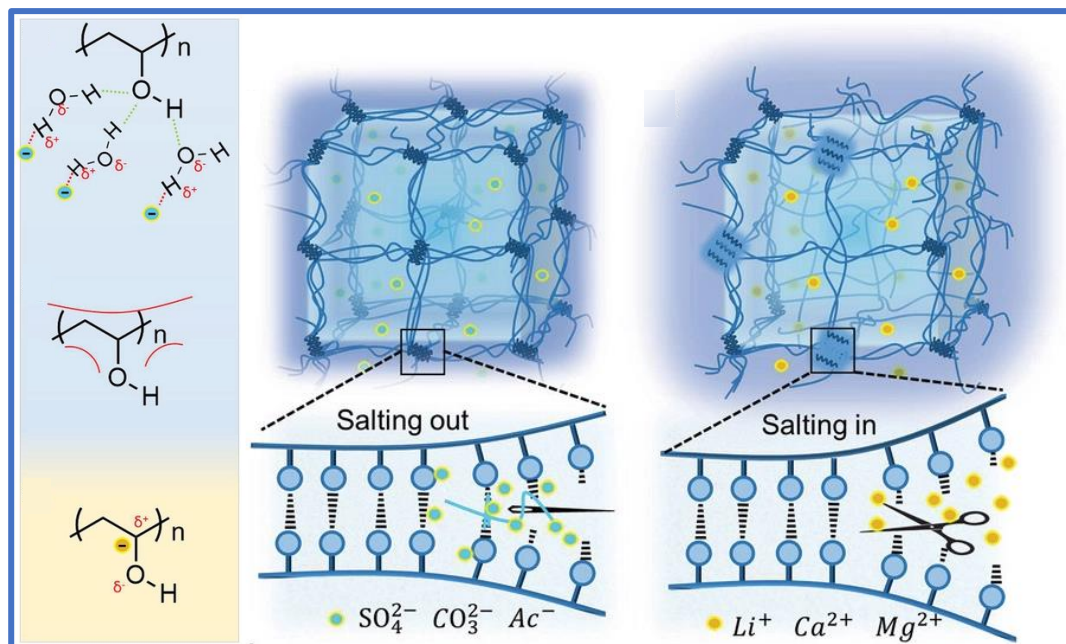
polymer networks during preparation or under load. The most typical phenomenon is that the hydrogel becomes hard and brittle with low water content. This section will summarize a set of solvent strategies for polymer gels to achieve the corresponding extreme mechanical properties, including high stretchability, tensile strength, fracture toughness, and fatigue threshold.

Hofmeister effect, introduced in 1888, demonstrated that various ions have different abilities to alter the solubility of proteins. Although its mechanism is still under debate,<sup>113</sup> has been widely used in various fields such as surface tension, ice nucleation and recrystallization, colloidal assembly, and hydrogel preparation. A strong gelatin hydrogel was fabricated solely based on gelatin via soaking in salt solutions.<sup>117</sup> This preparation of polymer gel does not contain any chemical modification or the addition of mechanical reinforcing filler. In brief, the gelatin solution with a designed shape (weak hydrogel) was immersed in  $(\text{NH}_4)_2\text{SO}_4$  solution to induce physically crosslinked domains via Hofmeister effect. During the immersion, the gelatin solubility in water decreased with the presence of high concentrations of  $(\text{NH}_4)_2\text{SO}_4$ , which resulted in precipitation of the gelatin, or the “salting-out” effect. These hydrogels based on virgin gelatin can withstand over 99% compressive strain at 12 MPa stress and 500% tensile strain at 3 MPa stress. Besides, the natural polymers, Hofmeister effect can also be applied in hydrogels with synthetic polymers.<sup>118</sup> A freeze-soak method, in which a frozen polymer solution is immersed in a saline solution, is reported to prepare hydrogels. This method can adjust the mechanical properties of hydrogels by tuning the aggregation of the hydrophilic polymer chains at the molecular level via the Hofmeister effect. With this solvent strategy, dynamic in-situ tuning of hydrogel mechanical properties is even achieved. This method selected PVA, composed of hydrophobic (CH<sub>2</sub>-CH<sub>2</sub>) backbone and hydrophilic (-OH) side-groups, as a polymer network. A typical Hofmeister series was found in PVA hydrogels (5 wt%), where the effect of ions follows the sequence  $\text{SO}_4^{2-} > \text{CO}_3^{2-} > \text{Ac}^- > \text{Cl}^- > \text{NO}_3^- > \text{I}^-$  and  $\text{K}^+ > \text{Na}^+ \approx \text{Cs}^+ > \text{Li}^+ \approx \text{Ca}^{2+} \approx \text{Mg}^{2+}$ . The obtained PVA hydrogels present extreme mechanical properties, including fracture strain of 2100%, strength of 15 MPa, and toughness of  $150 \text{ MJ m}^{-3}$ , which is even tougher than the solvent-free polymers like PDMS and synthetic rubber. Interestingly, the tough gel produced by salting-out salts can be softened by salting-in salts. After soaked in saturated  $\text{Na}_2\text{SO}_4$  solution, the PVA hydrogel became shrunk and opaque slightly. Then, the opaque gel was soaked in 3 M  $\text{CaCl}_2$  for 48 h, where it can be swelled back slightly and transformed into a transparent

hydrogel. Meanwhile, the corresponding strength, toughness and modulus were dynamically tuned from 2500 kPa, 15.53 MPa, and 153.41 MJ m<sup>-3</sup> to 34 kPa, 0.09 MPa, and 2.48 MJ m<sup>-3</sup>, respectively. This in-situ stiffness tunability offers attractive advantages and opportunities for applications requiring local tuning of material properties. In contrast, traditional material properties are set once produced or can only be tuned under extreme conditions such as high temperatures, which is impossible.<sup>119</sup>

In addition to the water system with salts, changing the solvent nature on molecular length can also enhance or tune the mechanical properties. In hydrogels or organic gels, small molecules are used as solvents in gels, which only play a role in swelling function. Due to the short length of molecules, they have limited possible interaction sites with the polymer network and with other solvent molecules. So, liquid oligomers or polymers are used as solvents for polymer gel, which offers the potential to introduce multivalent interactions between the main polymer network and other solvent molecules.<sup>69</sup> This approach can significantly enhance polymer gels' mechanical properties and stability. Importantly, such multivalences can enhance or finetune the performance of corresponding polymer gels by adjusting the molecule length of such oligomeric solvents. PEG was selected as the oligomeric solvent. Due to their terminal hydroxyl and ether bonds, PEG provides strong hydrogen bonding between hydrophilic polymers, ensuring monomer diversity and homogeneity of polymer gels. The superior mechanical properties of obtained PEGgel have been mentioned above, while the enhancement from the small molecule solvents system is presented here. Compared to the corresponding polymer gels generated in water or ethylene glycol as the liquid phase, the polymer gel based on macromolecular non-volatile PEG results in exceptional physical properties, such as high stretchability and toughness, rapid self-healing, and long-term stability under ambient conditions. With the same polymer network (P(HEMA-*co*-AAC)) and solvent volume ratio, the fracture strain of the PEG gel was 4335%, and the tensile strength was 218 kPa, while the corresponding hydrogels fractured at 617% and 150 kPa, and the EG gels fractured at 2382% and 106 kPa. The elastic modulus of PEGgel (78 kPa) is similar to EG gel (76 kPa), but lower than the hydrogel (125 kPa). The toughness of PEGgel was 5.66 MJ m<sup>-3</sup>, representing a 9.1-fold increase over the hydrogel (0.62 MJ m<sup>-3</sup>) and a 4.2-fold increase over the EG gel (1.35 MJ m<sup>-3</sup>). Moreover, the PEG solvent system can be extended to other polymer networks to form gels, showing better mechanical properties than the same network fabricated using hydrogels or EG gels.

This enhancement results from the increased long-range correlations of PEG molecules and polymer entanglements between polymer networks.



**Figure 10.** Schematics of the aggregation states of PVA polymer chains treated with different ions.<sup>112</sup>

#### 1.2.4 Electrical Performance

Next-generation intelligent healthcare sensing is a sophisticated system that monitors patients' physiological signs in real-time, evaluates their health conditions, and details the feedback data to doctors, making medical diagnosis and therapy more predictive and personalized.<sup>120</sup> Commercially used healthcare sensors are primarily composed of conventional rigid electronic materials, with obtrusive and hard supports to integrate with the human body. These devices undoubtedly cause discomfort to users and limitations for sensing because of their inadaptability to the soft nature of human tissues.<sup>121</sup> Polymer gels, with tissue-like mechanical properties, have shown great potential in wearable device, flexible electronics, and even implant devices. Numerous chemical and structural designs provide unlimited opportunities to tune the properties and performance of conductive polymer gels to match various demands for practical applications. Importantly, conductivity, a fundamental property, is the main resistance to applying polymer gels in the fields of flexible electronics. In this section, the solvent strategies to endow or enhance the conductivity for polymer gels were mainly discuss.

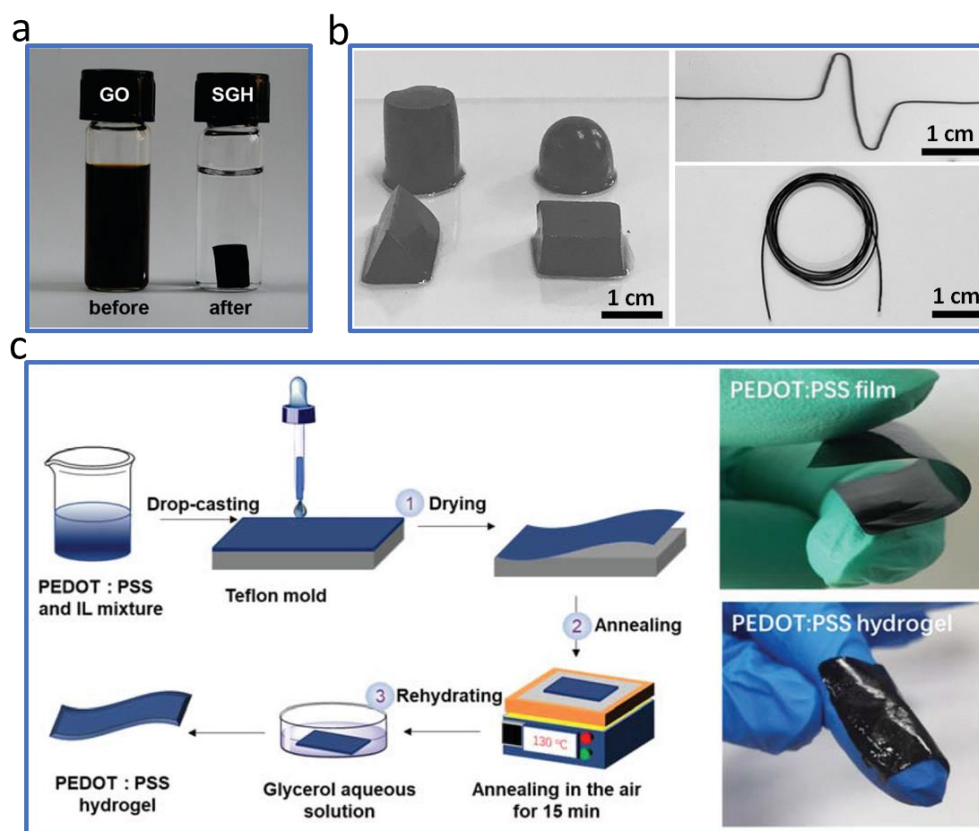
Graphene with single-atom thickness, flexible 2D structure, and exceptional physical and chemical properties have attracted intense interest in various technological fields,<sup>122</sup> such as chemical and biological sensors,<sup>123,124</sup> field-effect devices,<sup>125</sup> and energy storage systems.<sup>126</sup> Self-assembly of 2D graphene sheets into 3D structures is an important strategy to achieve highly conductive graphene structures for practical applications. Self-assembled graphene hydrogels were prepared by a one-step hydrothermal method.<sup>127</sup> Specifically, it can be easily prepared by heating a homogeneous graphene oxide aqueous dispersion (2 mg/mL, typical one) and sealing in a Teflon-lined autoclave at 180 °C for 12 h. The residual oxygen-containing functional groups on the graphene sheets can trap a large amount of water into the graphene network under high temperature and pressure to form graphene hydrogels. As the reduction reaction proceeds, the hydrophobicity of the graphene oxide sheets increases. With the help of water, more aggregates of graphene sheets are formed. These enhance the probability of  $\pi$ - $\pi$  stack formation and increase the number of crosslinks. Based on such 3D structures, the graphene hydrogels presented high electrical conductivity at 0.5 S m<sup>-1</sup> with extremely high water content (97.4%). Then, some biomolecules were able to be added to the graphene solutions to form functional graphene hydrogels with the same hydrothermal processing. For example, PEDOT:PSS, a biocompatible conducting polymer, has been widely studied in the last two decades, showing great potential in extensive applications, such as energy storage systems, organic electronics, and solar cells.<sup>128,129</sup> Due to its outstanding flexibility and high electrical conductivity, PEDOT:PSS is regarded as one of the most promising candidates for the fabrication of bio-electronic devices.<sup>130</sup> Hydrogels based on PEDOT:PSS, benefiting tissue-like mechanical properties and water-rich features, are considered suitable for bioelectronics. Most PEDOT:PSS hydrogels are fabricated by mixing insulated polymers with PEDOT:PSS, causing low electrical conductivities in the range of 10 S m<sup>-1</sup>, which is about several orders in magnitude lower than that of PEDOT films.<sup>131</sup> The low conductivity would seriously inhibit their applications in the emerging field of hydrogel bioelectronics.<sup>132</sup> Minimizing the use of insulating polymers, or even eliminating them, seems to be an effective strategy to improve the electrical conductivity of PEDOT:PSS hydrogels.<sup>133,134</sup> Thus, without the help of a polymer network, solvent strategies become the ideal method to fabricate PEDOT:PSS hydrogels with high conductivity. A PEDOT:PSS hydrogel with an extremely high conductivity of 880 S m<sup>-1</sup> was prepared by treating a commercial PEDOT:PSS (PH1000) suspension in 0.1 mol L<sup>-1</sup> sulfuric acid at a mildly elevated temperature of 90 °C without adding any other polymers

or crosslinkers.<sup>133</sup> To reach such high conductivity, this hydrogel only has a low solid content of 4 wt%. When PEDOT:PSS hydrogel's solid content is extremely low (0.78 wt%), its conductivity still reaches  $46 \text{ S m}^{-1}$ . The gelation mechanism was explained in detail as follows. Firstly, acid induces a conformational transition of the PEDOT chain from a random to an extended coil structure. This enhances the interactions between PEDOT chains, favoring the formation of 3D networks with physical crosslinks. Secondly, acid weakened the repulsion force between PEDOT:PSS chains. In the acidic medium, the PSS chains were partially protonated and removed from PEDOT:PSS complexes. Consequently, the  $\pi$ - $\pi$  stacking and hydrophobic attractions between PEDOT chains were enhanced, promoting the formation of physical crosslinks between PEDOT chains.

Interestingly, PEDOT:PSS tends to form micellar microstructures that consist of hydrophobic PEDOT-rich core and hydrophilic PSS-rich shell in an aqueous solution. Such separated structure will affect the electrical conductivity and mechanical properties of pure PEDOT:PSS hydrogels. Achieving a hybrid of rigid hydrophobic PEDOT network and soft hydrophilic PSS would be a feasible strategy. The organic solvent, owning high boiling point and miscibility with water, can serve as an additive to the aqueous PEDOT:PSS solution to facilitate the recrystallization of PEDOT-rich nanofibrils and chain rearrangement of PEDOT:PSS during the dry-annealing process.<sup>134</sup> Directly drying aqueous PEDOT:PSS solution always cause phase separation, including 1) rigid PEDOT crystalline domain, 2) disordered PEDOT:PSS semi-crystalline domain and 3) soft PSS domain. With the help of an organic solvent (dimethyl sulfoxide), these three domains can be controlled into a well-distributed network, forming a pure PEDOT:PSS hydrogel with high and stable conductivity ( $2000 \text{ S m}^{-1}$  in phosphate-buffered saline and  $4000 \text{ S m}^{-1}$  in deionized water) and good mechanical properties (low modulus of 2 MPa and high stretchability of over 35% strain in wet physiological environments).

Besides the thermal treatment based on solvents, a dry-annealing and rehydration method was developed to prepare PEDOT:PSS hydrogels by doping a series of ionic liquid.<sup>135</sup> The fabricated ionic liquid doped PEDOT:PSS hydrogels present a high electrical conductivity up to  $305 \text{ S cm}^{-1}$ . Such high electrical conductivity comes from the ion exchange induced nano-phase segregation of PEDOT chains. The whole preparation of this PEDOT:PSS hydrogel is simple, which only involves two steps: 1) drop-casting the mixture of PEDOT:PSS and ionic liquids on a mold and dried at room temperature, 2) annealed for 15 min and

soaked in the aqueous glycerol solution for 30 s to form the PEDOT:PSS hydrogels. The gelation of ionic liquid doped PEDOT:PSS is similar to the acid-based previous system. When the ionic liquids were mixed and dissolved in the PEDOT:PSS solution, the PSS was partially replaced by the anions in the ionic liquid, forming PEDOT-rich domains and PSS-rich domains, respectively. Then, the PEDOT-rich domains are electrically connected to offer efficient pathways for charge carriers. Thus, the charge carriers can move fast by hopping between these PEDOT-rich domains, significantly increasing electrical conductivity.



**Figure 11.** Solvent strategies to enhance the electrical performance of polymer gels. a) Hydrothermal reduction for fabricating graphene oxide hydrogels based on its aqueous dispersion.<sup>127</sup> b) Free-standing PEDOT:PSS hydrogels with different geometric shapes fabricated by solvent strategies.<sup>134</sup> c) PEDOT:PSS hydrogels prepared by dry-annealing and rehydration method.<sup>135</sup>

## 2 Work Objectives

i) PEGgel: a functional polymer gel using PEG as a solvent

Project objectives:

1. Establishments of the PEG solvent system for PEGgel  
*Compare the physical properties of hydrogel, ethylene glycol (EG) gel, and PEGgel based on the same polymer networks to confirm the advantages of the oligomer used as solvent*
2. Molecular mechanism of the enhancement of mechanical properties in the PEG system  
*Use various characterization methods to demonstrate the molecular mechanism, including NMR, FTIR, XRD, and CGMD*
3. Tunability of mechanical properties based on PEG solvent system  
*Change the volume fraction and molecular weight of PEG to fine-tune the physical properties of PEGgel*
4. Self-healing properties of PEGgels  
*Evaluate the self-healing properties of PEGgels. Compare the performance of hydrogels, EG gels, and PEGgels with different volume fractions and molecular weight of PEG*
5. Application of PEGgels  
*Demonstration of a self-healing pneumatic actuator fabricated using 3D printing*

(ii) Ionic PEGgel: introducing ions into PEGgel systems

1. Evaluation of the influence of ions on PEGgel  
*Compare the mechanical properties of PEGgel with different kinds and different concentrations of salts*
2. Molecular mechanism of the enhancement of mechanical properties from ions  
*Use various characterization methods to demonstrate the molecular mechanism of ions in PEGgel system, including FTIR, XRD, and CGMD*
3. Measurements of the electrical properties of Ionic PEGgel  
*Measure the conductivity, electrical stability, and sensing properties of ionic PEGgels*



### 4. Application of Ionic PEGgels

*Use Ionic PEGgel to serve as wearable strain sensors, temperature sensors, and flexible electrodes.*

(iii) Phase-separated PEGgel: introducing PPG into PEGgel systems to achieve *in-situ* phase-separation, leading to enhanced mechanical properties

#### 1. Confirmation of the *in situ* phase-separation in polymer gels

*Use various characterization methods to investigate the phase separation, including SEM, AFM, XRD, and DSC*

#### 2. Evaluation of the influence of *in-situ* phase-separation on PEGgel

*Compare the mechanical properties of phase-separated gels with different ratios of PEG and PPG*

#### 3. Application of Phase-separated PEGgels

*Combine shape-memory behavior with 3D printability to achieve actuation of soft 3D structures machines*

#### 4. Scalability of Phase-separated PEGgels

*Introduce ions into phase-separated PEGgel to fabricate polymer gels with the hierarchical structure, and achieve enhanced mechanical properties*

## 3 Results and Discussion

### 3.1 PEGgel

This chapter and associated sections are published in:

Wang, Z.; Cui, H.; Liu, M.; Grage, S. L.; Hoffmann, M.; Sedghamiz, E.; Wenzel, W.; Levkin, P. A., Tough, Transparent, 3D-Printable, and Self-Healing Poly(ethylene glycol)-Gel (PEGgel). *Advanced Materials* **2022**, *34* (11). DOI: 10.1002/adma.202107791

#### 3.1.1 Abstract

Polymer gels, such as hydrogels, consisting of cross-linked polymer chains and small molecule solvents, have been widely used in biomedical applications, flexible electronics, and soft machines due to the similarity of their mechanical properties to those of soft biological tissues. Polymer network design and its contribution to the properties of such materials have been extensively studied. This study demonstrates the critical influence of solvent nature on soft polymer gels' mechanical properties and performance. This section report a polymer gel system (PEGgel) based on a poly(hydroxyethyl methacrylate-*co*-acrylic acid) copolymerized in the presence of poly(ethylene glycol) (PEG) used as the liquid phase of the PEGgel. Compared to the corresponding hydrogel or ethylene glycol based gel, the PEGgel demonstrates exceptional physical properties, such as high stretchability and toughness, rapid self-healing, and long-term stability under ambient conditions. Depending on the molecular weight and fraction of PEG, the tensile strength of PEGgels varied from 0.22 MPa to 41.3 MPa, fracture strain from 12% to 4336%, modulus from 0.08 MPa to 352 MPa, and toughness from 2.89 MJ m<sup>-3</sup> to 56.23 MJ m<sup>-3</sup>. The influence of PEG on the mechanical properties was evaluated using the coarse-grain molecular dynamics (CGMD) model and solid-state NMR, revealing abundant weak hydrogen bonding leading to the observed enhancement of mechanical properties. Finally, this study demonstrated rapid self-healing of PEGgel materials and fabricated a self-healing pneumatic actuator by 3D printing of PEGgel structures. The enhanced mechanical properties of the PEGgel system could be extended to other polymer networks (both chemically and physically cross-linked). This study demonstrates the important influence of the liquid phase of polymer gels on their mechanical and other properties and highlights the potential for finetuning different physical

properties of gels through the use of PEG possessing weak but multiple hydrogen bond interactions with the polymer network. Such a simple 3D printable, self-healing and tough soft material holds promise for broad applications in wearable electronics, soft actuators and robotics.

#### 3.1.2 Introduction

Soft materials, benefiting from their low-modulus, deformable properties and diverse functionality, offer tremendous opportunities for applications in biomedicine,<sup>136</sup> flexible electronics,<sup>137,138</sup> soft robotics,<sup>139</sup> and soft actuators.<sup>140-142</sup> Polymer gels consist of physically or covalently cross-linked polymer chains and a liquid phase that is usually based on small molecule solvents.<sup>143</sup> These gels represent a class of soft materials with unique properties resembling soft biological tissues, such as tendons, ligaments, cartilage, muscles, and skin.<sup>121</sup> Hydrogels, obtained by cross-linking hydrophilic polymer chains in aqueous solutions,<sup>144</sup> possess the intrinsic low-modulus nature and tissue-like properties, which make them applicable to tissue engineering,<sup>145,146</sup> optical devices,<sup>147</sup> biomedicine<sup>109</sup> and actuators.<sup>148</sup>

In the pursuit of high performance, most research in the field of polymer gels has been focused on the chemical nature and polymer network architectures and their interactions,<sup>102</sup> such as ideal polymer networks,<sup>103-105</sup> interpenetrating polymer networks,<sup>106-108</sup> nano/micro composite polymer networks,<sup>109,110</sup> and hierarchically structured polymer networks.<sup>111,112</sup> The small molecule solvent is the second component of gels and is often considered to be a non-functional liquid that impregnates and expands a functional polymer network.

Recently, ionic liquids have been used to replace water in hydrogels,<sup>149</sup> resulting in soft materials with long-term stability.<sup>41</sup> Multicomponent solvent systems, in which water is mixed with organic solvents (such as glycerol,<sup>101</sup> ethylene glycol<sup>150</sup> and sorbitol<sup>97</sup>), were introduced into gel networks to maintain the performance of materials in harsh environments. However, because of the low molecular weight of solvents used and weak interactions with polymer networks, the reported “organo-hydrogels” possessed limited mechanical properties and showed spontaneous solvent leakage.<sup>150</sup> Furthermore, small molecules used as solvents in gels have limited number of possible interaction sites with the polymer network as well as with other solvent molecules. This study demonstrate that the use of

liquid oligomers or polymers as solvents for gel systems offers the potential to introduce multivalent interactions between the main polymer network as well as between other solvent molecules. This approach can be used to significantly change the mechanical properties and stability of polymer gels. Importantly, such multi-valency can be applied to enhance and finetune the physical properties of gels by changing the length of such oligomeric solvent molecules.

At room temperature, poly(ethylene glycol) (PEG) is a liquid ( $M_w < 600$  g/mol),<sup>73</sup> which has been widely used in chemistry, biology, biotechnology and medicine<sup>65</sup> and is currently approved for in vivo applications by the United States Food and Drug Administration.<sup>66</sup> In blends with polymers possessing side hydroxy groups, PEG was shown to provide strong hydrogen bonding between main chain ether groups and hydroxy groups.<sup>70,72</sup>

This study presents a polymer gel system (PEGgel) based on a poly(hydroxyethyl methacrylate-*co*-acrylic acid) (P(HEMA-*co*-AAc)) network copolymerized in the presence of small to average molecular weight PEG used as the liquid phase of the PEGgel (Figure 12a). Compared to the corresponding hydrogel generated using water or ethylene glycol as the liquid phase, the use of macromolecular non-volatile PEG results in a PEGgel with exceptional physical properties, such as high stretchability and toughness, rapid self-healing, and long-term stability under ambient conditions. Depending on the molecular weight and volume fraction of PEG, the tensile strength of PEGgels varied from 0.22 MPa to 41.3 MPa, fracture strain from 12% to 4336%, modulus from 0.08 MPa to 352 MPa, and toughness from 2.89 MJ m<sup>-3</sup> to 56.23 MJ m<sup>-3</sup>. The influence of PEG on the mechanical properties was evaluated using the coarse-grain molecular dynamics (CGMD) model and solid-state NMR. Finally, the experiment demonstrated rapid self-healing (approximately 1 min) and the possibility for 3D printing, by which the self-healing pneumatic actuator was fabricated. This study clearly demonstrates the important influence of the liquid phase of polymer gels on their mechanical and other properties, and highlights the potential for finetuning different physical properties of gels through the use of low-to-average molecular weight liquid polymers (e.g., PEG) possessing multiple hydrogen bond interactions with the polymer network. Such a simple soft material holds promise for broad applications in wearable electronics, soft actuators and robotics.

### 3.1.3 Results and Discussion

#### 3.1.3.1 *Concept of PEGgels*

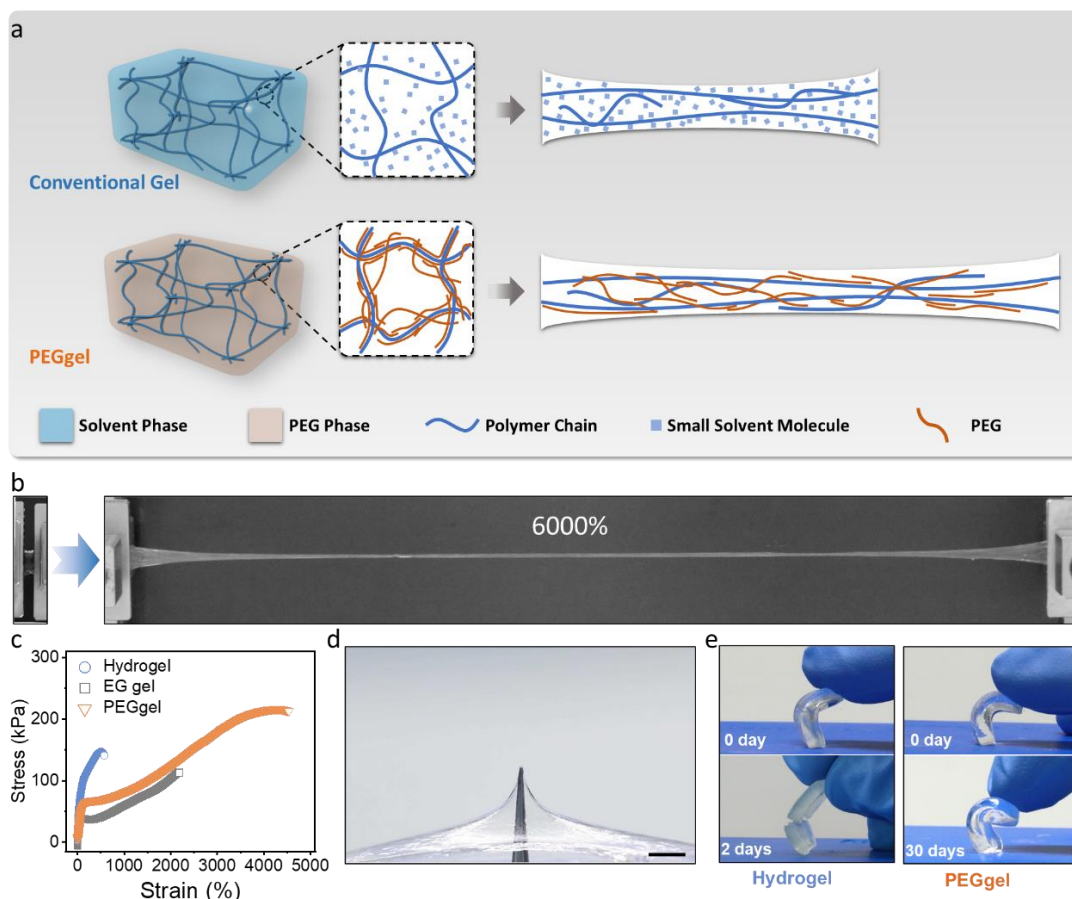
PEGgel and the corresponding ethylene glycol (EG) gel and hydrogel were synthesized by free radical copolymerization of 2-hydroxyethyl methacrylate (25 vol.%) and acrylic acid (25 vol.%) dissolved in PEG ( $M_w = 400$  g/mol), EG or water (50 vol.%), respectively, in the presence of a radical initiator. The prepolymer solutions were poured into a polytetrafluorethylene mold and cured by UV irradiation for 30 min (6 mW/cm<sup>2</sup>, 366 nm, room temperature). After polymerization, the gel blocks were detached from the mold and used for further investigations. The polymerization is confirmed by the FTIR analysis (Figure S1-1), in which the 1633 cm<sup>-1</sup> band corresponds to the stretching of the C=C on monomers disappeared after polymerization. The obtained PEGgel was immersed in PEG400 (containing 1mg/mL Sudan I) for one week. After one week soaking, the diameter of PEGgel swell from 20 mm into 40 mm (Figure S1-2), which confirms that the PEG is serving as fluid in polymer network. The obtained PEGgel could be stretched to 6000% of its original length at a rate of 50 mm/min without rupture (Figure 12b), while the corresponding hydrogel could be stretched to only 400% without damage. To confirm the enhancement of the mechanical properties of PEGgels, the performance of hydrogel, PEGgel and EG gel were compared by tensile tests (Figure 12c). All three samples were based on P(HEMA-*co*-AAc) with the same monomers: solvent volume ratio (1:1) and identical polymerization conditions (Table S1-1). After changing the solvent to PEG, the PEGgel showed a fracture strain of  $4335 \pm 340\%$  and a tensile strength of  $218 \pm 16$  kPa, while the corresponding hydrogel ruptured at  $617 \pm 175\%$  and  $150 \pm 9$  kPa and EG gel ruptured at  $2382 \pm 192\%$  and  $106 \pm 8$  kPa. The elastic modulus of PEGgel ( $78 \pm 13$  kPa) is similar with EG gel ( $76 \pm 9$  kPa), but lower than the hydrogel ( $125 \pm 32$  kPa). Notably, the toughness of PEGgel was  $5.66 \pm 0.58$  MJ m<sup>-3</sup>, representing to a 9.1-fold increase compared with the corresponding hydrogel ( $0.62 \pm 0.06$  MJ m<sup>-3</sup>) and a 4.2-fold increase compared with the corresponding EG gel ( $1.35 \pm 0.09$  MJ m<sup>-3</sup>). In addition, rheological master curves of frequency

dependence of the storage modulus ( $G'$ ) and loss modulus ( $G''$ ) for PEGgel, EG gel and hydrogel are presented in Figure S1-3. The  $G'$  of all the gels presented higher than  $G''$  in the low-frequency region ( $\omega \rightarrow 0$ ) without obvious crossover, which means that P(HEMA-co-AAc) chains were all tightly crosslinked in three solvents. For PEGgel, the gel status was still maintained under 120 °C (Figure S1-4). Interestingly, PEGgel and EG gel presented an obvious narrowing of  $G'$  and  $G''$  in the low frequency region, while hydrogel remained open towards the low frequency region. These different trends have shown the polymer chains are the most relaxed in EG gel, followed by PEGgel and the most fixed in hydrogel, which also is consistent with our previous tensile properties of gels in three solvent systems.

The extreme toughness of the PEGgel was also reflected in the excellent mechanical durability of this soft and elastic material demonstrated in the piercing test, in which tip of a stainless-steel pin (diameter, 1 mm) was used to pierce a gel membrane (14 × 30 mm in size and 2.5 mm thick) at a speed of 100 mm/min. The pin stretched the PEGgel membrane 4.5 cm above the membrane plane without piercing it, while the P(HEMA-co-AAc) hydrogel membrane was pierced when stretched only 1.5 cm by the pin (Movie S1-1, Figure 12d), demonstrating the high toughness of the PEGgel in comparison to the hydrogel. The absence of phase separation between the liquid PEG and P(HEMA-co-AAc) matrix was confirmed by the lack of visible light scattering and >95% transmittance of the PEGgel in the visible range (400-760 nm) (Figure S1-5).

Stability in open environment is also crucial for soft materials. To determine the stability of PEGgels, the hydrogel and PEGgels were stored in open air (25°C, 50% relative humidity) for 30 days. Due to the negligible evaporation from PEG, the PEGgel retained its flexibility for 30 days. The corresponding hydrogel became brittle after just 2 days and ruptured immediately upon bending, demonstrating the superior long-term stability of the PEGgel compared with the corresponding hydrogel (Figure 12e, Movie S1-2). The weight changes of PEGgel and hydrogel were recorded during storage of the gels in open air (25 °C, 50 ± 5% relative humidity)

over 30 days (Figure S1-6). The weight of PEGgel remained unchanged ( $\pm 1\%$ ), whereas the hydrogel lost 48% of its mass after one day, leading to the deterioration of its mechanical properties. After one month in storage under these conditions, the tensile stress-strain curve of PEGgel remained almost unchanged (Figure S1-7a), the strength decreased only marginally from 218 kPa to 200 kPa and the fracture strain was 3,200%. In contrast, the fracture strain of the corresponding hydrogel decreased from 460% to 11% after only one day (Figure S1-7b). The stability of PEGgels with different relative humidity was also investigated. EG gel and PEGgel were stored at 25 °C under saturated water vapor environment for 12h (Figure S1-8). Due to the higher density of Hydroxyl density, EG gel absorbed more water ( $37.8 \pm 1.4\%$ ) than PEGgel ( $9.6 \pm 1.5\%$ ) until balance. After absorbing water, the EG gel lost its edge and behaved more like a fluid, while the shape of PEGgel was still sharp. The weight change of PEGgel after storage at 25 °C for 12 h with different humidity was recorded in Figure S1-9a, which increased less than 5% at 50% relative humidity and below. The mechanical property is also preserved at 50% relative humidity and below in Figure S1-9b. The toughness of PEGgel after storage in saturated water vapor environment is still maintained at  $1.95 \pm 0.07 \text{ MJ m}^{-3}$ , which is still higher than those of the as-prepared hydrogels and EG-gels. The FTIR analysis was used to confirm the influence of humidity to PEGgels (Figure S1-9c), in which the band corresponds to the stretching of the H-O became wider and shifted from  $3438 \text{ cm}^{-2}$  to  $3405 \text{ cm}^{-2}$  with the relative humidity exceeding 50%. This might indicate that the water absorbed over 5% is free, which would destroy hydrogen bonds among PEG and polymer networks and then result the decline of mechanical properties.



**Figure 12.** Concept of PEGgels. a) Schematic illustration of the hydrogel and PEGgel structure. b) Photographs of PEGgel stretched 6000%. c) Representative tensile stress-strain curves of hydrogel, PEGgel and EG gel based on the same P(HEMA-*co*-AAc) polymer matrix and 50% solvent fraction. d) Photograph of a PEGgel membrane deformed by a sharp metal pin (pin diameter = 1 mm). Scale bar: 10 mm e) Hydrogel and PEGgel blocks bent immediately after preparation and after storage for 2 days and 30 days, demonstrating the long-term stability of the PEGgel compared with that of the hydrogel. Copyright 2022 Wiley-VCH.<sup>69</sup>

### 3.1.3.2 Molecular mechanism of PEGgels

(The following simulation was performed by Modan Liu and Elaheh Sedghamiz from Wolfgang Wenzel Group at the Institute of Nanotechnology, KIT as a part of the collaborative project. The following solid-state <sup>1</sup>H-NMR characterization was measured by Stephan L. Grage from Institute for Biological Interfaces IBG-2, KIT as a part of the collaborative project.)



To investigate the polymer network-solvent interactions within the gels and to clarify the molecular mechanisms underlying the experimentally observed mechanical properties of the gels, a coarse-grained (CG) molecular dynamics (MD) model was developed. In the coarse-graining process illustrated in Figure S1-10, the individual polymer chains were represented by beads for the polymer backbone and side-groups, whereas water and EG was represented by single spherical beads. PEG was modeled as a short linear chain with the same resolution as EG. All the CG beads were capable of forming either O-H...O or C-H...O hydrogen bonds, with the latter found to be essential to model the PEG conformation.<sup>151</sup> Full details of the CGMD simulation process, as well as the corresponding reduced units as  $\lambda_{CG}$  and  $\epsilon_{CG}$ , are presented in the Methods section.

The relaxed conformations of a single polymer chain of poly(2-hydroxyethyl methacrylate-*co*-acrylic acid), or P(HEMA-*co*-AAc) exhibited strikingly different behaviors when solvated in water, EG, and PEG (Figure 13a). The single polymer chain was the most compact in water, due to the hydrophobicity of the polymer backbone, while OH side-groups were exposed to form hydrogen bonds with water. In EG, all the molecular units were of similar miscibility and the single polymer chain remained as a polymer coil. When solvated in PEG, the short, linear PEG molecules wrapped around the P(HEMA-*co*-AAc) and served as mitigators in the polymer-PEG-polymer cross-linking. Figure 13b shows a snapshot highlighting an individual PEG molecule (bright red) forming H-bonds at both ends to connect different sites of a single P(HEMA-*co*-AAc) chain. In contrast to EG, PEG molecules in the polymer-solvent-polymer cross-links effectively introduced long-range correlations, thereby enhancing compaction of the polymer coil. The radii of gyration of the single polymer chains measured  $4.90 \lambda_{CG}$ ,  $12.62 \lambda_{CG}$  and  $10.36 \lambda_{CG}$  in water, EG, and PEG, respectively. The polymer-polymer interaction potential in water was much stronger ( $2\times$ ) than that of EG and PEG, indicating a polymer-water separation. Due to the high number of hydrogen donor and acceptor pairs in water, both the polymer-solvent and the solvent-solvent interaction energies in water were an order of magnitude larger than those in EG and PEG. In contrast, due to the similar miscibility of the polymer backbone and side groups in EG and PEG, the polymer uniformly mixed with the solvent molecules, leading to an open conformation of the solvated single polymer chain. The polymer-polymer interaction in PEG was just 8.5% larger than that in EG. Compared with the small, spherical water and EG

molecules, the large PEG molecules have reduced freedom of diffusion, which restrained the conformation of the P(HEMA-*co*-AAc) chains even in the dilute limit.

In CGMD simulations<sup>152</sup> of the elongation process up to 5000%, it is found that the strain-stress response of the polymer network was qualitatively consistent with the experimental data (Figure 12c and S11a). In the gel system, the CGMD simulations revealed different contributions to the overall mechanical response of the hydrogel, EG gel, and PEGgel upon stretching. A comprehensive analysis of the componential energy contribution from steric repulsion, hydrogen bonding and covalent bonds is presented in Figure 13c and Table S1-10. As for the solvation of single polymer chains, hydrogen bonding was the predominant contributor in the gel systems. Compared with the EG gel and PEGgel, the more inhomogeneous distribution of the water molecules in the hydrogel indicated a stronger polymer-solvent separation (Figure S1-11b). This led to a stiff mechanical response when the hydrogel got stretched.

In stark contrast, the polymer network in the EG gel remained homogeneously mixed at the molecular scale during the stretching process (Figure S1-11c). The EG solvent served as a mitigating medium linking the polymer chains, albeit in the form of short-range polymer-EG-polymer cross-links. Compared to water, the hydrogen bonding was less prevalent in the EG gel, leading to a soft response to the external stretching. The behavior of the PEGgel lay between the hydrogel and EG gel. The unique C-H...O hydrogen bond in the PEGgel was the predominant contributor to the hydrogen bond energy. The PEGgel had fewer OH groups compared to the hydrogel and EG gel as the OH groups from the solvent were located only on the termini of PEG. While the C-H...O bond was weaker than the O-H...O bond, the large number of ether groups on the PEG molecules facilitated frequent formation of C-H...O hydrogen bonds. The contribution from the H-bonds between the OH group on the polymer and the ether group of PEG is 9× smaller than that of the C-H...O bond energy. Among the three solvents, the total energy from the hydrogen bonding was the weakest in PEG. However, between the EG gel and PEGgel, the greater C-H...O H-bond energies in the PEG corresponded to a much larger number of H-bonds, which compensated for most of the energy difference. Overall, the presence of such frequent but weak cross-linking sites facilitated a pronounced polymer-polymer cross-linking.

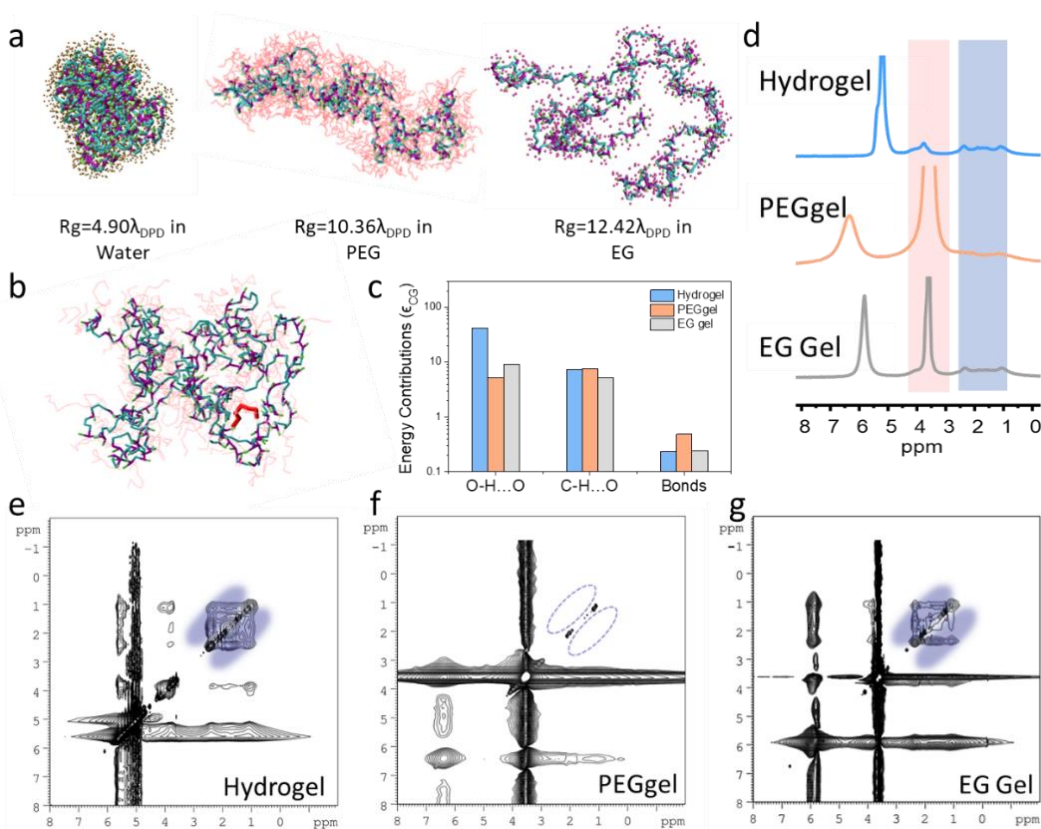
Moreover, the larger size of the PEG molecule, enhanced by the intramolecular hydrogen bonding, causes the solvent molecules to occupy distinct spaces among the polymer chains, thereby leading to local compression of the polymer network into a less homogeneously distributed pattern (Figure S1-11d). To quantify the entanglement, this study calculated the ensemble contour lengths for the polymer networks of the hydrogel, the EG gel and the PEGgel at 550% stretching using the Z1 method.<sup>153</sup> The contour length is a measure for the number of polymer units where the polymer has avoided the presence of another chain. A snapshot of the polymer network, with the highlighted entanglement sites between two polymer chains, is shown in Figure S1-11e. As summarized in Table S1-11, PEG has the shortest contour length, indicating a maximal polymer-polymer entanglement among the three gel systems. Larger entanglement is associated with improved mechanical properties,<sup>154,155</sup> as long as there are no knots,<sup>156,157</sup> which makes the polymer brittle.

To summarize, in the hydrogel, strong O-H...O hydrogen bonds and lack of miscibility with the solvent result in a stiff system. In the EG gel, the enhanced miscibility with the solvent means that EG can substitute easily for polymer-polymer interactions, resulting in a very soft system. For the PEGgel, the weak but abundant C-H...O hydrogen bonds generate a large number of variable interaction points that can accommodate the strain of the system. In contrast to the other two systems, the larger size of PEG generates more flexible long-range polymer-PEG-polymer cross-links. While these effects pertain to the individual scale, the larger polymer entanglement in the PEGgel may contribute somewhat to the improved mechanical properties<sup>155</sup> at longer length-scales.

To further elucidate the structural differences between the three gel systems, an in-situ two-dimensional solid-state <sup>1</sup>H-NMR characterization of these three gels was performed (Figure 13d). Indeed, in the 2D exchange spectrum of the hydrogel (Figure 13e), cross peaks connecting signals at 1.1 and 2.4 ppm, which indicate magnetization exchange between the methyl-groups (-CH<sub>3</sub>) and the backbone (-CH<sub>2</sub>-CH<sub>2</sub>-) of P(HEMA-*co*-AAc), respectively, can be clearly seen. In contrast, the cross peaks between 1.1 ppm and 2.4 ppm were not observed in the case of the PEGgel (Figure 13f). I note at this point that the strong signals at 3.8 ppm and 6.5 ppm arise from PEG, and would obscure potential cross peaks originating from the HEMA polymer. Nonetheless, the presence of spin diffusion within the HEMA polymer in the case of the hydrogel, and the absence of it in the PEGgel supports the proposed model of solvent-polymer interaction. The compact polymer clusters in the case

### 3.Results and Discussion

of the hydrogel lead to restricted motion and close proximities of the hydrogens in the sample, resulting in strong  $^1\text{H}$ - $^1\text{H}$  dipolar couplings and spin diffusion. In the PEGgel, on the other hand, the more elongated chains exhibit more motion and the hydrogens are further separated, leading to reduced spin diffusion. In the case of the EGgel, however, cross peaks between the methyl groups and the backbone within the HEMA polymers were again observed (Figure 13g). Again, the signals at 6.0 ppm and 3.8 ppm are solvent peaks, restricting the analysis to the region of below  $\sim 3$  ppm. The spin diffusion observed in the 2D exchange NMR experiments was further quantified by analyzing the intensity of the cross peaks connecting the signals at 1.1 ppm and 2.4 ppm as a function of the mixing time (Figure S1-12). The mixing time is a delay in the experiment, during which exchange processes such as spin diffusion occur. The intensity of the cross peaks (sum of both) was related to the intensity of the diagonal peaks (sum of the signals at 1.1 ppm and 2.4 ppm), and shows an increase with mixing time in the case of the hydrogel and EG gel, and nearly no cross peak intensity was detected in the case of the PEGgel. Thus, as opposed to water and EG in the hydrogel and EG gel, PEG seems to participate in the gel network formation with a larger molecule size, which further results in enhanced mechanical properties.



**Figure 13.** The CGMD simulation and the solid-state NMR investigation of the gel systems. a) CGMD simulated single chain conformations of P(HEMA-*co*-AAc) in water, PEG, and EG (from left to right). Size of the single chain, characterized by the calculated radius of gyration for the single-chain polymer. Atom groups in HEMA-*co*-AAc are color coded in accordance with the CG scheme in Figure S1-10. The solvent in the immediate vicinity of the polymer is shown as tan-color dots for water, violet-colored dots for EG, and pink short chains for PEG. b) A snapshot of the polymer-PEG-polymer cross-linking via H-bonding for the single P(HEMA-*co*-AAc) chain in PEG. The PEG highlighted in red forms an intra-polymer cross-linking unit. c) Componential contributions to the interaction potentials of the O-H...O hydrogen bonding, C-H...O hydrogen bonding and covalent bonds in three gels stretched to 550%. d) Solid state MAS <sup>1</sup>H-NMR spectra of hydrogel (blue), PEGgel (orange), and EG gel (gray). Anticipated inter- and intra-chain interactions are supported by 2D exchange <sup>1</sup>H-NMR experiments acquired under MAS using a mixing time of 100 ms of the hydrogel (e), PEGgel (f), and EG gel (g). The cross peaks arising from magnetization exchange between methyl-groups (-CH<sub>3</sub>) and copolymer backbone (-CH<sub>2</sub>-CH<sub>2</sub>-) in P(HEMA-*co*-AAc) are marked in blue, which connect the resonances at 1.1 and 2.4 ppm, respectively. Copyright 2022 Wiley-VCH.<sup>69</sup>

### 3.1.3.3 Tunable mechanical properties of PEGgels

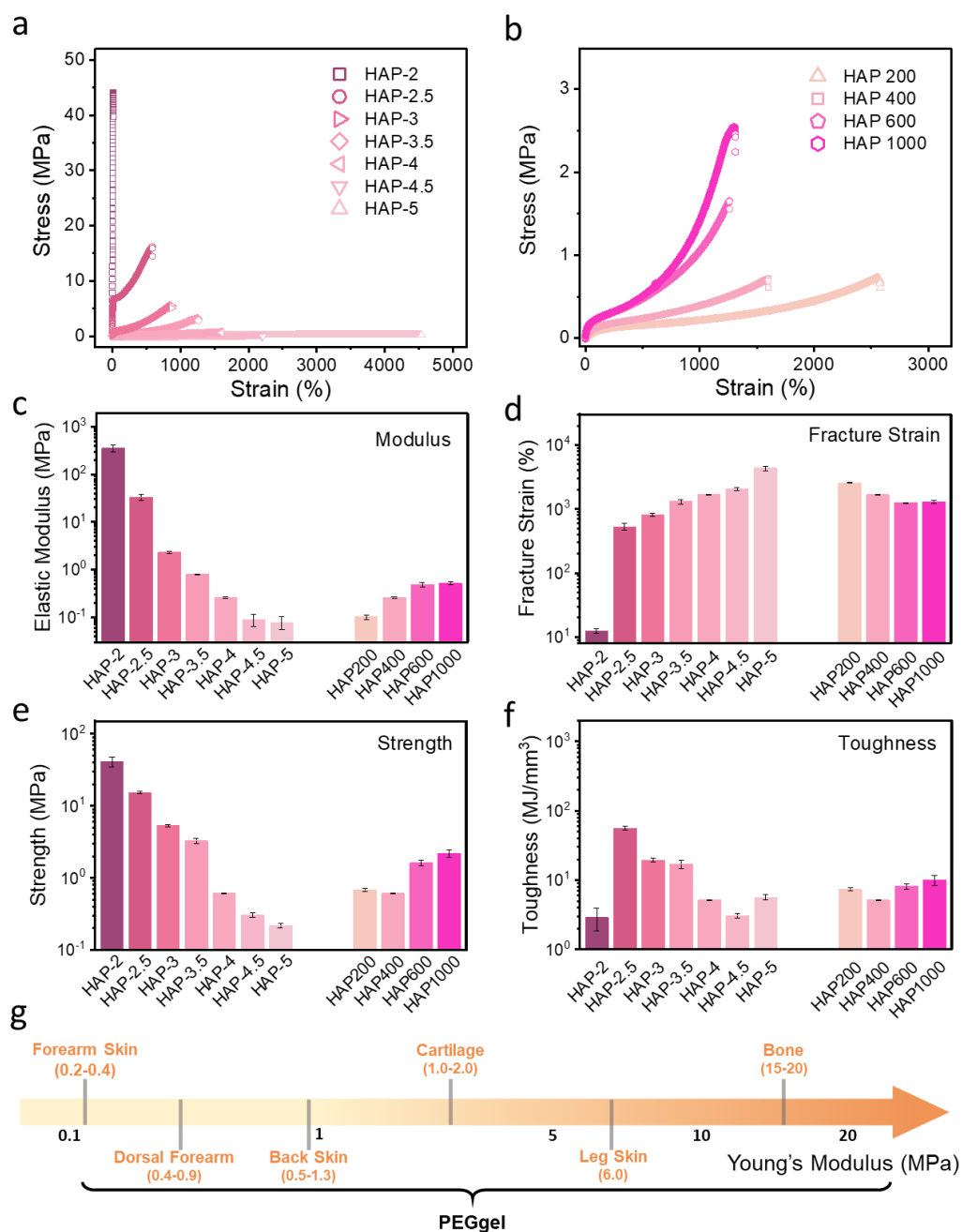
To further investigate the effect of solvent on the mechanical properties of the gel systems, this study varied the volume fraction of PEG and its molecular weight, thereby achieving tunability of the mechanical property of the P(HEMA-*co*-AAc) PEGgel (HAP). Prepolymer solutions of all samples (Tables S2 and S3) were added into a mold and exposed to UV for 30 min (6 mW/cm<sup>2</sup>, 366 nm, room temperature). All mechanical tests were performed in air, at room temperature, using a universal tester with a 100 N load cell and 100 mm/min load speed. The effect of PEG volume fraction on the mechanical properties of PEGgel (Figure 14a) was first evaluated using PEG 400 (400 g/mol) as a solvent. The tensile strength of the PEGgel obtained increased from 0.21 MPa (50 vol.%) to 41.29 MPa (20 vol.%) as the PEG 400 volume fraction decreased, while the fracture strain decreased from 4335% (50 vol.%) to 12% (20 vol.%). In addition, the elastic modulus of the gels showed a similar

pattern of changes, increasing from 0.078 MPa (50 vol.%) to 352 MPa (20 vol.%) as the volume fraction of PEG 400 decreased. In addition, the toughness of PEGgel could be tuned solely by changing the volume fraction of PEG from 50 to 20%, from 5.66 MJ m<sup>-3</sup> (50 vol.%) to 2.89 MJ m<sup>-3</sup>(20 vol.%). The differential scanning calorimetry analysis demonstrate same trend on T<sub>g</sub> change, which depends on the mobility of the polymer chain (Figure S1-13a). With PEG volume fraction decreasing, the T<sub>g</sub> of PEGgel increased from -38.8 °C (HAP-5) to -27.0 °C (HAP-4.5), -25.2 °C (HAP-4), -15.2 °C (HAP-3.5), -8.2 °C (HAP-3), 0.5 °C (HAP-2.5), and 22.3 °C (HAP-2). Here, lower volume fraction of PEG, serving as solvent, renders the polymer network less flexible, showing faster crack extension,<sup>158</sup> resulting in the higher elastic moduli and lower fracture strain of the gel.<sup>103</sup>

Next, this study evaluated the effect of the molecular weight of PEG used as a solvent on the mechanical properties of the PEGgel, with a constant PEG volume fraction of 60% (Figure 14b). The tensile strength of the PEGgel obtained with different PEGs increased from 0.60 MPa (PEG 200 g/mol) to 0.61 MPa (PEG 400 g/mol), 1.61 MPa (PEG 600 g/mol), and 2.20 MPa (PEG 1000 g/mol) as the molecular weight of PEG increased. However, as the molecular weight of PEG increased, the fracture strain of the PEGgel decreased from 2570% (PEG 200) to 1668% (PEG 400), 1244% (PEG 600), and 1280% (PEG 1000). The larger molecular weight of PEG provides more interactions among polymer chains of the network in the PEGgel, efficiently enhancing its tensile strength. In addition, the flexibility of the P(HEMA-*co*-AAc) polymer chain is reduced as the molecular weight of PEG increases, resulting in a further reduction in the fracture strain. Similarly, the elastic modulus and toughness of PEGgel can be tuned easily by changing the molecular weight of PEG. The difference on T<sub>g</sub> of these PEGgels also confirmed this trend (Figure S1-13b). With the larger PEG molecular weight, the T<sub>g</sub> of PEGgel behaved higher T<sub>g</sub>, in which the T<sub>g</sub> increased from -48.2 °C (HAP200) to -25.2 °C (HAP400), -23.6 °C (HAP600) and -18.6 °C (HAP1000). By increasing the molecular weight of PEG from 200 g/mol to 1000 g/mol, the elastic modulus and toughness of the corresponding PEGgels increased from 0.10 MPa and 7.36 MJ m<sup>-3</sup> to 0.52 MPa and 9.99 MJ m<sup>-3</sup>, respectively (Figure 14c and 14f). Moreover, cyclic tensile loading-unloading tests with gradual increase in strain was measured on HAP-4 to present the recovery in mechanical property (Figure S1-14). The obvious hysteresis loops demonstrate the energy dissipation in PEGgel during loading-unloading cycles. Interestingly, the second, third and fourth loading curves almost overlapped the previous

ones, indicating a rapid recovery of the network despite the energy dissipation during loading. Such rapid recovery is likely attributed to the reversible and dynamic hydrogen bonding between the P(HEMA-co-AAc) chains and PEG, which temporarily ruptured to dissipate energy upon loading and rapidly reformed during unloading.

Thus, the mechanical properties of PEGgels were tuned by changing the volume fraction and molecular weight of PEG, with an available range of tensile strength, fracture strain, elastic modulus, and toughness of 0.22-41.3 MPa, 12%-4336%, 0.08-352 MPa, and 2.89-56.23 MJ m<sup>-3</sup>, respectively (Figure 14c-f). Notably, the elastic modulus of PEGgels can be tuned within a broad range, from near 0.08 to 352 MPa, which covers the Young's modulus of most tissues in the human body (Figure 14g),<sup>159,160</sup> especially different skin types.<sup>161</sup> Overall, the PEGgel showed high ultimate stress and strain that well covered the values seen in many reported tough hydrogels and elastomers (Figure S1-15, Table S1-12). With such a broad range of elastic moduli, PEGgel represents a highly promising material platform for the development of human-compatible flexible devices,<sup>112</sup> such as wearable sensors, electronic skin and soft robots.<sup>162</sup>



**Figure 14.** The tunable mechanical properties of PEGgel. a) Representative stress-strain curves of PEGgels containing PEG 400 with volume fractions ranging from 20 vol.% (HAP-2) to 50 vol.% (HAP-5). b) Representative stress-strain curves of PEGgels composed of PEG 200 (HAP 200), 400 (HAP 400), 600 (HAP 400) and 1000 (HAP 1000), with constant PEG fraction of 40 vol.%. c-f) Modulus (c), fracture strain (d), strength (e), and toughness (f) of PEGgels mechanically tuned based on variation of PEG types and volume fractions. g) The range of elastic moduli of soft human tissues and corresponding PEGgels. Data represent the mean  $\pm$  standard deviation ( $n = 3$ ). Copyright 2022 Wiley-VCH.<sup>69</sup>



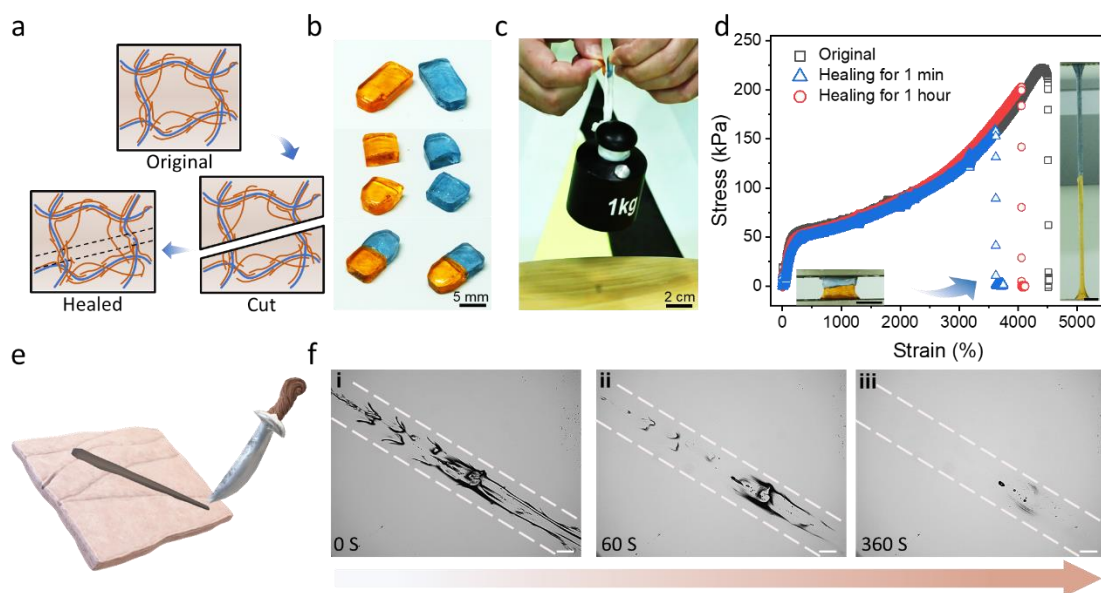
### 3.1.3.4 *Self-healing properties of PEGgels*

Physically cross-linked supramolecular networks (based on hydrogen bonding), which usually endow materials fast repair after damage,<sup>163</sup> have already been used to generate self-healing materials.<sup>164,165</sup> Owing to the diffusive nature of multivalent long PEG molecules wrapping around and non-covalently cross-linking the polymer network (Figure 15a), PEGgel demonstrates inherently rapid self-healing properties. To evaluate the self-healing, two PEGgel samples (HAP-5, 3 mm × 5 mm × 15 mm) stained with methyl blue and Sudan I were cut into two pieces and re-joined to allow repair (Figure 15b). After 1 min, the repaired gel could support 1 kg without damage (Figure 15c). The mechanical properties of this PEGgel after healing for different time periods are shown in Figure 15d. The tensile stress-strain curves of healed samples overlap almost completely with that of the original samples. After healing for 1 min without any external stimulus, the fracture strain of the sample reached 3600%, demonstrating a self-healing efficiency of  $49.1 \pm 8.7\%$  ( $n = 3$ ) measured by dividing the toughness of healed samples by the toughness of the original samples. After 1 h of healing, the PEGgel was stretched to 4000% (Figure 15d), representing a self-healing efficiency of  $70.2 \pm 3.0\%$  ( $n = 3$ ). After 1 h of healing, the hydrogels and EG gels showed significantly lower self-healing ratios (Figure S1-16). For hydrogels (50 vol.% water), the self-healing efficiency based on toughness was only 2.7% after 1 min, rising to only 18.5% after 1 hour. For EG gels, the self-healing ratio was only 1.3% and 12.2% after 1 min and 1 h of healing time, respectively. The self-healing efficiencies of PEGgels with different PEG ratios were also measured (Table S1-9). With a volume fraction of PEG is higher than 35 vol.%, the self-healing efficiency of these PEGgels exceeded 50% after healing for 1 hour (Figure S1-17). After longer time periods, HAP-4.5, HAP-4, HAP-3.5 achieved self-healing efficiencies of  $60.9 \pm 0.8\%$  (1 h),  $54.9 \pm 6.7\%$  (3 h), and  $63.8 \pm 5.0\%$  (6 h), respectively.

This study then performed surface scratch recovery tests to simulate skin wound healing (Figure 15e). A razor blade was used to make deep scratches (150-500  $\mu\text{m}$  wide and 1,000  $\mu\text{m}$  deep) on a PEGgel film (HAP-5). Optical microscopy images showed noticeable recovery after only 1 min and complete self-healing and disappearance of the wound within 6 min without any external stimulus (Figure 15f, Movie S1-3). The same scratch recovery tests were applied to the hydrogels and EG gels with same polymer network and solvent

ratio (Figure S1-18). After healing for 30 min, only the EG gel showed partial healing, with only the narrow parts of the scratch showing complete recovery. In contrast, only minimal healing of the hydrogel wound occurred. With the same polymer network and solvent ratio, the self-healing speed of PEGgel was significantly higher than that of the EG gel and hydrogel.

Rheology analyses were further used to demonstrate the self-healing process. Strain amplitude sweep was performed to analyse the elastic response of the PEGgel (Figure S1-19), and the critical strain regions of storage modulus ( $G'$ ) and loss modulus ( $G''$ ) were found to be 50% and 100% respectively, which is higher than EG gel (30% for  $G'$ , 40% for  $G''$ ) and hydrogel (20% for  $G'$ , 30% for  $G''$ ). The  $G'$  value was found to decrease rapidly above the critical strain region, indicating the damage of the gel network. Then, the PEGgel was subsequently subjected to a large amplitude oscillatory force (Figure S1-19d, 300% strain), and the  $G'$  value decreased from  $\sim 73.5$  to  $\sim 45.1$  kPa, indicating a loose network. After decreasing the amplitude (1% strain), the  $G'$  recovered ( $\sim 80$  s) to the initial value, and the PEGgel returned to the original state, indicating the quick recovery of the PEGgel inner network, confirming the self-healing capability based on the dynamic bonds. For EG gel, the recovery speed is faster than PEGgel ( $\sim 40$  s), resulting from the higher flexibility of the polymer chains in EG. But after the amplitude cycling, the EG gel is not able to recover back completely as PEGgel, which may result from the weaker long-range correlations of solvents. Due to the more fixed polymer network compared with PEGgel and EG gel, hydrogel showed poor self-healing property under such continuous small - large strain oscillation switch.



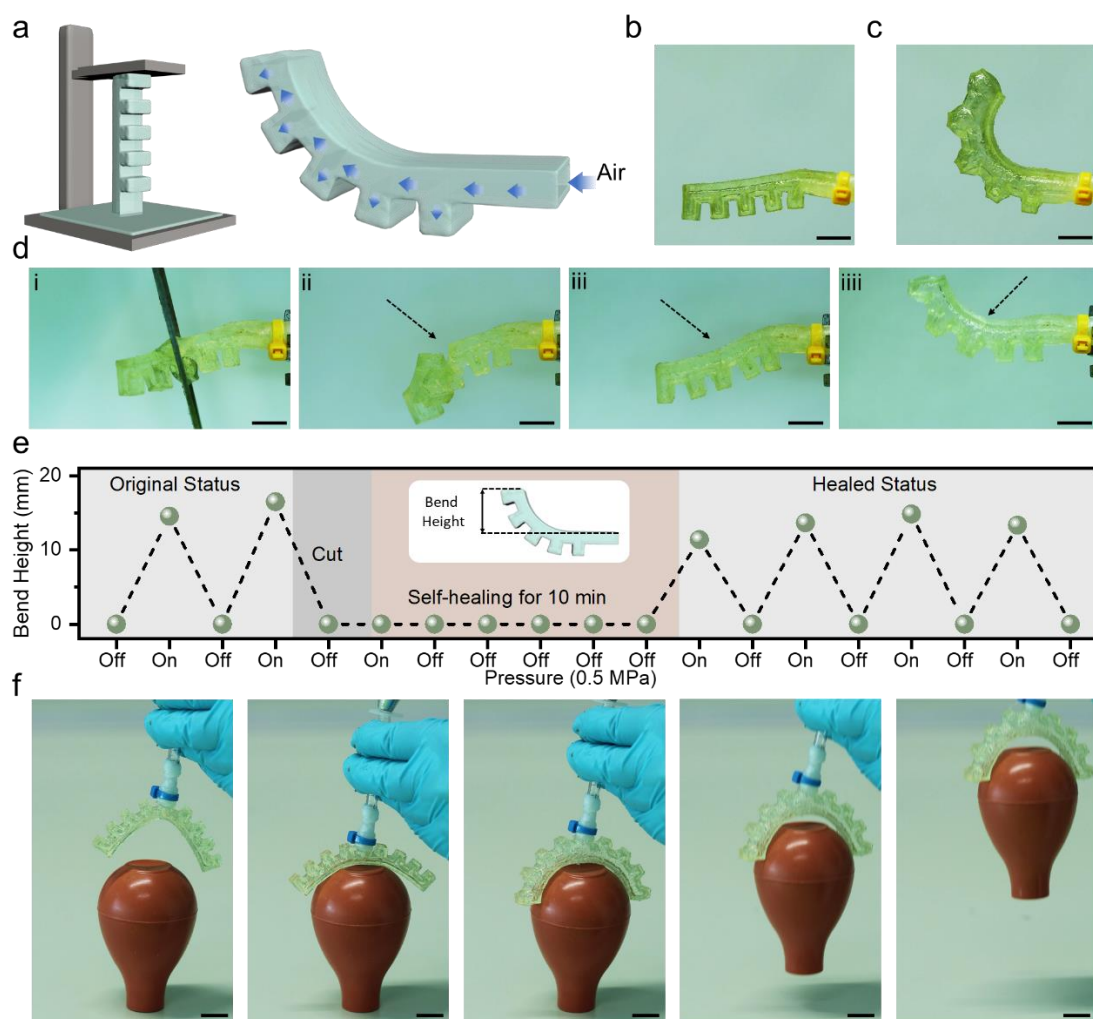
**Figure 15.** Self-healing properties of PEGgel. a) Self-healing mechanism of the PEGgel is based on the PEG functioning as a diffusive H-bonding molecular glue capable of cross-linking damaged polymer chains. b) The PEGgel (HAP-5) samples ( $3\text{ mm} \times 5\text{ mm} \times 15\text{ mm}$ ) stained with methyl blue and Sudan I cut into two pieces show complete healing within 1 min. c) Healed PEGgel sample supports 1 kg weight. d) Tensile stress-strain curves of PEGgel samples after different healing times. Inset photo shows gel stretched over 4000% after 1h of healing (scale bar: 5 mm). e) Schematic illustration of the scratch-healing test, simulating a skin tissue wound. f) The scratch wound on a PEGgel film (HAP-5,  $1000\text{ }\mu\text{m}$  thick) is completely healed after 360 s (scale bar:  $500\text{ }\mu\text{m}$ ). Copyright 2022 Wiley-VCH.<sup>69</sup>

### 3.1.3.5 *Soft actuators based on PEGgels*

Self-healing soft materials are indispensable for use as soft actuators and robots required to survive in dynamic and complex stress/strain environments in which they are vulnerable to mechanical damage that impairs their performance. To further explore the feasibility of using PEGgels in soft actuators and robots, a pneumatic soft actuator was fabricated through digital light processing (DLP) 3D printing technology based on HAP-4 gel (Figure 16a). A hollow structure with asymmetry above and below can be fabricated directly by 3D printing without the need to employ complex and multistep molding or casting manufacturing processes. Thus, this approach enables the geometric complexity and functionality of the

soft robots.<sup>166</sup> When the actuator is pressurized, the sawtooth part expands and deforms towards the non-sawtooth side, which causes a directed force that serves as an actuator. The 3D printed actuator with a hollow core generated is shown in Figure 16b. When pressure (0.5 MPa) was applied, the actuator bent, and then recovered after the pressure was released (Figure 16c and Movie S1-4). Due to the toughness and softness of the PEGgel, the soft actuator obtained was capable of repeatedly supporting a pair of steel scissors weighing 20 g (Figure S1-20 and Movie S1-5), representing 5.4 times its own weight (3.7 g). Since the pneumatic actuators are especially vulnerable to puncture damage, the self-healing properties of the 3D printed actuator were investigated after it was cut into two pieces (Figure 16d). The ability of the actuator to bend in response to the applied pressure was restored after 10 min of healing (Movie S1-6).

In detail, the performances of the actuator before cutting and after healing were analysed (Figure 16e). The actuator lost deformation ability after complete separation, because of the major leakage of the gas pressure applied. After healing for 10 min, the ability of actuator to bend with applied pressure was restored. Thus, the healing capacity of PEGgels allows the effective repair of damage, and therefore extends the operating lifetime of the actuators. Benefiting from the 3D printability of PEGgels, this study further prepared a soft actuator with two fingers (Figure S1-21) with the ability to bend into any direction under pressure to capture an object. In a proof-of-concept demonstration, this study used the actuator with two fingers to capture a soft rubber pipette bulb. When the pressure was applied, the two fingers of the actuator deformed and held the bulb tightly. Due to the softness of the gel, the bulb was not deformed and was lifted safely (Figure 16f, Movie S1-7). In summary, these soft materials based on PEG as a solvent can be easily shaped to form complex structures by 3D printing and heal after severe mechanical damage (scratches and even total separation), thus offering potential for application in the development of soft robots.



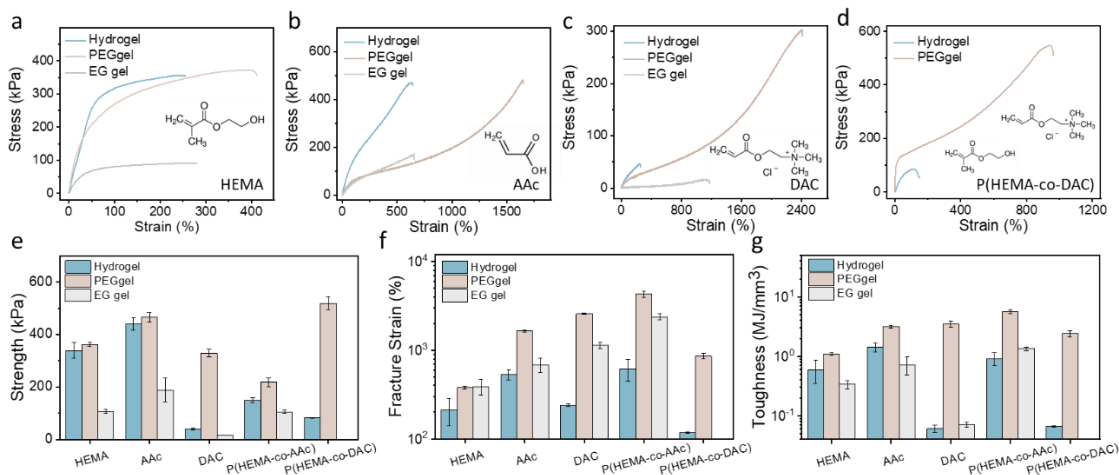
**Figure 16.** Use of 3D-printable self-healing PEGgel based soft actuators. a, b) Schematic diagram and photographs of a soft pneumatic actuator prepared from HAP-4 via digital light processing (DLP) 3D printing technology. c) Bending of the 3D printed actuator under 0.5 MPa air pressure. d) Healing of the actuator after total separation, and bending under 0.5 MPa air pressure after 10 min of healing. e) Quantification of the bend height of the soft actuator before cutting and after healing shows no distinguishable difference. The bend height is the vertical gap between the head and tail. The dotted line connects the data points. f) Design and fabrication of the actuator with two fingers to capture a soft rubber pipette bulb. Scale bars: 5 mm. Copyright 2022 Wiley-VCH.<sup>69</sup>

### 3.1.3.6 Generality and customizability

The PEGgel system can be extended to other polymer networks to form gels with better mechanical properties compared with the same network fabricated using hydrogels or EG

gels. HEMA was used to prepare hydrogel, EG gel and PEGgel by chemical cross-linking using polyethylene glycol diacrylate (PEGDA, 250 g/mol, 1 vol.% of monomer) (Figure 17a). The obtained PEGgel based on chemically cross-linked PHEMA exhibited a greater fracture strain (400%) compared with the hydrogel with the same polymer network (250%). Importantly, this enhanced performance in stretchability did not sacrifice tensile strength, with the fracture strength of PEGgel (375 kPa) being even slightly higher than that of the hydrogel (350 kPa). However, the EG gel with the same chemical composition as the PEGgel exhibited much weaker mechanical properties, with a fracture strain and tensile strength of 280% and 90 kPa, respectively. As shown in Figure 17b, the chemically cross-linked poly acrylic acid with PEGDA exhibited enhanced strength (from 440 kPa for the hydrogel and 186 kPa for the EG gel to 466 for the PEGgel), fracture strain (535% and 685%, to 1650%), and toughness ( $1.41 \text{ MJ m}^{-3}$  and  $0.72 \text{ MJ m}^{-3}$ , to  $3.15 \text{ MJ m}^{-3}$ ). The same phenomenon observed with anionic monomers occurred, when cationic monomers ([2-(acryloyloxy)-ethyl]-trimethyl ammonium chloride, DAC) were introduced into the PEGgel (Figure 17c). The chemically cross-linked DAC PEGgel showed tensile strength of 329 kPa, which is much higher than the strength of corresponding hydrogel (41 kPa) and EG gel (16 kPa). The toughness also increased from  $0.06 \text{ MJ m}^{-3}$  (hydrogel) and  $0.07 \text{ MJ m}^{-3}$  (EG gel) to  $3.45 \text{ MJ m}^{-3}$  (PEGgel). As shown in Figure 17d, the PEGgel fabricated based on physically cross-linked copolymer of HEMA and DAC exhibited a 5.4-fold increase in tensile strength (from 85 kPa to 547 kPa), a 7-fold increase on fracture strain (from 117% to 938%), and a massive 31-fold increase in toughness (from  $0.03 \text{ MJ m}^{-3}$  to  $1.07 \text{ MJ m}^{-3}$ ), compared with the corresponding hydrogel. All of these PEGgels with different polymer network presented enhancement on mechanical properties compared with corresponding hydrogels and EG gels. It may result from the abundant but relatively weak C-H...O hydrogen bonds between PEG and polymer network. Also, the increased long-range correlations and polymer entanglement facilitated the enhanced durability against fracture. Thus, these findings confirm that the improvement of mechanical property caused by the PEG used as a solvent can be extended to different polymer networks, showing universality and potential in functional soft matter preparation. Since the compatibility between PEG and various polymers has been widely confirmed,<sup>71,167,168</sup> our strategy is not restricted to the systems presented here. I foresee that this approach can be applied to design other tough and functional polymer gels for numerous practical applications.

### 3.Results and Discussion



**Figure 17.** Generality of PEGgel systems in different polymer networks. Representative stress-strain curves of hydrogel (blue), PEGgel (orange) and EG gel (gray) composed of chemically cross-linked poly(2-hydroxyethyl methacrylate) (a), chemically cross-linked poly(acrylic acid) (b), chemically cross-linked poly([2-(acryloyloxy)-ethyl]-trimethyl ammonium chloride) (c) and physically cross-linked copolymer of 2-hydroxyethyl methacrylate and [2-(acryloyloxy)-ethyl]-trimethyl ammonium chloride (d). e-g) Strength (e), Fracture Strain (f) and Toughness (g) of three types of gels with various polymer networks. All chemically cross-linked gel is achieving by adding PEGDA (1 vol.% of corresponding monomer). Data represent the mean  $\pm$  standard deviation ( $n = 3$ ). Copyright 2022 Wiley-VCH.<sup>69</sup>

#### 3.1.4 Materials and Methods

##### 3.1.4.1 *Materials*

Acrylic acid, hydroxyethyl methacrylate, [2-(acryloyloxy)-ethyl]-trimethyl ammonium chloride, polyethylene glycol diacrylate, I1173, and I819 were purchased from Sigma–Aldrich (Darmstadt, Germany). All forms of polyethylene glycol were purchased from Thermo Fisher (Schwerte, Germany). Ethanol and acetone were purchased from Merck (Darmstadt, Germany). All chemicals were used as received. All aqueous solutions were prepared with deionized water.

##### 3.1.4.2 *Preparation of gels*

All samples, including hydrogels, EG gels and PEGgels, were prepared by UV-induced one-pot sequential polymerization. Monomers, a photo initiator, and solvents were mixed in amber bottles. After vortexing for 3 min, a clear solution was obtained. All samples were initiated under 366 nm UV light (6 mW/cm<sup>2</sup>) for 30 min. The specific prepolymer compositions are shown in Tables S1–S7. For PEG1000, the solution mixing was finished at 60°C.

##### 3.1.4.3 *3D printing of PEGgel*

The PEGgel containing 40 vol.% of PEG 400 and 60 vol.% of P(HEMA-co-AAc) was used as the ink for 3D printing with a digital light processing printer (Miicraft prime 110). I819 was selected for use as the photo initiator at 10 mg mL<sup>-1</sup>. The curing time for every layer (thickness: 100 µm) was 30 s.

##### 3.1.4.4 *Characterization*

The tensile performance of samples was tested using the AGS-X Series Universal Electromechanical Test Frame (Shimadzu Inc., Japan). For tensile tests, samples were molded into a dumbbell shape (thickness, 1-2 mm thick; 2 mm width, 2 mm; length, 8 mm); three samples were prepared for each tensile experiment. The tensile speed was set at 100 mm/min. The elastic modulus was calculated from the slope of tensile stress-strain curves at 5%-10% strain area. The self-healing efficiency was calculated by dividing the toughness of healed samples by the toughness of the original samples. The molecular weight of samples



was determined by gel permeation chromatography (GPC) in dimethylacetamide phase (data shown in Table S1-8). The dynamic viscoelasticity of the samples was measured by ARES G2 (TA Instruments) rheometer via small amplitude oscillatory shear experiments. The samples were placed under a 13 mm-diameter parallel plate. In the strain sweep tests, the shear strain ( $\gamma$ ) was from 0.01 to 800% at the frequency of 10 rad s<sup>-1</sup> and temperature of 25 °C. In the frequency sweep tests, the angular frequency ( $\omega$ ) was from 1 to 100 rad s<sup>-1</sup> at specified temperatures with the shear strain ( $\gamma$ ) of 0.5%. The master curves at a reference temperature of 25 °C were scaled by time-temperature superposition. In the temperature sweep measurements, the temperature was varied from 25 to 120 °C (5 °C min<sup>-1</sup>) at a frequency of 10 rad s<sup>-1</sup> with the shear strain of 1%.

#### 3.1.4.5 *Coarse-grained molecular dynamic simulation*

The CGMD simulations was built by Modan Liu and Elaheh Sedghamiz from Wolfgang Wenzel Group at the Institute of Nanotechnology, KIT as a part of the collaborative project. CGMD simulations were performed to reproduce initial configurations of the polymer network and investigate the mechanical properties during stretching. A schematic diagram of the CGMD simulations is shown in Figure S1-4. The force-field parameters for the CGMD were fitted to reproduce the tensile stress-strain curves of hydrogel, PEGgel and EG gel based on the same P(HEMA-*co*-AAc) polymer matrix and 50% solvent fraction (representative curves shown in Figure 12c).

The corresponding CG length  $\lambda_{CG}$  was set at 1 nm and the characteristic molecular mass  $m_{CG}$  was set at 100Da. The covalent bonds in the backbone of P(HEMA-*co*-AAc) and between the backbone and the side group in HEMA was considered with a bonding strength of 40.0  $\epsilon_{CG}$ . Similar to the Kremer-Grest polymer model, the steric repulsion was modeled as a truncated and shifted Lennard-Jones potential. Hydrogen bonding was characterized by the Morse potential. The non-bonded interactions among the different CG beads are listed in Table S1-10.

The polymer chains of P(HEMA-*co*-AAc) were assigned a fixed length of 600 monomer units, in a random mixture of HEMA:AAc=36:64. The polymer chains were packed in a  $30 \lambda_{CG} \times 30 \lambda_{CG} \times 20 \lambda_{CG}$  simulation box by PACKmol. The corresponding CG bead solvent

(water, EG, and PEG) were added to fill the simulation box and went through a simulated annealing process to reach a relaxed state at ambient temperature and pressure.

Upon stretching, the simulation box is elongated in the  $z$ -direction whereas in the  $x$ - $y$  plane the cross-sectional area shrinks to preserve the overall volume. The stretching is applied every  $2000 \tau_{CG}$  with an engineering rate of 0.01 to slowly deform the box dimensions until a 50-times elongation is reached in the  $z$ -direction. Average values for the componential contributions to the interaction potential of the steric effect, the hydrogen bonds, and the covalent bonds recorded over the last  $1000 \tau_{CG}$  during each deformation are shown in Table S1-10. As a limitation of this model, the time series of the energetics showed only minor fluctuations across the whole stretching time span, where critical events, such as the rupture during stretching, can be implied in transitional behaviors for some observables however the definitive critical behaviors cannot be covered. In the post-processing of the MD data, the number of O-H...O and C-H...O hydrogen bonds were calculated based on the Morse potential. The tensile stress  $\sigma$  with respect to the stress tensor in the  $z$ -direction was calculated by:

$$\sigma = (1 + \mu)(P - P_{zz})$$

where  $\mu$  is the Poisson's ratio, which is estimated to decrease from 0.7 to 0.5 during the elongation in the  $z$ -direction.<sup>169,170</sup>

#### 3.1.4.6 *NMR Measurement*

The solid-state  $^1\text{H}$ -NMR characterization was measured by Stephan L. Grage from Institute for Biological Interfaces IBG-2, KIT as a part of the collaborative project. 2D exchange  $^1\text{H}$ -NMR spectra was measured under MAS of 20 kHz for different mixing times in the range from 0-300 ms (Figure 13d-g). The pulse sequence of this experiment is identical to that used in NOESY spectroscopy in solution NMR<sup>171</sup>, however, the physical mechanisms leading to cross peaks are different in solids or large molecules such as polymers. While in solution NMR of small molecules, cross peaks are caused by cross relaxation, spin diffusion is the dominating mechanism in solids. Cross peaks in solution indicate a proximity (within a distance of  $\sim 5\text{\AA}$ ) of the spins corresponding to the signals linked by the cross peak. Spin diffusion, however, has a larger distance range as magnetization is exchanging within a larger  $^1\text{H}$  spin network. Cross peaks caused by this effect depend on the  $^1\text{H}$ - $^1\text{H}$  dipolar

couplings within the spin network, and are influenced by molecular mobility and proximity of the  $^1\text{H}$  spins. 2D exchange NMR hence allows to distinguish a compact polymer with reduced local mobility and loose polymer chains, where strong or weak spin diffusion is anticipated, respectively.

Solid state  $^1\text{H}$  NMR measurements were performed using a 500-MHz widebore Bruker Avance III spectrometer. The PEGel, hydrogel and EG gel of copolymer of hydroxyethyl methylacrylate and acrylic acid were filled into 3.2 mm rotors and measured within ~1 day after production of the gels. The  $^1\text{H}$ -NMR spectra were acquired under magic angle spinning (MAS) with a spinning speed of 20 kHz using a triple-resonant (HCN) MAS probe (Bruker) equipped with a low resonator. A  $90^\circ$ -pulse of 3.2  $\mu\text{s}$  was used. The acquisition time was 20ms, and 32 scans with a recycle delay of 3s were averaged in case of the 1-dimensional  $^1\text{H}$ -NMR spectra. To get insight into the proximities and molecular mobility, 2D exchange experiments were conducted using a NOESY pulse sequence and mixing times of 0, 10, 30, 100, 300 ms. 400 increments covering 13.33 ppm were used in the indirect dimension, and 8 scans were averaged with a recycle delay of 3s.

## 3.1.5 Supporting Information

**Table S1-1.** Prepolymer composition of physically cross-linked P(HEMA-*co*-AAc) Gel.

	P(HEMA- <i>co</i> - AAc)-Hydrogel	P(HEMA- <i>co</i> - AAc)-EG Gel	P(HEMA- <i>co</i> - AAC)-PEGel
AAc (mL)	1	1	1
HEMA (mL)	1	1	1
I1173 ( $\mu$ L)	10	10	10
Solvent (mL)	2 (water)	2 (EG)	2 (PEG 400)

**Table S1-2.** Prepolymer composition of HAP with different types of PEG.

	HAP200	HAP400	HAP600	HAP1000
HEMA	1.2	1.2	1.2	1.2
AAC (mL)	1.2	1.2	1.2	1.2
I1173 ( $\mu$ L)	12	12	12	12
PEG (mL)	1.6 (PEG 200)	1.6 (PEG 400)	1.6 (PEG 600)	1.6 (PEG 1000)

**Table S1-3.** Prepolymer composition of HAP with different ratios of PEG.

	HAP-2	HAP-	HAP-3	HAP-	HAP-4	HAP-	HAP-5
HEMA	1.6	1.5	1.4	1.3	1.2	1.1	1
AAC	1.6	1.5	1.4	1.3	1.2	1.1	1
I1173( $\mu$ L)	16	15	14	13	12	11	10
PEG400	0.8	1	1.2	1.4	1.6	1.8	2

### 3.Results and Discussion

**Table S1-4.** Prepolymer composition of chemically cross-linked PEGgels.

	Cross-linked HEMA	Cross-linked AAc	Cross-linked DAC
Monomer (mL)	1 (HEMA)	1 (AAc)	1 (DAC)
PEGDA ( $\mu$ L)	10	10	10
I1173 ( $\mu$ L)	10	10	10
PEG400 (mL)	1	1	1

**Table S1-5.** Prepolymer composition of chemically cross-linked hydrogels.

	Cross-linked	Cross-linked AAc	Cross-linked DAC
Monomer (mL)	1 (HEMA)	1 (AAc)	1 (DAC)
PEGDA ( $\mu$ L)	10	10	10
I1173 ( $\mu$ L)	10	10	10
Water (mL)	1	1	1

**Table S1-6.** Prepolymer composition of chemically cross-linked EG gels.

	Cross-linked	Cross-linked AAc	Cross-linked DAC
Monomer (mL)	1 (HEMA)	1 (AAc)	1 (DAC)
PEGDA ( $\mu$ L)	10	10	10
I1173 ( $\mu$ L)	10	10	10
EG (mL)	1	1	1

**Table S1-7.** Prepolymer composition of physically cross-linked P(HEMA-co-DAC) gel.

### 3.Results and Discussion

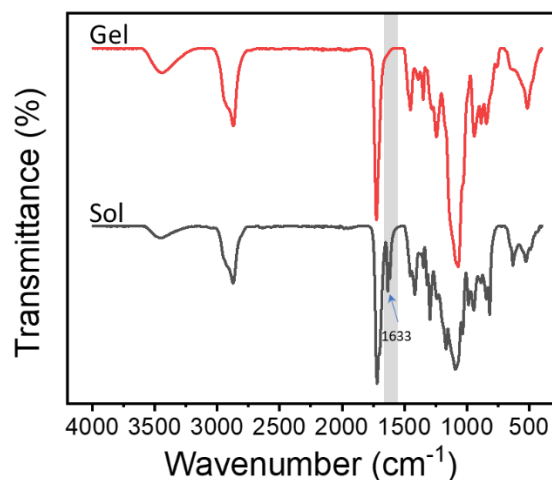
	P(HEMA- <i>co</i> -DAC)-Hydrogel	P(HEMA- <i>co</i> -DAC)-PEGel
DAC (mL)	1	1
HEMA (mL)	1	1
I1173 ( $\mu$ L)	10	10
Solvent (mL)	2 (water)	2 (PEG 400)

**Table S1-8.** Molecular weight of commercial PEG.

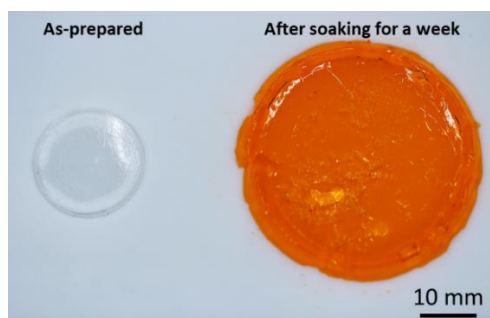
	PEG 200	PEG 400	PEG 600	PEG 1000
<i>Mn</i> (g/mol)	131	430	710	1431
<i>Mw</i> (g/mol)	180	487	793	1510
<i>Mw/Mn</i>	1.373	1.129	1.103	1.056

**Table S1-9.** Healing efficiency of PEGgels with different ratio of PEG.

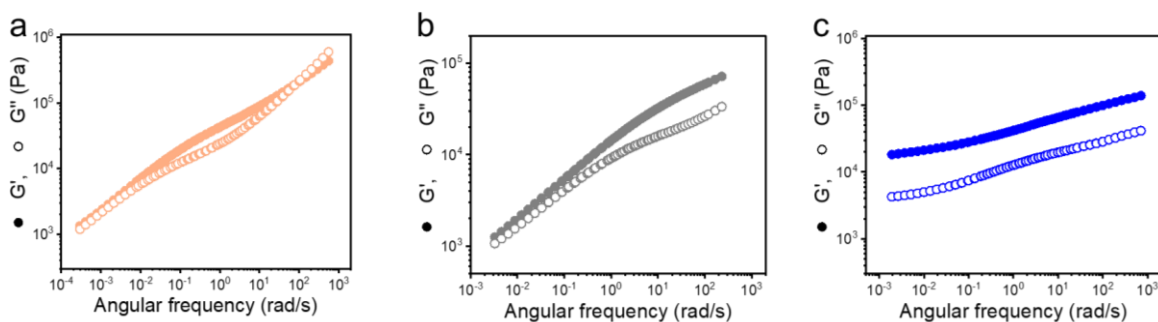
	HAP-5	HAP-4.5	HAP-4	HAP-3.5	HAP-3	HAP-2.5
Healing efficiency (%)	70.2 $\pm$ 3.0	60.9 $\pm$ 0.8	54.9 $\pm$ 6.7	63.8 $\pm$ 5.0	17.8 $\pm$ 4.3	2.5 $\pm$ 1.6



**Figure S1-1.** FTIR spectrums of the PEGgels before (sol, black) and after (gel, red) polymerization.

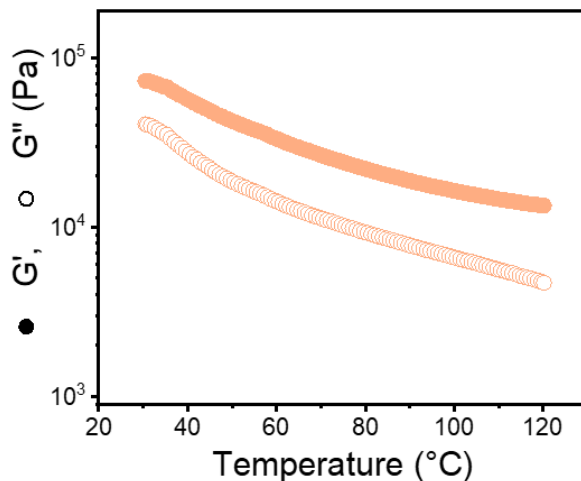


**Figure S1-2.** Photograph of as-prepared PEGgel and PEGgel after one week of soaking in PEG 400 containing Sudan I 1 mg mL<sup>-1</sup>.

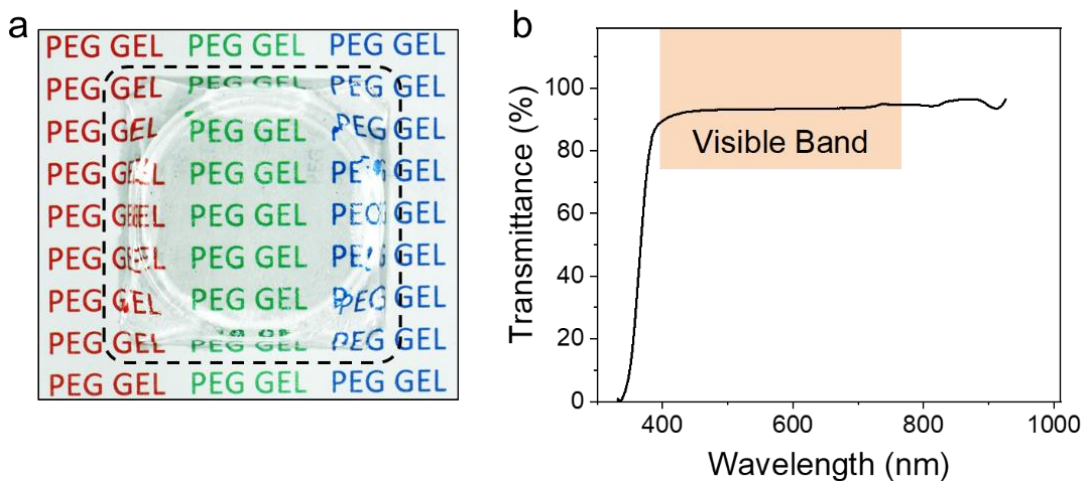


**Figure S1-3.** Frequency dependence of storage modulus ( $G'$ ) and loss modulus ( $G''$ ) for PEGgel (a), EG gel (b), and hydrogel (c). The master curves were obtained by time-temperature superposition (TTS) and shifted horizontally by the indicating factors. PEGgel and EG gel were test under 5 °C, 25 °C, 45 °C, 65 °C, 85 °C, and 105 °C, while hydrogel

was test under 5 °C, 25 °C, 45 °C, 65 °C, and 85 °C for boiling of water. During the frequency sweep tests, the angular frequency was from 0.1 to 100 rad s<sup>-1</sup> at specified temperatures with the shear strain of 1%.

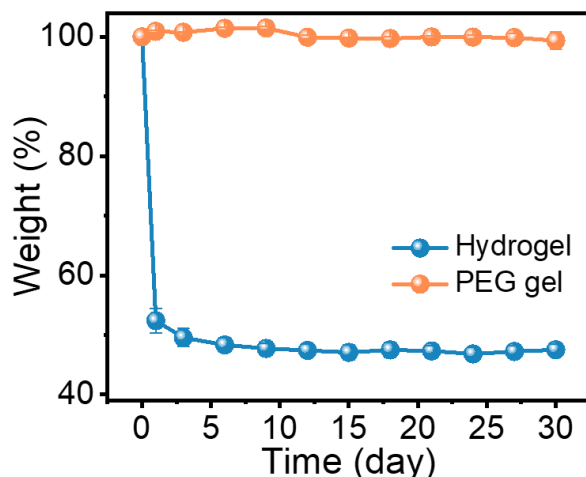


**Figure S1-4.** Temperature dependence of storage modulus ( $G'$ ) and loss modulus ( $G''$ ) for PEGgel. The temperature ( $T$ ) was varied from 25 to 120 °C (5 °C min<sup>-1</sup>) at a frequency of 10 rad s<sup>-1</sup> with the shear strain of 1%.

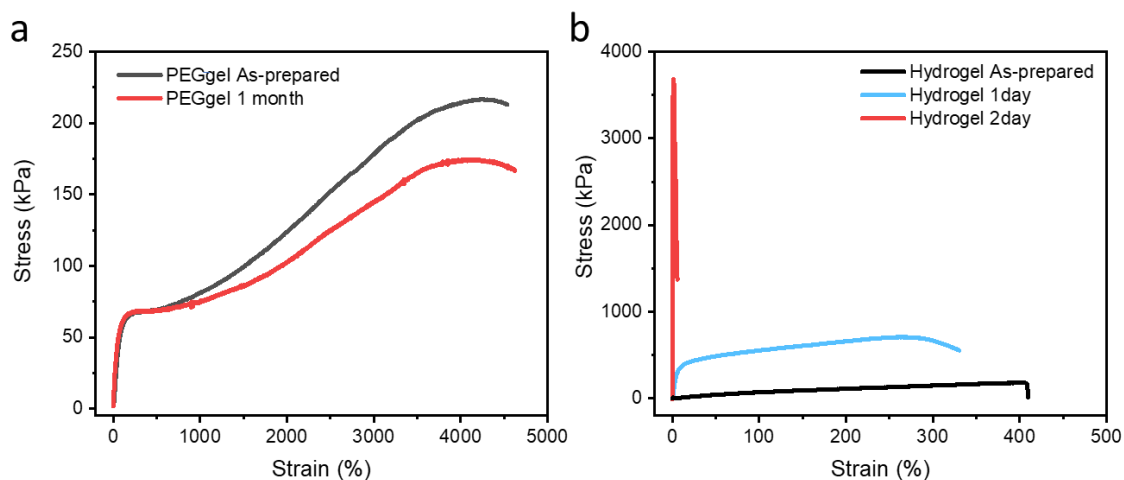


**Figure S1-5.** a) Photograph of the transparent PEGgel placed on paper with a colored logo. b) Transmittance spectrum of the PEGgel polymerized in situ in standard cuvettes. Average transmittance: >95%.

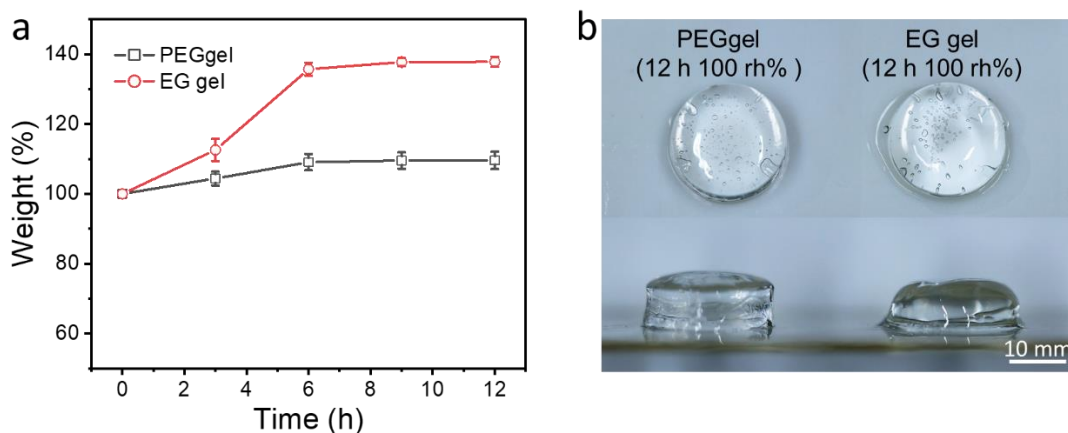




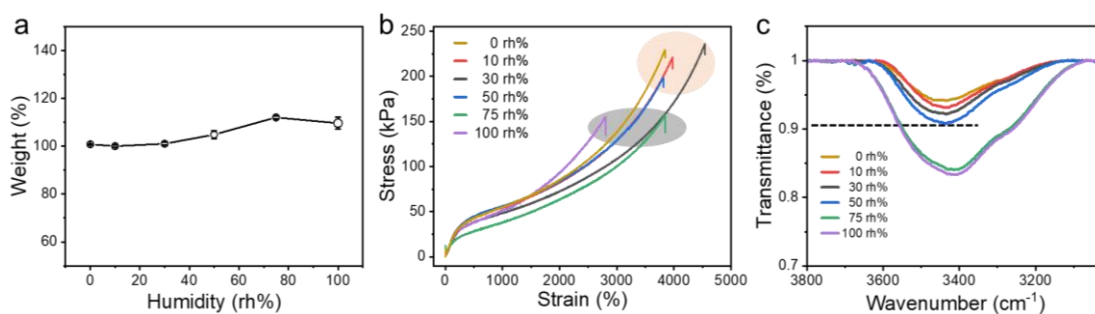
**Figure S1- 6.** The weight change of hydrogel and PEGgel with the same polymer network (copolymer of hydroxyethyl methacrylate and acrylic acid, P(HEMA-co-AAc)) and solvent ratio 50%) measured over 30 days. After storage in air (25 °C, 50% relative humidity), the P(HEMA-co-AAc) hydrogel lost flexibility and broke on bending. In contrast, P(HEMA-co-AAc) PEGgel (HAP) retained flexibility for >1 month.



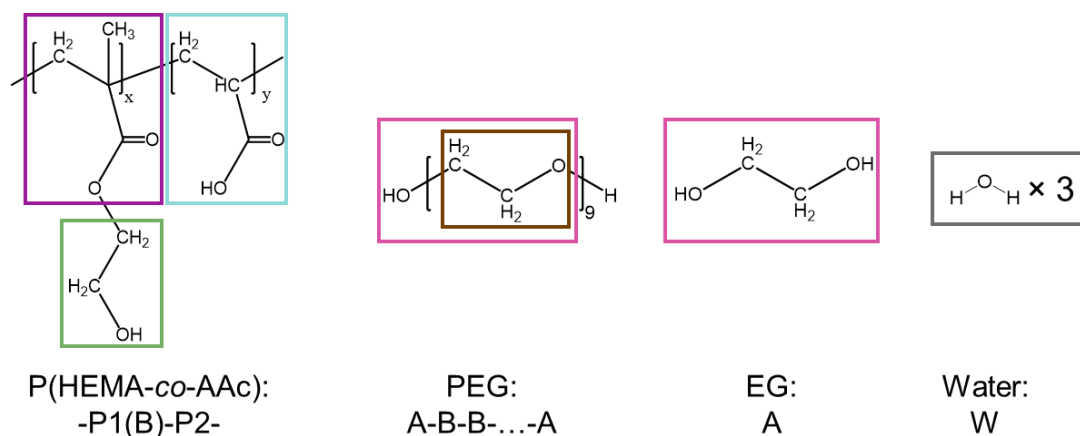
**Figure S1- 7.** Representative tensile stress-strain curves of PEGgel (a) and hydrogel (b) as prepared and after storage at room temperature and 50% relative humidity for different time periods.



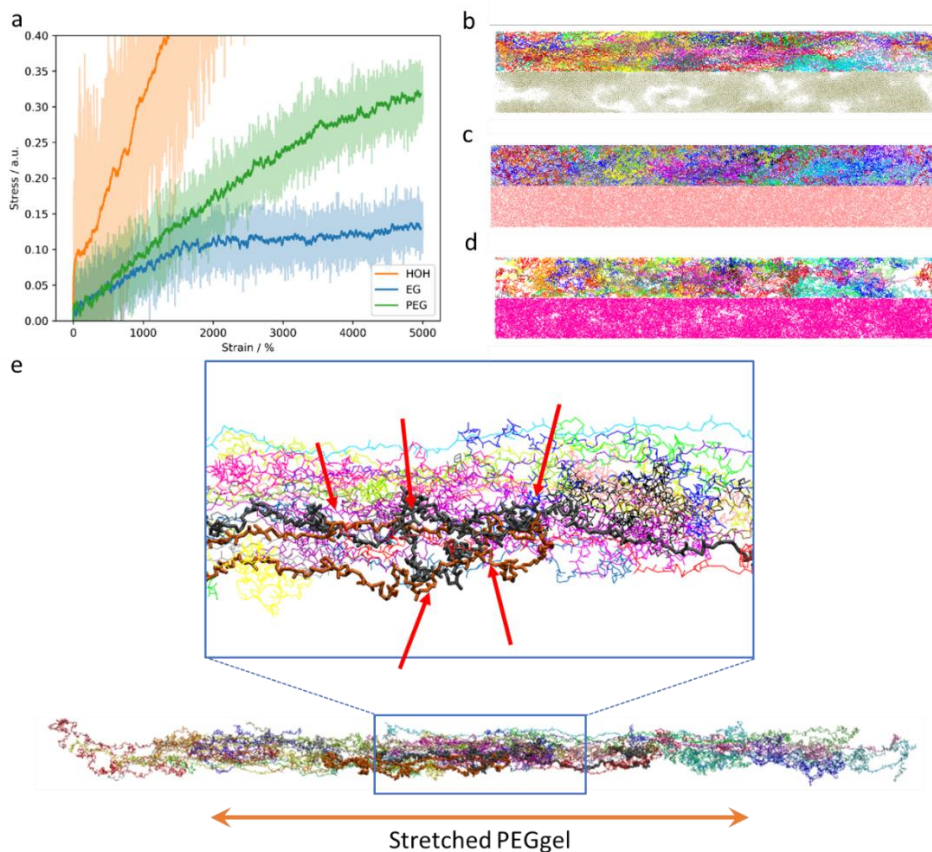
**Figure S1-8.** a) The weight change of PEGgel and EG gel under saturated water vapor environment. Five samples were stored at 25 °C for 12 h, whose weight were measured every three hours. b) photographs of PEGgel and EG gel after storage at saturated water vapor environment for 12 h. the shape of PEGgel was still sharp, while the EG gel lost its edge and behaved more like a fluid.



**Figure S1-9.** a) The weight change of PEGgel with different relative humidity environment. For each relative humidity environment, five samples were stored at 25 °C for 12 h, to ensure water vapor is fully absorbed. b) Representative tensile stress-strain curves of PEGgels after storage at 25 °C and various relative humidity for 12 h. c) FTIR analysis of PEGGels after storage at 25 °C and various relative humidity for 12 h.



**Figure S1-10.** Schematic illustration of the coarse-grained molecular dynamics model. The polymer chains consist of two-component P1-B HEMA monomers and one-component P2 AAac monomers. EG is represented as a single type A CG bead. Three water molecules are grouped into a type W bead, and PEG is represented as a short chain of type A-B-...-A beads.



**Figure S1-11.** a) Strain-stress calculation from the CGMD simulation. The transparent shade corresponds to the raw stress-strain data and the thick lines correspond to the moving average. Side views of the snapshots of stretching in the coarse-grained molecular dynamic simulations performed for a) hydrogel, b) EG gel and c) PEGgel. The polymer network (upper panel) is colored per polymer chain and the solvents (lower panel) are color-coded to correspond with the scheme. For the hydrogel and the PEGgel, the non-homogeneous distribution of the polymer networks is represented by the highly populated versus vacant areas for the polymer network as well as the solvent distribution. d) A snapshot of the polymer entanglement in the PEGgel under external strain. When the polymer network is stretched (indicated by the orange arrows), the individual polymer chains reorganize in the PEGgel (the polymer chains are color-coded per chain; the PEG solvent is omitted for clarity). In the magnified diagram, the chains highlighted in black and brown become entangled at certain sites (indicated by the red arrows). These figure come from the CGMD simulation done by Modan Liu and Elaheh Sedghamiz from Wolfgang Wenzel Group at the Institute of Nanotechnology, KIT as a part of the collaborative project.

**Table S1-10.** Componential contributions to the interaction potential of the steric effect, the hydrogen bonds, and the covalent bonds. P-P: interaction among (both intra- and inter chain interactions) P(HEMA-co-AAc) chains; P-S: Interaction between P(HEMA-co-AAc) chain and solvent molecules; S-S: interactions among solvent molecules.

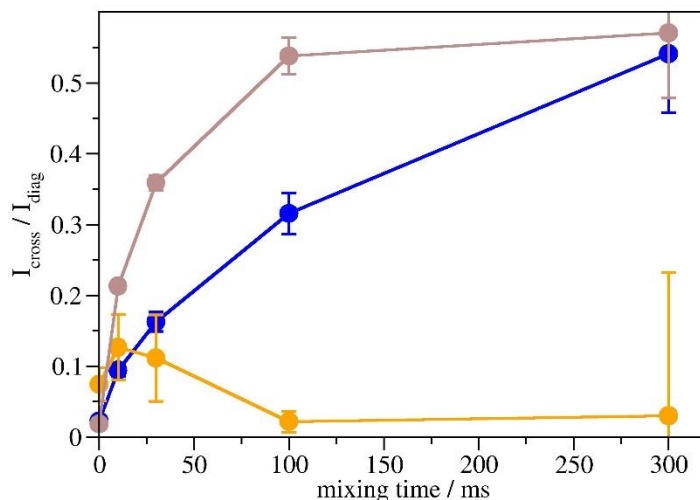
<b>Energy contributions (<math>\epsilon_{CG}</math>)</b>	<b>Hydrogel</b>	<b>EG gel</b>	<b>PEGgel</b>
the steric effect	0.1382	0.1044	0.0873
the steric effect P-P	0.0325	0.0117	0.0162
the steric effect P-S	0.025	0.0482	0.0278
the steric effect S-S	0.0807	0.0445	0.0433
<b>Hydrogen bonds</b>	<b>49.75</b>	<b>14.37</b>	<b>12.715</b>
Hydrogen bonds P-P	7.1	7.1	9.9
Hydrogen bonds P-S	10.8	3.72	1.52
Hydrogen bonds S-S	31.85	3.55	1.295
<b>O-H...O</b>	<b>42.3</b>	<b>9.15</b>	<b>5.151</b>
O-H...O P-P	3.05	3.08	4.3
O-H...O P-S	7.4	2.57	0.55
O-H...O S-S	31.85	3.5	0.301
<b>C-H...O</b>	<b>7.45</b>	<b>5.22</b>	<b>7.564</b>
C-H...O P-P	4.05	4.02	5.6

### 3.Results and Discussion

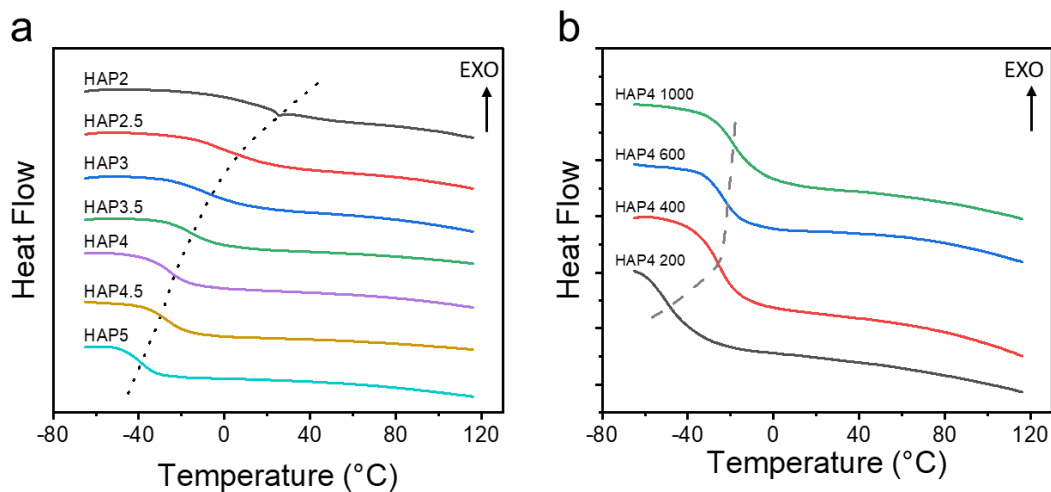
C-H...O P-S	3.4	1.15	0.97
C-H...O S-S	0	0.05	0.994
<b>Covalent bonds</b>	<b>0.235</b>	<b>0.242</b>	<b>0.478</b>
Covalent bonds P-P	0.235	0.242	0.237
Covalent bonds S-S	0	0	0.241

**Table S1-11.** Contour lengths for polymer-polymer entanglement.  $L_{pp}$  refers to the average number of polymer units in units of the monomer size  $\lambda_{CG}$  where the chain needs to bend to avoid another chain. The shorter the contour length, the larger the entanglement.

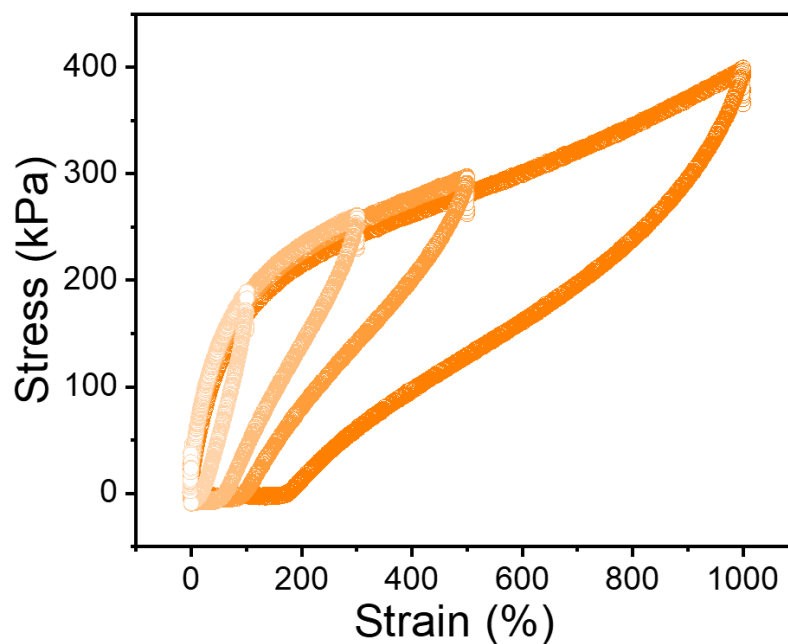
Solvent	Contour length $L_{pp}$ ( $\lambda_{CG}$ )
Water	43.40
EG	47.45
PEG	40.48



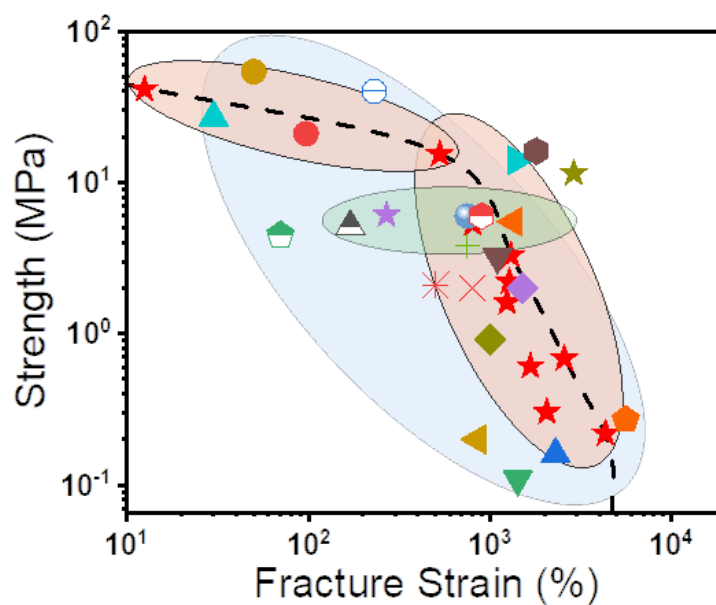
**Figure S1-12.** Build-up curves of the intensity of the cross peak connecting signals at 1.1 ppm and 2.4 ppm from hydrogel (blue), PEGgel (orange), and EG gel (gray). The ratio of the cross peak intensity (sum of the intensity of both cross peaks) and the intensity of the diagonal peaks (sum of the diagonal peaks at 1.1 ppm and 2-4 ppm) is plotted as a function of the mixing time. The intensity of the cross peaks connecting the signals at 1.1 ppm and 2.4 ppm as a function of the mixing time. Herein, the EG gel exhibits the largest cross peak intensity. It is because that using EG as a solvent increases the mobility of the polymers such that, from an NMR point of view, the system approaches a solution NMR situation. Then, cross relaxation rather than spin diffusion, could lead to nuclear overhauser effect (NOE) related cross peaks.



**Figure S1-13.** DSC spectrums of PEGgels with different PEG volume fraction (a) and different PEG molecular weight (b).



**Figure S1-14.** The representative tensile loading-unloading curves of the HAP-4 to different strains (100%, 300%, 500%, 1000%). Four cycles were continuous and without rest time. The loading-unloading speed was maintained at 100 mm/min.



**Figure S1-15.** Comparison of ultimate tensile strength versus ultimate tensile strain of PEGgel (pink) to reported tough hydrogels (blue) and elastomers (green).



**Table S1-12.** Comparison of ultimate tensile strength versus ultimate tensile strain of PEGgel to reported tough hydrogels and some elastomers.

<b>Paper</b>	<b>Materials Design</b>	<b>Fracture Strain (%)</b>	<b>Strength (MPa)</b>
This work	Oligomer Solvent	12-4336	0.2-41.3
2002. Nanocomposite Hydrogels: A Unique Organic–Inorganic Network Structure with Extraordinary Mechanical, Optical, and Swelling/De-swelling Properties	Nanocomposite	1424	0.109
2003. Double-Network Hydrogels with Extremely High Mechanical Strength	Double network	97	21
2012. Highly stretchable and tough hydrogels (Nature)	Double network	2300	0.16
2013. Physical hydrogels composed of polyampholytes demonstrate high toughness and viscoelasticity	Supramolecular structure	1500	2
2014. “Nonswellable” Hydrogel Without Mechanical Hysteresis	Ideal network	850	0.2
2015. A Novel Design Strategy for Fully Physically Linked Double Network Hydrogels with Tough, Fatigue Resistant, and Self-Healing Properties	Double network	5600	0.27
2015. Molecularly Engineered Dual-Crosslinked Hydrogel with Ultrahigh	Dual-Crosslinking	750	6

### 3.Results and Discussion

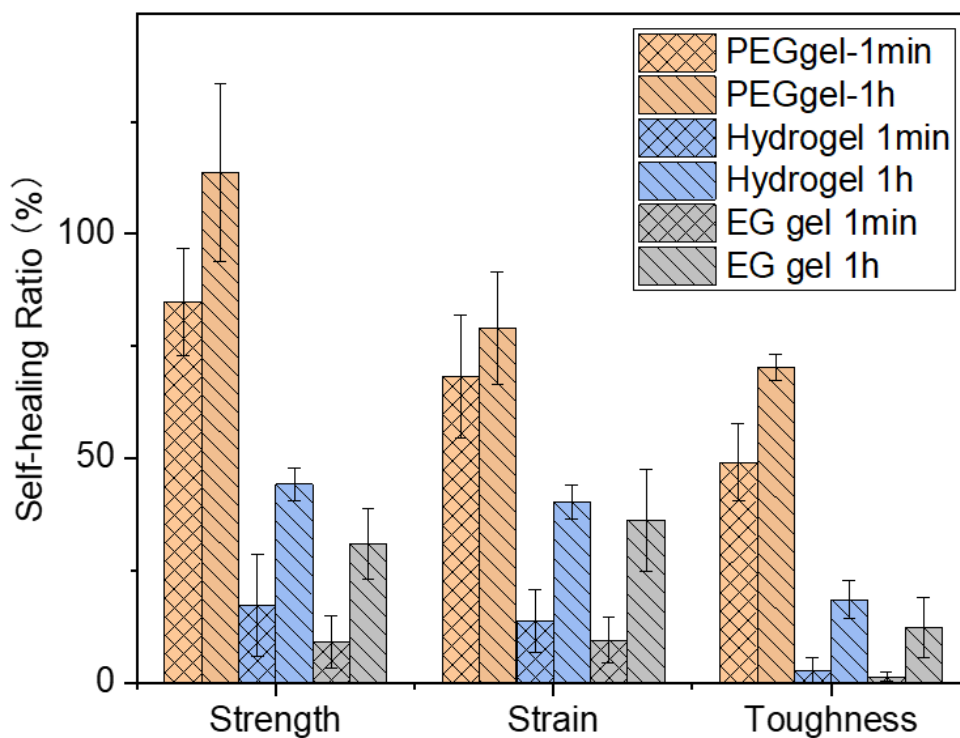
Mechanical Strength, Toughness, and Good Self-Recovery			
2015. Oppositely Charged Polyelectrolytes Form Tough, Self-Healing, and Rebuildable Hydrogels	Supramolecular structure	750	3.8
2015. Weak Hydrogen Bonding Enables Hard, Strong, Tough, and Elastic Hydrogels	Hybrid network	800	2
2016. A Universal Soaking Strategy to Convert Composite Hydrogels into Extremely Tough and Rapidly Recoverable Double-Network Hydrogels	Soaking strategy	500	2.1
2016. Freezing Molecular Orientation under Stretch for High Mechanical Strength but Anisotropic Hydrogels	Freezing Molecular Orientation	230	40
2016. High-Strength and High-Toughness Double-Cross-Linked Cellulose Hydrogels: A New Strategy Using Sequential Chemical and Physical Cross-Linking	Double Cross-Linking	70	4.5
2016. A Mineralized High Strength and Tough Hydrogel for Skull Bone Regeneration	Mineralization	269	6.1
2018. A Facile Method to Fabricate Anisotropic Hydrogels with Perfectly Aligned Hierarchical Fibrous Structures	Aligned Hierarchical Fibrous Structures	50	54
2019. Anisotropic tough multilayer hydrogels with programmable orientation	programmable orientation	30	27

### 3.Results and Discussion

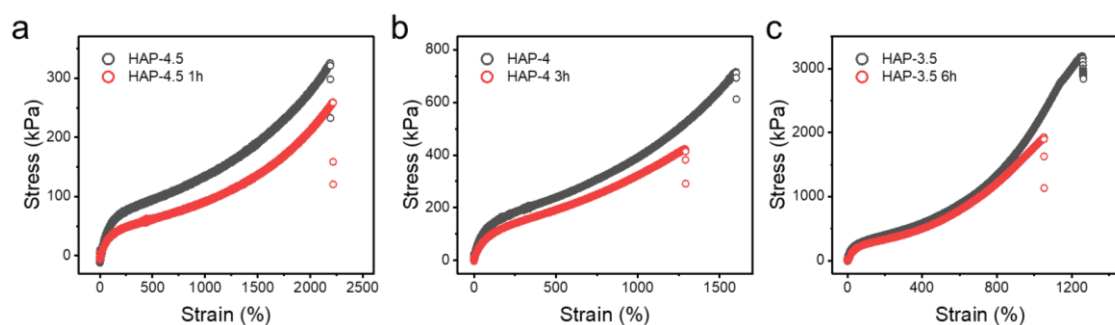
---

2021. Strong tough hydrogels via the synergy of freeze-casting and salting out	Hierarchical structures	1400	14
2021. Fracture, fatigue, and friction of polymers in which entanglements greatly outnumber cross-links	Entanglements	1100	3.2
2021. Toughening hydrogels through force-triggered chemical reactions that lengthen polymer strands	Lengthen polymer strands	1000	0.92
2021. Tough hydrogels with rapid self-reinforcement	Strain-induced crystallization	1350	5.5
1987. Uniaxial Extension and Compression in Stress-Strain Relations of Rubber	Synthetic rubber	900	6
2014. Mechanical characterization of bulk Sylgard 184 for microfluidics and microengineering	PDMS	170	5.13

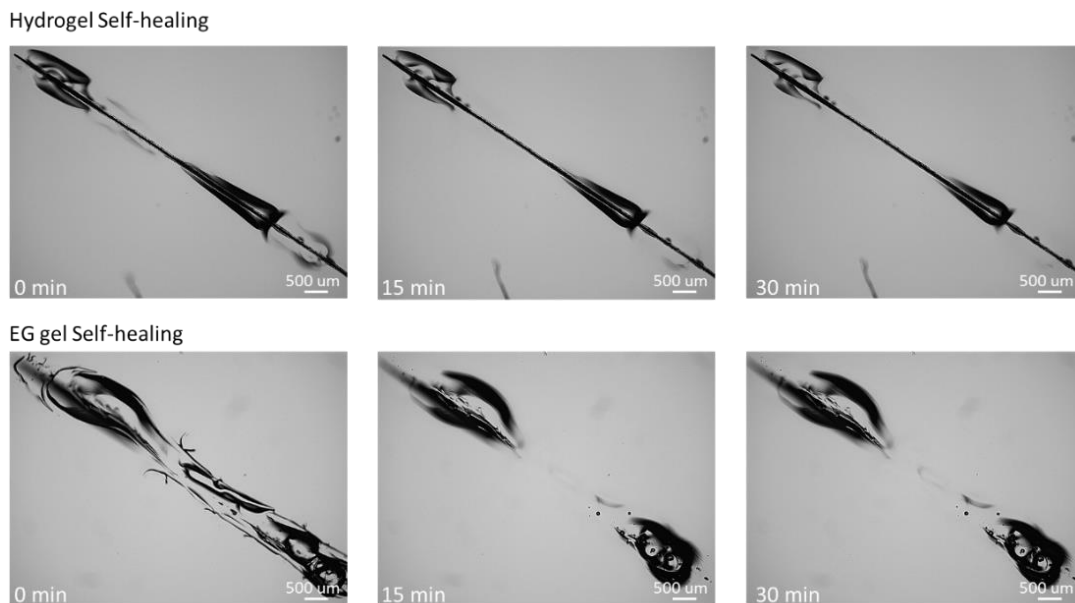
---



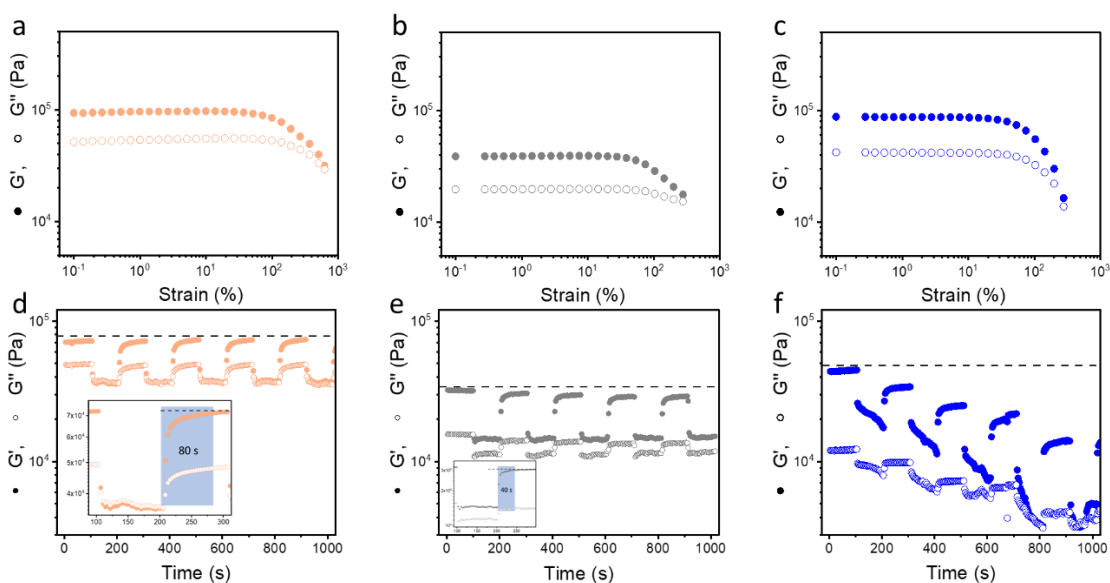
**Figure S1-16.** Self-healing ratio of hydrogel, PEGgel and EG gel on strength, strain (fracture) and toughness with different healing time.



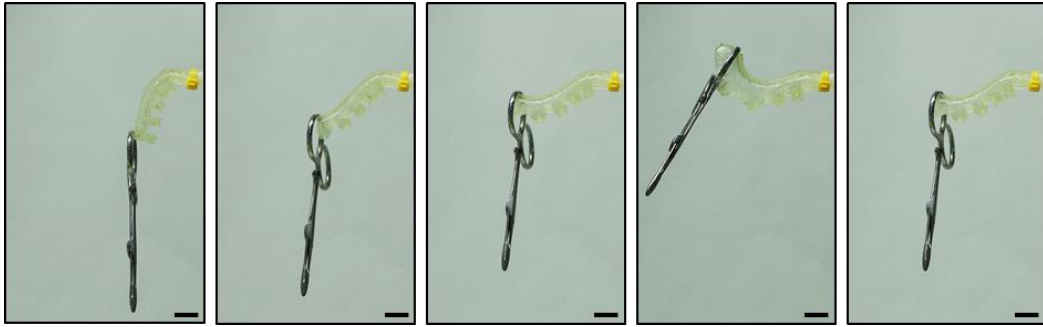
**Figure S1-17.** Representative tensile stress-strain curves of PEGgel samples with different PEG volume fraction after different healing times. Black circle is as-prepared sample, and red circle is healed sample.



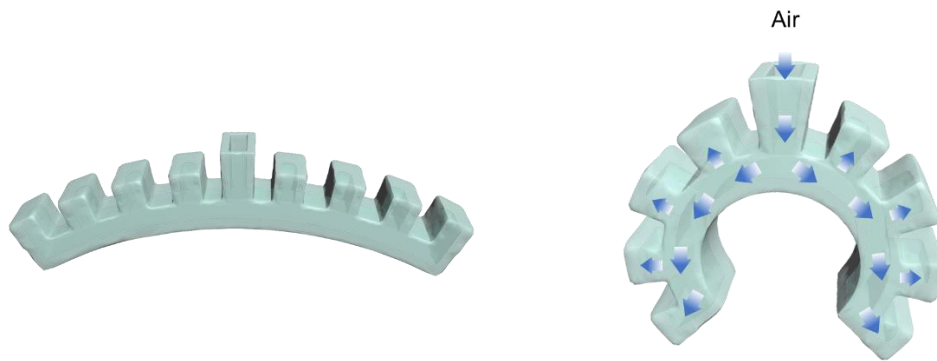
**Figure S1-18.** Partial healing of a scratch wound on the hydrogel and EG gel after 30 min. Scale bars: 500  $\mu\text{m}$ .



**Figure S1-19.** Rheology analyses of the self-healing property. The storage moduli ( $G'$ ) and loss moduli ( $G''$ ) of PEGgel (a), EG gel (b), and hydrogel (c) from strain amplitude sweep at 25  $^{\circ}\text{C}$  with frequency of 10 rad/s.  $G'$  and  $G''$  of PEGgel (d), EG gel (e), and hydrogel (f) from continuous strain sweep with alternate small oscillation force ( $\gamma = 1\%$  strain) and large one ( $\gamma = 300\%$ ) at 25  $^{\circ}\text{C}$  with frequency of 10 rad/s.



**Figure S1-20.** The 3D printed actuator used to lift a pair of steel scissors weighing 20 g. Scale bars: 5 mm.



**Figure S1-21.** Schematic diagram of a soft pneumatic actuator with two fingers for capture.

## 3.2 Ionic PEGgel

This chapter and associated sections are published in:

Wang, Z.; Lai, Y.; Chiang, Y.; Scheiger, J. M.; Li, S.; Dong, Z.; Cai, Q.; Liu, S.; Hsu, S.; Chou, C.; Levkin, P. A. Tough, Self-healing, and Conductive Elastomer --- Ionic PEGgel. *ACS Applied Materials & Interfaces* **2022**, Just Accepted, DOI: 10.1021/acsami.2c14394

### 3.2.1 Abstract

Ionically conductive elastomers are necessary for realizing human-machine interfaces, bioelectronic applications, or durable wearable sensors. Current design strategies, however, often suffer from solvent leakage and evaporation, or from poor mechanical properties. This section reports a strategy to fabricate ionic elastomers (IHP) demonstrating high conductivity ( $0.04 \text{ S m}^{-1}$ ), excellent electrochemical stability ( $> 60,000$  cycles), ultra-stretchability (up to 1400%), high toughness ( $7.16 \text{ MJ m}^{-3}$ ), fast self-healing property enabling restoration of ionic conductivity within seconds, as well as no solvent leakage. The ionic elastomer is composed of in-situ formed physically cross-linked poly(2-hydroxyethyl methacrylate) networks and poly(ethylene glycol) (PEG). The long molecular chains of PEG serve as a solvent for dissolving electrolytes, improve its long-term stability, reduce solvent leakage, and ensure the outstanding mechanical properties of the IHP. Surprisingly, the incorporation of ions into PEG simultaneously enhances the strength and toughness of the elastomer. The strengthening and toughening mechanisms were further revealed by molecular simulation. This study demonstrates applications of the IHPs as (a) flexible sensors for strain or temperature sensing, (b) skin electrodes for recording electrocardiograms, and (c) a tough and sensing material for pneumatic artificial muscles. The proposed strategy is simple, easily scalable, and can further inspire the design of novel ionic elastomers for ionotronics applications.

### 3.2.2 Introduction

Driven by the rising demand for wearable, lightweight, conformal instruments in the current Internet of Things era,<sup>172</sup> flexible electronics are developed to enable a wide variety of applications such as biomedicine,<sup>173,174</sup> healthcare,<sup>175</sup> brain-computer interfacing,<sup>176</sup> and soft robotics.<sup>139</sup> Despite significant achievements in this field,<sup>177</sup> most of the current electronic devices rely on electrons to conduct signals,<sup>178,179</sup> as opposed to biological systems which transmit information mostly using ions.<sup>180,181</sup> Ionically conductive soft materials or ionically conductive elastomers (ICE) bridge the gap between humans and machines on both mechanical and electrical properties,<sup>131,182</sup> and could thus revolutionize human-machine interfaces and flexible electronics.<sup>183-186</sup> To meet the stringent requirements of soft machines, ICEs have to possess ionic conductivity, excellent mechanical properties (high toughness, thermal stability, etc.), or even self-healing property.<sup>187-190</sup>

Currently, the major strategy to design ICEs is based on embedding elastomer networks into liquid electrolytes, such as electrolyte salts dissolved in polar solvents<sup>191</sup> or ionic liquids.<sup>192</sup> The resulting ICEs, such as ionic hydrogels and ionic liquid gels,<sup>41</sup> typically have a high ionic conductivity but suffer from leakage of liquids and solvent evaporation. In solvent-infused ICEs, the elastic polymer network is embedded in liquid ionic electrolytes. This feature guarantees the continuity of the conductive phase during deformation. However, on the other hand, too many solvated ionic electrolytes fail to be effectively bonded with polymer networks and thus give rise to instability or poor performance, like electrolyte leakage. To overcome these problems, solvent-free systems were developed by mixing electrolyte salts with monomers and further polymerizing to obtain flexible polymer networks.<sup>189</sup> In such systems, ions are directly bound to the polymer network through electrostatic interactions or metal-ligand coordination rather than solely serving as mobile charge carriers.<sup>187,189,190</sup> However, the choice of polymer networks for solvent-free ICEs is limited by the low solubility of electrolytes in potential monomers or polymers. Also, without solvents, the ionic conductivity of most solvent-free ICEs is lower than  $0.02 \text{ S m}^{-1}$ .<sup>193</sup> Thus, there is room for improvements to increase the versatility of materials and the performance of corresponding devices (Table S1-4).

Inspired by both advantages and drawbacks of current strategies, balancing the interactions between the ionic electrolyte, the solvent, and the elastic network appears to be a promising



strategy to improve the performance of ICEs. Previously, a polymer gel in which PEG served as solvent (PEGgel) was developed, presenting tunable mechanical properties, fast self-healing property, and remarkable stability under ambient conditions.<sup>69</sup> PEG is a good solvent for various electrolytes giving it excellent ionic conductivity, as evidenced by its extensive use in the field of solid polymer electrolytes in battery research.<sup>194</sup> However, solid electrolytes solely based on PEG usually show poor mechanical properties due to the absence of elastic network components.<sup>195</sup> PEG was also blended with other elastic polymers and electrolytes for ICE fabrication.<sup>196</sup>

This study hypothesized that adding electrolytes into the PEGgel system could create an ICE,<sup>197</sup> in which the electrolyte, solvent (PEG), and the polymer networks are dynamically, non-covalently, but strongly bound together. This would merge the advantages of both liquid-infused and liquid-free ICEs, i.e., no solvent leakage or evaporation, 3D printability, as well as excellent mechanical and electrical properties. Additionally, PEGgels are inherently self-healing, a desirable property for producing long-lasting electronic devices. Using the above strategy, this study fabricated both tough and self-healing ICE (Figure 18a), which demonstrated simultaneous improvement of the toughness and strength after the introduction of cations (including Li<sup>+</sup>, Na<sup>+</sup>, K<sup>+</sup>, and the choline cation). Such simultaneous improvement of toughness and strength is usually exclusive to material design. The mechanism of this interesting behavior was revealed by molecular simulation, providing a valuable concept for future ICE design. This study further showed 3D printability, high transparency, ultra-stretchability (up to 1400%), high toughness (7.16 MJ m<sup>-3</sup>), as well as fast self-healing of ion-conductivity. Examples of application of the developed material as wearables, skin electrodes for recording electrocardiograms or for creating artificial muscles with sensing properties demonstrate the potential of this concept and material in ionotronics.

### 3.2.3 Result and Discussion

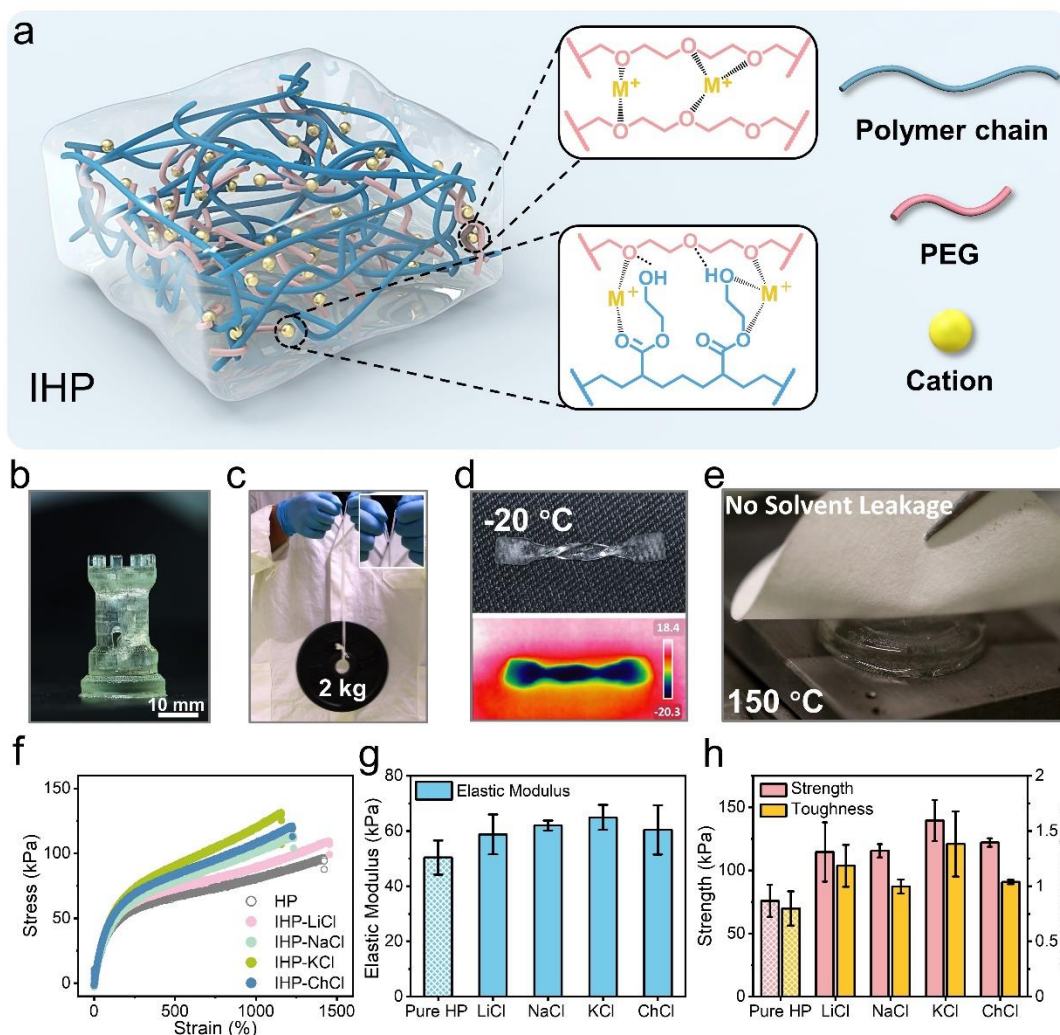
#### 3.2.3.1 *Concept of Ionic PEGgels*

In a typical preparation process, 3 mol kg<sup>-1</sup> of lithium chloride (LiCl) was dissolved in PEG 400 at 90°C. LiCl was chosen for its high solubility in PEG.<sup>198</sup> 2-Hydroxyethyl methacrylate and Irgacure 1173 were dissolved in the LiCl PEG solution in defined ratios (Table S1-1). The prepolymer solutions were cured in a polytetrafluoroethylene mould by UV irradiation (366 nm, 5 mW cm<sup>-2</sup>) for 30 min at room temperature. The polymerization completion was confirmed by Fourier transform infrared spectroscopy (Figure S2-1). IHP does not contain chemical cross-linkers but forms a physically cross-linked network based on hydrogen bonds, ionic coordination, and entanglements among poly(2-hydroxyethyl methacrylate) (PHEMA) and PEG.<sup>199</sup> Wide-angle X-ray scattering (WAXS) was used to investigate the microstructure of the IHP (Figure S2-2a). It confirms that IHP has an amorphous structure at room temperature with no diffraction peaks other than the amorphous halo. This indicates that LiCl is fully dissolved in the PEG rather than crystallization. Due to its amorphous structure, the obtained IHP possesses high transmittance > 95% in the visible spectrum (400-760 nm) (Figure S2-2b). Stretched IHP (300% strain) becomes almost invisible in front of a colored background (Figure S2-3a). This high transparency is essential for applications of conductive elastomers as transparent actuators or sensors requiring good optical transparency.<sup>200,201</sup> With the help of PEG as the solvent, IHP presented superior 3D printability in Figure 18b, where a towel with a spiral staircase inside was built.

After introducing 3 mol kg<sup>-1</sup> of LiCl into the polymer network, an IHP rod (cross-section: 15 mm × 3 mm) could withstand a 2 kg barbell plate without fracture (Figure 18c). Interestingly, IHP maintained its flexibility at -20°C and sustained twisting without breaking, demonstrating satisfying mechanical performance even at low temperatures (Figure 18d). At a high temperature (100°C), physically cross-linked IHP was able to lift and maintain its shape (Figure S2-3b), resulting from the strong physical cross-linking and non-volatility of PEG. From tensile stress-strain curves of IHPs at different temperatures, fracture strains above 1200% (1250% at -20°C, 1300% at 25°C, and 1640% at 100°C) were determined (Figure S2-3c). Furthermore, the solvent leakage test was applied to IHPs (Figure 18e, Figure S2-4, and Movie S2-1), showing no leakage at room temperature and 150°C. Even after continuous compression (50% strain, 10000 cycles) and tensile (100% stain, 10000

cycles) loading-unloading performed at room temperature and around 50% relative humidity over 36 h, the weight of IHP remained almost the same with the as-prepared status (Figure S2-5). This demonstrates that the obtained IHP can operate under a wide range of working temperatures resulting from the stable solvent and strong non-covalent interactions between the polymer network and PEG as solvent.

To show the generality and versatility of this ICE design strategy, a series of IHPs containing 0.1 mol kg<sup>-1</sup> of LiCl, NaCl, KCl, or choline chloride (ChCl) were prepared (Figure 18f). All IHPs showed higher modulus, strength, and toughness than the PHEMA PEGgel (HP) without added salts. With the change in the salt types, the elastic modulus increased from 50.4 ± 6.2 kPa (HP) to 58.8 ± 7.2 kPa (IHP-LiCl), 62.0 ± 1.8 kPa (IHP-NaCl), and 65.0 ± 4.5 kPa (IHP-KCl), reflecting stronger interpolymer chain interactions (Figure 18g). The strength and toughness increased from 75.9 ± 12.7 kPa and 0.80 ± 0.16 MJ m<sup>-3</sup> (HP), to 114.6 ± 23.5 kPa and 1.18 ± 0.19 MJ m<sup>-3</sup> (IHP-LiCl), 115.6 ± 5.2 kPa and 0.99 ± 0.06 MJ m<sup>-3</sup> (IHP-NaCl), 139.6 ± 16.3 kPa and 1.38 ± 0.30 MJ m<sup>-3</sup> (IHP-KCl), respectively (Figure 18h). Interestingly, for all cases, even small amounts (0.1 mol kg<sup>-1</sup>) of salts added to HP enhanced both strength (>50%) and toughness (>25%). Often, strength and toughness are mutually exclusive properties: stronger materials tend to be more brittle, whereas materials with lower strength can be deformed to a larger extent and thus tend to be tougher, i.e., can dissipate more energy before breaking.<sup>202</sup> Besides inorganic salts, the organic salts choline chloride was found to give a similar enhancement of the strength and toughness (60% and 30%, respectively), which indicates the generality of this strategy.



**Figure 18.** Overview of the IHPs. a) Illustration of the mechanism of enhancement of mechanical properties of IHP through the metal cation. b) Image of a 3D-printed tower with a spiral staircase inside based on IHP. c) Image demonstrating the remarkably high strength of the IHP (3 M LiCl, 35 mm × 15 mm × 3 mm), by sustaining a dumbbell (2 kg). d) Top: Image demonstrating the mechanical stability under extreme temperatures (twisted at -20°C). Bottom: Image from a thermal camera at the same time. e) Image demonstrating the no solvent leakage of the IHP under 150 °C, in which the paper retained dry after peeling from the IHP surface. Representative tensile curves (f), elastic modulus (g), strength, and toughness (h) of IHPs with different salt types at 0.1 mol kg<sup>-1</sup>. Error bars represent standard deviation (n = 3).

3.2.3.2 *Mechanical and electrochemical properties of Ionic PEGgels*

Besides the diversity of the current ICE design strategy, further performance improvement is also accessible. By increasing the molar concentration of salts, the mechanical properties of IHP can be enhanced (Figure 19a). When increasing the concentration of LiCl from 0 to 3.0 mol kg<sup>-1</sup>, the strength of the IHP increased from 0.08 ± 0.01 MPa (HP) to 1.18 ± 0.13 MPa (IHP-3) (Figure 19b) and the toughness increased from 0.80 ± 0.16 MJ m<sup>-3</sup> (HP) to 7.16 ± 1.05 MJ m<sup>-3</sup> (IHP-3). Notably, both the strength and toughness of the IHP increased (roughly 14.7 and 8.9 times, respectively) with increasing content of LiCl, breaking the trade-off between strength and toughness again. Upon the introduction of LiCl into HP, the elastic modulus could be tuned from 50 kPa (HP) to 177 kPa (IHP-3), achieving a 3.5-fold increase (Figure S2-6a). Such an increase may stem from the strong ionic coordination between Li<sup>+</sup> and the side groups of polymer chains such as hydroxyl and ester groups, which is confirmed by FT-IR in Figure S2-7. However, the fracture strain remained almost constant at around 1400%, exhibiting only 9.5% fluctuations (Figure S2-6b). For pursuing higher strength and toughness, the fraction of PEG in IHP-3 was tuned (Figure S2-6c and S2-6d). When the fraction of PEG decreased from 50 wt% to 30 wt%, the strength and toughness increased from 1.18 MPa and 7.16 MJ m<sup>-3</sup> to 10.04 MPa and 16.99 MJ m<sup>-3</sup> respectively. The strength of the resulting material is higher than that of the previously reported solvent-free ICE (7.6 MPa).<sup>189</sup>

The differential scanning calorimetry (DSC) analysis confirmed the same phenomenon, where the T<sub>g</sub> of the IHP increased from -51.0°C (HP) to -23.5°C (IHP-3), respectively (Figure S2-8). Notably, the DSC curves of all IHPs presented a smooth trend after their glass transition without any sharp endothermic or exothermic peaks until 150°C. The thermal stability was further confirmed by thermogravimetric analysis (TGA). As evident from Figure S2-9, the TGA plots of IHP-3 presented a negligible weight loss (< 3%) up to 250°C, demonstrating a wide operation window from -23.5 to 250°C. On the other hand, the mechanical properties IHP reversibly change upon heating or cooling (Figure S2-3).

The addition of ions also significantly enhanced the recovery property of the IHPs. The continuous cyclic tensile test was performed to evaluate the mechanical recovery of HP and IHP-3. As shown in Figure 19c, the second (300% strain), third (500 % strain), and fourth (1000%) loading curves overlap, indicating an immediate recovery of the network to the

original state despite the energy dissipation during loading. Without the toughening effect of ions, HP could only present fast recovery after 100% strain in a cyclic tensile test. After 300% strain, the damage to HP is irreversible (Figure S2-10a). Moreover, HP demonstrates a larger hysteresis than IHP-3, demonstrating its inability to recover the energy dissipation occurring during the loading-unloading cycles fully. The rapid recovery of IHP-3 is likely attributed to the reversible and dynamic interactions between the polymer chains and Li<sup>+</sup> cations, which can be ruptured to dissipate energy upon loading, followed by rapid reforming.

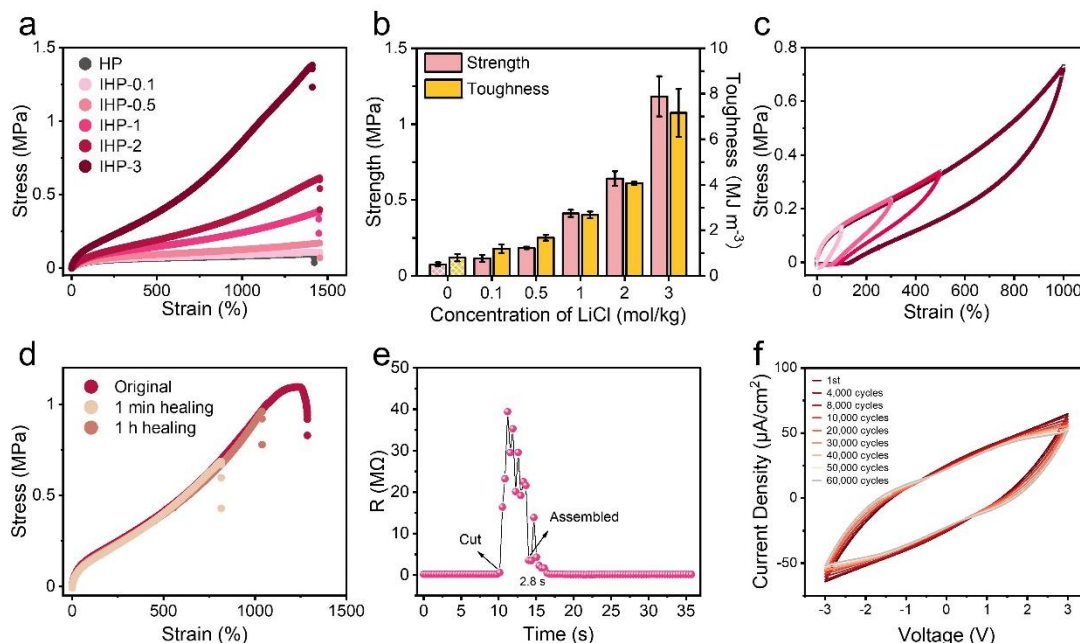
Additionally, robust and tough IHP-3 showed good self-healing abilities (Figure 19d), owing to the mobility of polymer chains and multiple interactions (e.g., hydrogen bonds, ion coordination) between polymer chains and PEG. When the sample was cut into two separate pieces, which were gently brought back into contact, polymer chains could diffuse across the interface over time and form entanglements or bonds with the network on the other side, thereby mechanically healing the cut sample in ambient conditions. The healing efficiency, defined as the ratio between the work required to break the healing joint and that required to break the virgin sample by tensile deformation, reached 38% after 1 min healing and 63% after 1 h healing. Without ion restrictions, HP owned the higher flexibility of PEGs and PHEMA chains than IHP, showing faster self-healing property (68% self-healing ratio after 1 min). In comparison, the self-healing ratio of HP was still 68% after healing for 1 h (Figure S2-10b). This result demonstrates that introducing ions into HP slightly reduced the flexibility of PEGs and PHEMA chains, but did not reduce the overall self-healing ability of IHP.

The ionic conductivity is the most important property of ICEs, but is often traded off for acceptable mechanical properties. In our system, adding LiCl enhanced the mechanical properties and increased the ionic conductivity of IHP. Herein, the conductivity was measured with the alternating current impedance method in ambient conditions and determined by  $C = T/(S \times R_b)$ , with T being the sample thickness, S the area of the sample, and R<sub>b</sub> the bulk resistance (Figure S2-11). Since the ionic conductivity is typically proportional to the effective number of mobile ions, the ionic conductivity of the IHPs increases from  $1.13 \times 10^{-4} \text{ S m}^{-1}$  (HP) to  $0.04 \text{ S m}^{-1}$  (IHP-3) upon the increase of the concentration of LiCl from 0 to  $3.0 \text{ mol kg}^{-1}$ . Even when the PEG fraction decreased to 40 wt%, the ionic conductivity was still  $0.01 \text{ S m}^{-1}$  (Figure S2-11f). To determine the

environmental influence on the performance of IHP, its ionic conductivity was measured for different conditions (Figure S2-12). After being stored in ambient conditions (around 50 % relative humidity and 25°C) for 7 days, the ionic conductivity of IHP-3 increased to 0.06 S m<sup>-1</sup> owing to the absorption of water. After drying IHP -3 in a vacuum, the conductivity of IHP-3 decreased to 0.005 S m<sup>-1</sup>. After being stored in 100 % relative humidity for 12 h, the ionic conductivity of IHP-3 further increased to 0.29 S m<sup>-1</sup>. This conductivity is close to those of most live tissues (0.01-3 S m<sup>-1</sup>), making the IHPs suitable for use as flexible and wearable ionotronics related to the human body.<sup>203</sup>

The real-time resistance changes of IHP-3 were recorded during cutting, assembling, and self-healing (Figure 19e). After cutting, the resistance of IHP-3 immediately increased from 188 kΩ to 40 MΩ as expected for an open circuit. After bringing the two parts of IHP-3 together, the resistance dropped to 197 kΩ after only 2.8 s, showing rapid self-healing of the conductivity of the material after damage. Cyclic voltammetry was used to demonstrate the electrochemical stability of IHP-3. The current density of IHP-3 under large scanning voltage ( $\pm 3$  V, 500 mV s<sup>-1</sup>) remained 90% after 10,000 cycles and 81% after 60,000 cycles (Figure 19f).

In summary, introducing ions into HP results in extraordinary mechanical versatility in terms of high stretchability (1400%), satisfying self-healing (68% at 1 h), and quick self-recovery. Importantly, both the strength and the toughness of the IHPs increase by increasing the concentration of LiCl, improving by a factor of 14.7- and 8.9-times, respectively. Also, IHP presents its rapid self-healing in ion-conducting (2.8 s) and displays outstanding electrochemical stability. Self-healing of the mechanical performance and conductive properties is necessary to maintain the performance and to lengthen the lifetime of ionotronic devices, which are often subject to external damages such as stretches or cuts. Thus, IHP is a very promising ionically conductive material for human-compatible flexible devices,<sup>112</sup> such as wearable sensors, electronic skin, and soft robots.<sup>162</sup>



**Figure 19.** Mechanical and electrochemical properties of IHPs. a) Representative stress-strain curves of IHPs with different LiCl concentrations, in which IHP-x corresponds to HP with x mol kg<sup>-1</sup> LiCl. b) Strength and toughness of IHPs with different LiCl concentrations. Error bars are standard deviations (n = 3). c) Continuous cyclic tensile loading-unloading curves of IHP-3 with strain going to 100%, 300%, 500%, and 1000%. d) Representative stress-strain curves of IHP-3 with increasing healing time after the cut. e) Resistance change of IHP-3 during the cut and assembling process. f) Cyclic linear sweep voltammetry curves of the IHP-3 with a scanning speed of 500 mV s<sup>-1</sup> after 60,000 cycles.

### 3.2.3.3 Molecular dynamics simulation of PEGgels and Ionic PEGgels

(The following simulation was performed by Yu-Cheng Lai and Ya-Tang Chiang from Chia-Ching Chou Group at the Institute of Applied Mechanics, College of Engineering, National Taiwan University as a part of the collaborative project.)

To understand the ion-induced improvement of the mechanical properties, molecular dynamics (MD) simulation was used to investigate the molecular structure of HP and IHP. Details about the applied model can be found in the Materials and Methods part. Firstly, the influence of PEG on Li<sup>+</sup>-cations was evaluated in terms of the radius of gyration ( $R_g$ ), which provides an understanding of polymer structure under a microscopic system. After introducing Li<sup>+</sup>-cations into HP, the average  $R_g$  of PEG chains decreased from 7.4 Å to 5.0



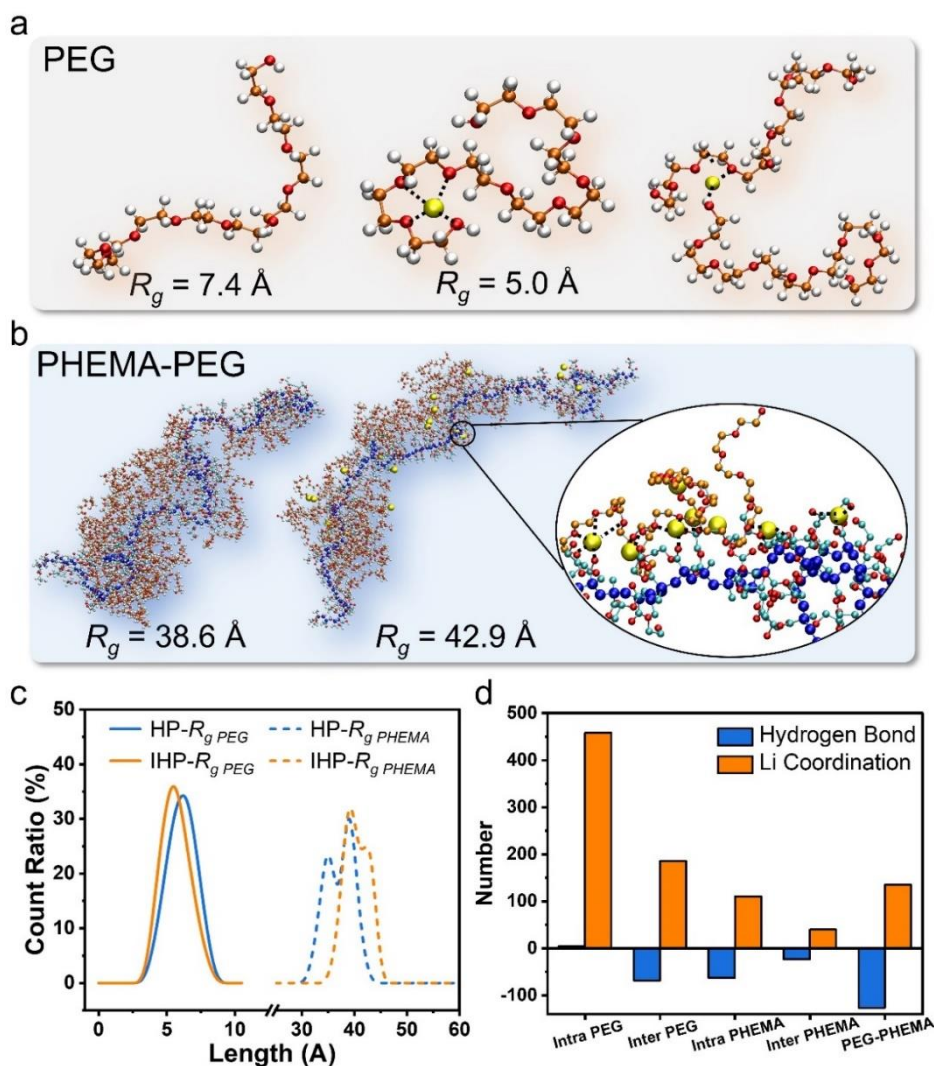
Å, due to strong coordination bonds between Li<sup>+</sup>-cations and O atoms in the PEG chains. The PEG in the presence of Li<sup>+</sup> ions behaved more compactly than the one without Li<sup>+</sup> (Figure 20a and Movie S2-2), since coordination between Li and O is much stronger than hydrogen bonds.<sup>204,205</sup> In the presence of Li<sup>+</sup>, the end-to-end distance ( $L_{e-e}$ ) of PEGs, a basic mechanical parameter quantifying the expansion of a polymer, decreased from 18.5 Å (HP) to 7.8 Å (IHP) (Figure S2-13c). The decreased  $L_{e-e}$  implies PEGs were curlier and more fixed in IHP than those in HP. In addition, the coordination of Li<sup>+</sup> between two PEGs was observed, which efficiently dissipates energy during deformation.

In contrast, Li<sup>+</sup>-cations had the opposite effect on PHEMA (Figure 20b and 20c and Movie S2-3). The  $R_g$  of PHEMA increased from 38.6 Å (HP) to 42.9 Å (IHP), which makes the PHEMA chains more relaxed. Similarly,  $L_{e-e}$  of PHEMA increased from 114.1 Å (HP) to 137.4 Å (IHP), showing a higher expansion and potentially higher flexibility with the presence of Li<sup>+</sup>. To explain the opposite effects on PEG and PHEMA, the numbers of PEG molecules around each PHEMA chain within a radius of 3 Å in HP and IHP were evaluated and compared. These PEG molecules serve as a bridge between PEG phase and PHEMA chains. The number of PEG molecules around each PHEMA chain in IHP was 43% lower than the number in HP (Figure S2-14). Less PEG molecules around the PHEMA directly reduced restrictions on PHEMA, making it more stretched out and flexible. The reason for the decrease in the number of PEG molecules around PHEMA can be summarized as: 1) PEG molecules attracted by Li<sup>+</sup>-cations were less likely to form hydrogen bonds with PHEMA; 2) Li<sup>+</sup>-cations, serving as an inserter, maintained a certain distance between the oxygen atoms in order to form coordination bonds and reach the lowest energy point. Without coordination bonds, hydrogen bonds were the dominant interactions between the molecules, and the length of the oxygen at both ends of the hydrogen bond is about 3 Å; after forming coordination bonds, the average distance between the oxygen atoms increased to 3.5 Å. Therefore, once Li ions are presented between PEG and PHEMA, the chances for PEG to form hydrogen bonds with PHEMA may reduce, leading to fewer PEG chains around PHEMA in IHP.

To further explain the difference in mechanical properties between HP and IHP, the hydrogen bonds and coordination bonds were counted (Figure 20d). After adding Li<sup>+</sup>-cations, most hydrogen bonds were replaced by Li-O coordination. The number of coordination bonds formed between PEG-PEG, PHEMA-PEG, and PHEMA-PHEMA was larger than

the number of hydrogen bonds lost. Even more, the potential energy of a single Li-O coordination bond is higher than a single hydrogen bond. Thus, the coordination bonds replaced corresponding hydrogen bonds, providing more energy with IHP to enhance strength efficiency.

In summary, the weak hydrogen bonds were replaced by strong Li-O coordination bonds after the introduction of lithium ions, even with a slight increase in numbers. Based on these numerous and stronger Li-O coordination bonds, the IHP presents higher strength than HP. Then, due to the energy difference between Li-O coordination bonds and hydrogen bonds, the number of PEGs around PHEMA chains reduced, making PHEMA chains more flexible, which maintains the large deformation during tensile. The IHP successfully addressed the trade-off between strength and toughness based on these two changes.



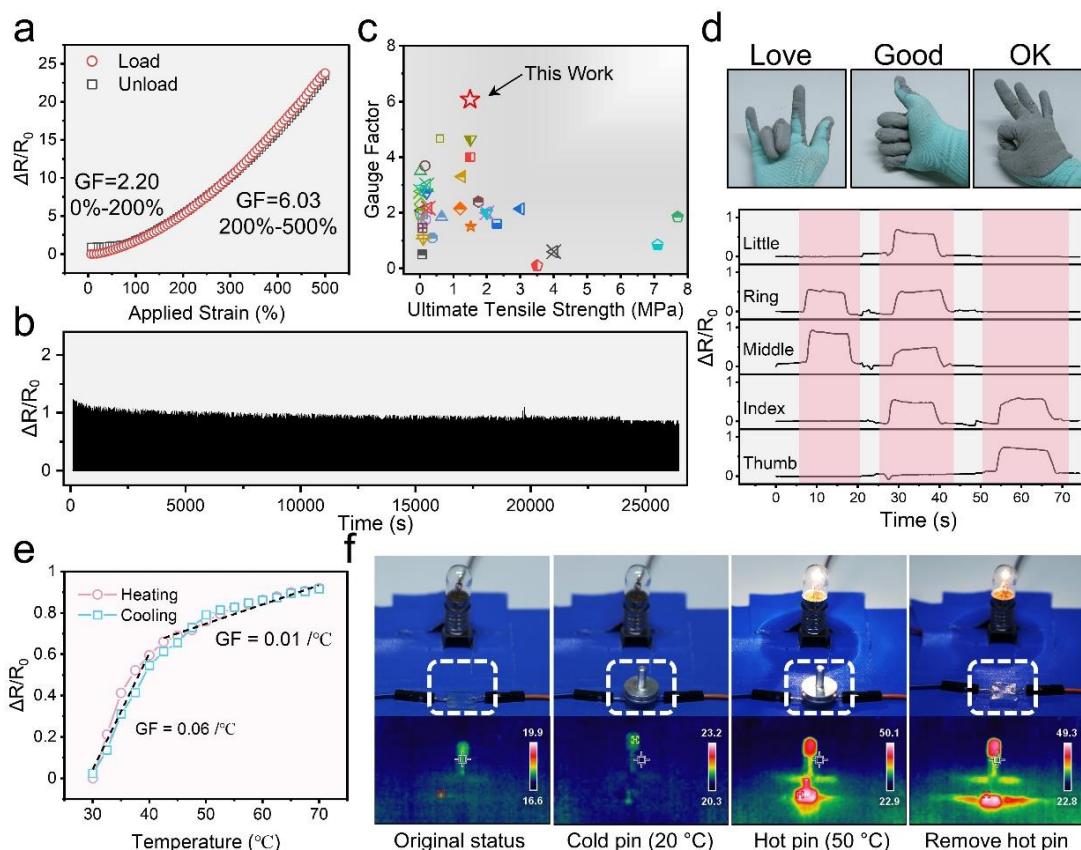
**Figure 20.** Molecular dynamics simulation of HP and IHP. Representative snapshots for PEG molecule (a) and PHEMA polymer chain (b) in HP and IHP. In PEG molecules, the orange spheres are carbon atoms, white spheres are hydrogen atoms, and red spheres are oxygen atoms. In PHEMA polymer chain, the blue spheres are carbon atoms, red spheres are oxygen atoms, and deeper blue spheres are the backbone carbon atoms of the PHEMA. Hydrogen atoms of PHEMA are not displayed due to their simplicity. Yellow spheres are Li cations. c) Distribution of the radius of gyration ( $R_g$ ) of PEG (solid line) and PHEMA (dotted line) in HP (blue) and IHP (orange). d) The number change of hydrogen bond (blue) and Li coordination (orange) in HP and IHP, containing intra PEG, inter PEG, intra PHEMA, inter PHEMA, and PEG-PHEMA. These results come from the simulation, which is performed by Yu-Cheng Lai and Ya-Tang Chiang from Chia-Ching Chou Group at the Institute of Applied Mechanics, College of Engineering, National Taiwan University as a part of the collaborative project.

#### 3.2.3.4 *Sensing property of Ionic PEGgels*

The excellent mechanical properties and good conductivity of IHP make it a promising soft material for applications as flexible sensors. Figure 21a presents the relative change in resistance of IHP-3 (3 mol kg<sup>-1</sup> LiCl),  $\Delta R/R_0$ , as a function of the applied tensile strain up to 500%. When the strain was applied, the resistance of IHP increased accordingly, whereas releasing the strain restored the resistance to the original value, indicating the feasibility of IHP-3 on a reliable strain sensor. The reliable and repeatable sensing ability of IHP-3 was further demonstrated by measuring the relative resistance change,  $\Delta R/R_0$ , for 1500 cyclic loading-unloading cycles (0-100% strain) (Figure 21b). After 1500 loading-unloading cycles, the  $\Delta R/R_0$  remained about 100% for 100% strain. The sensitivity or gauge factor (GF) is defined as  $GF = (\Delta R/R_0)/\varepsilon$ , where  $\varepsilon$  is the applied strain. IHP showed a sensitivity of 2.2 at 0-200% strain, rapidly increasing to 6.03 at 200-500% strain. The performance of IHP-3 strain sensor in this work was compared with other reported strain sensors based on self-healing ionic elastomers. The two key parameters, GF and strength, were used to evaluate the performance: the former presents the precise signal capture, and the latter means stability during operation. As shown in Figure 21c, the IHP-3 strain sensor developed in this work outperforms most strain sensors based on self-healing ionic elastomers (Table S1-3).

To further demonstrate the potential of IHP-3 as wearable sensors, IHP-3 was directly attached to the skin to monitor diverse human activities. An IHP-3 sensor was fixed onto the index finger of a volunteer. Bending of the index finger by 30°, 60°, and 90° stretched the IHP-3 sensor to different extents, which resulted in a repeatable resistance change ratio of 30%, 60%, and 120% (Figure S2-15), respectively, which were quantitatively correlated to bending angles. To further illustrate the application of such strain sensors for strain sensing capability, the sensors were implemented onto a glove to detect human hand gestures (Figure 21d). Specifically, five strain sensors were mounted on a commercial fabric glove near the joints to maximize the deformations upon bending (Figure S2-16). Besides strain sensing, IHP-3 can work as a pressure sensor with compression mode. An unprecedented linear increase in  $\Delta R/R_0$  was observed upon increasing the pressure from 0 to 100 kPa, which offers high signal capture and transformation accuracy. As shown in Figure S2-17, IHP demonstrated good recovery during 500 kPa loading-unloading cycles, and a stable GF at 0.24% kPa<sup>-1</sup> during 0-100 kPa.

Additionally, IHP presented a temperature sensing property, owing to the resistance change ratio being a function of the temperature from 30 °C to 70 °C during the heating and cooling processes (Figure 21e). The resistance change ratio of the hydrogel dramatically raised with increasing temperature and decreased during the cooling process, showing almost consistent trends of resistance change. During a heating-cooling cycle, the trend of resistance change can be divided into two regions, with a sensitivity of 0.06 °C<sup>-1</sup> during 30°C - 40°C and 0.01 °C<sup>-1</sup> during 40°C - 70°C. The obtained sensitivity is much higher than that of previously reported temperature sensors based on soft materials.<sup>206-210</sup> Here, the thermal sensing property of IHP comes from the mobility change of ions upon temperature variation, which was confirmed by the increasing ionic conductivity of IHP with temperature rise (Figure S2-18). The cyclic heating-cooling processing was also measured on IHP-3 (Figure S2-19). After 50 heating-cooling cycles from 30°C to 50°C, the thermal sensing property was still maintained effective as the original. The temperature sensing performance can be understood as follows: Elevated temperatures lead to a greater segmental motion of polymer chains, facilitating ion transport and reducing resistance.<sup>189</sup> Then, IHP was connected to a circuit with a DC power supplier and a light bulb (Figure 21f, and Movie S2-4). Without external stimulus, the light bulb emitted a faint light, indicating a stable and low current loop on the cold pin. After putting a hot pin (50°C) on the surface of IHP, the light bulb instantly lighted up due to the temperature-induced decrease of the resistance. When the hot pin was removed, the temperature of IHP was still about 50°C, maintaining the brightness of bulb.



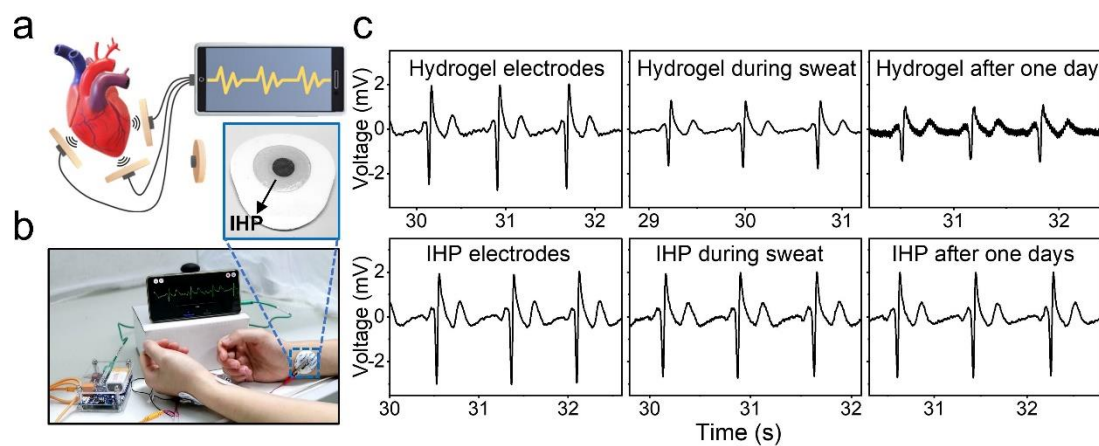
**Figure 21.** Sensing properties of IHPs. a) Dependence of relative resistance change on the applied tensile strain for IHP-3. b) relative change of resistance of IHP-3 upon cyclic tensile loading/unloading tests (0-100% strain) over 1500 times. c) Comparison of IHP-3 with previously reported strain sensors based on self-healing ICE, in terms of gauge factor and ultimate tensile strength. The hollow red pentacle represents this work. d) IHP-3 were integrated into gloves for detecting human hand gestures. The relative changes of the resistance of five fingers depending on the hand pose were used to convert sign language into an electric signal (left to right: “Love”, “Good” and “OK”). e) the relative change of the resistance of IHP-3 in dependence of the temperature during 30°C - 70°C. f) Images of light bulb controlled by the temperature sensor with putting cold or hot metal pin and removing the pin.

### 3.2.3.5 Ionotronics based on IHPs

To further explore the feasibility of IHP for flexible devices, IHP (0.1 mol kg<sup>-1</sup> KCl) was used as flexible electrodes for ECG signal capture and compared to hospital-grade gel electrodes (Meditrace 450 Foam Electrodes, Kendall) in Figure 22a. Both of two types of

electrodes were attached to the same locations (wrists of both hands and the back of the left hand), as shown in Figure 22b. The ECG signal collected by both electrodes under normal condition, during sweating, and after one day were investigated and compared in Figure 22c. The ECG signals attained with IHP electrodes were comparable to those of the commercial hydrogel electrodes (Figure 22c, left). During sweating, the ECG signals recorded by IHP electrodes remained relatively consistent with those recorded under normal conditions. A dampened ECG signal was observed based on the hydrogel electrodes, resulting from sweat pooling which decreased the contact area between the hydrogel and the skin. Since PEG serves as a solvent in IHP, sweat is absorbed by IHP and minimally affects the physical appearance of IHP electrodes, which is confirmed visually (Figure S2-20). Furthermore, the durability of these two types of electrodes was compared after one day. The ECG signals attained with IHP electrodes were relatively consistent over time. In contrast, the signal based on the hydrogel decreased significantly after one day and presented a high signal-noise ratio. The impedance of hydrogel and IHP electrodes under these three conditions was also investigated (Figure S2-21), which shows similar changes. During the sweating and after one day, the impedance of the hydrogel electrode increased more than 100 times compared with the fresh one. For IHP, the impedance remained almost the same under different conditions. Compared with the commercial hydrogel electrodes, IHP electrodes presented similar acquisition capability, better moisture resistance, and better durability, showing potential in health-related applications such as monitoring and diagnosis.

Moreover, the IHP-3 was fabricated into a pneumatic artificial muscle with sensing ability as shown in Figure S2-22a, showing the potential application in soft robotics. IHP-3 was used to seal up an open tube, deforming in response to changes in gas pressure from the tube. The IHP-3 was stretched during inflating and recovered in response to inhaling. The flexibility and high strength of IHP-3 offer a repeatable deformation to the obtained pneumatic artificial muscle (Figure S2-22b). Due to the strain sensing property of IHP-3, the action of device can be transmitted into resistance change. As shown in Figure S2-22c, when the tube was inflated, the IHP-3 was stretched, presenting an increased resistance. While the tube was pumped out, the resistance of IHP-3 decreased to the original values. Then, a hanging ring was cast onto the IHP-3 membrane for lifting objects. The pneumatic artificial muscle was able to lift a weight of 200 g, which is more than 20 times its weight (Figure S2-22d, Movie S2-5).



**Figure 22.** Ionotronics based on IHPs. a) A schematic of ECG signal real-time monitor, including flexible electrodes and intelligent display terminal. b) Photograph of the IHP electrodes attached to the skin for achieving ECG signal capture and display. c) ECG signals recorded based on commercial hydrogel electrodes (top row) and IHP electrodes (bottom row) under normal conditions (left), during sweating (middle), and after one day (right).



#### 3.2.4 Materials and Methods

##### 3.2.4.1 *Materials*

2-hydroxyethyl methacrylate, sodium chloride, potassium chloride, and Irgacure 1173 were purchased from Sigma-Aldrich (Darmstadt, Germany). Poly ethylene glycol ( $M_w = 400 \text{ g mol}^{-1}$ ), lithium chloride, and choline chloride were purchased from Thermal Fisher (Schwerte, Germany). All chemicals were used as received.

##### 3.2.4.2 *Preparation of Ionic PEGgels*

All samples were prepared via UV-induced one-pot sequential polymerization. Various salts and PEG were firstly mixed and stirred at  $90^\circ\text{C}$  for 12 h, obtaining transparent and uniform solutions. Then, monomers, photo initiator were added into the obtained PEG and mixed in brown bottles. After stirring through a vortex for 1 min, a clear prepolymer solution was obtained. And all of samples are initiated under 366 nm UV light ( $5 \text{ mW cm}^{-2}$ ) for 30 min. The specific prepolymer compositions are shown in Table S2-1 and S2-2. Without external explanation, IHP-3 presents PEGgel based on poly(2-hydroxyethyl methacrylate) with  $3 \text{ mol kg}^{-1}$  of lithium chloride. The maximum LiCl concentration in PEG400 was found to be around  $3 \text{ mol kg}^{-1}$ .

##### 3.2.4.3 *Mechanical Characterization*

The samples were tested by using AGS-X Universal tester (Shimadzu Inc., Japan). Three samples were prepared for each tensile experiment. For tensile tests, the tested samples are shaped into dumbbell with 1-2 mm thickness, 2 mm width and 8 mm length. The tensile speed was set at  $100 \text{ mm min}^{-1}$ . The self-healing efficiency is calculated by dividing toughness of healed samples by the toughness of original samples. Three samples were tested as parallel samples.

##### 3.2.4.4 *Material Characterization*

All IR measurements were performed on a Bruker Alpha II ATR-IR from  $400\text{-}4000 \text{ cm}^{-1}$  at  $25^\circ\text{C}$ . The transmission of samples was measured using a UV-Vis spectrometer (Lambda 35, Perkin Elmer) with a wavelength range of 400-800 nm. The thickness of the samples is  $300 \mu\text{m}$ . Three samples were tested as parallel samples, and every sample was scanned 24

times. The Differential scanning calorimetry (DSC) measurements were performed on a TA DSC 2500 instrument, in a sealed 40  $\mu$ L aluminium crucibles under nitrogen atmosphere. Samples with 3 - 5 mg were analyzed by using a heat/cool/heat cycle with a heating or cooling rate of 20  $^{\circ}\text{C min}^{-1}$ . In this cyclic thermal measurement, the samples were heated from -90  $^{\circ}\text{C}$  to 150  $^{\circ}\text{C}$ , then cooled to -90  $^{\circ}\text{C}$  and reheated to 150  $^{\circ}\text{C}$ . The glass transition temperature ( $T_g$ ) was determined in the second heat run to eliminate possible interference from the polymer's thermal history.

#### 3.2.4.5 *Electrochemical Measurement*

Impedance spectra of IHPs were performed in frequency ranging from  $10^5$  to 0.1 Hz under amplitude of 10 mV utilizing Reference 1010 (Gamry). The ionic conductivity was tested a configuration of stainless steel / IHP / Stainless steel. The measurement of ionic conductivity was conducted at 25  $^{\circ}\text{C}$ , following the equation  $C = T / (R_b \times S)$ , where  $R_b$  represented the bulk resistance according to impedance spectra, T represented the thickness of samples and S was the area of the stainless steel. Three samples (diameter of 10 mm and thickness of 2 mm) were tested at room temperature as parallel samples.

Sensing properties were tested with LCR Meter (LCR-6100, RS) and AGS-X Universal tester. Universal tester controlled the applied pressure and strain, while LCR Meter recorded the resistance in real-time during loading/unloading (potential: 1V). The size of strain and pressure sensor was 10  $\times$  5  $\times$  3 mm. For the temperature sensing, samples were clamped by the metal clip, and connected to the LCR meter. The size of sensing part was 10  $\times$  7  $\times$  3 mm. The temperature sensors were immersed in silicon oil for uniform and rapid temperature conduction (also for isolating the water). For temperature sensing curve, every temperature point was recorded after holding for 10 min at corresponding temperature. Heating-cooling cycles were achieved by transferring sensors between two oil baths (one was 30  $^{\circ}\text{C}$ , and the other one was 55  $^{\circ}\text{C}$ ). Without specific explanation, all samples were tested after polymerization immediately. All the experiments related to the human body were processed on Z. Wang.

#### 3.2.4.6 *Molecular dynamics simulation*

##### *Model Building*

In this study, molecular dynamics simulation is used to investigate the molecular structure of PEG-PHEMA organgel in the pure and LiCl solution and the effect of LiCl on the interaction between the polymers to link the mechanical properties at the macro scale. All simulations were carried out using full atomistic models. Two models were built in this research: a pure model contains PEG and PHEMA, while the other one contains PEG, PHEMA, Li<sup>+</sup> and Cl<sup>-</sup>. In LiCl model, optimized polymer structures of one 9-mer PEG and one 100-mer PHEMA were built by Winmostar V10.2.4<sup>216</sup> and were set as replicate unit. Next, 323 PEG polymers, 10 PHEMA polymers and Li<sup>+</sup>, Cl<sup>-</sup> ions with concentration of 3 M were packed into a 150 Å x 150 Å x 150 Å cube using PACKMOL.<sup>217</sup> Each polymer or ion is oriented at least 2 Å apart from each other. In the final step, pure model was obtained by removing Li<sup>+</sup> and Cl<sup>-</sup> ions from LiCl model. The initial model of our simulation is shown in Figure S2-13a and S2-13b.

All force field parameters were built using the general Amber force field (GAFF),<sup>218</sup> which has been repeatedly tested to be compatible on PEG<sup>219-222</sup> and PHEMA.<sup>223,224</sup> The cutoffs for van der Waals (vdW) potentials and short-range electrostatic interactions were set to 10 Å. The Particle-Particle-Particle-Mesh (PPPM) method<sup>225</sup> was used to recover long-range electrostatic interactions. Antechamber<sup>226</sup> was used to assign electrostatic point charges on polymers by the AM1-BCC method,<sup>227,228</sup> a charge scheme suggest by GAFF.<sup>218</sup> This GAFF/AM1-BCC method has been widely used in small molecules and polymers.<sup>229-232</sup> As for Li<sup>+</sup> and Cl<sup>-</sup> ions, charges were set as +1 and -1. Molecular dynamics simulations were performed using Large-scale Atomic/Molecular Massively Parallel Simulator (LAMMPS).<sup>233</sup> The equations of motion were integrated using the velocity-Verlet algorithm with a timestep of 1 fs. The model was equilibrated at NPT ensemble at 1 atmosphere and 300K for 20ns to achieve the fully relaxed systems. The Nose-Hoover temperature thermostat and pressure barostat for NPT simulations was used with a damping relaxation time of 0.1ps and 1ps respectively. Equilibrium state was check by the stableness of density, volume, and root-mean-square distance (RMSD). After equilibrium, a 10 ns NPT MD simulation under same condition is carried out for data collection. Visual molecular dynamics program (VMD)<sup>234</sup> was used for visualizations and further postprocessing analysis.

#### *Polymer structure and flexibility*

Two characteristic lengths, end-to-end distance, and radius of gyration,<sup>235</sup> were selected to analysis the structure and flexibility of a single polymer. End-to-end distance,  $\langle L_{e-e} \rangle$ , is calculated by measuring the distance between head atom and tail atom. Radius of gyration,  $\langle R_g \rangle$ , was called a more reasonable measure of polymer size because changes in  $\langle R_g \rangle$  do not change the conditionally expected shape from spherical, while changes in  $\langle R \rangle$  do<sup>236</sup>. Three characteristic lengths' formulae are list in (1) ~ (3).

$$\langle R \rangle = \langle |r_{\text{head}} - r_{\text{tail}}| \rangle \quad (1)$$

$$\langle R_g^2 \rangle = \frac{\sum_{i=1}^N \langle (r_i - \bar{r})^2 \rangle}{N} \quad (3)$$

Where  $r_{\text{head}}$ ,  $r_{\text{tail}}$  represent the position of head atom and tail atom,  $w_i, r_i$  represents the mass and position of the i-th atom, and  $\bar{r}$  is the center of mass of the polymer. The distribution of three characteristic lengths were plot and analysis to determine the effect of LiCl to polymers.

#### *Definition of Hydrogen bond and Lithium-Oxygen coordinate bond*

Hydrogen bond in our work is counted if matches two conditions: (1) The distance between acceptor and donor is smaller than 3 Å (2) The angle between donor, hydrogen and acceptor is larger than 150 degree.<sup>237</sup>

For the Lithium-Oxygen coordinate bond, one must satisfy that the distance between Lithium ion and oxygen atom should be smaller than 2.4 Å. According to Shannon's experiment,<sup>238</sup> average Lithium-Oxygen distance is 2.159 Å. Therefore, a cutoff which is larger than the average value is selected due to the oscillating of atoms in our simulation.

## 3.2.5 Supporting Information

**Table S2-1.** Prepolymer composition of ionic poly(2-Hydroxyethyl methacrylate) PEGgel (IHP) based on LiCl.

	HP	IHP-0.1	IHP-0.5	IHP-1	IHP-2	IHP-3
PEG400 (g)	1	1	1	1	1	1
HEMA (g)	1	1	1	1	1	1
I1173 ( $\mu\text{L}$ )	5	5	5	5	5	5
LiCl (mg)	0	4.2	21	42	84	126

**Table S2-2.** Prepolymer composition of IHPs with various salts.

	IHP-LiCl	IHP-NaCl	IHP-KCl	IHP-ChCl
PEG400 (g)	1	1	1	1
HEMA (g)	1	1	1	1
I1173 ( $\mu\text{L}$ )	5	5	5	5
Salt (mg)	4.2 (LiCl)	5.8 (NaCl)	7.5 (KCl)	14.0 (ChCl)

### 3.Results and Discussion

**Table S2-3.** Summary of strain sensors based on self-healing ICE, in terms of gauge factor and ultimate tensile strength.

Paper	Ultimate Tensile Strength (MPa)	Sensitivity	Reference
<b>This Work</b>	1.5	6.03	
<b>2020</b> -Transparent Stretchable Dual-Network Ionogel with Temperature Tolerance for High-Performance Flexible Strain Sensors	2.3	1.6	239
<b>2019</b> -A transparent, stretchable, stable, self-adhesive ionogel-based strain sensor for human motion monitoring	0.017	3.5	240
<b>2020</b> - A facile strategy for fabricating multifunctional ionogel based electronic skin	0.056	1.6	241
<b>2019</b> - Self-Healing, Adhesive, and Highly Stretchable Ionogel as a Strain Sensor for Extremely Large Deformation	0.035	20	242
<b>2020</b> -Transparent, mechanically robust, and ultrastable ionogels enabled by hydrogen bonding between elastomers and ionic liquids	1.75	2.4	41
<b>2020</b> -Mechanically Robust, Elastic, and Healable Ionogels for Highly Sensitive Ultra-Durable Ionic Skins	1.52	1.51	243
<b>2020</b> - Robust Physically Linked Double-Network Ionogel as a Flexible Bimodal Sensor	0.37	1.1	244
<b>2021</b> -3D Printable, Highly Stretchable, Superior Stable Ionogels Based on Poly(ionic liquid) with Hyperbranched Polymers as Macro-cross-linkers for High-Performance Strain Sensors	0.25	2.77	245
<b>2019</b> -Highly Stretchable, Fatigue-Resistant, Electrically Conductive, and Temperature-Tolerant Ionogels for High-Performance Flexible Sensors	0.036	2.08	246
<b>2021</b> -Flexible, transparent, and antibacterial ionogels toward highly sensitive strain and temperature sensors	3.5	0.1	247
<b>2020</b> -Ionoskins: Nonvolatile, Highly Transparent, Ultrastretchable Ionic Sensory Platforms for Wearable Electronics	0.2	2.72	248
<b>2021</b> - Ultra-Sensitive and Stretchable Ionic Skins for High-Precision Motion Monitoring	0.204	3	249
<b>2021</b> - Adaptive Ionogel Paint from Room-Temperature Autonomous Polymerization of $\alpha$ -Thioctic Acid for Stretchable and Healable Electronics	2	2	250
<b>2021</b> - Highly Stretchable and Reconfigurable Ionogels with Unprecedented Thermoplasticity and Ultrafast Self-Healability Enabled by Gradient-Responsive Networks	0.1	1.07	251
<b>2019</b> -Highly Stretchable Organogel Ionic Conductors with Extreme-Temperature Tolerance	0.048	2.86	252

### 3.Results and Discussion

<b>2019-</b> Transparent, Highly Stretchable, Rehealable, Sensing, and Fully Recyclable Ionic Conductors Fabricated by One-Step Polymerization Based on a Small Biological Molecule	0.152	3.69	211
<b>2021-</b> Highly Transparent, Stretchable, and Conductive Supramolecular Ionogels Integrated with Three-Dimensional Printable, Adhesive, Healable, and Recyclable Character	1.51	4.64	253
<b>2021-</b> Self-Adhesive, Stretchable, Biocompatible, and Conductive Nonvolatile Eutectogels as Wearable Conformal Strain and Pressure Sensors and Biopotential Electrodes for Precise Health Monitoring	1.2	2.15	254
<b>2021-</b> Highly Stretchable, Transparent, and Self-Adhesive Ionic Conductor for High-Performance Flexible Sensors	0.09	1.95	255
<b>2021-</b> A novel strategy for fabricating highly stretchable and highly conductive photoluminescent ionogels via an in situ self-catalytic cross-linking reaction in ionic liquids	0.02	1.93	256
<b>2019-</b> Highly stretchable and nonvolatile gelatin-supported deep eutectic solvent gel electrolyte-based ionic skins for strain and pressure sensing	0.067	0.5	257
<b>2021-</b> A Mechanically Robust and Versatile Liquid-Free Ionic Conductive Elastomer	1.5	4	189
<b>2021-</b> Self-healing, anti-freezing and highly stretchable polyurethane ionogel as ionic skin for wireless strain sensing	3	2.14	258
<b>2020-</b> Polymeric Complex-Based Transparent and Healable Ionogels with High Mechanical Strength and Ionic Conductivity as Reliable Strain Sensors	7.7	1.85	259
<b>2019-</b> Transparent and stretchable triboelectric nanogenerator for self-powered tactile sensing	0.17	1.76	260
<b>2020-</b> 3D Printable Strain Sensors from Deep Eutectic Solvents and Cellulose Nanocrystals	1.25	3.3	261
<b>2020-</b> Hierarchically Crosslinked Gels Containing Hydrophobic Ionic Liquids towards Reliable Sensing Applications	2	2	262
<b>2017-</b> Patternable transparent and conductive elastomers towards flexible tactile/strain sensors	0.08	1.45	61
<b>2021-</b> Underwater Communication and Optical Camouflage Ionogels	0.6	4.67	263
<b>2021-</b> Block Copolymer-Based Supramolecular Ionogels for Accurate On-Skin Motion Monitoring	0.65	1.85	264
<b>2018-</b> Extremely Stretchable, Stable, and Durable Strain Sensors Based on Double-Network Organogels	0.03	2.3	265
<b>2021-</b> Multifunctional Liquid-Free Ionic Conductive Elastomer Fabricated by Liquid Metal Induced Polymerization	0.25	2.17	190

### 3.Results and Discussion

**Table S2-4.** Summary of recently reported ionic conductive elastomers, in terms of ultimate tensile strength, conductivity, 3D printability, transparency and self-healing.

Paper	Ultimate Tensile Strength (MPa)	Conductivity (S/m)	3D-printability	Transparency	Self-healing	Type
This Work	10.04	0.04	yes	0.95	0.68	PEG as Solution
<b>2020</b> -Transparent Stretchable Dual-Network Ionogel with Temperature Tolerance for High-Performance Flexible Strain Sensors	2.3	0.102	no	0.93	no	Ionic Liquid
<b>2019</b> -A transparent, stretchable, stable, self-adhesive ionogel-based strain sensor for human motion monitoring	0.017	0.015	yes	0.93	no	Ionic Liquid
<b>2020</b> - A facile strategy for fabricating multifunctional ionogel based electronic skin	0.056	0.049	no	0.9	no	Ionic Liquid
<b>2019</b> - Self-Healing, Adhesive, and Highly Stretchable Ionogel as a Strain Sensor for Extremely Large Deformation	0.035	0.1	no	no	0.95	Ionic Liquid
<b>2020</b> -Transparent, mechanically robust, and ultrastable ionogels enabled by hydrogen bonding between elastomers and ionic liquids	1.75	0.004	no	0.95	no	Ionic Liquid
<b>2020</b> -Mechanically Robust, Elastic, and Healable Ionogels for Highly Sensitive Ultra-Durable Ionic Skins	2.52	0.12	no	no	0.99	Ionic Liquid
<b>2020</b> - Robust Physically Linked Double-Network Ionogel as a Flexible Bimodal Sensor	0.37	0.012	no	0.8	no	Ionic Liquid
<b>2021</b> -3D Printable, Highly Stretchable, Superior Stable Ionogels Based on Poly(ionic liquid) with Hyperbranched Polymers as Macro-cross-linkers for High-Performance Strain Sensors	0.25	0.58	yes	no	no	Ionic Liquid
<b>2019</b> -Highly Stretchable, Fatigue-Resistant, Electrically Conductive, and Temperature-Tolerant Ionogels for High-Performance Flexible Sensors	0.036	1.9	no	no	no	Ionic Liquid
<b>2021</b> -Flexible, transparent, and antibacterial ionogels toward highly sensitive strain and temperature sensors	3.5	0.045	no	0.943	no	Ionic Liquid
<b>2020</b> -Ionoskins: Nonvolatile, Highly Transparent, Ultrastretchable Ionic	0.2	0.133	no	0.985	no	Ionic Liquid

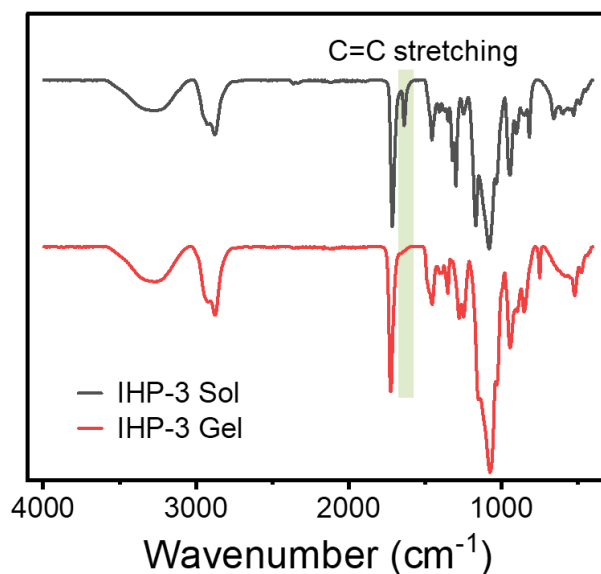


### 3.Results and Discussion

Sensory Platforms for Wearable Electronics						
<b>2021-</b> Ultra-Sensitive and Stretchable Ionic Skins for High-Precision Motion Monitoring	0.204	-	no	no	no	Ionic Liquid
<b>2021-</b> Adaptive Ionogel Paint from Room-Temperature Autonomous Polymerization of $\alpha$ -Thioctic Acid for Stretchable and Healable Electronics	0.2	0.023	no	0.95	0.9	Ionic Liquid
<b>2021-</b> Highly Stretchable and Reconfigurable Ionogels with Unprecedented Thermoplasticity and Ultrafast Self-Healability Enabled by Gradient-Responsive Networks	0.1	0.3	no	no	0.917	Ionic Liquid
<b>2019-</b> Highly Stretchable Organogel Ionic Conductors with Extreme-Temperature Tolerance	0.048	0.079	no	0.93	no	Ionic Liquid
<b>2021-</b> Highly Transparent, Stretchable, and Conductive Supramolecular Ionogels Integrated with Three-Dimensional Printable, Adhesive, Healable, and Recyclable Character	1.51	2.25	yes	0.93	no	Ionic Liquid
<b>2021-</b> A Transparent, Highly Stretchable, Solvent-Resistant, Recyclable Multifunctional Ionogel with Underwater Self-Healing and Adhesion for Reliable Strain Sensors	0.72	0.091	no	0.92	0.99	Ionic Liquid
<b>2021-</b> Highly Stretchable, Transparent, and Self-Adhesive Ionic Conductor for High-Performance Flexible Sensors	0.09	0.0164	no	0.9	no	Ionic Liquid
<b>2021-</b> A novel strategy for fabricating highly stretchable and highly conductive photoluminescent ionogels via an in situ self-catalytic cross-linking reaction in ionic liquids	0.02	0.1	no	no	no	Ionic Liquid
<b>2021-</b> Self-healing, anti-freezing and highly stretchable polyurethane ionogel as ionic skin for wireless strain sensing	3	1.4	no	0.95	0.95	Ionic Liquid
<b>2020-</b> Polymeric Complex-Based Transparent and Healable Ionogels with High Mechanical Strength and Ionic Conductivity as Reliable Strain Sensors	7.7	1.97	no	0.85	1	Ionic Liquid
<b>2020-</b> Hierarchically Crosslinked Gels Containing Hydrophobic Ionic Liquids towards Reliable Sensing Applications	2	0.07	no	80.5	no	Ionic Liquid
<b>2021-</b> Underwater Communication and Optical Camouflage Ionogels	0.6	0.025	no	0.966	1	Ionic Liquid

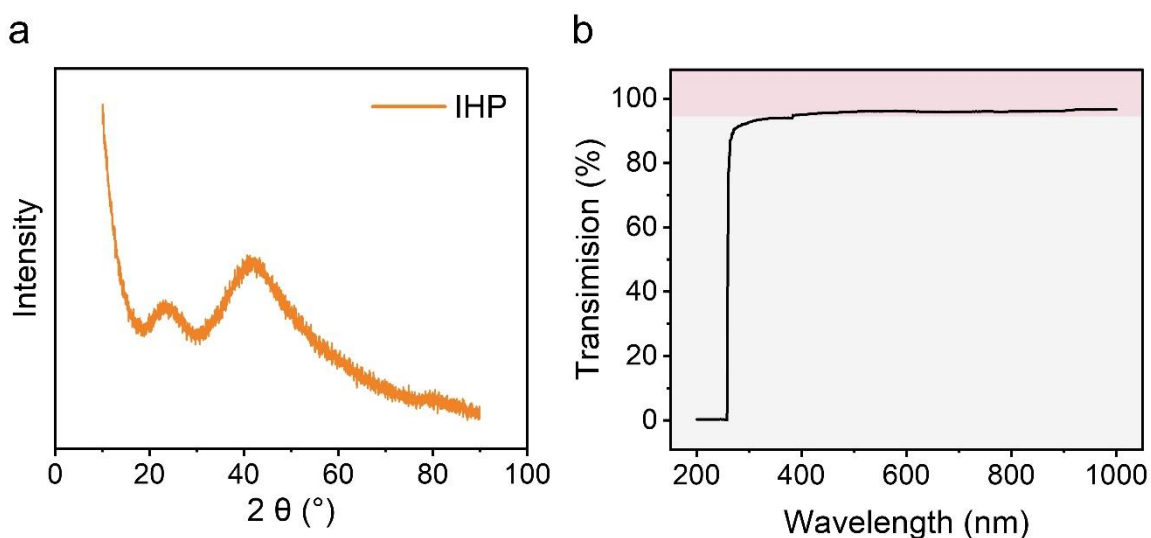
### 3.Results and Discussion

<b>2021-</b> Block Copolymer-Based Supramolecular Ionogels for Accurate On-Skin Motion Monitoring	0.65	1.78	no	0.8	no	Ionic Liquid
<b>2019-</b> Transparent and stretchable triboelectric nanogenerator for self-powered tactile sensing	0.17	1.9	no	no	no	Ionic Liquid
<b>2019-</b> Highly stretchable and nonvolatile gelatin-supported deep eutectic solvent gel electrolyte-based ionic skins for strain and pressure sensing	0.067	0.25	no	no	no	Deep Eutectic Solvents
<b>2020-</b> 3D Printable Strain Sensors from Deep Eutectic Solvents and Cellulose Nanocrystals	1.25	0,08	yes	no	no	Deep Eutectic Solvents
<b>2017-</b> Patternable transparent and conductive elastomers towards flexible tactile/strain sensors	0.08	0.2	no	0.81	no	Deep Eutectic Solvents
<b>2021-</b> A Mechanically Robust and Versatile Liquid-Free Ionic Conductive Elastomer	7.16	0.00528	yes	0.9	0.4	Solvent-free
<b>2019-</b> Transparent, Highly Stretchable, Rehealable, Sensing, and Fully Recyclable Ionic Conductors Fabricated by One-Step Polymerization Based on a Small Biological Molecule	0.152	0.0028	no	0.85	0.86	Solvent-free
<b>2021-</b> Dynamically Crosslinked Dry Ion-Conducting Elastomers for Soft Iontronics	0.262	0.02	no	0.78	0.96	Solvent-free
<b>2020-</b> Stretchable, Transparent, and Thermally Stable Triboelectric Nanogenerators Based on Solvent-Free Ion-Conducting Elastomer Electrodes	0.34	0.00047	no	0.915	no	Solvent-free
<b>2022-</b> Hierarchical Response Network Boosts Solvent-Free Ionic Conductive Elastomers with Extreme Stretchability, Healability, and Recyclability for Ionic Sensors	0.6	0.00054	no	0.9	no	Solvent-free
<b>2022-</b> Solvent-free adhesive ionic elastomer for multifunctional stretchable electronics	0.418	0.007	no	0.92	no	Solvent-free
<b>2018-</b> Highly stretchable and transparent ionic conducting elastomers	0.25	0.0000127	no	0.924	no	Solvent-free
<b>2021-</b> An Intrinsically Conductive Elastomer for Thromboembolism Diagnosis	0.4	0.000056	no	0.97	no	Solvent-free

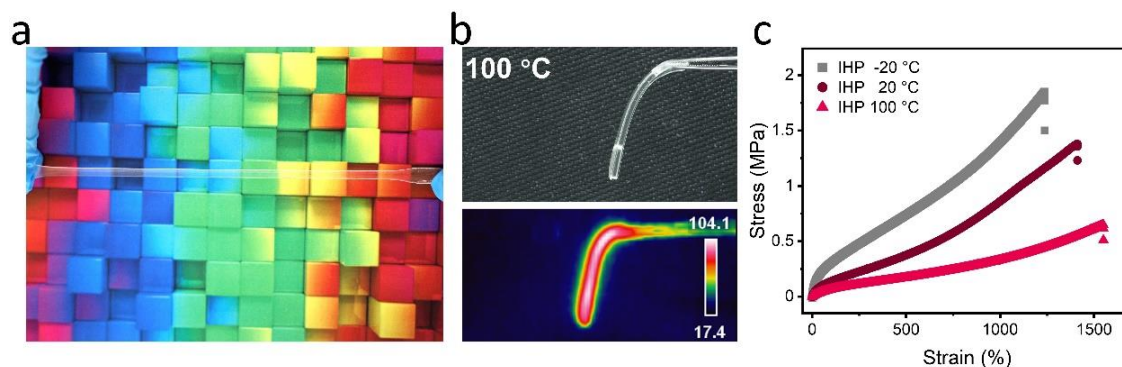


**Figure S2-1.** Fourier transform infrared spectrum of IHP-3 before (sol) and after (gel) UV initiation, demonstrating the disappearance of C=C stretching bands at 1600-1700 $\text{cm}^{-1}$ .

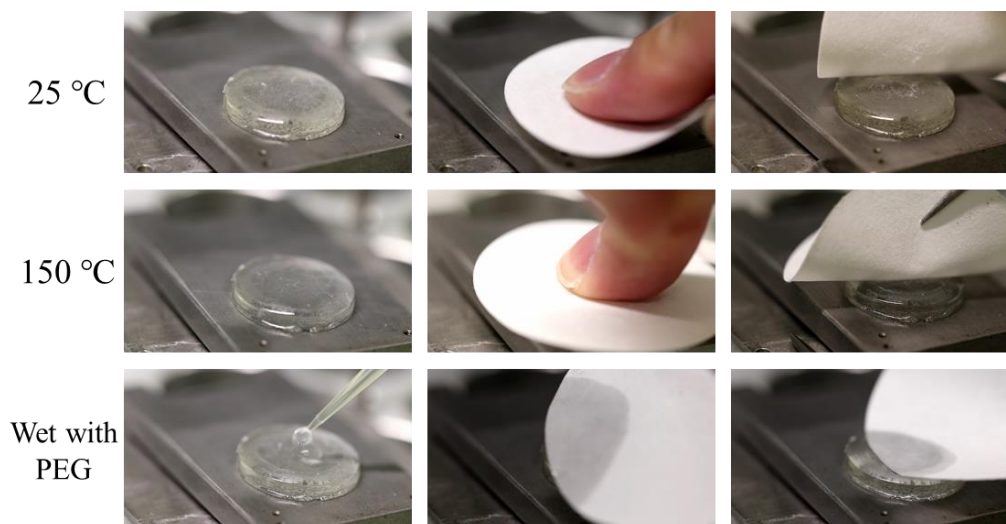
There is no band at 1600-1700  $\text{cm}^{-1}$  (C=C stretching) after UV initiation, confirming the completion of the polymerization and absence of the acrylate monomers after UV irradiation.



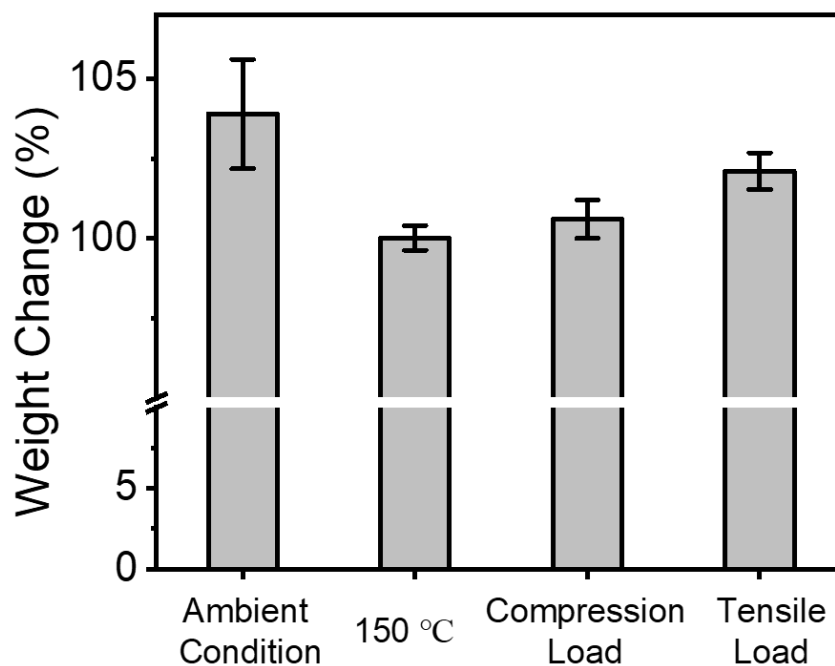
**Figure S2-2.** a) WAXS spectra of IHP-3, showing the amorphous halo. b) Transmittance spectrum of a 1 mm thick IHP-3.



**Figure S2-3.** a) Photograph of transparent IHP film stretched up to 300% strain. b) Top: Images demonstrating the mechanical stability under extreme temperatures (lifted at 100°C). Bottom: Images from a thermal camera at the same time. c) Representative stress-strain curves of IHP-3 under different temperatures.



**Figure S2-4.** Solvent leakage measurements for IHP-3. A dry filter paper was used to evaluate the solvent leakage of the IHP elastomer. A piece of filter paper was pressed to the surface of IHP-3 at 25°C with about 10 N pressure for 5 s. Photograph of the paper after detaching it from the IHP-3 shows no visible wetting and/or contamination of the paper by PEG. The surface of paper remained dry and clean. The same experiment was performed for IHP-3 at 150°C. As shown in Figure below, the filter paper remained dry after being in contact with the IHP-3 for 20 s. However, when the surface of IHP-3 was additionally wetted by PEG, the PEG was absorbed by paper immediately when touching the surface of IHP-3. These results demonstrate the leakage-free nature of IHP due to the multiple (although weak) interactions between PEG and the PHEMA matrix, as opposed to the ICES based on small molecule solvents that have tendency to leak out of the network.



**Figure S2-5.** Weight change of IHP-3 samples under different conditions. Ambient condition: sample of IHP-3 was stored under ambient condition for one week; 150°C: an IHP-3 sample was stored in an oven at 150°C for one week; Compression load: an IHP-3 sample underwent 10,000 cycles of 50% strain compression with a speed of 10 %/s at room temperature for 28 h; Tensile Load: an IHP-3 sample undergone 10,000 cycles of 100% strain tensile with a speed of 100 mm/min at room temperature for 36 h. Error bars are standard deviations ( $n = 3$ ).

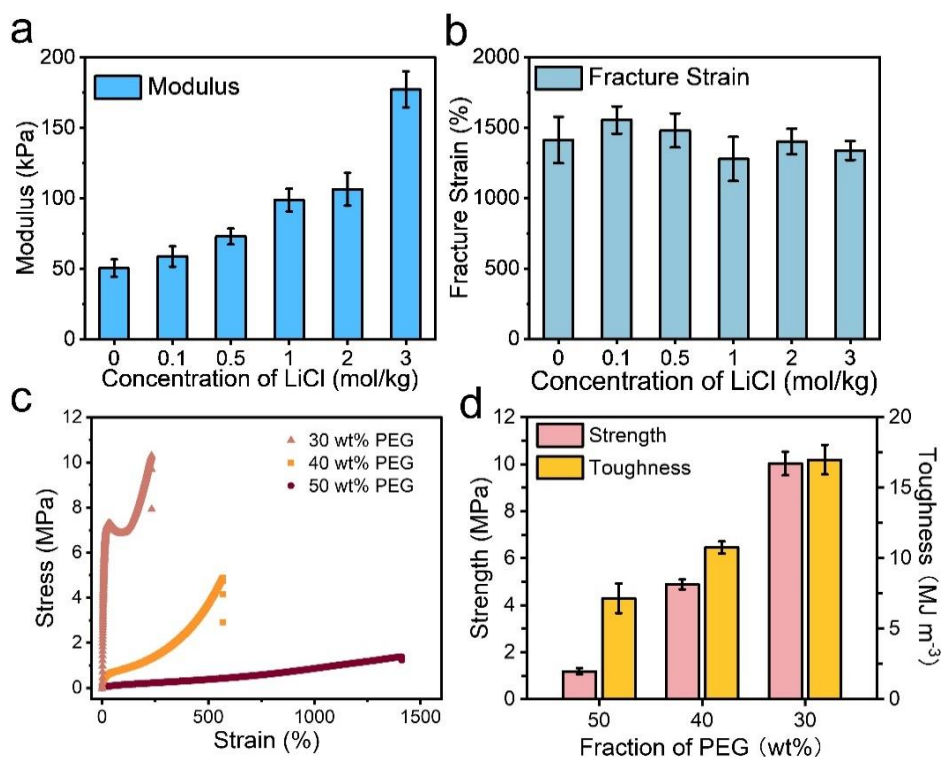
After being stored in ambient condition (room temperature, around 50% relative humidity) for one week, the weight of IHP-3 increased slightly by 3.9%, due to the absorption of water from the air. After being stored in an oven at 150°C for one week (around 50% relative humidity), the weight did not change at all. Also, after undergoing 10,000 cycles of 50% strain compression and 100% strain tensile at room temperature for 36 h, the weight changes of IHP-3 are below 2% compared to the as-prepared sample.

### 3.Results and Discussion

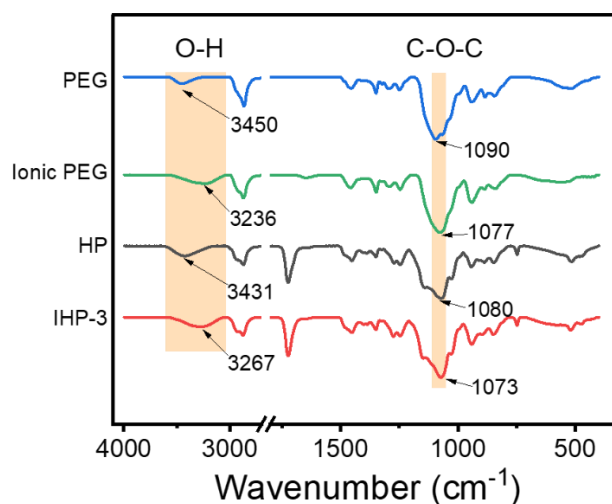
**Table S2-5.** Comparison of mechanical property of IHP-3 before and after drying. Drying processing: 120°C in the oven with a vacuum (0.1 mbar) for 24 h.

	Weight Change (%)	Strength (MPa)	Toughness (MJ m <sup>-3</sup> )	Elastic Modulus (kPa)	Fracture Strain (%)
As-prepared	100	1.18 ± 0.13	7.16 ± 1.05	177 ± 13	1336 ± 67
After Drying	99.07 ± 0.99	1.35 ± 0.12	7.41 ± 0.53	169.6 ± 7.7	1225 ± 29

To investigate the effects of the dry processing on mechanical properties, the as-prepared IHP-3 was stored at 120°C in the oven with a vacuum (0.1 mbar) for 24 h. The weight of IHP-3 decreased to 99.07% of as-prepared samples, due to the water in the raw material before polymerization. The toughness and elastic modulus lightly increase from 1.18MPa and 7.16 MJ m<sup>-3</sup> to 1.35 MPa and 7.41 MJ m<sup>-3</sup>, respectively.

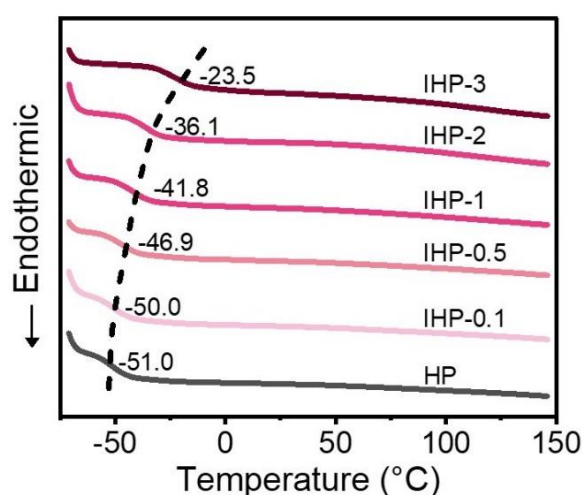


**Figure S2-6.** Fracture strain (a) and modulus (b) of IHP (50 wt% PEG) with different concentrations of LiCl. c) Representative stress-strain curves of IHPs (3 mol kg<sup>-1</sup> LiCl) with different PEG fraction. d) Strength and toughness of IHPs (3 mol kg<sup>-1</sup> LiCl) with different PEG fraction. Error bars are standard deviations (n = 3).

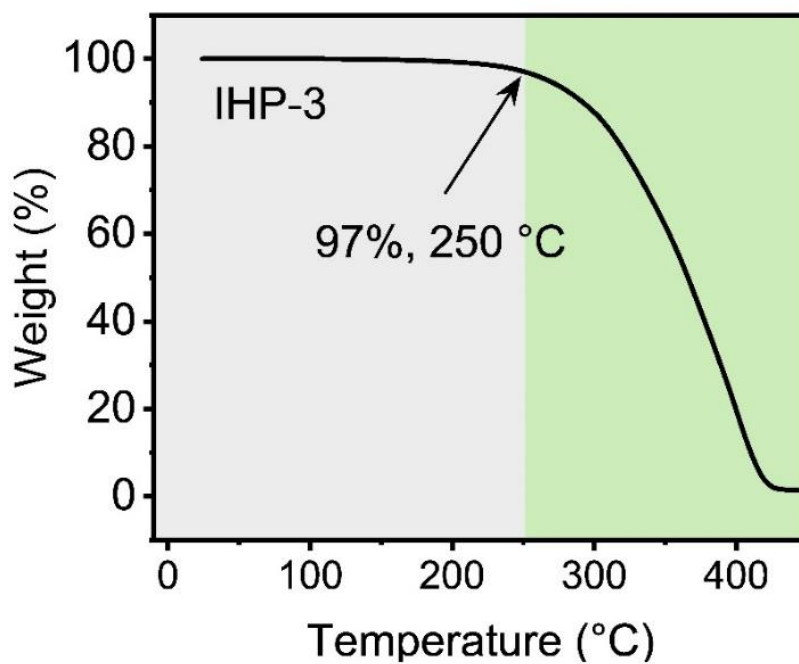


**Figure S2-7.** Fourier transform infrared spectrum of PEG, Ionic PEG (containing 3 mol kg<sup>-1</sup> LiCl), HP, and IHP-3.

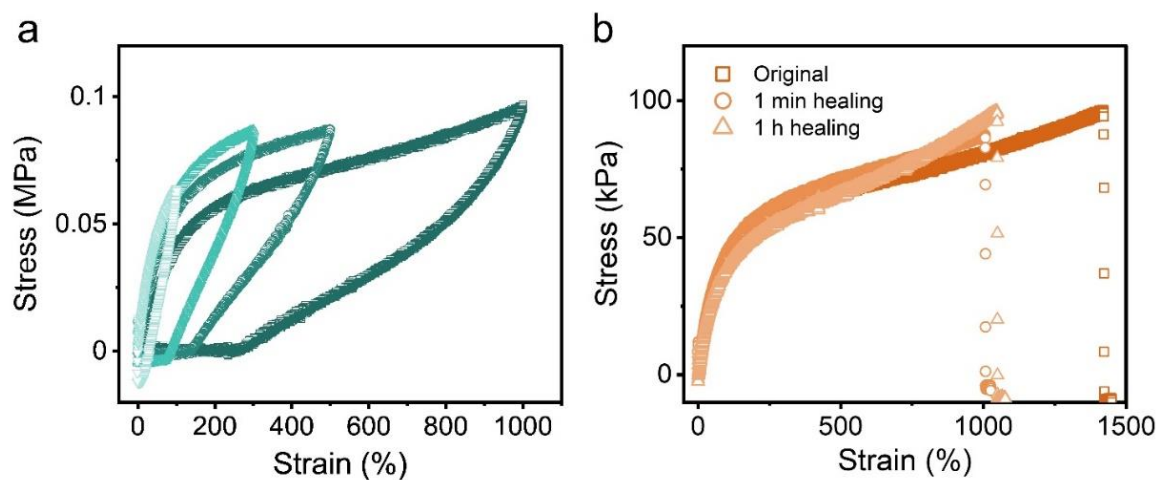
For the Li-O interactions, after the addition of LiCl, the peak corresponding to the stretching of O-H in PEG exhibited a shift from 3450 cm<sup>-1</sup> to 3236 cm<sup>-1</sup>, and became wider, indicating the lithium ions coordinated to the ends of PEG chains. Also, the peak of O-H in the elastomer shifted from 3431 cm<sup>-1</sup> (HP) to 3267 cm<sup>-1</sup> (IHP-3), after introducing LiCl. This further confirmed that lithium ions have interactions between PHEMA and PEG. Moreover, the interactions between lithium ions and C-O-C in PEG and elastomer were also confirmed. The peaks of C-O-C in both PEG and elastomer presented a shift from 1090 cm<sup>-1</sup> and 1080 cm<sup>-1</sup> to 1077 cm<sup>-1</sup> and 1073 cm<sup>-1</sup>, after adding LiCl.



**Figure S2-8.** Differential scanning calorimetry (DSC) analysis of IHPs with different concentrations of LiCl. IHP-x corresponds to HP with x mol kg<sup>-1</sup> LiCl.

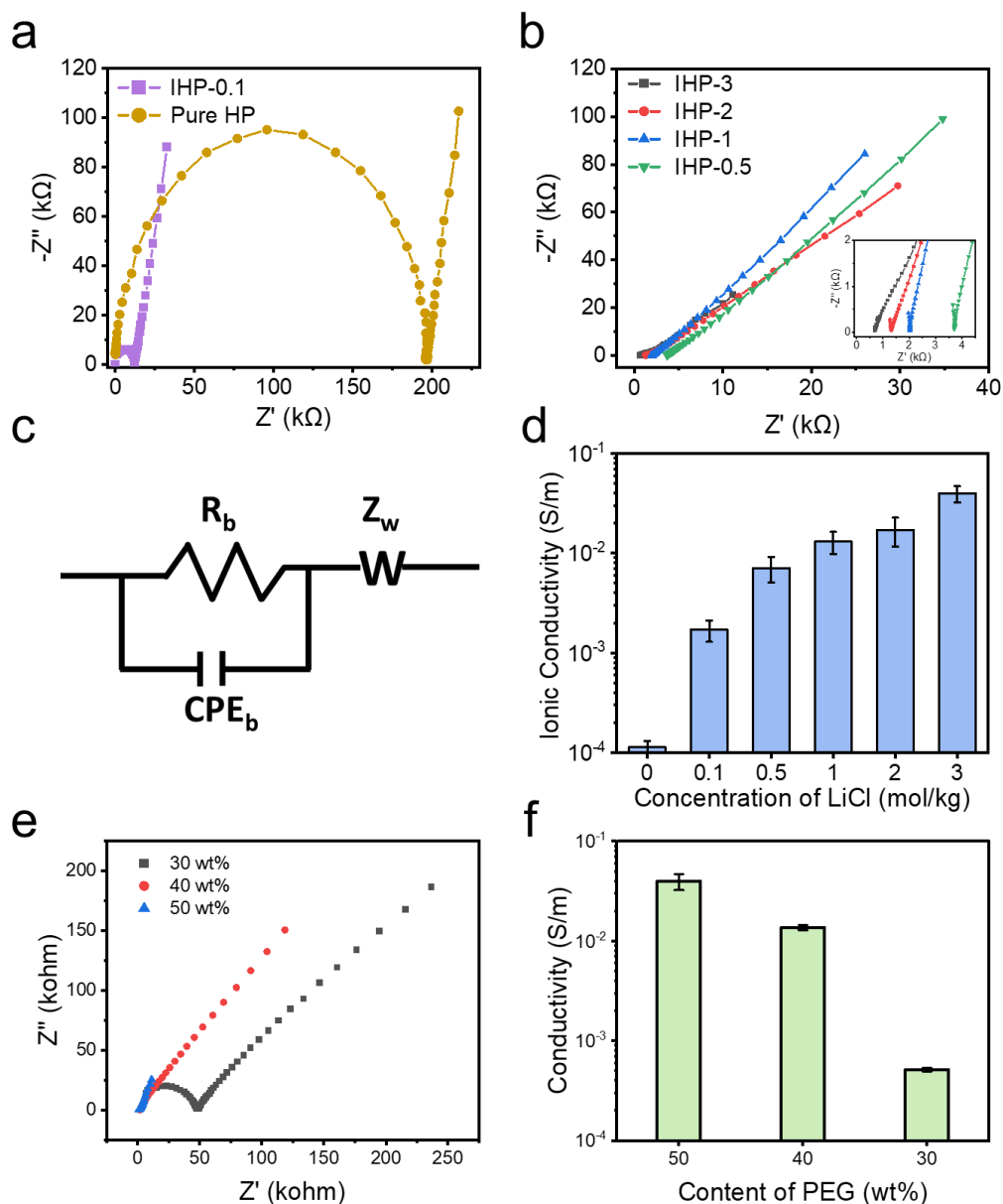


**Figure S2-9.** Thermal gravimetric analysis (TGA) spectrum of IHP-3.

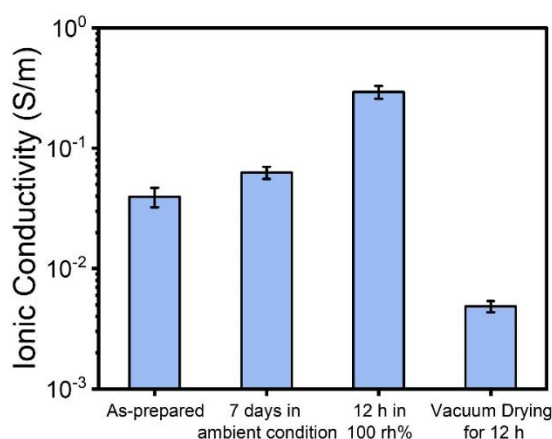


**Figure S2-10.** a) Continuous cyclic tensile loading-unloading curves of HP, in which strain increased from 100% to 300%, 500%, and 1000%. b) Representative stress-strain curves of HP with increasing healing time after cut.

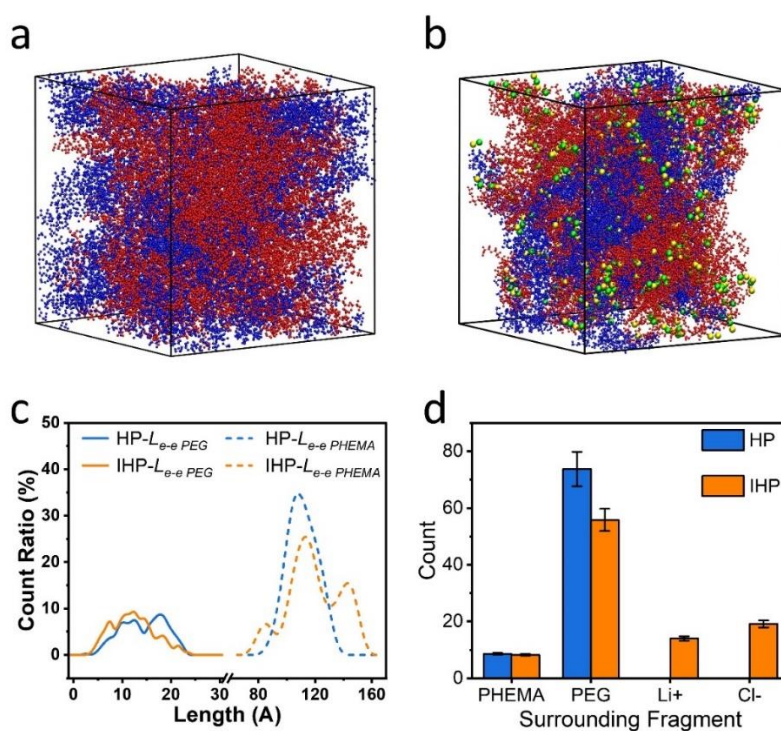




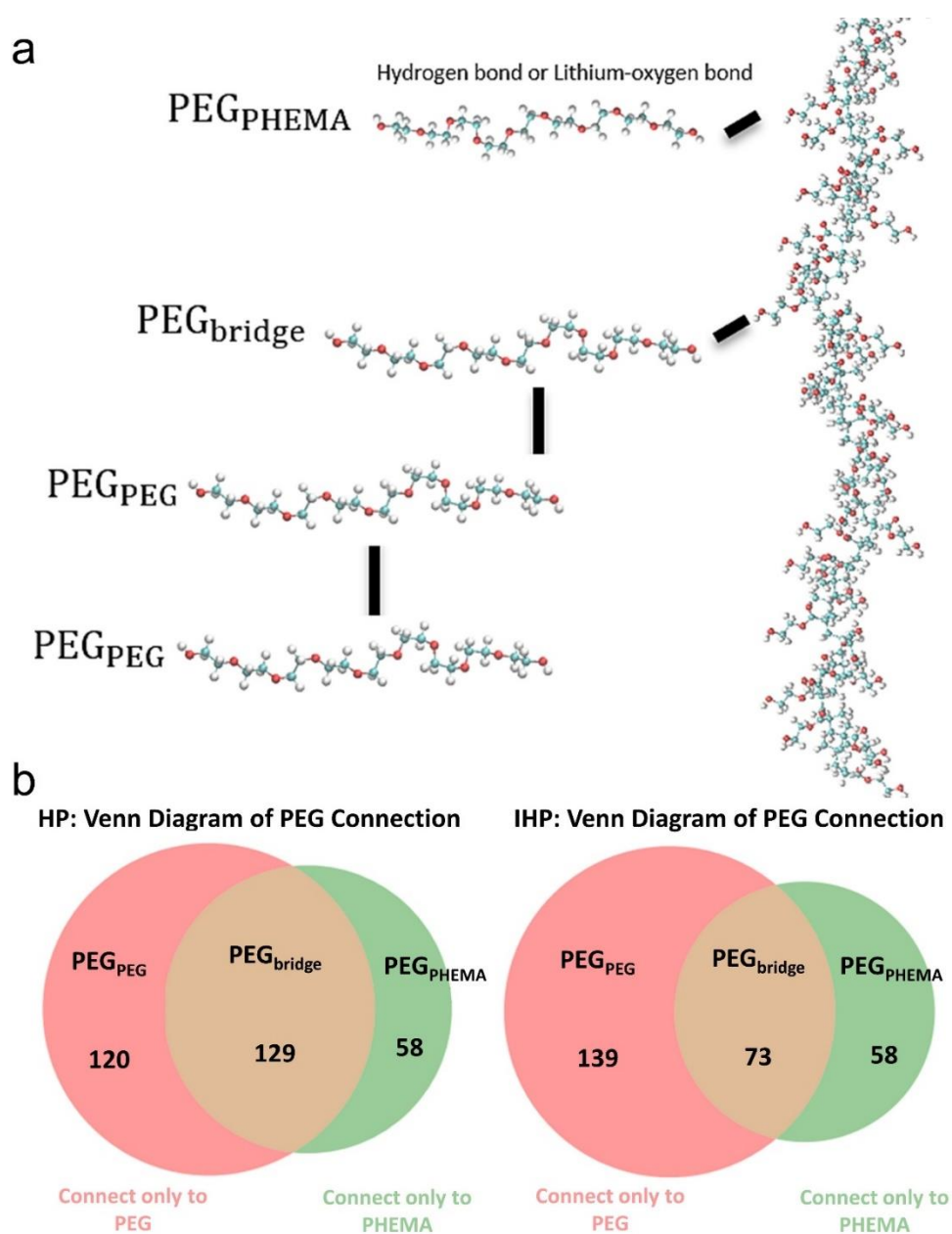
**Figure S2-11.** a) and b) Impedance spectra of IHPs (diameter of 10 mm and thickness of 1mm) with different content of LiCl at 25 °C, 50 rh%. c) The equivalent circuit of the tested model. In the equivalent circuit,  $R_b$  is the bulk resistance of the polymer electrolytes (calculated from the real axis intercept) and  $CPE_b$  is used to fit bulk capacitance. The straight line in the lower frequencies corresponds to the Warburg impedance  $Z_w$ . d) Ionic conductivity of the IHPs with different LiCl concentrations. e) Impedance spectra of IHPs with different PEG weight fractions at 25 °C, 50 rh% (3 mol kg<sup>-1</sup> LiCl). f) Ionic conductivity of the IHPs with different PEG weight fractions. Error bars present standard deviation (n = 3).



**Figure S2-12.** Ionic conductivity of the IHP-3 under different environments. Error bars present standard deviation ( $n = 3$ ).



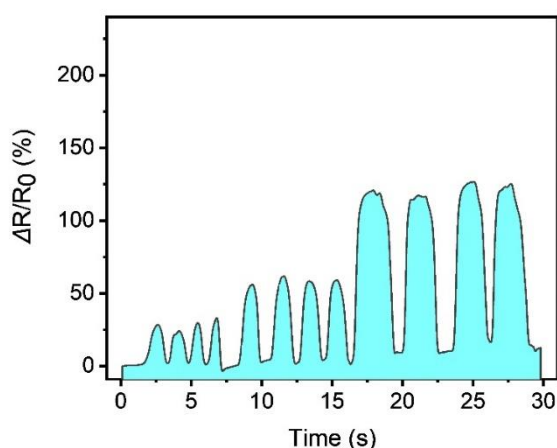
**Figure S2-13.** The initial model of HP (a) and IHP (b). c) Distribution of the end-to-end length ( $L_{e-e}$ ) of PEG (solid line) and PHEMA (dotted line) in HP (blue) and IHP (orange). d) Number of various elements around PEG in HP and IHP. These results come from the simulation, which is performed by Yu-Cheng Lai and Ya-Tang Chiang from Chia-Ching Chou Group at the Institute of Applied Mechanics, College of Engineering, National Taiwan University as a part of the collaborative project.



**Figure S2-14.** a) Schematic diagram of PEG with different conditions. b) Statistic result of PEG molecules with different conditions in HP and IHP. These results come from the simulation, which is performed by Yu-Cheng Lai and Ya-Tang Chiang from Chia-Ching Chou Group at the Institute of Applied Mechanics, College of Engineering, National Taiwan University as a part of the collaborative project.

To investigate the microstructure in PHEMA-PEG gel, this part organizes PEG molecules into 3 partitions based on their connected molecules (Figure S2-10a). If a PEG molecule connects to PHEMA polymer only whether with hydrogen bond or with coordinate bond, it is denoted as PEG<sub>PHEMA</sub>. If a PEG molecule connects to PEG molecules only, it is denoted as PEG<sub>PEG</sub>. If a PEG molecule connects to PEG and PHEMA polymer simultaneously, it is denoted as PEG<sub>connect</sub> since this PEG molecule connects two phases, polymer network, and solvent. Finally, if a PEG molecule does not connect to any molecule through hydrogen bond or coordinate bond, it is denoted as PEG<sub>isolate</sub>.

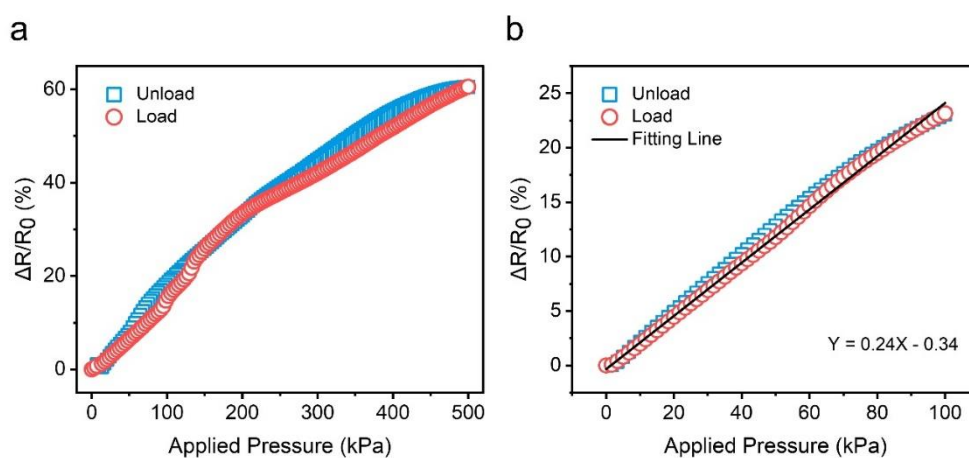
The statistical result is shown as Venn diagram and plot in Figure S2-10b. It is observed that there is a 17% increase in PEG<sub>PEG</sub> and a 43% decrease in PEG<sub>connect</sub> in LiCl system. The number of PEG<sub>PHEMA</sub> in both system in this simulation remains similar. The result shows that the percentage of PEG molecules which connect between PEG and PHEMA decreases, while the percentage of PEG molecules which connect other PEG increases. This may lead to a stronger interaction between PEG solvent system and a weaker interaction between PEG and PHEMA networks. Another observation is that PEG<sub>isolate</sub> increases from 7 to 44 in LiCl system. This result implies that strong interactions between lithium ions in gel and oxygen in PEG may eventually curl PEG molecules themselves together, causing an isolated PEG increase. These results show that the addition of LiCl in PEG-PHEMA gel increases the interaction in PEG solvent, decreases the interaction between PHEMA and PEG molecules, and most important of all, maintains the connectivity in the LiCl system.



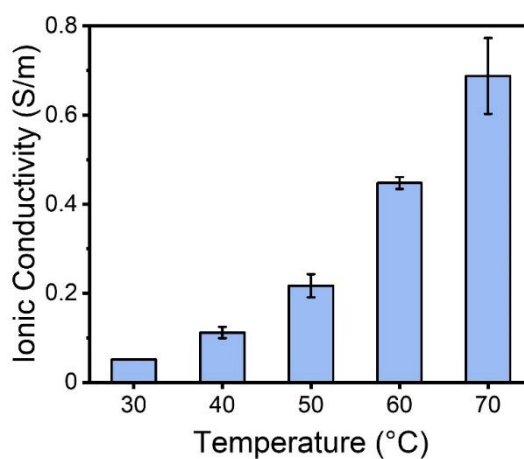
**Figure S2-15.** Relative change of resistance of IHP-3 during finger bending.



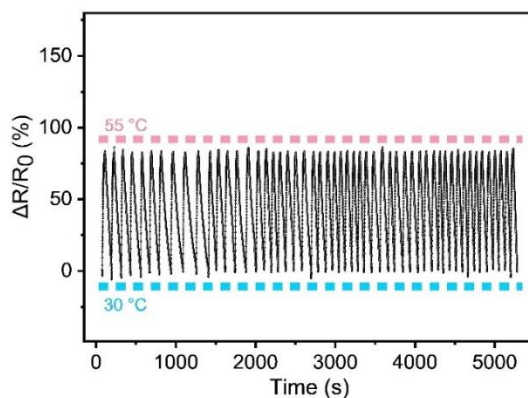
**Figure S2-16.** Schematic of fabric glove (black) with five strain sensors (pink).



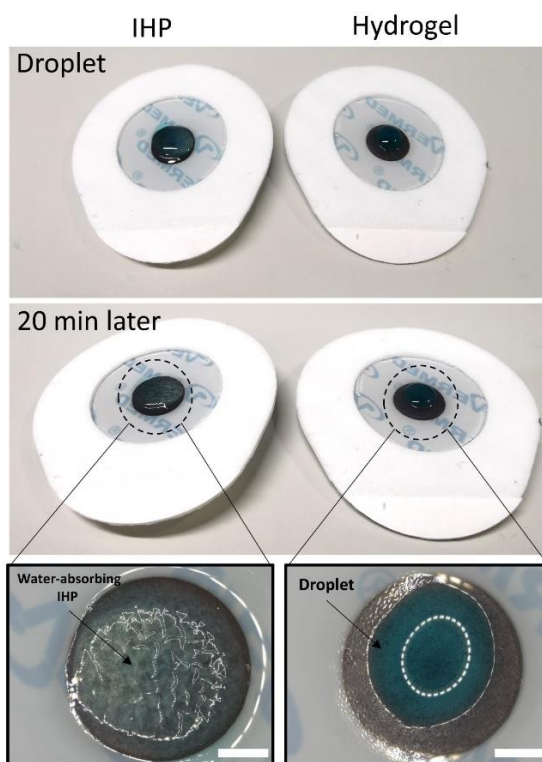
**Figure S2-17.** The resistance change of IHP-3 during pressure loading-unloading with 500 kPa (a) and 100 kPa (b).



**Figure S2-18.** Ionic conductivity of IHP-3 with different temperatures. Error bars present standard deviation (n = 3).

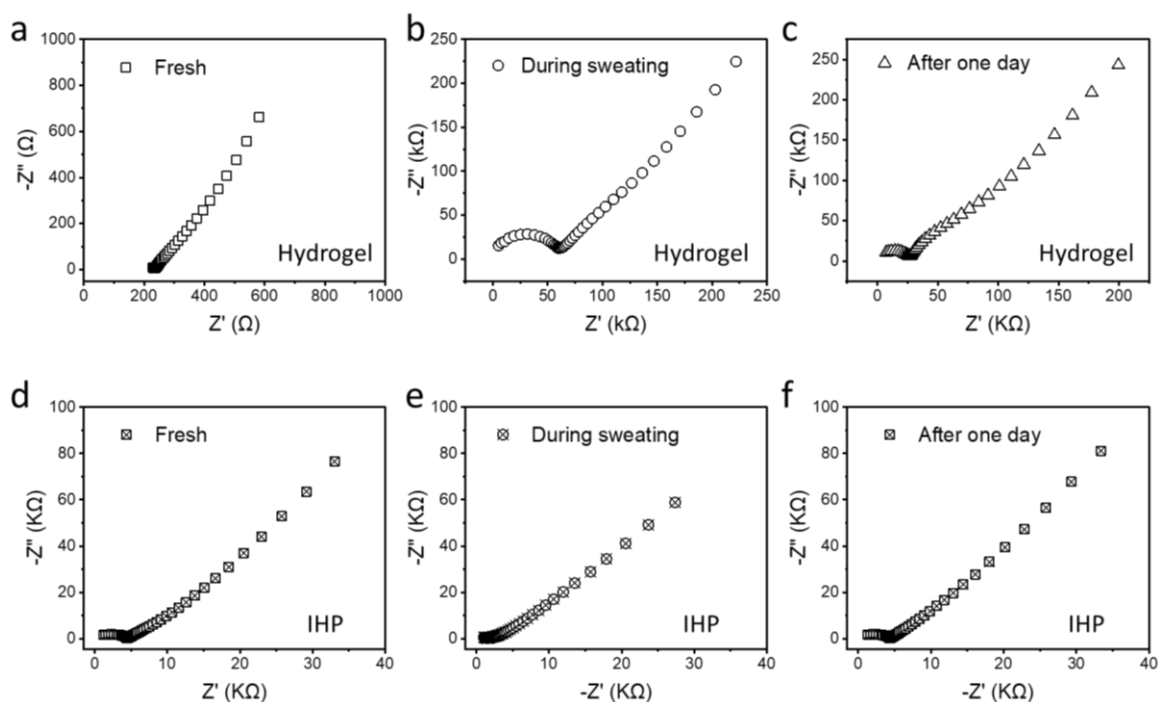


**Figure S2-19.** The resistance change of IHP-3 upon cyclic temperature change (30 °C to 55°C, 50 cycles).



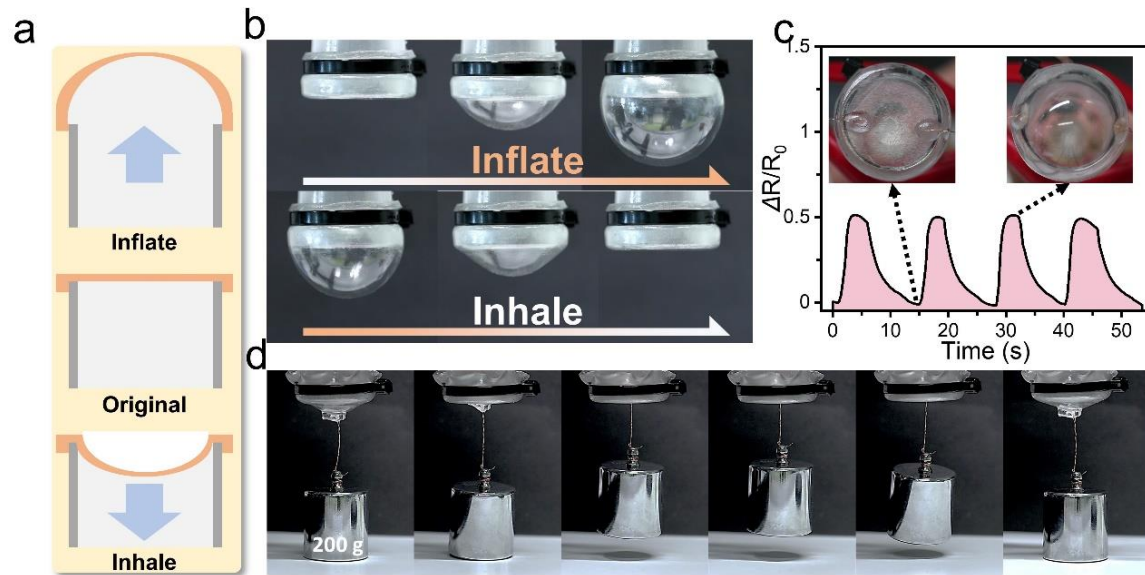
**Figure S2-20.** Photos of water absorption of an IHP electrode (left) and a commercial hydrogel electrode (right). The droplet contains NaCl (2 mg mL<sup>-1</sup>) and methyl blue (0.5 mg mL<sup>-1</sup>). The dotted ring in the center of the bottom right image is the reflection of microscope lens in droplet. Scale bar = 2 mm.

A droplet of aqueous solution (20  $\mu$ L) was placed on the surfaces of IHP and hydrogel electrodes. After 20 min, IHP absorbed the droplet and presented swollen rough surface. For hydrogel, the droplet appearance did not change.



**Figure S2-21.** The impedance of the hydrogel and IHP electrodes under different conditions. The aluminum tape and NaCl aqueous solution ( $2 \text{ mg mL}^{-1}$ ) were used to mimic skin and sweat, respectively. “During sweating” means  $20 \mu\text{L}$  of NaCl aqueous solution ( $2 \text{ mg mL}^{-1}$ ) was placed between the aluminum tape and electrodes. “After one day” means that IHP and commercial hydrogel electrodes were stored in ambient conditions for one day.

For sweating condition, about  $20 \mu\text{L}$  of NaCl aqueous solution was added to the surface of the aluminum tape. The impedance of hydrogel electrode increased more than 100 times under sweating condition and after one day. For IHP, the impedance remained almost the same after one day and even decreased slightly (possibly due to water absorption) under sweating conditions (Figure S2-21).



**Figure S2-22.** a) a schematic of artificial muscle with sensing property. b) Photograph of IHP based pneumatic artificial muscle during inflating and inhaling. c) The relative change of resistance of fabricated artificial muscle during working. d) Photograph of IHP-3 lifting a 200 g weight.



### 3.3 Phase-separated PEGgel

#### 3.3.1 Abstract

Polymer gel consists of a cross-linked polymer network infused with a solvent, whereby the network structure is strongly influenced by the solvent nature and affinity. Nano/micro scale-sized phase separation is considered as an efficient way to enhance the mechanical properties of materials. This study developed a simple and efficient method for the fabrication of tough phase-separated polymer gels by polymerizing 2-hydroxyethyl methacrylate (HEMA) in a mixture of poly(ethylene glycol) (PEG) and poly(propylene glycol) (PPG). The polymerized elastic networks present distinct solubility in PEG (highly soluble) and PPG (poorly soluble due to the existing methyl on the main chain), resulting in a macroscopically homogeneous covalent network with *in-situ* phase separation. The resulting phase-separated H<sub>6</sub>E<sub>4</sub>P<sub>6</sub> demonstrates high strength (8.0 MPa), favorable fracture strain (430%), and large toughness (17.0 J m<sup>-3</sup>). The separated phases endow the polymer gel with shape-memory property, which, together with 3D printability, can be used for various soft machine applications. Finally, ions were incorporated into PEG/PPG solvent to achieve a hierarchical interaction in polymer gels ranging from ionic interactions (nano-level) to interactions between phase separated regions at the micrometer scale. Such a hierarchical structure further enhanced the strength and toughness of polymer gels, showing high fracture strength (12.2 MPa) and fracture energy (54 kJ m<sup>-2</sup>).

#### 3.3.2 Introduction

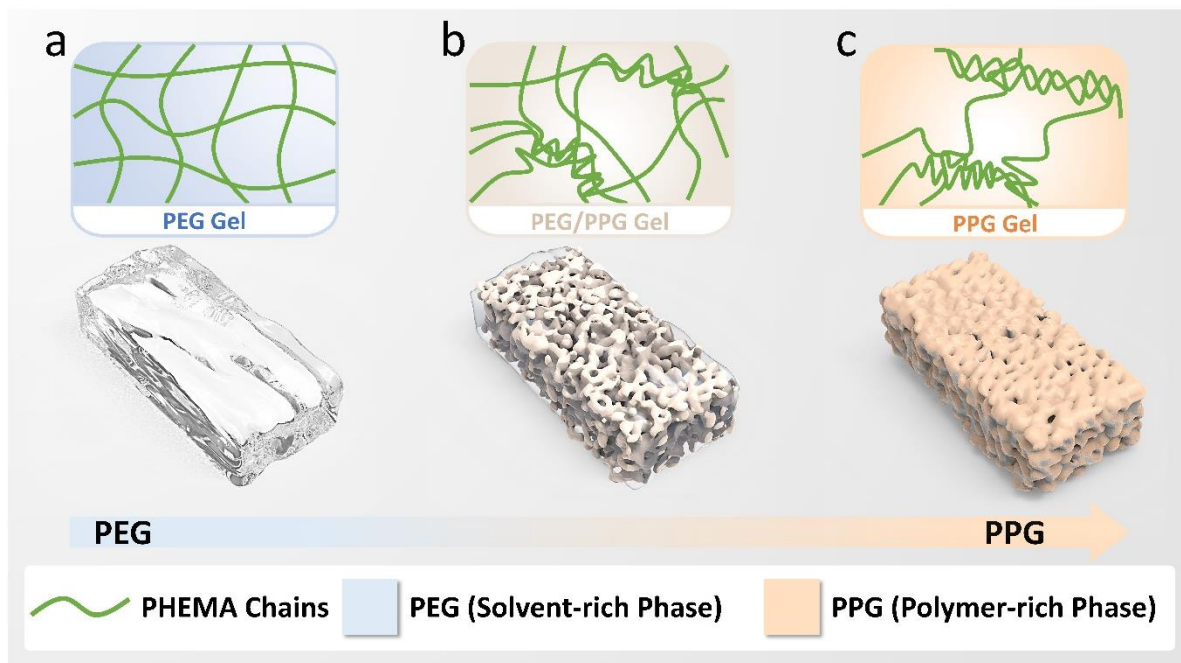
Soft materials, due to their tissue-like mechanical properties, show great promise as ideal materials for applications as diverse as tissue engineering, flexible electronics, bio-adhesives, and soft robotics.<sup>266-269</sup> Soft materials with various chemical functionalities, electrical properties, and mechanical properties have been developed to meet these engineering demands.<sup>270-272</sup> However, engineered soft materials still typically suffer from poor mechanical properties, resulting in poor reliability and premature failure under harsh application environments.<sup>273</sup> In nature, the hierarchical structures, widely existing in the biological tissues, have been proved to enhance the mechanical properties,<sup>274</sup> where destroying the packed hierarchical structures requires more energy per unit area than the single structure.<sup>275</sup> Thus, creating a hierarchical structure across multiple scales by combing

materials with contrasting properties would be a feasible strategy. Recent studies have demonstrated that hard components, such as fibers<sup>276</sup> and metal particles,<sup>277</sup> can largely improve the mechanical properties of soft materials.<sup>278</sup> Besides these embedded hard components, in-situ forming hard domains with nano/micro-scale in soft materials would be interesting, which avoids the problems of mixture and compatibility.

Polymer gels, one of the most promising soft materials, consist of cross-linked polymer network systems infused with plenty of solvents.<sup>108</sup> The internal structure of gels, which is strongly influenced by solvent affinity, determines their optical, electrical, and mechanical properties.<sup>97</sup> With good solvents, a gel swells extensively, becoming highly transparent and elastic. With poor solvents, a gel shrinks, usually showing opaque due to the internal phase separation. These separated phases can efficiently enhance the mechanical properties of polymer gels (such as modulus, strength, and toughness), especially under micro/nanoscale.<sup>279-281</sup> Abundant efforts are devoted to designing tough polymer gels with phase separations, which usually involve laborious processing such as solvent exchange,<sup>282</sup> multistep syntheses,<sup>283</sup> and post-freezing casting<sup>284</sup>. These shortcomings result in dimensional instability and poor processability, severely limiting the further application of phase-separated gels.

This study demonstrates a strategy to fabricate phase-separated gel by polymerizing 2-hydroxyethyl methacrylate (HEMA) in a mixture of poly(ethylene glycol) (PEG) and poly(propylene glycol) (PPG). Using PEG/PPG as solvent avoids solvent leakage, evaporation, and toxicity. Then, the polymerized elastic networks present distinct solubility in PEG (highly soluble) and PPG (poorly soluble due to the existing methyl on the main chain), resulting in a macroscopically homogeneous covalent network with *in-situ* phase separation (Figure 24). In detail, the polymer-rich phase with hydrogen bonds dissipates energy and strengthens the gel; and the solvent-rich phase enables large strain. The separated phases were confirmed by various characterizations, endow polymer gel high strength (8.0 MPa) and outstanding toughness (17.0 MJ m<sup>-3</sup>). Based on the separated phases, the obtained polymer gel exhibits shape memory behavior. Combining the 3D printability and shape memory behavior, the phase-separated gel can be shaped into complex structures directly and used for various soft machines. Finally, this study incorporated ions into PEG/PPG solvent to achieve a hierarchical enhancement in polymer gels covering the phase separation (micro-level) and ionic interactions (nano-level), showing the scalability of this solvent

strategy for phase separation. Such a hierarchical structure enhanced strength and toughness, showing high fracture strength (12.2 MPa) and fracture energy (54 kJ m<sup>-2</sup>). The proposed strategy offers fundamental and extensible materials for various soft machines and further inspires the design of novel soft materials.



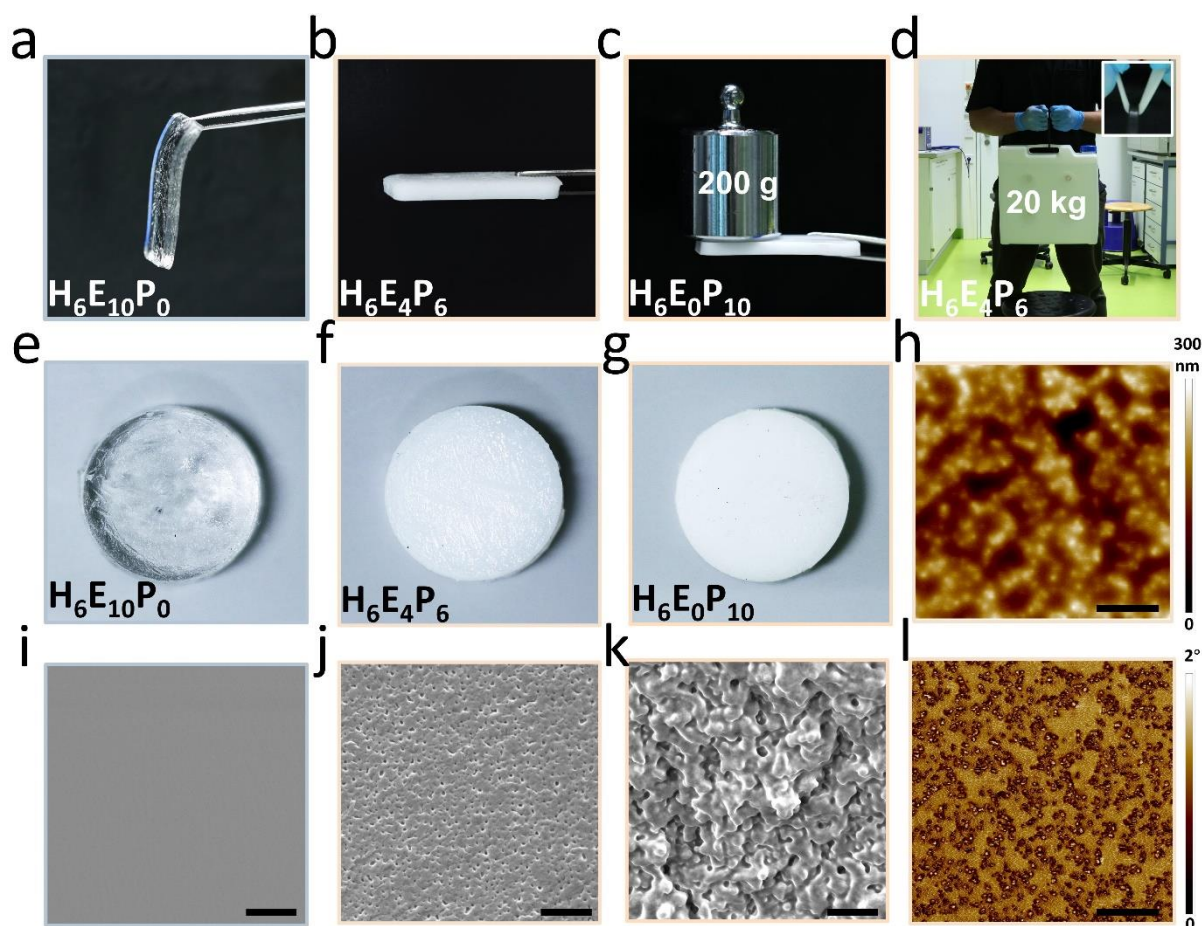
**Figure 23.** Schematic illustrations of *in-situ* phase-separated polymer gels using mixed oligomer solvents. a) In pure PEG solvent, the PHEMA swells in PEG forms a uniform, transparent, and elastic network, resulting from the high solubility. b) In mixed solvents of PEG and PPG, PHEMA swells in PEG to create highly solvated and soft domains and aggregates in PPG to form poorly solvated and stiff domains. Soft domains connect the stiff domains to form an extremely tough gel. c) In PPG gel, the poor solubility induced strong hydrogen bonds between PHEMA chains, driving aggregation to form separated stiff domains surrounded by PPG.

### 3.3.3 Result and Discussion

#### 3.3.3.1 *Concept of Phase-separated Gels*

Poly 2-hydroxyethyl methacrylate (PHEMA) was selected as the main polymer network with 60 wt% of gel mass to form pure PEG gel, PEG/PPG gel, and PPG gel, respectively. All samples were synthesized by mixing 2-hydroxyethyl methacrylate, corresponding

solvents, and a photo-initiator with a pre-designed ratio (Table S3-1) and polymerizing under UV light ( $5 \text{ mW cm}^{-2}$ , 366 nm, room temperature) for 30 min. The pure PEG gel, pure PPG gel, and polymer gel based on the mixture of PEG and PPG exhibited stark differences in optical and mechanical properties. PHEMA is compatible with PEG, which forms a homogeneous PEG gel ( $\text{H}_6\text{E}_{10}\text{P}_0$ ) with high transparency and flexibility (Figure 25a). By contrast, PPG has poor compatibility with PHEMA due to the presence of additional methyl groups on the main chain, which leads to a white and hard PPG gel (Figure 25c,  $\text{H}_6\text{E}_0\text{P}_{10}$ ). In the mixture of PEG and PPG, the obtained polymer gel ( $\text{H}_6\text{E}_4\text{P}_6$ ) can hold itself naturally without bending (Figure 25b) and even lift 20 kg weight without damage, harmoniously combining elasticity and strength, which correspond to the pure PEG gel and the PPG gel respectively. Phase separation (Figure 25e-g) is freely apparent based on the white color of polymer gel with PPG. In detail, the UV-Vis spectrum was used to evaluate the transparency of the samples (Figure S3-1, thickness: 300  $\mu\text{m}$ ). With the increasing fraction of PPG, the average transmittance during 400-800 nm decreased from 99% ( $\text{H}_6\text{E}_{10}\text{P}_0$ ) to 39% ( $\text{H}_6\text{E}_0\text{P}_{10}$ ), which means that the globules of the polymers are increased with the added PPG. The SEM result also confirms this. For  $\text{H}_6\text{E}_{10}\text{P}_0$ , the topography of the cross-section is smooth and uniform (Figure 25i), indicating a homogeneously disperse network. In  $\text{H}_6\text{E}_0\text{P}_{10}$ , the polymer-rich phase is separated and obvious, forming the microparticles in PPG (Figure 25k). In the middle,  $\text{H}_6\text{E}_4\text{P}_6$  also has the obvious phase separation, while the hard polymer-rich domains were mixed or connected with soft solvent-rich domains. Under atomic force microscopy (AFM), similar results were confirmed (Figure S3-2). The AFM images of  $\text{H}_6\text{E}_{10}\text{P}_0$  and  $\text{H}_6\text{E}_0\text{P}_{10}$  showed distinct morphologies, the former being smooth and the latter rough. The  $\text{H}_6\text{E}_4\text{P}_6$  also had a rough morphology but smaller polymer-rich domains than the  $\text{H}_6\text{E}_4\text{P}_{10}$ , showing a bicontinuous phase structure with a microscale based on the mixture of PEG and PPG (Figure 25h-l). To exclude the influence of polymer crystallization from mixture solvents, wide-angle X-ray scattering was performed to investigate the nanostructure of polymer gels (Figure S3-3). It confirms that all polymer gels based on PEG and PPG solvents have an amorphous structure with no diffraction peaks other than the amorphous halo. This indicates that the polymer-rich domains mainly depend on the aggregation of polymer chains in poor solvents rather than ordered crystallization.



**Figure 24.** Overview and structural characterization of the phase-separated gel. (a to c) Photographs of pure PEGgel (H<sub>6</sub>E<sub>10</sub>P<sub>0</sub>), pure PPG gel (H<sub>6</sub>E<sub>0</sub>P<sub>10</sub>) and PEG/PPG gel (H<sub>6</sub>E<sub>4</sub>P<sub>6</sub>). "H<sub>x</sub>" means that HEMA accounts for x tens percentage in the prepolymer solution; "E<sub>y</sub>" or "P<sub>z</sub>" means that PEG or PPG account for y or z tens percentage in the mixed solvents, respectively. The size of these three gels are all 3\*15\*38 mm a) H<sub>6</sub>E<sub>10</sub>P<sub>0</sub> presents soft and flexible, achieving natural bending and sagging. b) H<sub>6</sub>E<sub>4</sub>P<sub>6</sub> can hold itself without bending. c) H<sub>6</sub>E<sub>0</sub>P<sub>10</sub> behaves stiff, which can hold 200 g weight without bending. d) H<sub>6</sub>E<sub>0</sub>P<sub>10</sub> can lift 20 kg weight without damage. e-g) Photos of phase-separated gels with different solvent ratios, showing decreasing transparency with the increasing content of PPG. The diameter of all samples is 10 mm. h-j) SEM image of phase-separated gels with different solvent ratios. k) AFM image and l) phase image of H<sub>6</sub>E<sub>4</sub>P<sub>6</sub>, collected simultaneously (field of view 20 μm × 20 μm). All scale bars are 5 μm.

#### 3.3.3.2 *Mechanical Properties of Phase-separated Gels*

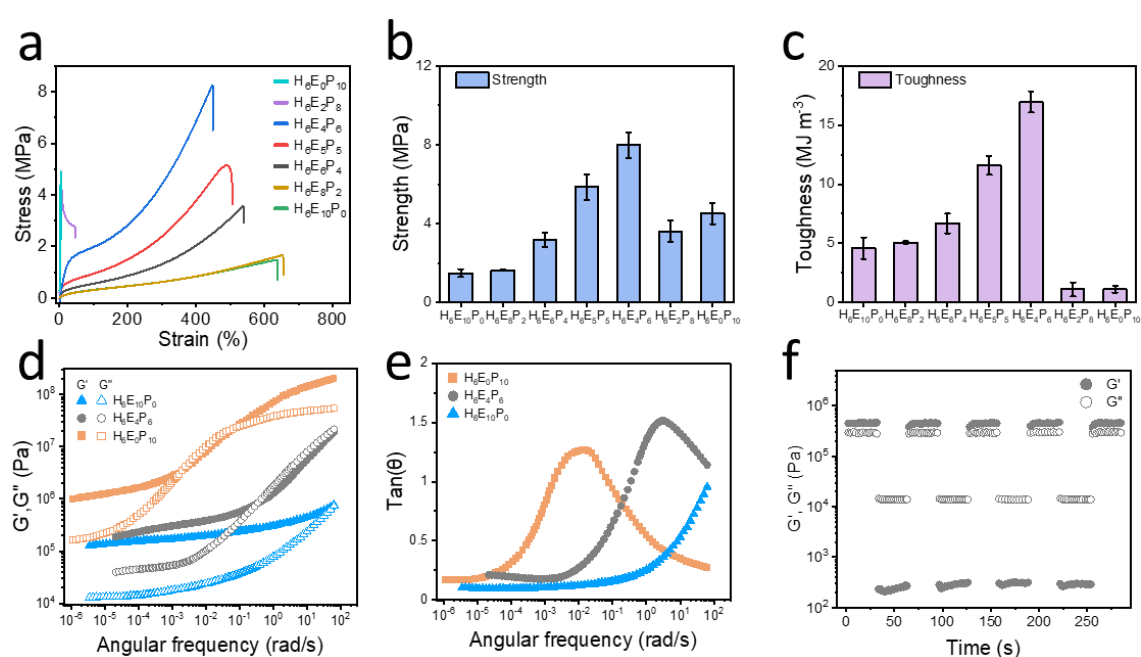
To further investigate the effect of solvent combinations on the mechanical properties of the polymer gels, the volume fractions of PPG were varied, thereby efficiently achieving tunability of the mechanical property of phase-separated gel. The typical tensile stress-strain curves of the polymer gels contain the same content of polymer networks (60 wt%) only with different solvent compositions. (Figure 26a-c, Figure S3-4) The pure PEG gel ( $H_6E_{10}P_0$ ) is soft and elastic with a low elastic modulus of  $0.71 \pm 0.08$  MPa, normal fracture stress of  $1.48 \pm 0.20$  MPa, and high fracture elongation of  $650\% \pm 72\%$ . With the increasing content of PPG, phase separation occurs and increases in the polymer gels, making the polymer gels stronger and less elastic than  $H_6E_{10}P_0$ . When the ratio of PPG to PEG is less than 60 wt%, the phase-separated gel is still soft and elastic, with fracture elongation higher than 400%. When the content of PPG reaches 80 wt%, the gels become glassy-like, showing an abrupt increase in elastic modulus from  $12.8 \pm 3.9$  MPa ( $H_6E_4P_6$ ) to  $29.1 \pm 4.2$  MPa ( $H_6E_2P_8$ ) and sudden decrease in fracture elongation at break from  $430\% \pm 28\%$  ( $H_6E_4P_6$ ) to  $6.4\% \pm 0.3\%$  ( $H_6E_2P_8$ ). Further increasing the PPG to 100%, the obtained  $H_6E_0P_{10}$  presents stiff and brittle with a high elastic modulus of  $124 \pm 21$  MPa, fracture stress of  $4.51 \pm 0.54$  MPa, and tiny fracture elongation of  $4.8\% \pm 0.4\%$ . Toughness is highly relevant to elongation and strength. In this phase separation model, the  $H_6E_4P_6$  performs the highest fracture stress ( $8.0 \pm 0.7$  MPa) and maintains favorable fracture strain ( $430\% \pm 28\%$ ), resulting in the outstanding toughness ( $17.0 \pm 0.9$  MJ m<sup>-3</sup>), which is 3.7 times of  $H_6E_0P_{10}$  ( $4.58 \pm 0.92$  MJ m<sup>-3</sup>) and 15.5 times of  $H_6E_0P_{10}$  ( $1.1 \pm 0.3$  MJ m<sup>-3</sup>). Notably, this simultaneous improvement of strength and toughness usually conflicts with material design. In a pure PEG environment, the polymer networks are highly solvated, where few hydrogen bonds form between the polymer chains since solvent separates the polymer chains, resulting in soft and stretchable  $H_6E_{10}P_0$ . Conversely, in PPG, the polymer networks are poorly solvated, forming abundant hydrogen bonds and entanglements between polymer chains, further behaving stiff and brittle. This study addresses this trade-off by forming the polymer chains in a mixture of good and poor solvents. This leads to poorly solvated domains (stiff, glass-like) and highly solvated domains (elastic, gel-like) in the same network, which synergistically toughen and strengthen the polymer gel.

The dynamic responsive properties of the phase-separated gel were investigated by using an oscillatory strain rheometer. According to the strain sweep test (Figure S3-5), the linear viscoelastic regions of H<sub>6</sub>E<sub>10</sub>P<sub>0</sub>, H<sub>6</sub>E<sub>4</sub>P<sub>6</sub>, and H<sub>6</sub>E<sub>0</sub>P<sub>10</sub> exhibit a high dependence on the contents of soft domains. With the decrease of PEG, the linear viscoelastic region decreases from 5% (H<sub>6</sub>E<sub>10</sub>P<sub>0</sub>) to 1% (H<sub>6</sub>E<sub>4</sub>P<sub>6</sub>) and 0.1% (H<sub>6</sub>E<sub>0</sub>P<sub>10</sub>). This indicates that the soft domains can provide a reversible response to the dynamic loadings under larger strain than stiff domains. Then, this study choose the corresponding linear strain to measure the dynamic master curves of modulus and frequencies for the three samples by time-temperature superposition. The rheological master curves of angular frequency dependence ( $\omega$ ) of the storage modulus ( $G'$ ), loss modulus ( $G''$ ), and loss factor ( $\tan\theta$ ) at a reference temperature of 30 °C are presented in Figure 26d and 26e. Due to the exitance of separated domains, the H<sub>6</sub>E<sub>4</sub>P<sub>6</sub> and H<sub>6</sub>E<sub>0</sub>P<sub>10</sub> exhibit a typical rubbery plateau region. In converse, H<sub>6</sub>E<sub>10</sub>P<sub>0</sub> only presents a terminal region during the same frequency range. In the H<sub>6</sub>E<sub>0</sub>P<sub>10</sub>, the sample without many elastic and soft domains presents a transition region at moderate to high frequencies (over 0.1 rad s<sup>-1</sup>).

Additionally, the  $G'$  of all samples shows a platform in the low-frequency region ( $\omega \rightarrow 0$ ). This results from the strong physical cross-links in gel networks, which prevent the network chains from slipping. With the increasing content of stiff domains, the plateau modulus ( $G_p, \omega \rightarrow 0$ ) of gels increases from 130 kPa (H<sub>6</sub>E<sub>10</sub>P<sub>0</sub>) to 200 kPa (H<sub>6</sub>E<sub>4</sub>P<sub>6</sub>), and 1000 kPa (H<sub>6</sub>E<sub>0</sub>P<sub>10</sub>). Thus, the stiff domains immensely enhance the strength of the network matrix. Meanwhile, the  $\tan\theta$  is a key parameter to characterize the energy-dissipation property of materials. As the stiff domain increases, the peak of  $\tan\theta$  shifts to the low-frequency region. The H<sub>6</sub>E<sub>4</sub>P<sub>6</sub>, combining soft domains and stiff domains in one network matrix, demonstrates a higher value of  $\tan\theta$  at moderate to high frequencies than both the pure soft and pure stiff domains. This result validates that the separated stiff domains play a dominant role in the energy dissipation of polymer gels.

Rheology analyses were further used to demonstrate the recovery properties of phase-separated gels. A strain amplitude sweep was performed to analyze the elastic response of the samples, and the critical strain regions of  $G'$  and  $G''$  were found to be 0.05% and 100%, respectively, according to the performance under the previous strain sweep test. In Figure 26f and S3-6, the  $G'$  values of all samples were found to decrease rapidly above the critical

strain region, indicating the nonlinear behavior of the gel network involving its damage. For  $H_6E_{10}P_0$ , the  $G'$  value decreased from  $\approx 230$  kPa to  $\approx 54$  kPa after the amplitude increased from 0.05% to 100%, indicating an impaired network. After decreasing the amplitude to 0.05% strain, the  $G'$  of  $H_6E_{10}P_0$  takes around 20 s to recover to 200 kPa. For  $H_6E_4P_6$ , the original  $G'$  value is  $\approx 450$  kPa, then the recovery process takes 16 s to achieve the  $G'$  value recovery from 0.23 kPa (100% strain) back to  $\approx 450$  kPa (0.05% strain). For  $H_6E_0P_{10}$ , the recovery is shorter than  $H_6E_4P_6$ , which takes only 14 s. According to such continuous small-large strain oscillation switch test, the improvement in recovery properties from the separated stiff domains is confirmed.



**Figure 25.** Mechanical properties of the phase-separated gel. a) Representative stress-strain curves of polymer gels with different compositions of PEG and PPG. Strength (b) and toughness (c) of polymer gels with different compositions of PEG and PPG. Data represent the mean  $\pm$  standard deviation ( $n = 3$ ). d) Frequency dependence of storage modulus ( $G'$ ) and loss modulus ( $G''$ ) for  $H_6E_{10}P_0$ ,  $H_6E_4P_6$ , and  $H_6E_0P_{10}$ . The master curves were obtained by time-temperature superposition (TTS) at a reference temperature of 30 °C. All samples were tested at 30 °C, 50 °C, 75 °C, 100 °C, 125 °C, and 150 °C. During the frequency sweep tests, the angular frequency was increased from 0.1 to 100  $rad\ s^{-1}$  at specified temperatures with the shear strain of 0.01% to 1%. e) Master curves for the  $\tan\theta$  of  $H_6E_{10}P_0$ ,  $H_6E_4P_6$ , and  $H_6E_0P_{10}$ . f)  $G'$  and  $G''$  of  $H_6E_4P_6$  under continuous strain sweep with alternate small

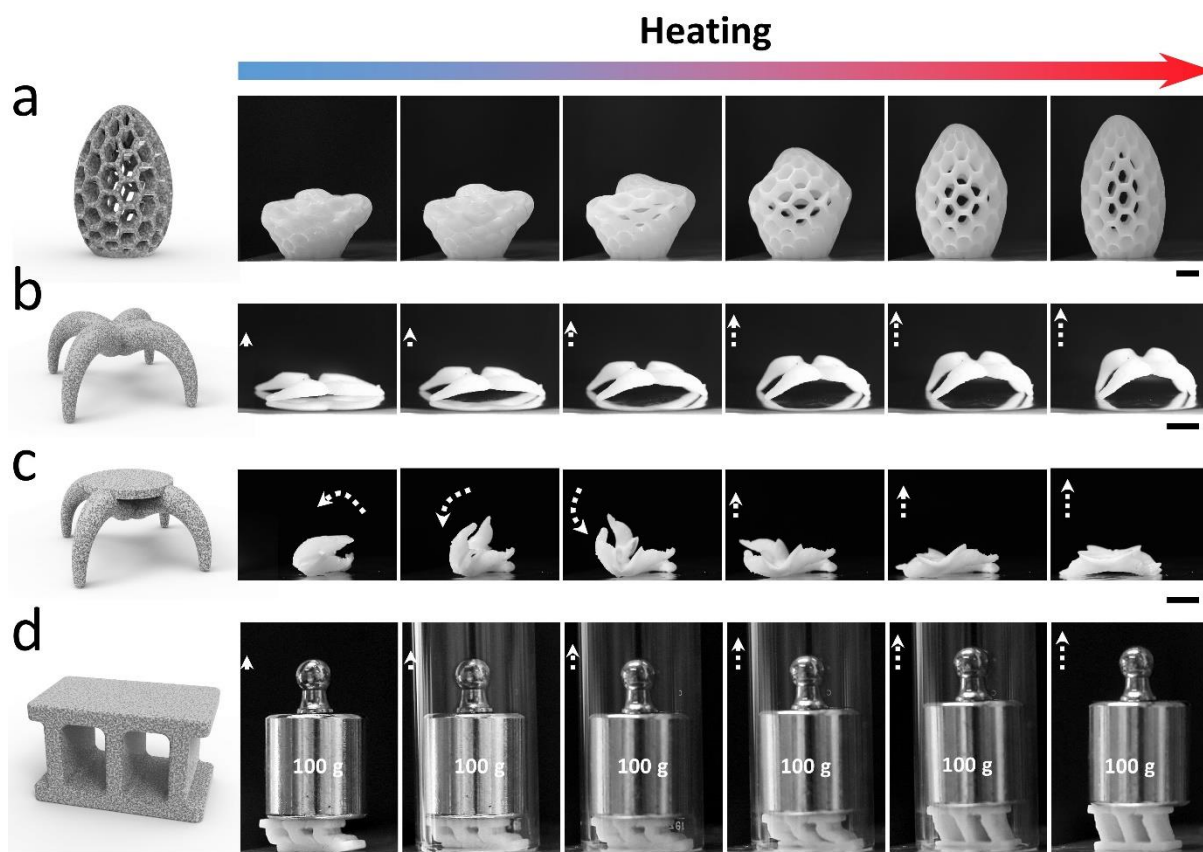


oscillation force ( $\gamma = 0.05\%$  strain) and large one ( $\gamma = 100\%$ ) at 30 °C with frequency of 10 rad/s.

#### 3.3.3.3 *4D printing of Phase-separated Gels*

The unique microstructure with separated and different domains enables the gel with shape-memory properties. The phase-separated gel (H<sub>6</sub>E<sub>4</sub>P<sub>6</sub>) has two glass transition temperatures (Figure S3-6). The soft solvent-rich domains show a low  $T_{g1}$  of -43.9 °C, and the stiff polymer-rich domains show a high  $T_{g2}$  of 75.3 °C. The shape-memory behavior was demonstrated by deforming (or called 'programming') the gel at an elevated temperature over  $T_{g2}$  (80 °C) and cooling back to room temperature to preserve the programmed shape. Above  $T_{g2}$ , the phase-separated gel becomes rubbery, providing a driving force for the elastic recovery of polymer chains.

Consequently, the gel would lose the previously programmed shape and recover to the original shape above  $T_{g2}$ , showing the shape-memory behavior. With the help of digital light processing technology, the photo-initiated gel can be 3D printed into various complex structures. Here, the 3D printability and shape-memory behavior were combined to achieve the 4D printing base on phase-separated gels. As shown in Figure 27a and Movie S3-1, the hexagonal hollow egg-shaped structure was programmed at a compressive collapsed state and quickly recovered to the original shape after heating over 80 °C in 20 s. Moreover, a quadruped model was directly printed and programmed into a lying-down state at room temperature. After heating over 80 °C, the quadruped model can stand by itself (Figure 27b, and Movie S3-2). A quadruped model with a small table was designed and printed to achieve more complex actions. From the folded status, the small item can turn itself over and stand in the designed direction (Figure 27c and Movie S3-3). Furthermore, due to the high strength of the phase-separated gel, the printed soft actuator can lift 100 g during heating, which is 116 times its own weight of 0.86 g (Figure 27d and Movie S3-4). Such a combination of superb mechanical properties and 4D printability demonstrates the great potential of phase-separated gels in various soft machines such as medical devices, wearable devices, and soft robots.

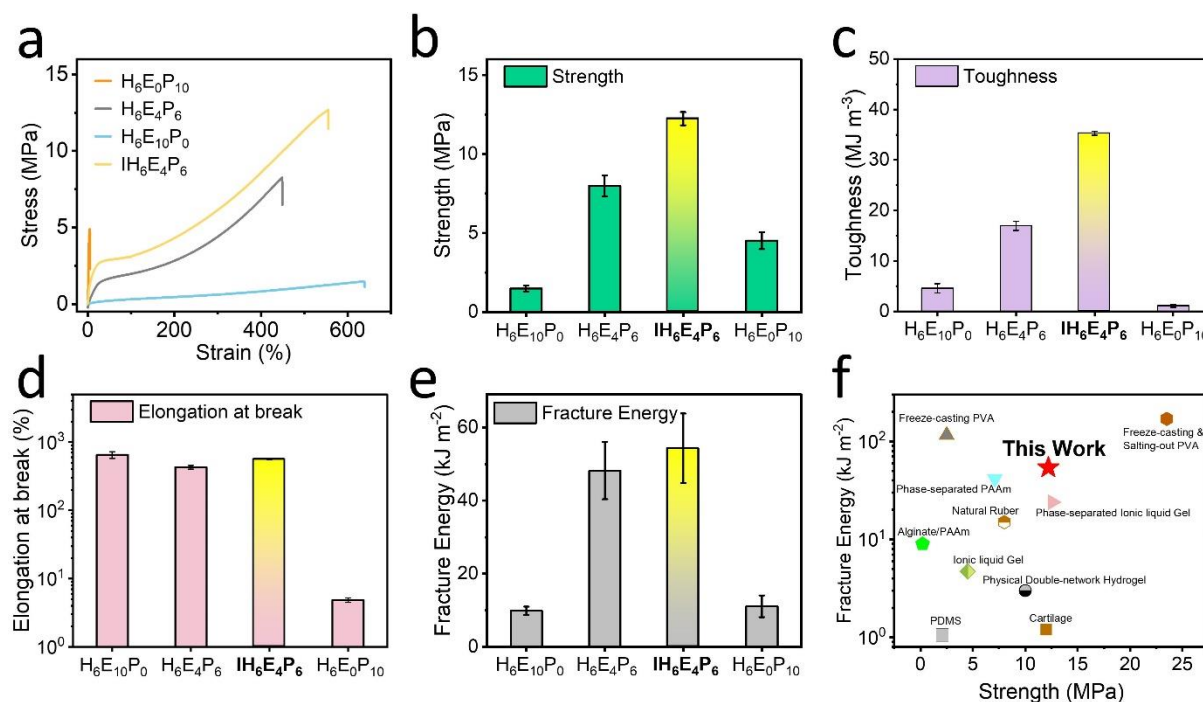


**Figure 26.** 4D printing of the phase-separated gel. a) The shape-memory behavior of a 3D printed hexagonal hollow egg-shaped structure, recovery from the collapsed state back to the original. b) The 3D-printed quadruped model can stand by itself after heating. c) The 3D-printed quadruped model with a small table can turn itself over and stand in the right direction after heating. d) The printed actuator can jack up 100g weight after heating, which is 116 times its own weight (0.86 g). The samples with complex 3D structures were prepared by DLP 3D Printer based on H<sub>6</sub>E<sub>4</sub>P<sub>6</sub> directly (Table S3-2). All heating processing (over 80 °C) was achieved by plate heating at the bottom and a heat gun at the top. The left column is the model designed for printing. All scale bars are 5 mm.

#### 3.3.3.4 Scalability of Phase-separated Gels

The current solvent strategy for *in-situ* phase separation efficiently improved the mechanical properties of polymer gels, which mainly occur at the microscale. To show the scalability of the current strategy, ions were added into the phase-separated gels to enhance the mechanical properties at the nanoscale. Such good compatibility and scalability between the ionic method and phase-separated strategy enable toughening and strengthening of a polymer gel

with hierarchical structures. The ionic  $\text{H}_6\text{E}_4\text{P}_6$  ( $\text{IH}_6\text{E}_4\text{P}_6$ ) was prepared by mixing Lithium chloride ( $3 \text{ mol kg}^{-1}$  in PEG) with a prepolymer solution of  $\text{H}_6\text{E}_4\text{P}_6$  and UV polymerized (Table S3-2). The hierarchical structure of  $\text{IH}_6\text{E}_4\text{P}_6$  consists of reversible ionic bonds at the  $\sim 0.1 \text{ nm}$  scale, oligomer solvents (PEG and PPG) at the  $\sim 1 \text{ nm}$  scale, a cross-linked polymer network at the  $\sim 10 \text{ nm}$  scale, and separated soft and stiff phase at the  $\sim 1 \mu\text{m}$  scale. Based on such a hierarchical structure,  $\text{IH}_6\text{E}_4\text{P}_6$  presents higher strength ( $12.2 \pm 0.4 \text{ MPa}$ ) and larger toughness ( $35.3 \pm 0.4 \text{ MJ m}^{-3}$ ) compared to the  $\text{H}_6\text{E}_4\text{P}_6$  (Figure 28a-c). Importantly, based on  $\text{H}_6\text{E}_4\text{P}_6$ , simultaneous toughening and strengthening are achieved again. With the help of ionic bonds in the networks, the fracture strain of  $\text{IH}_6\text{E}_4\text{P}_6$  is even higher than  $\text{H}_6\text{E}_4\text{P}_6$ , reaching  $560\% \pm 6\%$  (Figure 28d). Furthermore, the fracture energy of  $\text{IH}_6\text{E}_4\text{P}_6$  reached up to  $54.2 \pm 9.5 \text{ kJ m}^{-2}$  (Figure 28e), which is over five times  $\text{H}_6\text{E}_{10}\text{P}_0$  ( $9.9 \pm 1.1 \text{ kJ m}^{-2}$ ). A rough performance summary, including tough polymer gels, biological tissue, and some commercial elastomers, is presented in Figure 28f. Current  $\text{IH}_6\text{E}_4\text{P}_6$  outperforms most commercial or natural materials compared to fracture energy and strength.



**Figure 27.** Scalability of phase-separation strategy for fabricating super tough gels with hierarchical structures. a) Representative stress-strain curves of  $\text{H}_6\text{E}_{10}\text{P}_0$ ,  $\text{H}_6\text{E}_4\text{P}_6$ ,  $\text{H}_6\text{E}_0\text{P}_{10}$ , and  $\text{IH}_6\text{E}_4\text{P}_6$ . Strength (b), toughness (c), elongation at break (d), and fracture energy (e) of these polymer gels. f) A comparison between this work and cartilage, natural rubber, PDMS, and various gels regarding fracture energy to fracture strength.

### 3.3.4 Materials and Methods

#### 3.3.4.1 *Materials*

Hydroxyethyl methacrylate, and 2-hydroxy-2-methylpropiophenon (I1173) were purchased from Sigma-Aldrich (Darmstadt, Germany). Poly ethylene glycol ( $M_w = 400$  g/mol) and Poly propylene glycol ( $M_w = 425$  g/mol) were purchased from Thermal Fisher (Schwerte, Germany). All chemicals were used as received.

#### 3.3.4.2 *Preparation of Phase-separated gels*

All of the samples were prepared via UV-induced one-pot sequential polymerization. HEMA, PEG, PPG, and photo-initiator were mixed in brown bottles with designed ratios and vortex stirred for 2 min, obtaining transparent and uniform solutions. Moreover, the samples are initiated under 366 nm UV light ( $5 \text{ mW/cm}^2$ ) for 30 min. The specific prepolymer compositions are shown in Table S3-1.

#### 3.3.4.3 *Mechanical Characterization*

The samples were tested using an AGS-X Universal tester (Shimadzu Inc., Japan). Three samples were prepared for each tensile experiment. For tensile tests, the tested samples are shaped into dumbbells with 1-2 mm thickness, 2 mm width, and 10 mm length. The tensile speed was set at 100 mm/min. Three samples were tested as parallel samples.

The fracture energy was measured by pure shear tests.<sup>108,111</sup> Two identical samples were loaded under the sample setup as a pair to obtain one fracture energy value. One was notched, and the other one was unnotched. For the notched samples, an initial 20% width was cut in the middle of the long edge towards the center of the samples, and the specimen was loaded at a strain rate of  $100 \text{ mm min}^{-1}$ . All specimens had microstructure alignment parallel to the height direction. The critical strain ( $\epsilon_c$ ) for notched samples was obtained from the strain at maximum stress. The unnotched pairing samples were subsequently loaded over  $\epsilon_c$ . The fracture energy ( $\Gamma$ ) was obtained by multiplying the area under the stress-strain ( $\sigma$ - $\epsilon$ ) curve of the unnotched specimens with the length of the sample ( $L$ ) as  $\Gamma = L \int_0^{\epsilon_c} \sigma d\epsilon$ .

The dynamic viscoelasticity of the samples was measured by ARES G2 (TA Instruments) rheometer via small amplitude oscillatory shear experiments. The samples were placed under a 8 mm-diameter parallel plate.

#### 3.3.4.4 *Material Characterization*

The transmission of samples was measured using a UV-Vis spectrometer (Lambda 35, Perkin Elmer) with a wavelength range of 400 - 800 nm. The thickness of the samples is 300  $\mu\text{m}$ . Three samples were tested parallel, and every sample was scanned 24 times. The Differential scanning calorimetry (DSC) measurements were performed on a TA DSC 2500 instrument in sealed 40  $\mu\text{L}$  aluminum crucibles under a nitrogen atmosphere. Samples with 3 - 5 mg were analyzed using a heat/cool/heat cycle with a heating or cooling rate of 20  $^{\circ}\text{C}/\text{min}$ . In this cyclic thermal measurement, the samples were heated from room temperature to 250  $^{\circ}\text{C}$ , cooled to -90  $^{\circ}\text{C}$  and reheated to 250  $^{\circ}\text{C}$ . The glass transition temperature ( $T_g$ ) was determined in the second heat run to eliminate possible interference from the polymer's thermal history.

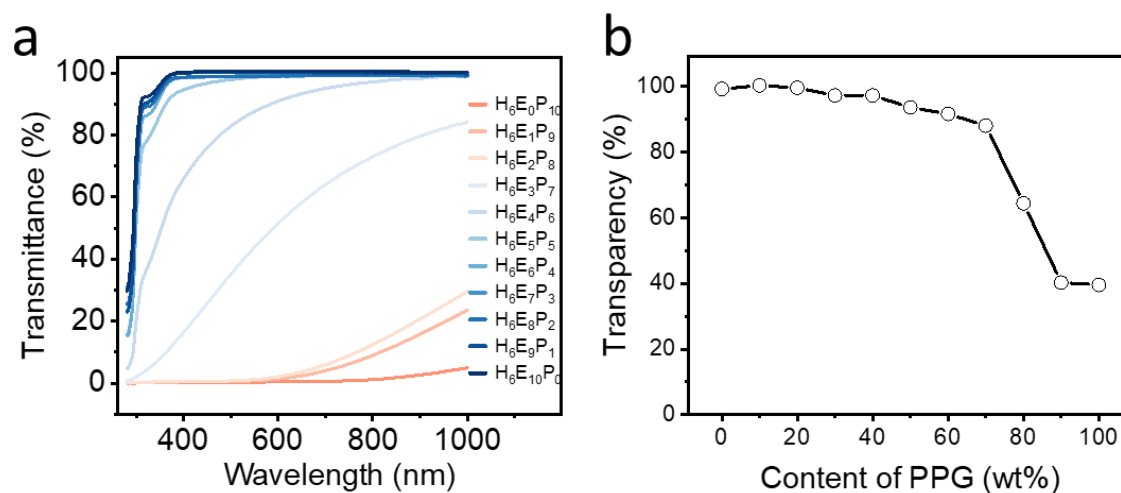
## 3.3.5 Supporting Information

**Table S3-1.** Prepolymer composition of phase-separated PEGgel with different ratio of PEG/PPG.

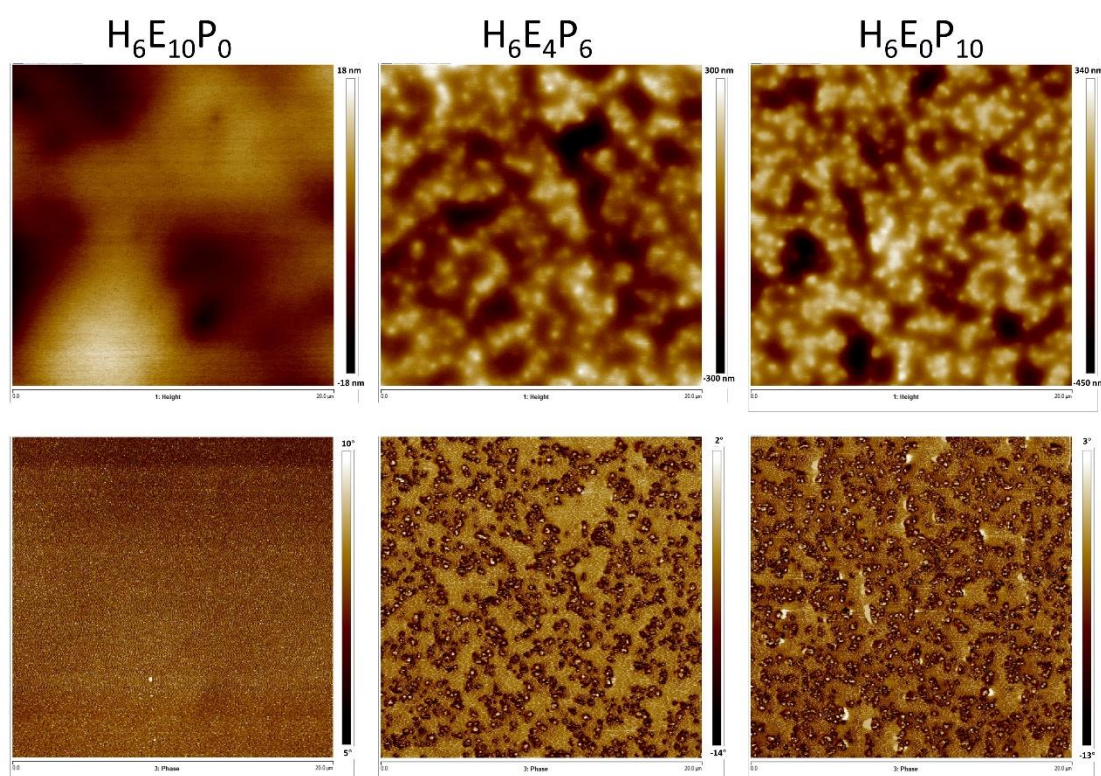
	H <sub>6</sub> E <sub>10</sub> P <sub>0</sub>	H <sub>6</sub> E <sub>8</sub> P <sub>2</sub>	H <sub>6</sub> E <sub>6</sub> P <sub>4</sub>	H <sub>6</sub> E <sub>5</sub> P <sub>5</sub>	H <sub>6</sub> E <sub>4</sub> P <sub>6</sub>	H <sub>6</sub> E <sub>2</sub> P <sub>8</sub>	H <sub>6</sub> E <sub>0</sub> P <sub>10</sub>
HEMA (g)	2.4	2.4	2.4	2.4	2.4	2.4	2.4
PEG (g)	1.6	1.28	0.96	0.8	0.64	0.32	0
PPG (g)	0	0.32	0.64	0.8	0.96	1.28	1.6
I1173 (μL)	12	12	12	12	12	12	12

**Table S3-2.** Prepolymer composition of H<sub>6</sub>E<sub>4</sub>P<sub>6</sub> for 3D printing and IH<sub>6</sub>E<sub>4</sub>P<sub>6</sub>.

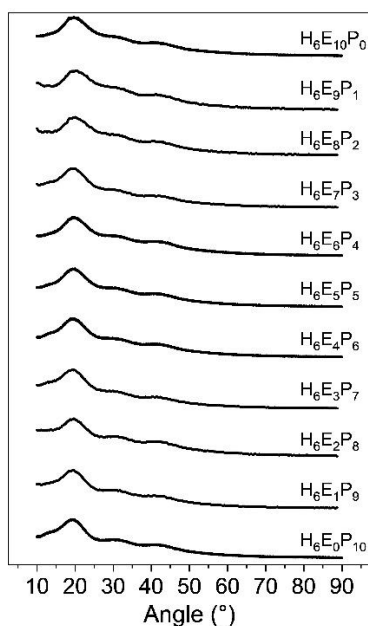
	H <sub>6</sub> E <sub>4</sub> P <sub>6</sub> for 3D Printing	IH <sub>6</sub> E <sub>0</sub> P <sub>10</sub>
HEMA (g)	2.4	2.4
PEG (g)	0.64	0.64
PPG (g)	0.96	0.96
Initiator	12 mg (I819)	12 μL (I1173)
LiCl (g)	-	0.081



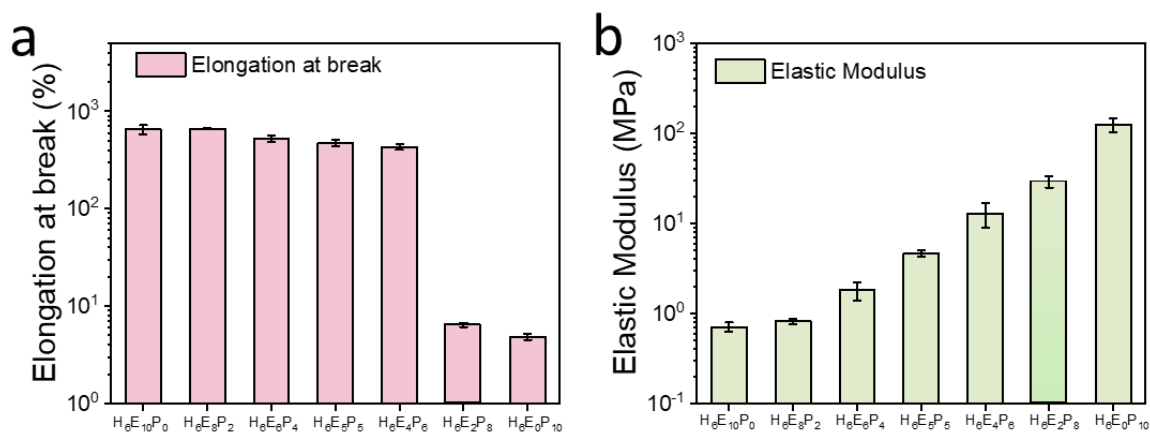
**Figure S3-1.** a) UV–Vis transmittance spectra of phase-separated gels prepared on glass support. b) The average transparency during 400-800 nm of polymer gels. The thickness of all samples is around 300  $\mu\text{m}$ . Globules of the polymers are increased from  $H_6E_{10}P_0$  to  $H_6E_0P_{10}$  by changing the composition of the polymerization mixtures.



**Figure S3-2.** AFM image (top) and phase image (bottom) of  $H_6E_{10}P_0$ ,  $H_6E_4P_6$ , and  $H_6E_0P_{10}$  collected simultaneously (field of view  $20\ \mu\text{m} \times 20\ \mu\text{m}$ ).

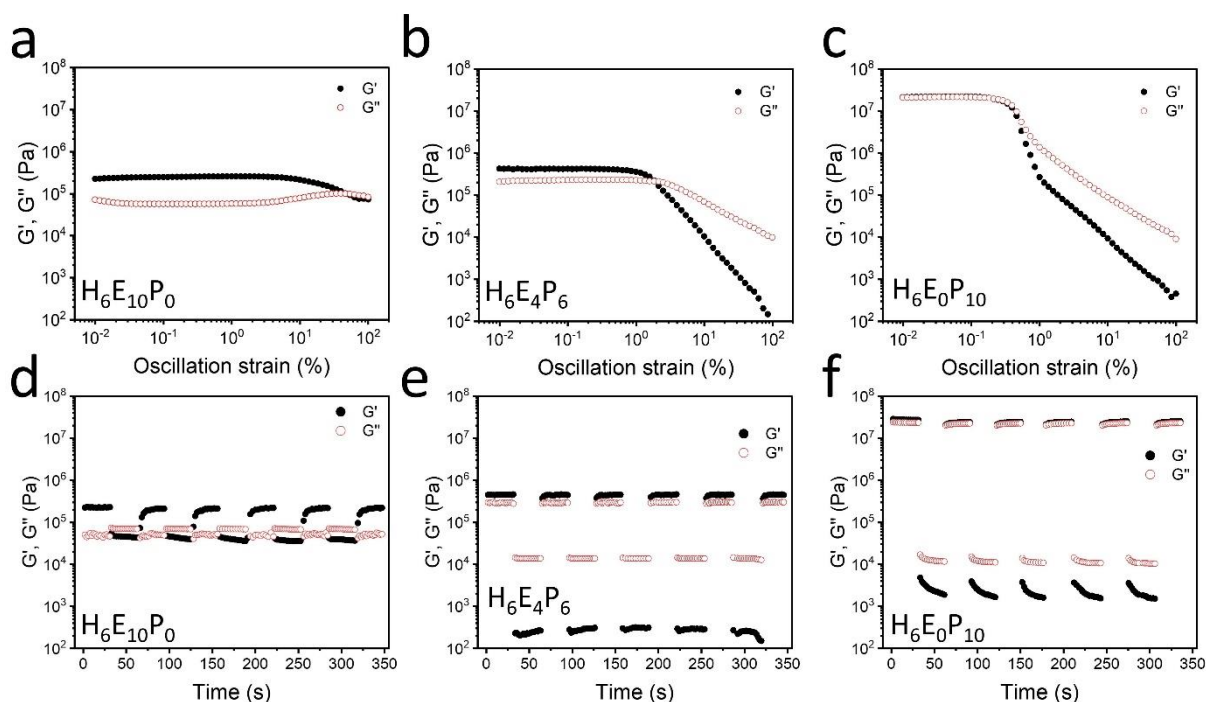


**Figure S3-3.** XRD of phase-separated gels prepared on glass support. The thickness of all samples is around  $300\ \mu\text{m}$ . Globules of the polymers are increased from  $H_6E_0P_{10}$  to  $H_6E_{10}P_0$  by changing the composition of the polymerization mixtures.

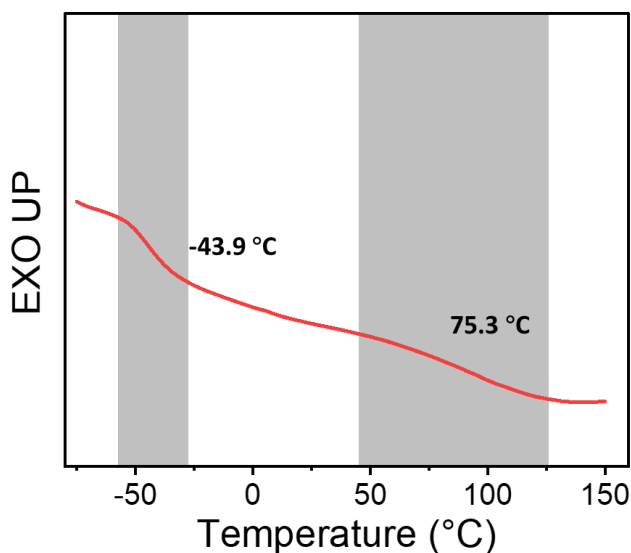


**Figure S3-4.** Elongation at break (a) and elastic modulus (b) of polymer gels with different compositions of PEG and PPG. Data represent the mean  $\pm$  standard deviation ( $n = 3$ ).





**Figure S3-5.** Rheology analyses of the recovery property. Storage moduli ( $G'$ ) and loss moduli ( $G''$ ) of  $H_6E_{10}P_0$  (a),  $H_6E_4P_6$  (b), and  $H_6E_0P_{10}$  (c) from strain amplitude sweep at 30 °C with frequency of 10 rad/s.  $G'$  and  $G''$  of  $H_6E_{10}P_0$  (d),  $H_6E_4P_6$  (e), and  $H_6E_0P_{10}$  (f) from continuous strain sweep with alternate small oscillation force ( $\gamma = 0.05\%$  strain) and large one ( $\gamma = 100\%$ ) at 30 °C with frequency of 10 rad/s.



**Figure S3-6.** Differential scanning calorimetry (DSC) trace of  $H_6E_4P_6$ , showing two  $T_g$ . The lower  $T_{g1}$  is -43.9 °C from the soft solvent-rich domains. The higher  $T_{g2}$  is 75.3 °C from the stiff polymer-rich domains.

## 4 Conclusions and Outlook

### 4.1 Conclusions

Within this thesis, three functional tough polymer gels were designed and fabricated by utilizing proposed concept claiming the importance of the solvent in defining a gel's properties. The three gel systems reported here, and based on the PEG as a solvent, are called PEGgel (Chapter 3.1), Ionic PEGgel (Chapter 3.2) and phase-separated PEGgel (Chapter 3.3).

In Chapter 3.1, a universal method for fabrication of tough gels using PEG as a solvent is developed. PEGgels based on P(HEMA-*co*-AAc) presented superior and versatile properties, in terms of long-lasting performance (>1 month), high stretchability (6000% at 50 mm/min), transparency (95% for visible light), rapid self-healing (1 min) and 3D printability. The abundant but relatively weak C-H...O hydrogen bonding added considerably to the overall stiffness of the PEGgel, with the increased long-range correlations and polymer entanglement facilitating the enhanced durability against fracture. Then, varying the volume fraction or molecular weight of PEG, the PEGgel exhibited tunable mechanical properties over a large window of properties with tensile strength increased from 0.22 MPa to 41.3 MPa, fracture strain from 12% to 4336%, elastic modulus from 0.08 MPa to 352 MPa, and toughness from 2.89 MJ m<sup>-3</sup> to 56.23 MJ m<sup>-3</sup>. Based on this simple but multi-functional gel, self-healing pneumatic actuators were fabricated, showing potential of PEGgel in broad applications in soft actuators and robots. Last but not least, the PEGgel system was successfully applied to other polymer networks, showing generality and customizability. Since the compatibility between PEG and various polymers has been widely confirmed, PEGgels offer great promise for application in various serviceable functions that can be extended to a various platform to meet the needs of a variety of areas ranging from biomedical applications to flexible electronics and soft robots.

Chapter 3.2 focused on the ionic PEGgel. It was shown that adding ionic into PEGgel allowed us to fabricate versatile ionic PEGgels. The typical ionic PEGgel is composed of in-situ formed physically cross-linked poly(2-hydroxyethyl methacrylate) networks and poly(ethylene glycol) (PEG). The long molecular chains of PEG serve as a solvent for dissolving electrolytes, improve its long-term stability, reduce solvent leakage, and ensure

the outstanding mechanical properties of the ionic PEGgel. Incorporating ions into PEG simultaneously enhances the strength and toughness of the polymer gels, showing an impressive ionic conductivity ( $0.04 \text{ S m}^{-1}$ ), stretchability of up to 1400%, high toughness ( $7.16 \text{ MJ m}^{-3}$ ), fast self-healing of ion-conducting (2.8 s), as well as thermal and electrochemical stability ( $> 60,000$  cycles). By tuning the fraction of PEG, the strength and toughness of IHP-3 could be further improved to 10.04 MPa and  $16.9 \text{ MJ m}^{-3}$  separately. This section demonstrated applications of the ionic PEGgel as a) strain and temperature sensors, showing high sensitivity of resistance change at  $6.03$  and  $0.06 \text{ }^\circ\text{C}^{-1}$ , respectively; b) skin electrodes to capture ECG signals with improved stability compared to commercial hydrogel electrodes; c) a tough and elastic material for pneumatic artificial muscles.

In the Chapter 3.3, a simple and efficient method is presented for fabricating tough phase-separated polymer gels using PEG and PPG as solvents with two distinct compatibilities with polymer networks. After polymerizing the monomer in the mixture solvent of PEG and PPG, the *in-situ* phase separations are formed. During deformation, the stiff polymer-rich phase dissipates energy, while the soft solvent-rich phase maintains the large strain. The resulting H<sub>6</sub>E<sub>4</sub>P<sub>6</sub> demonstrates high strength (8.0 MPa), favorable fracture strain (430%), and large toughness ( $17.0 \text{ J m}^{-3}$ ). The separated phases endow the polymer gel with shape memory property, which can be used for various soft machines combined with 3D printability. For the scalability of this solvent strategy, ions were incorporated into PEG/PPG solvent to achieve a hierarchical enhancement in polymer gels covering from the ionic interactions (nano-level) to phase separation (micro-level). Such a hierarchical structure further enhanced the strength and toughness of polymer gels, showing high fracture strength (12.2 MPa) and fracture energy ( $54 \text{ kJ m}^{-2}$ ).

### 4.2 Outlook

Although various polymer gels based on PEG have shown admirable performance, some challenges remain, including fatigue resistance, anti-swelling properties, humidity stability, and even friction resistance. All of these mentioned challenges are difficult to solve only by solvent strategies. Due to the compatibility or scalability of solvent strategies, combining the design of polymer networks with solvent strategies seem to be a promising approach to achieving novel soft materials covering large spaces of functionalities. Although we mainly present the polymer gels based on PEG and PPG in this thesis, there are many oligomer choices for potential polymer gels. Also, endowing various functions into polymer gels can also be achieved by modifying the oligomer molecules.

Besides the “big” challenges above, some small goals can be tried based on current findings and results.

1. The toughening mechanism of oligomers used as a solvent is still not completely elucidated. More advanced technologies can be used to monitor the polymer gels from the nanoscale to the microscale during deforming. This would help us to understand the energy dissipation mechanism for further design of novel polymer gels.
2. With the 3D printability, this series of PEGgels can be integrated into other actuator designs and potentially generate advanced soft machines, actuators, and functional components of robotics devices.
3. Adding further active, dynamic, or functional fillers into the PEGgel can endow the PEGgel with various admirable functionalities, such as electrical conductivity and magnetic or fluorescent properties. This can make the PEGgel more meaningful for practical applications.
4. Some stimuli-responsive oligomers or polymer fluids can be used as solvents to prepare polymer gels. Imagining the polymer gel owning both stimuli-responsive solvents and networks is exciting.
5. Learning the mechanics of natural systems may hint at the design of novel polymer gels. For example, the ordered distribution of soft and hard phases can be achieved by high-resolution 3D printing technologies, such as two-photon absorption 3D printing or two-step absorption 3D printing.

6. The tissue adhesion based on oligomer gels would also be an interesting research topic. Diffusing polymer chains from adhesives into tissue was an efficient way to build strong adhesion. It is possible to achieve it by using oligomers with suitable polymer lengths.

## 5 Appendix

### 5.1 List of Figures

- Figure 1. A picture of a jellyfish swimming taken at Musée océanographique de Monaco. Jellyfish, the oldest multi-organ animal group in nature, contains more than 95% of water as solvent in the body. They can move, sense, and grow up based on such a completely soft gel-like system. What do we need to create artificial soft functional machines similar to jellyfish? ..... XII
- Figure 2. Schematic illustration of gelation mechanism of organogels. (a) Polymer chains self-assembly into physically cross-linked organogels. (b) Cross-linkers connect polymer chains to form chemically cross-linked organogels. (c) Solvents swell cross-linked bulk polymers to prepare organogels. (d) Monomer solutions are polymerized to form organogels. .... 16
- Figure 3. Strategies to fabricate IL gels. a) Top-down strategy to fabricate IL gels by mixing polymers and ILs. b) Bottom-up strategy to fabrication of IL gels based on the polymerization of monomers in ILs. .... 23
- Figure 4. a) Schematic description of IL gels based on poly (ethyl acrylate) and 1-ethyl-3-methylimidazolium bis(trifluoromethylsulfonyl)imide with their mechanical properties and potential applications.<sup>41</sup> b) Schematics of IL gels with in situ phase separation and their performance.<sup>42</sup> ..... 24
- Figure 5. a) Schematic illustration of the fabrication of Sulfonated lignin-Fe<sup>3+</sup>-DES eutectogel from hydrogel by the method of solvent replacement.<sup>58</sup> b) Scheme illustration of the preparation of PAA gel in the presence of DES.<sup>59</sup> c) Schematic illustration of the strong, tough, and ultra-stretchable eutectogel based on tetramethylammonium chloride and acrylic acid.<sup>63</sup> ..... 30
- Figure 6. a) Schematic illustration of eutectogel based on copolymer of acrylic amide/choline chloride and maleic acid/choline chloride polymerizable DES.<sup>64</sup> b) Schematic illustration for the preparation of cellulose nanocrystals/poly DES in situ composites and network of dynamic interfacial hydrogen bonds.<sup>62</sup> ..... 31

- Figure 7. Schematic structure of high energy-dissipation polymer-fluid-gels (PFGs) design.<sup>74</sup> .....34
- Figure 8. Slippery surfaces based on polymer gels with solvent strategies. a) Schematic illustration of the preparation and reconfiguration of hetero network organohydrogels.<sup>86</sup> b) Rational design of ionic liquid gel surfaces with easy-sliding and ultradurable features.<sup>89</sup> 37
- Figure 9. Anti-freezing and anti-hydration polymer gels based on functional solvent strategies. a) Salt addition in solvents for anti-freezing hydrogel.<sup>100</sup> b) Solvent displacement for the fabrication of tough organohydrogels.<sup>97</sup> c) solvent mixture for the fabrication of hydrogel with long-lasting moisture and extreme temperature tolerance.<sup>101</sup> .....41
- Figure 10. Schematics of the aggregation states of PVA polymer chains treated with different ions.<sup>112</sup> .....44
- Figure 11. Solvent strategies to enhance the electrical performance of polymer gels. a) Hydrothermal reduction for fabricating graphene oxide hydrogels based on its aqueous dispersion.<sup>127</sup> b) Free-standing PEDOT:PSS hydrogels with different geometric shapes fabricated by solvent strategies.<sup>134</sup> c) PEDOT:PSS hydrogels prepared by dry-annealing and rehydration method.<sup>135</sup> .....47
- Figure 12. Concept of PEGgels. a) Schematic illustration of the hydrogel and PEGgel structure. b) Photographs of PEGgel stretched 6000%. c) Representative tensile stress-strain curves of hydrogel, PEGgel and EG gel based on the same P(HEMA-*co*-AAc) polymer matrix and 50% solvent fraction. d) Photograph of a PEGgel membrane deformed by a sharp metal pin (pin diameter = 1 mm). Scale bar: 10 mm e) Hydrogel and PEGgel blocks bent immediately after preparation and after storage for 2 days and 30 days, demonstrating the long-term stability of the PEGgel compared with that of the hydrogel. Copyright 2022 Wiley-VCH.<sup>69</sup> .....56
- Figure 13. The CGMD simulation and the solid-state NMR investigation of the gel systems. a) CGMD simulated single chain conformations of P(HEMA-*co*-AAc) in water, PEG, and EG (from left to right). Size of the single chain, characterized by the calculated radius of gyration for the single-chain polymer. Atom groups in HEMA-*co*-AAc are color coded in accordance with the CG scheme in Figure S1-10. The solvent in the immediate vicinity of the polymer is shown as tan-color dots for water, violet-colored dots for EG, and pink short

chains for PEG. b) A snapshot of the polymer-PEG-polymer cross-linking via H-bonding for the single P(HEMA-*co*-AAc) chain in PEG. The PEG highlighted in red forms an intrapolymer cross-linking unit. c) Componential contributions to the interaction potentials of the O-H...O hydrogen bonding, C-H...O hydrogen bonding and covalent bonds in three gels stretched to 550%. d) Solid state MAS <sup>1</sup>H-NMR spectra of hydrogel (blue), PEGgel (orange), and EG gel (gray). Anticipated inter- and intra-chain interactions are supported by 2D exchange <sup>1</sup>H-NMR experiments acquired under MAS using a mixing time of 100 ms of the hydrogel (e), PEGgel (f), and EG gel (g). The cross peaks arising from magnetization exchange between methyl-groups (-CH<sub>3</sub>) and copolymer backbone (-CH<sub>2</sub>-CH<sub>2</sub>-) in P(HEMA-*co*-AAc) are marked in blue, which connect the resonances at 1.1 and 2.4 ppm, respectively. Copyright 2022 Wiley-VCH.<sup>69</sup> .....61

Figure 14. The tunable mechanical properties of PEGgel. a) Representative stress-strain curves of PEGgels containing PEG 400 with volume fractions ranging from 20 vol.% (HAP-2) to 50 vol.% (HAP-5). b) Representative stress-strain curves of PEGgels composed of PEG 200 (HAP 200), 400 (HAP 400), 600 (HAP 400) and 1000 (HAP 1000), with constant PEG fraction of 40 vol.%. c-f) Modulus (c), fracture strain (d), strength (e), and toughness (f) of PEGgels mechanically tuned based on variation of PEG types and volume fractions. g) The range of elastic moduli of soft human tissues and corresponding PEGgels. Data represent the mean ± standard deviation (n = 3). Copyright 2022 Wiley-VCH.<sup>69</sup> .....64

Figure 15. Self-healing properties of PEGgel. a) Self-healing mechanism of the PEGgel is based on the PEG functioning as a diffusive H-bonding molecular glue capable of cross-linking damaged polymer chains. b) The PEGgel (HAP-5) samples (3 mm × 5 mm × 15 mm) stained with methyl blue and Sudan | cut into two pieces show complete healing within 1 min. c) Healed PEGgel sample supports 1 kg weight. d) Tensile stress-strain curves of PEGgel samples after different healing times. Inset photo shows gel stretched over 4000% after 1h of healing (scale bar: 5 mm). e) Schematic illustration of the scratch-healing test, simulating a skin tissue wound. f) The scratch wound on a PEGgel film (HAP-5, 1000 μm thick) is completely healed after 360 s (scale bar: 500 μm). Copyright 2022 Wiley-VCH.<sup>69</sup> .....67

Figure 16. Use of 3D-printable self-healing PEGgel based soft actuators. a, b) Schematic diagram and photographs of a soft pneumatic actuator prepared from HAP-4 via digital light



processing (DLP) 3D printing technology. c) Bending of the 3D printed actuator under 0.5 MPa air pressure. d) Healing of the actuator after total separation, and bending under 0.5 MPa air pressure after 10 min of healing. e) Quantification of the bend height of the soft actuator before cutting and after healing shows no distinguishable difference. The bend height is the vertical gap between the head and tail. The dotted line connects the data points. f) Design and fabrication of the actuator with two fingers to capture a soft rubber pipette bulb. Scale bars: 5 mm. Copyright 2022 Wiley-VCH.<sup>69</sup> ..... 69

Figure 17. Generality of PEGgel systems in different polymer networks. Representative stress-strain curves of hydrogel (blue), PEGgel (orange) and EG gel (gray) composed of chemically cross-linked poly(2-hydroxyethyl methacrylate) (a), chemically cross-linked poly(acrylic acid) (b), chemically cross-linked poly([2-(acryloyloxy)-ethyl]-trimethyl ammonium chloride) (c) and physically cross-linked copolymer of 2-hydroxyethyl methacrylate and [2-(acryloyloxy)-ethyl]-trimethyl ammonium chloride (d). e-g) Strength (e), Fracture Strain (f) and Toughness (g) of three types of gels with various polymer networks. All chemically cross-linked gel is achieving by adding PEGDA (1 vol.% of corresponding monomer). Data represent the mean  $\pm$  standard deviation (n = 3). Copyright 2022 Wiley-VCH.<sup>69</sup> ..... 71

Figure 18. Overview of the IHPs. a) Illustration of the mechanism of enhancement of mechanical properties of IHP through the metal cation. b) Image of a 3D-printed tower with a spiral staircase inside based on IHP. c) Image demonstrating the remarkably high strength of the IHP (3 M LiCl, 35 mm  $\times$  15 mm  $\times$  3 mm), by sustaining a dumbbell (2 kg). d) Top: Image demonstrating the mechanical stability under extreme temperatures (twisted at -20°C). Bottom: Image from a thermal camera at the same time. e) Image demonstrating the no solvent leakage of the IHP under 150 °C, in which the paper retained dry after peeling from the IHP surface. Representative tensile curves (f), elastic modulus (g), strength, and toughness (h) of IHPs with different salt types at 0.1 mol kg<sup>-1</sup>. Error bars represent standard deviation (n = 3). ..... 100

Figure 19. Mechanical and electrochemical properties of IHPs. a) Representative stress-strain curves of IHPs with different LiCl concentrations, in which IHP-x corresponds to HP with x mol kg<sup>-1</sup> LiCl. b) Strength and toughness of IHPs with different LiCl concentrations. Error bars are standard deviations (n = 3). c) Continuous cyclic tensile loading-unloading

curves of IHP-3 with strain going to 100%, 300%, 500%, and 1000%. d) Representative stress-strain curves of IHP-3 with increasing healing time after the cut. e) Resistance change of IHP-3 during the cut and assembling process. f) Cyclic linear sweep voltammetry curves of the IHP-3 with a scanning speed of 500 mV s<sup>-1</sup> after 60,000 cycles. .... 104

Figure 20. Molecular dynamics simulation of HP and IHP. Representative snapshots for PEG molecule (a) and PHEMA polymer chain (b) in HP and IHP. In PEG molecules, the orange spheres are carbon atoms, white spheres are hydrogen atoms, and red spheres are oxygen atoms. In PHEMA polymer chain, the blue spheres are carbon atoms, red spheres are oxygen atoms, and deeper blue spheres are the backbone carbon atoms of the PHEMA. Hydrogen atoms of PHEMA are not displayed due to their simplicity. Yellow spheres are Li cations. c) Distribution of the radius of gyration ( $R_g$ ) of PEG (solid line) and PHEMA (dotted line) in HP (blue) and IHP (orange). d) The number change of hydrogen bond (blue) and Li coordination (orange) in HP and IHP, containing intra PEG, inter PEG, intra PHEMA, inter PHEMA, and PEG-PHEMA. These results come from the simulation, which is performed by Yu-Cheng Lai and Ya-Tang Chiang from Chia-Ching Chou Group at the Institute of Applied Mechanics, College of Engineering, National Taiwan University as a part of the collaborative project..... 107

Figure 21. Sensing properties of IHPs. a) Dependence of relative resistance change on the applied tensile strain for IHP-3. b) relative change of resistance of IHP-3 upon cyclic tensile loading/unloading tests (0-100% strain) over 1500 times. c) Comparison of IHP-3 with previously reported strain sensors based on self-healing ICE, in terms of gauge factor and ultimate tensile strength. The hollow red pentacle represents this work. d) IHP-3 were integrated into gloves for detecting human hand gestures. The relative changes of the resistance of five fingers depending on the hand pose were used to convert sign language into an electric signal (left to right: "Love", "Good" and "OK"). e) the relative change of the resistance of IHP-3 in dependence of the temperature during 30°C - 70°C. f) Images of light bulb controlled by the temperature sensor with putting cold or hot metal pin and removing the pin. .... 110

Figure 22. Ionotronics based on IHPs. a) A schematic of ECG signal real-time monitor, including flexible electrodes and intelligent display terminal. b) Photograph of the IHP electrodes attached to the skin for achieving ECG signal capture and display. c) ECG signals

recorded based on commercial hydrogel electrodes (top row) and IHP electrodes (bottom row) under normal conditions (left), during sweating (middle), and after one day (right).

..... 112

Figure 23. Schematic illustrations of *in-situ* phase-separated polymer gels using mixed oligomer solvents. a) In pure PEG solvent, the PHEMA swollen in PEG forms a uniform, transparent, and elastic network, resulting from the high solubility. b) In mixed solvents of PEG and PPG, PHEMA swells in PEG to create highly solvated and soft domains and aggregates in PPG to form poorly solvated and stiff domains. Soft domains connect the stiff domains to form an extremely tough gel. c) In PPG gel, the poor solubility induced strong hydrogen bonds between PHEMA chains, driving aggregation to form separated stiff domains surrounded by PPG. .... 139

Figure 24. Overview and structural characterization of the phase-separated gel. (a to c) Photographs of pure PEGgel ( $H_6E_{10}P_0$ ), pure PPG gel ( $H_6E_0P_{10}$ ) and PEG/PPG gel ( $H_6E_4P_6$ ). "H<sub>x</sub>" means that HEMA accounts for x tens percentage in the prepolymer solution; "E<sub>y</sub>" or "P<sub>z</sub>" means that PEG or PPG account for y or z tens percentage in the mixed solvents, respectively. The size of these three gels are all 3\*15\*38 mm a)  $H_6E_{10}P_0$  presents soft and flexible, achieving natural bending and sagging. b)  $H_6E_4P_6$  can hold itself without bending. c)  $H_6E_0P_{10}$  behaves stiff, which can hold 200 g weight without bending. d)  $H_6E_0P_{10}$  can lift 20 kg weight without damage. e-g) Photos of phase-separated gels with different solvent ratios, showing decreasing transparency with the increasing content of PPG. The diameter of all samples is 10 mm. h-j) SEM image of phase-separated gels with different solvent ratios. k) AFM image and l) phase image of  $H_6E_4P_6$ , collected simultaneously (field of view 20  $\mu\text{m} \times 20 \mu\text{m}$ ). All scale bars are 5  $\mu\text{m}$ . .... 141

Figure 25. Mechanical properties of the phase-separated gel. a) Representative stress-strain curves of polymer gels with different compositions of PEG and PPG. Strength (b) and toughness (c) of polymer gels with different compositions of PEG and PPG. Data represent the mean  $\pm$  standard deviation (n = 3). d) Frequency dependence of storage modulus ( $G'$ ) and loss modulus ( $G''$ ) for  $H_6E_{10}P_0$ ,  $H_6E_4P_6$ , and  $H_6E_0P_{10}$ . The master curves were obtained by time-temperature superposition (TTS) at a reference temperature of 30 °C. All samples were tested at 30 °C, 50 °C, 75 °C, 100 °C, 125 °C, and 150 °C. During the frequency sweep

tests, the angular frequency was increased from 0.1 to 100  $\text{rad s}^{-1}$  at specified temperatures with the shear strain of 0.01% to 1%. e) Master curves for the  $\tan\theta$  of  $\text{H}_6\text{E}_{10}\text{P}_0$ ,  $\text{H}_6\text{E}_4\text{P}_6$ , and  $\text{H}_6\text{E}_0\text{P}_{10}$ . f)  $G'$  and  $G''$  of  $\text{H}_6\text{E}_4\text{P}_6$  under continuous strain sweep with alternate small oscillation force ( $\gamma = 0.05\%$  strain) and large one ( $\gamma = 100\%$ ) at 30 °C with frequency of 10 rad/s. .... 144

Figure 26. 4D printing of the phase-separated gel. a) The shape-memory behavior of a 3D printed hexagonal hollow egg-shaped structure, recovery from the collapsed state back to the original. b) The 3D-printed quadruped model can stand by itself after heating. c) The 3D-printed quadruped model with a small table can turn itself over and stand in the right direction after heating. d) The printed actuator can jack up 100g weight after heating, which is 116 times its own weight (0.86 g). The samples with complex 3D structures were prepared by DLP 3D Printer based on  $\text{H}_6\text{E}_4\text{P}_6$  directly (Table S3-2). All heating processing (over 80 °C) was achieved by plate heating at the bottom and a heat gun at the top. The left column is the model designed for printing. All scale bars are 5 mm. .... 146

Figure 27. Scalability of phase-separation strategy for fabricating super tough gels with hierarchical structures. a) Representative stress-strain curves of  $\text{H}_6\text{E}_{10}\text{P}_0$ ,  $\text{H}_6\text{E}_4\text{P}_6$ ,  $\text{H}_6\text{E}_0\text{P}_{10}$ , and  $\text{IH}_6\text{E}_4\text{P}_6$ . Strength (b), toughness (c), elongation at break (d), and fracture energy (e) of these polymer gels. f) A comparison between this work and cartilage, natural rubber, PDMS, and various gels regarding fracture energy to fracture strength. .... 147

## 5.2 List of Tables

Table 1. Common small molecule solvents for organogels.....	17
Table 2. Some common examples of cations and anions used in the formation of corresponding ionic liquid and thereby admirable properties, and changes of water miscibility with anion type. ....	25
Table 3. General Formula for the Classification of DESs. <sup>47</sup> .....	26
Table 4. Representative sampling of common constituents of Type III DESs used in previous studies. <sup>51</sup> .....	29

### 5.3 List of Abbreviations

PEG	Poly ethylene glycol
PEGgel	Poly ethylene glycol gel
PPG	Poly propylene glycol
FDA	U.S. Food and Drug Administration
PDMS	Polydimethylsiloxane
EG	Ethylene glycol
HEMA	2-Hydroxyethylmethacrylat
AAc	Acrylic Acid
DAC	[2-(acryloyloxy)-ethyl]-trimethyl ammonium chloride
PDMS	Poly dimethyl siloxane
ChCl	Choline Chloride
TGA	Thermogravimetric Analysis
DSC	Differential Scanning Calorimetry
AFM	Atomic Force Microscopy
SEM	Scanning Electron Microscope
XRD	X-ray diffraction
ATR FT-IR	Attenuated Total Reflexion Fourier Transform Infrared Spectroscopy
GPC	Gel Permeation Chromatography
NMR	Nuclear Magnetic Resonance
PXRD	Powder X-ray Diffractometry
UV-Vis	Ultra-Violet-Visible
G'	Storage Modulus
G''	Loss Modulus
vol%	Volume Percent
wt%	Weight Percent
CGMD	Coarse-Grain Molecular Dynamics
$M_w$	Mass Average Molar Mass
$M_n$	Number Average Molar Mass
$\delta$	Chemical Shift
$\lambda$	Wavelength
$\theta$	Angle of Incidence
GF	Gauge Factor or Sensitivity

## 5.4 Curriculum Vitae

### Personal Data

---

Name	Zhenwu Wang
Email	wangzhenwuup@gmail.com

---

### Education

---

10.2019-12.2022	PhD studies Karlsruhe Institute of Technology (KIT), Germany Institute of Biological and Chemical Systems – Functional Molecular Systems (IBCS-FMS) Supervisor: Prof. Pavel A. Levkin Research Topic: Functional Polymer Gels
-----------------	--

---

## 5.5 Publications and Conference Contributions

### *Publications* (Since 2019.10)

1. **Wang, Z.**; Cui, H.; Liu, M.; Grage, S. L.; Hoffmann, M.; Sedghamiz, E.; Wenzel, W.; Levkin, P. A., Tough, Transparent, 3D-Printable, and Self-Healing Poly(ethylene glycol)-Gel (PEGgel). *Advanced Materials* **2022**, *34* (11). DOI: 10.1002/adma.202107791
2. **Wang, Z.**; Lai, Y.; Chiang, Y.; Scheiger, J. M.; Li, S.; Dong, Z.; Cai, Q.; Liu, S.; Hsu, S.; Chou, C.; Levkin, P. A. Tough, Self-healing, and Conductive Elastomer --- Ionic PEGgel. *ACS Applied Materials & Interfaces* **2022**, Just Accepted, DOI: 10.1021/acsami.2c14394
3. **Wang, Z.**; Cui, H.; Li, S.; Feng, X.; Aghassi-Hagmann, J.; Azizian, S.; Levkin, P. A., Facile Approach to Conductive Polymer Microelectrodes for Flexible Electronics. *ACS Applied Materials & Interfaces* **2021**, *13* (18), 21661-21668. DOI: 10.1021/acsami.0c22519
4. **Wang, Z.**; Heck, M.; Yang, W.; Wilhelm, M.; Levkin, P. A. Tough PEGgels by In-situ Phase Separation for 4D Printing. In preparation.
5. **Wang, Z.**; Cong, Y.; Fu, J., Stretchable and tough conductive hydrogels for flexible pressure and strain sensors. *Journal of Materials Chemistry B* **2020**, *8* (16), 3437-3459. DOI: 10.1039/c9tb02570g
6. Wei, H.; **Wang, Z.**; Zhang, H.; Huang, Y.; Wang, Z.; Zhou, Y.; Xu, B. B.; Halila, S.; Chen, J., Ultrastretchable, Highly Transparent, Self-Adhesive, and 3D-Printable Ionic Hydrogels for Multimode Tactical Sensing. *Chemistry of Materials* **2021**, *33* (17), 6731-6742. DOI: 10.1021/acs.chemmater.1c01246
7. Scheiger, J. M.; Hoffmann, M.; Falkenstein, P.; **Wang, Z.**; Rutschmann, M.; Scheiger, V. W.; Grimm, A.; Urbschat, K.; Sengpiel, T.; Matysik, J.; Wilhelm, M.; Levkin, P. A.; Theato, P., Inverse Vulcanization of Norbornenylsilanes: Soluble Polymers with Controllable Molecular Properties via Siloxane Bonds. *Angewandte Chemie - International Edition* **2022**, *61* (16). DOI: 10.1002/anie.202114896
8. Li, S.; Scheiger, J. M.; **Wang, Z.**; Dong, Z.; Welle, A.; Trouillet, V.; Levkin, P. A., Substrate-Independent and Re-Writable Surface Patterning by Combining



---

Polydopamine Coatings, Silanization, and Thiol-Ene Reaction. *Advanced Functional Materials* **2021**, 31 (50). DOI: 10.1002/adfm.202107716

### ***Conference Contributions***

---

12.2022	Oral presentation
2022 MRS Fall Meeting	
Functional Polymer Gels Based on Oligomer Fluids	
06.2022	Oral presentation
Max Planck Institute for the Physics of Complex Systems Workshop---Intelligent Machines? – Self-Organized Nonlinear Dynamics of Machines across Scales	
3D-Printable, Tough and Self-Healing Elastomer for Soft Machines	
06.2022	Oral presentation
Materials DAY	
Functional Polymer Gels based on PEG Fluids	
06.2022	Oral presentation
BioInterfaces International Graduate School RETREAT	
06.2021	Poster presentation
BioInterfaces International Graduate School RETREAT	
10.2022	Poster presentation
7th International Conference on Multifunctional, Hybrid and Nanomaterials	

---

## 6 Literature

- 1 Ajayaghosh, A. & Praveen, V. K.  $\pi$ -Organogels of Self-Assembled p-Phenylenevinylenes: Soft Materials with Distinct Size, Shape, and Functions. *Accounts of Chemical Research* **40**, 644-656, doi:10.1021/ar7000364 (2007).
- 2 Simmons, B. *et al.* Spatial Compartmentalization of Nanoparticles into Strands of a Self-Assembled Organogel. *Nano Letters* **2**, 1037-1042, doi:10.1021/nl015691r (2002).
- 3 Jones, M.-C. *et al.* Self-Assembled Nanocages for Hydrophilic Guest Molecules. *Journal of the American Chemical Society* **128**, 14599-14605, doi:10.1021/ja065462c (2006).
- 4 Liu, D.-E., Chen, Q., Long, Y.-B., Ma, J. & Gao, H. A thermo-responsive polyurethane organogel for norfloxacin delivery. *Polymer Chemistry* **9**, 228-235, doi:10.1039/C7PY01803G (2018).
- 5 O'Bryan, C. S. *et al.* Self-assembled micro-organogels for 3D printing silicone structures. *Science* **3**, e1602800, doi:10.1126/sciadv.1602800 (2017).
- 6 Zhu, L. *et al.* Ice-phobic Coatings Based on Silicon-Oil-Infused Polydimethylsiloxane. *ACS Applied Materials & Interfaces* **5**, 4053-4062, doi:10.1021/am400704z (2013).
- 7 Urata, C., Dunderdale, G. J., England, M. W. & Hozumi, A. Self-lubricating organogels (SLUGs) with exceptional syneresis-induced anti-sticking properties against viscous emulsions and ices. *Journal of Materials Chemistry A* **3**, 12626-12630, doi:10.1039/C5TA02690C (2015).
- 8 Howell, C. *et al.* Self-Replenishing Vascularized Fouling-Release Surfaces. *ACS Applied Materials & Interfaces* **6**, 13299-13307, doi:10.1021/am503150y (2014).
- 9 Yao, X. *et al.* Self-Replenishable Anti-Waxing Organogel Materials. *Angewandte Chemie International Edition* **54**, 8975-8979, doi: 10.1002/anie.201503031 (2015).
- 10 Brochard, F. & de Gennes, P. G. Dynamical Scaling for Polymers in Theta Solvents. *Macromolecules* **10**, 1157-1161, doi:10.1021/ma60059a048 (1977).
- 11 Patel, S. K. & Cohen, C. Dynamic light scattering from swollen poly(dimethylsiloxane) networks. *Macromolecules* **25**, 5252-5258, doi:10.1021/ma00046a022 (1992).
- 12 Introduction: Ionic Liquids. *Chemical Reviews* **117**, 6633-6635, doi:10.1021/acs.chemrev.7b00246 (2017).
- 13 Vekariya, R. L. A review of ionic liquids: Applications towards catalytic organic transformations. *Journal of Molecular Liquids* **227**, 44-60, doi: 10.1016/j.molliq.2016.11.123 (2017).

- 14 Correia, D. M. *et al.* Ionic Liquid–Polymer Composites: A New Platform for Multifunctional Applications. *Advanced Functional Materials* **30**, 1909736, doi: 10.1002/adfm.201909736 (2020).
- 15 Boeck, G. Paul Walden (1863–1957): the man behind the Walden inversion, the Walden rule, the Ostwald-Walden-Bredig rule and Ionic liquids. *ChemTexts* **5**, 6, doi:10.1007/s40828-019-0080-9 (2019).
- 16 Patel, D. D. & Lee, J.-M. Applications of ionic liquids. *The Chemical Record* **12**, 329-355, doi: 10.1002/tcr.201100036 (2012).
- 17 Dong, K., Liu, X., Dong, H., Zhang, X. & Zhang, S. Multiscale Studies on Ionic Liquids. *Chemical Reviews* **117**, 6636-6695, doi:10.1021/acs.chemrev.6b00776 (2017).
- 18 Izgorodina, E. I., Seeger, Z. L., Scarborough, D. L. A. & Tan, S. Y. S. Quantum Chemical Methods for the Prediction of Energetic, Physical, and Spectroscopic Properties of Ionic Liquids. *Chemical Reviews* **117**, 6696-6754, doi:10.1021/acs.chemrev.6b00528 (2017).
- 19 Zhang, Z., Song, J. & Han, B. Catalytic Transformation of Lignocellulose into Chemicals and Fuel Products in Ionic Liquids. *Chemical Reviews* **117**, 6834-6880, doi:10.1021/acs.chemrev.6b00457 (2017).
- 20 Zhang, S., Zhang, J., Zhang, Y. & Deng, Y. Nanoconfined Ionic Liquids. *Chemical Reviews* **117**, 6755-6833, doi:10.1021/acs.chemrev.6b00509 (2017).
- 21 Domańska, U. Solubilities and thermophysical properties of ionic liquids. *Pure and Applied Chemistry* **77**, 543-557, doi:doi:10.1351/pac200577030543 (2005).
- 22 Lassègues, J.-C., Grondin, J. & Talaga, D. Lithium solvation in bis(trifluoromethanesulfonyl)imide-based ionic liquids. *Physical Chemistry Chemical Physics* **8**, 5629-5632, doi:10.1039/B615127B (2006).
- 23 Takada, A., Imaichi, K., Kagawa, T. & Takahashi, Y. Abnormal Viscosity Increment Observed for an Ionic Liquid by Dissolving Lithium Chloride. *The Journal of Physical Chemistry B* **112**, 9660-9662, doi:10.1021/jp800633x (2008).
- 24 Swatloski, R. P., Spear, S. K., Holbrey, J. D. & Rogers, R. D. Dissolution of Cellulose with Ionic Liquids. *Journal of the American Chemical Society* **124**, 4974-4975, doi:10.1021/ja025790m (2002).
- 25 Zhu, S. *et al.* Dissolution of cellulose with ionic liquids and its application: a mini-review. *Green Chemistry* **8**, 325-327, doi:10.1039/B601395C (2006).
- 26 Tan, S. S. Y. *et al.* Extraction of lignin from lignocellulose at atmospheric pressure using alkylbenzenesulfonate ionic liquid. *Green Chemistry* **11**, 339-345, doi:10.1039/B815310H (2009).
- 27 Sun, N. *et al.* Complete dissolution and partial delignification of wood in the ionic liquid 1-ethyl-3-methylimidazolium acetate. *Green Chemistry* **11**, 646-655, doi:10.1039/B822702K (2009).

- 28 Welton, T. Room-Temperature Ionic Liquids. Solvents for Synthesis and Catalysis. *Chemical Reviews* **99**, 2071-2084, doi:10.1021/cr980032t (1999).
- 29 Hallett, J. P. & Welton, T. Room-Temperature Ionic Liquids: Solvents for Synthesis and Catalysis. 2. *Chemical Reviews* **111**, 3508-3576, doi:10.1021/cr1003248 (2011).
- 30 Martins, M. A. P., Frizzo, C. P., Moreira, D. N., Zanatta, N. & Bonacorso, H. G. Ionic Liquids in Heterocyclic Synthesis. *Chemical Reviews* **108**, 2015-2050, doi:10.1021/cr078399y (2008).
- 31 Pârvulescu, V. I. & Hardacre, C. Catalysis in Ionic Liquids. *Chemical Reviews* **107**, 2615-2665, doi:10.1021/cr050948h (2007).
- 32 Han, X. & Armstrong, D. W. Ionic Liquids in Separations. *Accounts of Chemical Research* **40**, 1079-1086, doi:10.1021/ar700044y (2007).
- 33 Kang, X., Sun, X. & Han, B. Synthesis of Functional Nanomaterials in Ionic Liquids. *Advanced Materials* **28**, 1011-1030, doi: 10.1002/adma.201502924 (2016).
- 34 Lu, J., Yan, F. & Texter, J. Advanced applications of ionic liquids in polymer science. *Progress in Polymer Science* **34**, 431-448, doi: 10.1016/j.progpolymsci.2008.12.001 (2009).
- 35 Hapiot, P. & Lagrost, C. Electrochemical Reactivity in Room-Temperature Ionic Liquids. *Chemical Reviews* **108**, 2238-2264, doi:10.1021/cr0680686 (2008).
- 36 Izák, P., Hovorka, Š., Bartovský, T., Bartovská, L. & Crespo, J. G. Swelling of polymeric membranes in room temperature ionic liquids. *Journal of Membrane Science* **296**, 131-138, doi: 10.1016/j.memsci.2007.03.022 (2007).
- 37 Susan, M. A. B. H., Kaneko, T., Noda, A. & Watanabe, M. Ion Gels Prepared by in Situ Radical Polymerization of Vinyl Monomers in an Ionic Liquid and Their Characterization as Polymer Electrolytes. *Journal of the American Chemical Society* **127**, 4976-4983, doi:10.1021/ja045155b (2005).
- 38 Scott, M. P., Rahman, M. & Brazel, C. S. Application of ionic liquids as low-volatility plasticizers for PMMA. *European Polymer Journal* **39**, 1947-1953, doi: 10.1016/S0014-3057(03)00129-0 (2003).
- 39 Brehm, M., Pulst, M., Kressler, J. & Sebastiani, D. Triazolium-Based Ionic Liquids: A Novel Class of Cellulose Solvents. *The Journal of Physical Chemistry B* **123**, 3994-4003, doi:10.1021/acs.jpcc.8b12082 (2019).
- 40 Noda, A. & Watanabe, M. Highly conductive polymer electrolytes prepared by in situ polymerization of vinyl monomers in room temperature molten salts. *Electrochimica Acta* **45**, 1265-1270, doi: 10.1016/S0013-4686(99)00330-8 (2000).
- 41 Cao, Z., Liu, H. & Jiang, L. Transparent, mechanically robust, and ultrastable ionogels enabled by hydrogen bonding between elastomers and ionic liquids. *Materials Horizons* **7**, 912-918, doi:10.1039/C9MH01699F (2020).
- 42 Wang, M. *et al.* Tough and stretchable ionogels by in situ phase separation. *Nature Materials*, doi:10.1038/s41563-022-01195-4 (2022).

- 43 Abbott, A. P., Capper, G., Davies, D. L., Rasheed, R. K. & Tambyrajah, V. Novel solvent properties of choline chloride/urea mixtures. *Chemical Communications*, 70-71, doi:10.1039/B210714G (2003).
- 44 Abbott, A. P., Boothby, D., Capper, G., Davies, D. L. & Rasheed, R. K. Deep Eutectic Solvents Formed between Choline Chloride and Carboxylic Acids: Versatile Alternatives to Ionic Liquids. *Journal of the American Chemical Society* **126**, 9142-9147, doi:10.1021/ja048266j (2004).
- 45 Nardecchia, S. *et al.* Phase Behavior of Elastin-Like Synthetic Recombinamers in Deep Eutectic Solvents. *Biomacromolecules* **13**, 2029-2036, doi:10.1021/bm300200e (2012).
- 46 Abbott, A. P., Capper, G. & Gray, S. Design of Improved Deep Eutectic Solvents Using Hole Theory. *ChemPhysChem* **7**, 803-806, doi: 10.1002/cphc.200500489 (2006).
- 47 Hansen, B. B. *et al.* Deep Eutectic Solvents: A Review of Fundamentals and Applications. *Chemical Reviews* **121**, 1232-1285, doi:10.1021/acs.chemrev.0c00385 (2021).
- 48 Płotka-Wasyłka, J., de la Guardia, M., Andruch, V. & Vilková, M. Deep eutectic solvents vs ionic liquids: Similarities and differences. *Microchemical Journal* **159**, 105539, doi: 10.1016/j.microc.2020.105539 (2020).
- 49 Pollet, P., Davey, E. A., Ureña-Benavides, E. E., Eckert, C. A. & Liotta, C. L. Solvents for sustainable chemical processes. *Green Chemistry* **16**, 1034-1055, doi:10.1039/C3GC42302F (2014).
- 50 Halder, A. K. & Cordeiro, M. N. D. S. Probing the Environmental Toxicity of Deep Eutectic Solvents and Their Components: An In Silico Modeling Approach. *ACS Sustainable Chemistry & Engineering* **7**, 10649-10660, doi:10.1021/acssuschemeng.9b01306 (2019).
- 51 Smith, E. L., Abbott, A. P. & Ryder, K. S. Deep Eutectic Solvents (DESs) and Their Applications. *Chemical Reviews* **114**, 11060-11082, doi:10.1021/cr300162p (2014).
- 52 Ruß, C. & König, B. Low melting mixtures in organic synthesis – an alternative to ionic liquids? *Green Chemistry* **14**, 2969-2982, doi:10.1039/C2GC36005E (2012).
- 53 Mota-Morales, J. D. *et al.* Free-radical polymerizations of and in deep eutectic solvents: Green synthesis of functional materials. *Progress in Polymer Science* **78**, 139-153, doi: 10.1016/j.progpolymsci.2017.09.005 (2018).
- 54 Hong, S. *et al.* A stretchable and compressible ion gel based on a deep eutectic solvent applied as a strain sensor and electrolyte for supercapacitors. *Journal of Materials Chemistry C* **8**, 550-560, doi:10.1039/C9TC05913J (2020).
- 55 Li, R. a., Chen, G., Fan, T., Zhang, K. & He, M. Transparent conductive elastomers with excellent autonomous self-healing capability in harsh organic solvent environments. *Journal of Materials Chemistry A* **8**, 5056-5061, doi:10.1039/D0TA00050G (2020).

- 56 Wang, J., Zhang, S., Ma, Z. & Yan, L. Deep eutectic solvents eutectogels: progress and challenges. *Green Chemical Engineering* **2**, 359-367, doi: 10.1016/j.gce.2021.06.001 (2021).
- 57 Oweyung, R. E., Sonkusale, S. R. & Panzer, M. J. Influence of Hydrogen Bond Donor Identity and Intentional Water Addition on the Properties of Gelatin-Supported Deep Eutectic Solvent Gels. *The Journal of Physical Chemistry B* **124**, 5986-5992, doi:10.1021/acs.jpcc.0c03361 (2020).
- 58 Li, R. a. *et al.* Highly transparent, self-healing conductive elastomers enabled by synergistic hydrogen bonding interactions. *Chemical Engineering Journal* **393**, 124685, doi: 10.1016/j.cej.2020.124685 (2020).
- 59 Wan, Y. *et al.* Superstrong yet water-detachable eutectogel adhesives. *Chemical Engineering Journal* **442**, 136289, doi: 10.1016/j.cej.2022.136289 (2022).
- 60 Wang, J., Ma, Z., Wang, Y., Shao, J. & Yan, L. Ultra-Stretchable, Self-Healing, Conductive, and Transparent PAA/DES Ionic Gel. *Macromolecular Rapid Communications* **42**, 2000445, doi: 10.1002/marc.202000445 (2021).
- 61 Li, R. a., Chen, G., He, M., Tian, J. & Su, B. Patternable transparent and conductive elastomers towards flexible tactile/strain sensors. *Journal of Materials Chemistry C* **5**, 8475-8481, doi:10.1039/C7TC02703F (2017).
- 62 Li, X., Liu, J., Guo, Q., Zhang, X. & Tian, M. Polymerizable Deep Eutectic Solvent-Based Skin-Like Elastomers with Dynamic Schemochrome and Self-Healing Ability. *Small* **18**, 2201012, doi: 10.1002/sml.202201012 (2022).
- 63 Zhang, K. *et al.* Polymerizable deep eutectic solvent-based mechanically strong and ultra-stretchable conductive elastomers for detecting human motions. *Journal of Materials Chemistry A* **9**, 4890-4897, doi:10.1039/D0TA11508H (2021).
- 64 Li, R. a. *et al.* Autonomous Self-Healing, Antifreezing, and Transparent Conductive Elastomers. *Chemistry of Materials* **32**, 874-881, doi:10.1021/acs.chemmater.9b04592 (2020).
- 65 Harris, J. M. in *Poly(Ethylene Glycol) Chemistry: Biotechnical and Biomedical Applications* (ed J. Milton Harris) 1-14 (Springer US, 1992).
- 66 Chen, J., Spear, S. K., Huddleston, J. G. & Rogers, R. D. Polyethylene glycol and solutions of polyethylene glycol as green reaction media. *Green Chemistry* **7**, 64-82, doi:10.1039/B413546F (2005).
- 67 Zalipsky, S. & Harris, J. M. in *Poly(ethylene glycol)* Vol. 680 ACS Symposium Series Ch. 1, 1-13 (American Chemical Society, 1997).
- 68 Kuo, P.-L., Tsao, C.-H., Hsu, C.-H., Chen, S.-T. & Hsu, H.-M. A new strategy for preparing oligomeric ionic liquid gel polymer electrolytes for high-performance and nonflammable lithium ion batteries. *Journal of Membrane Science* **499**, 462-469, doi: 10.1016/j.memsci.2015.11.007 (2016).

- 69 Wang, Z. *et al.* Tough, Transparent, 3D-Printable, and Self-Healing Poly(ethylene glycol)-Gel (PEGgel). *Advanced Materials* **34**, 2107791, doi: 10.1002/adma.202107791 (2022).
- 70 Coleman, M. M., Skrovanek, D. J., Hu, J. & Painter, P. C. Hydrogen bonding in polymer blends. 1. FTIR studies of urethane-ether blends. *Macromolecules* **21**, 59-65, doi:10.1021/ma00179a014 (1988).
- 71 Zhang, M., Li, X. H., Gong, Y. D., Zhao, N. M. & Zhang, X. F. Properties and biocompatibility of chitosan films modified by blending with PEG. *Biomaterials* **23**, 2641-2648, doi: 10.1016/S0142-9612(01)00403-3 (2002).
- 72 Mattia, J. & Painter, P. A Comparison of Hydrogen Bonding and Order in a Polyurethane and Poly(urethane-urea) and Their Blends with Poly(ethylene glycol). *Macromolecules* **40**, 1546-1554, doi:10.1021/ma0626362 (2007).
- 73 Bailey, F. E. *Poly(ethylene oxide)* / F. E. Bailey, Jr., and J. V. Koleske. (Academic Press, 1976).
- 74 Wei, H. *et al.* Ultrastretchable, Highly Transparent, Self-Adhesive, and 3D-Printable Ionic Hydrogels for Multimode Tactical Sensing. *Chemistry of Materials* **33**, 6731-6742, doi:10.1021/acs.chemmater.1c01246 (2021).
- 75 Amini, S. *et al.* Preventing mussel adhesion using lubricant-infused materials. *Science* **357**, 668-673, doi:doi:10.1126/science.aai8977 (2017).
- 76 Kreder, M. J., Alvarenga, J., Kim, P. & Aizenberg, J. Design of anti-icing surfaces: smooth, textured or slippery? *Nature Reviews Materials* **1**, 15003, doi:10.1038/natrevmats.2015.3 (2016).
- 77 Wong, T.-S. *et al.* Bioinspired self-repairing slippery surfaces with pressure-stable omniphobicity. *Nature* **477**, 443-447, doi:10.1038/nature10447 (2011).
- 78 Li, J., Ueda, E., Paulssen, D. & Levkin, P. A. Slippery Lubricant-Infused Surfaces: Properties and Emerging Applications. *Advanced Functional Materials* **29**, 1802317, doi: 10.1002/adfm.201802317 (2019).
- 79 Hou, X. *et al.* Interplay between materials and microfluidics. *Nature Reviews Materials* **2**, 17016, doi:10.1038/natrevmats.2017.16 (2017).
- 80 Zhao, H., Sun, Q., Deng, X. & Cui, J. Earthworm-Inspired Rough Polymer Coatings with Self-Replenishing Lubrication for Adaptive Friction-Reduction and Antifouling Surfaces. *Advanced Materials* **30**, 1802141, doi: 10.1002/adma.201802141 (2018).
- 81 Zhang, P., Zhao, C., Zhao, T., Liu, M. & Jiang, L. Recent Advances in Bioinspired Gel Surfaces with Superwettability and Special Adhesion. *Advanced Science* **6**, 1900996, doi: 10.1002/advs.201900996 (2019).
- 82 Liu, M., Wang, S., Wei, Z., Song, Y. & Jiang, L. Bioinspired Design of a Superoleophobic and Low Adhesive Water/Solid Interface. *Advanced Materials* **21**, 665-669, doi: 10.1002/adma.200801782 (2009).

- 83 Xue, Z. *et al.* A Novel Superhydrophilic and Underwater Superoleophobic Hydrogel-Coated Mesh for Oil/Water Separation. *Advanced Materials* **23**, 4270-4273, doi: 10.1002/adma.201102616 (2011).
- 84 Liu, H., Zhang, P., Liu, M., Wang, S. & Jiang, L. Organogel-based Thin Films for Self-Cleaning on Various Surfaces. *Advanced Materials* **25**, 4477-4481, doi: 10.1002/adma.201301289 (2013).
- 85 Yao, X. *et al.* Self-Replenishable Anti-Waxing Organogel Materials. *Angewandte Chemie International Edition* **54**, 8975-8979, doi: 10.1002/anie.201503031 (2015).
- 86 Gao, H. *et al.* Adaptive and freeze-tolerant heteronetwork organohydrogels with enhanced mechanical stability over a wide temperature range. *Nature Communications* **8**, 15911, doi:10.1038/ncomms15911 (2017).
- 87 Manabe, K. *et al.* Controllable Broadband Optical Transparency and Wettability Switching of Temperature-Activated Solid/Liquid-Infused Nanofibrous Membranes. *ACS Nano* **10**, 9387-9396, doi:10.1021/acsnano.6b04333 (2016).
- 88 Yao, X., Ju, J., Yang, S., Wang, J. & Jiang, L. Temperature-Driven Switching of Water Adhesion on Organogel Surface. *Advanced Materials* **26**, 1895-1900, doi: 10.1002/adma.201304798 (2014).
- 89 Ding, Y. *et al.* Ionic-Liquid-Gel Surfaces Showing Easy-Sliding and Ultradurable Features. *Advanced Materials Interfaces* **2**, 1500177, doi: 10.1002/admi.201500177 (2015).
- 90 Bai, Y. *et al.* Transparent hydrogel with enhanced water retention capacity by introducing highly hydratable salt. *Applied Physics Letters* **105**, 151903, doi:10.1063/1.4898189 (2014).
- 91 Yuk, H., Zhang, T., Parada, G. A., Liu, X. & Zhao, X. Skin-inspired hydrogel-elastomer hybrids with robust interfaces and functional microstructures. *Nature Communications* **7**, 12028, doi:10.1038/ncomms12028 (2016).
- 92 Kong, W. *et al.* Muscle-Inspired Highly Anisotropic, Strong, Ion-Conductive Hydrogels. *Advanced Materials* **30**, 1801934, doi: 10.1002/adma.201801934 (2018).
- 93 Morelle, X. P. *et al.* Highly Stretchable and Tough Hydrogels below Water Freezing Temperature. *Advanced Materials* **30**, 1801541, doi: 10.1002/adma.201801541 (2018).
- 94 Zhang, X.-F. *et al.* Inorganic Salts Induce Thermally Reversible and Anti-Freezing Cellulose Hydrogels. *Angewandte Chemie International Edition* **58**, 7366-7370, doi: 10.1002/anie.201902578 (2019).
- 95 Wu, J. *et al.* Extremely Deformable, Transparent, and High-Performance Gas Sensor Based on Ionic Conductive Hydrogel. *ACS Applied Materials & Interfaces* **11**, 2364-2373, doi:10.1021/acsaami.8b17437 (2019).
- 96 Zhao, X. *et al.* Bioinspired ultra-stretchable and anti-freezing conductive hydrogel fibers with ordered and reversible polymer chain alignment. *Nature Communications* **9**, 3579, doi:10.1038/s41467-018-05904-z (2018).



- 97 Chen, F. *et al.* Rational Fabrication of Anti-Freezing, Non-Drying Tough Organohydrogels by One-Pot Solvent Displacement. *Angewandte Chemie International Edition* **57**, 6568-6571, doi:10.1002/anie.201803366 (2018).
- 98 Rong, Q. *et al.* Anti-freezing, Conductive Self-healing Organohydrogels with Stable Strain-Sensitivity at Subzero Temperatures. *Angewandte Chemie International Edition* **56**, 14159-14163, doi: 10.1002/anie.201708614 (2017).
- 99 Han, L. *et al.* Mussel-Inspired Adhesive and Conductive Hydrogel with Long-Lasting Moisture and Extreme Temperature Tolerance. *Advanced Functional Materials* **28**, 1704195, doi: 10.1002/adfm.201704195 (2018).
- 100 Morelle, X. P. *et al.* Highly Stretchable and Tough Hydrogels below Water Freezing Temperature. *Advanced Materials* **30**, 1801541, doi:10.1002/adma.201801541 (2018).
- 101 Han, L. *et al.* Mussel-Inspired Adhesive and Conductive Hydrogel with Long-Lasting Moisture and Extreme Temperature Tolerance. *Advanced Functional Materials* **28**, 1704195, doi:10.1002/adfm.201704195 (2018).
- 102 Zhao, X. *et al.* Soft Materials by Design: Unconventional Polymer Networks Give Extreme Properties. *Chemical Reviews* **121**, 4309-4372, doi:10.1021/acs.chemrev.0c01088 (2021).
- 103 Kamata, H., Akagi, Y., Kayasuga-Kariya, Y., Chung, U.-i. & Sakai, T. "Nonswellable" Hydrogel Without Mechanical Hysteresis. *Science* **343**, 873-875, doi:10.1126/science.1247811 (2014).
- 104 Sakai, T. *et al.* Design and Fabrication of a High-Strength Hydrogel with Ideally Homogeneous Network Structure from Tetrahedron-like Macromonomers. *Macromolecules* **41**, 5379-5384, doi:10.1021/ma800476x (2008).
- 105 Huang, X., Nakagawa, S., Li, X., Shibayama, M. & Yoshie, N. A Simple and Versatile Method for the Construction of Nearly Ideal Polymer Networks. *Angewandte Chemie International Edition* **59**, 9646-9652, doi: 10.1002/anie.202001271 (2020).
- 106 Gong, J. P., Katsuyama, Y., Kurokawa, T. & Osada, Y. Double-Network Hydrogels with Extremely High Mechanical Strength. *Advanced Materials* **15**, 1155-1158, doi:10.1002/adma.200304907 (2003).
- 107 Zhao, X. Multi-scale multi-mechanism design of tough hydrogels: building dissipation into stretchy networks. *Soft Matter* **10**, 672-687, doi:10.1039/C3SM52272E (2014).
- 108 Sun, J.-Y. *et al.* Highly stretchable and tough hydrogels. *Nature* **489**, 133-136, doi:10.1038/nature11409 (2012).
- 109 Yan, C. & Pochan, D. J. Rheological properties of peptide-based hydrogels for biomedical and other applications. *Chemical Society Reviews* **39**, 3528-3540, doi:10.1039/B919449P (2010).

- 110 Prince, E. & Kumacheva, E. Design and applications of man-made biomimetic fibrillar hydrogels. *Nature Reviews Materials* **4**, 99-115, doi:10.1038/s41578-018-0077-9 (2019).
- 111 Hua, M. *et al.* Strong tough hydrogels via the synergy of freeze-casting and salting out. *Nature* **590**, 594-599, doi:10.1038/s41586-021-03212-z (2021).
- 112 Wu, S. *et al.* Poly(vinyl alcohol) Hydrogels with Broad-Range Tunable Mechanical Properties via the Hofmeister Effect. *Advanced Materials* **33**, 2007829, doi: 10.1002/adma.202007829 (2021).
- 113 Jungwirth, P. & Cremer, P. S. Beyond Hofmeister. *Nature Chemistry* **6**, 261-263, doi:10.1038/nchem.1899 (2014).
- 114 Pegram, L. M. & Record, M. T. Hofmeister Salt Effects on Surface Tension Arise from Partitioning of Anions and Cations between Bulk Water and the Air–Water Interface. *The Journal of Physical Chemistry B* **111**, 5411-5417, doi:10.1021/jp070245z (2007).
- 115 Wu, S. *et al.* Ion-specific ice recrystallization provides a facile approach for the fabrication of porous materials. *Nature Communications* **8**, 15154, doi:10.1038/ncomms15154 (2017).
- 116 Du, R. *et al.* Specific ion effects directed noble metal aerogels: Versatile manipulation for electrocatalysis and beyond. *Science Advances* **5**, eaaw4590, doi: 10.1126/sciadv.aaw4590 (2019).
- 117 He, Q., Huang, Y. & Wang, S. Hofmeister Effect-Assisted One Step Fabrication of Ductile and Strong Gelatin Hydrogels. *Advanced Functional Materials* **28**, 1705069, doi: 10.1002/adfm.201705069 (2018).
- 118 Wu, S. *et al.* Poly(vinyl alcohol) Hydrogels with Broad-Range Tunable Mechanical Properties via the Hofmeister Effect. *Advanced Materials* **33**, 2007829, doi: 10.1002/adma.202007829 (2021).
- 119 Capadona, J. R., Shanmuganathan, K., Tyler, D. J., Rowan, S. J. & Weder, C. Stimuli-Responsive Polymer Nanocomposites Inspired by the Sea Cucumber Dermis. *Science* **319**, 1370-1374, doi: 10.1126/science.1153307 (2008).
- 120 Kim, J., Campbell, A. S., de Ávila, B. E.-F. & Wang, J. Wearable biosensors for healthcare monitoring. *Nature Biotechnology* **37**, 389-406, doi:10.1038/s41587-019-0045-y (2019).
- 121 Liu, X., Liu, J., Lin, S. & Zhao, X. Hydrogel machines. *Materials Today* **36**, 102-124, doi: 10.1016/j.mattod.2019.12.026 (2020).
- 122 Novoselov, K. S. *et al.* Electric Field Effect in Atomically Thin Carbon Films. *Science* **306**, 666-669, doi:doi:10.1126/science.1102896 (2004).
- 123 Fowler, J. D. *et al.* Practical Chemical Sensors from Chemically Derived Graphene. *ACS Nano* **3**, 301-306, doi:10.1021/nn800593m (2009).

- 124 Lu, C.-H., Yang, H.-H., Zhu, C.-L., Chen, X. & Chen, G.-N. A Graphene Platform for Sensing Biomolecules. *Angewandte Chemie International Edition* **48**, 4785-4787, doi: 10.1002/anie.200901479 (2009).
- 125 Gilje, S., Han, S., Wang, M., Wang, K. L. & Kaner, R. B. A Chemical Route to Graphene for Device Applications. *Nano Letters* **7**, 3394-3398, doi:10.1021/nl0717715 (2007).
- 126 Zhu, J., Yang, D., Yin, Z., Yan, Q. & Zhang, H. Graphene and Graphene-Based Materials for Energy Storage Applications. *Small* **10**, 3480-3498, doi: 10.1002/sml.201303202 (2014).
- 127 Xu, Y., Sheng, K., Li, C. & Shi, G. Self-Assembled Graphene Hydrogel via a One-Step Hydrothermal Process. *ACS Nano* **4**, 4324-4330, doi:10.1021/nn101187z (2010).
- 128 Lipomi, D. J., Tee, B. C. K., Vosgueritchian, M. & Bao, Z. Stretchable Organic Solar Cells. *Advanced Materials* **23**, 1771-1775, doi: 10.1002/adma.201004426 (2011).
- 129 Groenendaal, L., Jonas, F., Freitag, D., Pielartzik, H. & Reynolds, J. R. Poly(3,4-ethylenedioxythiophene) and Its Derivatives: Past, Present, and Future. *Advanced Materials* **12**, 481-494, doi: 10.1002/(SICI)1521-4095(200004)12:7<481::AID-ADMA481>3.0.CO;2-C (2000).
- 130 Kayser, L. V. & Lipomi, D. J. Stretchable Conductive Polymers and Composites Based on PEDOT and PEDOT:PSS. *Advanced Materials* **31**, 1806133, doi: 10.1002/adma.201806133 (2019).
- 131 Yuk, H., Lu, B. & Zhao, X. Hydrogel bioelectronics. *Chemical Society Reviews* **48**, 1642-1667, doi:10.1039/C8CS00595H (2019).
- 132 Mawad, D. *et al.* A conducting polymer with enhanced electronic stability applied in cardiac models. *Science Advances* **2**, e1601007, doi:doi:10.1126/sciadv.1601007 (2016).
- 133 Yao, B. *et al.* Ultrahigh-Conductivity Polymer Hydrogels with Arbitrary Structures. *Advanced Materials* **29**, 1700974, doi: 10.1002/adma.201700974 (2017).
- 134 Lu, B. *et al.* Pure PEDOT:PSS hydrogels. *Nature Communications* **10**, 1043, doi:10.1038/s41467-019-09003-5 (2019).
- 135 Wang, J. *et al.* Ultra-High Electrical Conductivity in Filler-Free Polymeric Hydrogels Toward Thermoelectrics and Electromagnetic Interference Shielding. *Advanced Materials* **34**, 2109904, doi: 10.1002/adma.202109904 (2022).
- 136 Caló, E. & Khutoryanskiy, V. V. Biomedical applications of hydrogels: A review of patents and commercial products. *European Polymer Journal* **65**, 252-267, doi:10.1016/j.eurpolymj.2014.11.024 (2015).
- 137 Liu, Y. *et al.* Soft and elastic hydrogel-based microelectronics for localized low-voltage neuromodulation. *Nature Biomedical Engineering* **3**, 58-68, doi:10.1038/s41551-018-0335-6 (2019).

- 138 Wang, Z., Cong, Y. & Fu, J. Stretchable and tough conductive hydrogels for flexible pressure and strain sensors. *Journal of Materials Chemistry B* **8**, 3437-3459, doi:10.1039/C9TB02570G (2020).
- 139 Li, T. *et al.* Fast-moving soft electronic fish. *Science Advances* **3**, e1602045, doi:10.1126/sciadv.1602045 (2017).
- 140 Zhang, Y. S. & Khademhosseini, A. Advances in engineering hydrogels. *Science* **356**, eaaf3627, doi:10.1126/science.aaf3627 (2017).
- 141 Correa, S. *et al.* Translational Applications of Hydrogels. *Chemical Reviews*, doi:10.1021/acs.chemrev.0c01177 (2021).
- 142 Yuk, H. *et al.* Hydraulic hydrogel actuators and robots optically and sonically camouflaged in water. *Nature Communications* **8**, 14230, doi:10.1038/ncomms14230 (2017).
- 143 Wichterle, O. & LÍM, D. Hydrophilic Gels for Biological Use. *Nature* **185**, 117-118, doi:10.1038/185117a0 (1960).
- 144 Yang, H. *et al.* Fabricating hydrogels to mimic biological tissues of complex shapes and high fatigue resistance. *Matter*, doi: 10.1016/j.matt.2021.03.011 (2021).
- 145 Lee, K. Y. & Mooney, D. J. Hydrogels for Tissue Engineering. *Chemical Reviews* **101**, 1869-1880, doi:10.1021/cr000108x (2001).
- 146 Nguyen, K. T. & West, J. L. Photopolymerizable hydrogels for tissue engineering applications. *Biomaterials* **23**, 4307-4314, doi: 10.1016/S0142-9612(02)00175-8 (2002).
- 147 Guo, J. *et al.* Highly Stretchable, Strain Sensing Hydrogel Optical Fibers. *Advanced Materials* **28**, 10244-10249, doi: 10.1002/adma.201603160 (2016).
- 148 Kim, Y., Yuk, H., Zhao, R., Chester, S. A. & Zhao, X. Printing ferromagnetic domains for untethered fast-transforming soft materials. *Nature* **558**, 274-279, doi:10.1038/s41586-018-0185-0 (2018).
- 149 Gao, N. *et al.* Crystal-confined freestanding ionic liquids for reconfigurable and repairable electronics. *Nature Communications* **10**, 547, doi:10.1038/s41467-019-08433-5 (2019).
- 150 Rong, Q. *et al.* Anti-freezing, Conductive Self-healing Organohydrogels with Stable Strain-Sensitivity at Subzero Temperatures. *Angewandte Chemie International Edition* **56**, 14159-14163, doi:10.1002/anie.201708614 (2017).
- 151 Kozłowska, M., Goclon, J. & Rodziewicz, P. Intramolecular Hydrogen Bonds in Low-Molecular-Weight Polyethylene Glycol. *ChemPhysChem* **17**, 1143-1153, doi: 10.1002/cphc.201501182 (2016).
- 152 Elaheh, S., Modan, L. & Wolfgang, W. *Research Square*, doi:10.21203/rs.3.rs-151096/v1 (2021).

- 153 Kröger, M. Shortest multiple disconnected path for the analysis of entanglements in two- and three-dimensional polymeric systems. *Computer Physics Communications* **168**, 209-232, doi: 10.1016/j.cpc.2005.01.020 (2005).
- 154 Balani, K., Verma, V., Agarwal, A. & Narayan, R.
- 155 Brown, H. R. & Russell, T. P. Entanglements at Polymer Surfaces and Interfaces. *Macromolecules* **29**, 798-800, doi:10.1021/ma951123k (1996).
- 156 Qin, J. & Milner, S. T. Tubes, Topology, and Polymer Entanglement. *Macromolecules* **47**, 6077-6085, doi:10.1021/ma500755p (2014).
- 157 Stauch, T. & Dreuw, A. Knots “Choke Off” Polymers upon Stretching. *Angewandte Chemie International Edition* **55**, 811-814, doi: 10.1002/anie.201508706 (2016).
- 158 Zhang, E., Bai, R., Morelle, X. P. & Suo, Z. Fatigue fracture of nearly elastic hydrogels. *Soft Matter* **14**, 3563-3571, doi:10.1039/C8SM00460A (2018).
- 159 Cox, T. R. & Erler, J. T. Remodeling and homeostasis of the extracellular matrix: implications for fibrotic diseases and cancer. *Disease Models & Mechanisms* **4**, 165-178, doi:10.1242/dmm.004077 (2011).
- 160 Butcher, D. T., Alliston, T. & Weaver, V. M. A tense situation: forcing tumour progression. *Nature Reviews Cancer* **9**, 108-122, doi:10.1038/nrc2544 (2009).
- 161 Diridollou, S. *et al.* Skin ageing: changes of physical properties of human skin in vivo. *Int J Cosmet Sci* **23**, 353-362, doi:10.1046/j.0412-5463.2001.00105.x (2001).
- 162 Qi, D., Zhang, K., Tian, G., Jiang, B. & Huang, Y. Stretchable Electronics Based on PDMS Substrates. *Advanced Materials* **33**, 2003155, doi: 10.1002/adma.202003155 (2021).
- 163 Pena-Francesch, A., Jung, H., Demirel, M. C. & Sitti, M. Biosynthetic self-healing materials for soft machines. *Nature Materials* **19**, 1230-1235, doi:10.1038/s41563-020-0736-2 (2020).
- 164 Cordier, P., Tournilhac, F., Soulié-Ziakovic, C. & Leibler, L. Self-healing and thermoreversible rubber from supramolecular assembly. *Nature* **451**, 977-980, doi:10.1038/nature06669 (2008).
- 165 Chen, Y., Kushner, A. M., Williams, G. A. & Guan, Z. Multiphase design of autonomic self-healing thermoplastic elastomers. *Nature Chemistry* **4**, 467-472, doi:10.1038/nchem.1314 (2012).
- 166 Patel, D. K. *et al.* Highly Stretchable and UV Curable Elastomers for Digital Light Processing Based 3D Printing. *Advanced Materials* **29**, 1606000, doi: 10.1002/adma.201606000 (2017).
- 167 Mohapatra, A. K., Mohanty, S. & Nayak, S. K. Effect of PEG on PLA/PEG blend and its nanocomposites: A study of thermo-mechanical and morphological characterization. *Polymer Composites* **35**, 283-293, doi: 10.1002/pc.22660 (2014).

- 168 Rolim, W. R. *et al.* Antimicrobial Activity and Cytotoxicity to Tumor Cells of Nitric Oxide Donor and Silver Nanoparticles Containing PVA/PEG Films for Topical Applications. *ACS Applied Materials & Interfaces* **11**, 6589-6604, doi:10.1021/acsami.8b19021 (2019).
- 169 Liu, J., Wu, S., Zhang, L., Wang, W. & Cao, D. Molecular dynamics simulation for insight into microscopic mechanism of polymer reinforcement. *Physical Chemistry Chemical Physics* **13**, 518-529, doi:10.1039/C0CP00297F (2011).
- 170 Wang, L. *et al.* Stress-strain behavior of block-copolymers and their nanocomposites filled with uniform or Janus nanoparticles under shear: a molecular dynamics simulation. *Physical Chemistry Chemical Physics* **18**, 27232-27244, doi:10.1039/C6CP05853A (2016).
- 171 Jeener, J., Meier, B. H., Bachmann, P. & Ernst, R. R. Investigation of exchange processes by two-dimensional NMR spectroscopy. *The Journal of Chemical Physics* **71**, 4546-4553, doi:10.1063/1.438208 (1979).
- 172 Li, H., Ma, Y. & Huang, Y. Material innovation and mechanics design for substrates and encapsulation of flexible electronics: a review. *Materials Horizons* **8**, 383-400, doi:10.1039/D0MH00483A (2021).
- 173 Yang, Y. & Gao, W. Wearable and flexible electronics for continuous molecular monitoring. *Chemical Society Reviews* **48**, 1465-1491, doi:10.1039/C7CS00730B (2019).
- 174 Kim, R.-H. *et al.* Waterproof AlInGaP optoelectronics on stretchable substrates with applications in biomedicine and robotics. *Nature Materials* **9**, 929-937, doi:10.1038/nmat2879 (2010).
- 175 Webb, R. C. *et al.* Epidermal devices for noninvasive, precise, and continuous mapping of macrovascular and microvascular blood flow. *Science Advances* **1**, e1500701, doi:10.1126/sciadv.1500701.
- 176 Zhang, Y. *et al.* Climbing-inspired twining electrodes using shape memory for peripheral nerve stimulation and recording. *Science Advances* **5**, eaaw1066, doi:10.1126/sciadv.aaw1066.
- 177 Someya, T., Bao, Z. & Malliaras, G. G. The rise of plastic bioelectronics. *Nature* **540**, 379-385, doi:10.1038/nature21004 (2016).
- 178 Lacour, S. P., Courtine, G. & Guck, J. Materials and technologies for soft implantable neuroprostheses. *Nature Reviews Materials* **1**, 16063, doi:10.1038/natrevmats.2016.63 (2016).
- 179 Feiner, R. & Dvir, T. Tissue-electronics interfaces: from implantable devices to engineered tissues. *Nature Reviews Materials* **3**, 17076, doi:10.1038/natrevmats.2017.76 (2017).
- 180 Tian, B. & Lieber, C. M. Nanowired Bioelectric Interfaces. *Chemical Reviews* **119**, 9136-9152, doi:10.1021/acs.chemrev.8b00795 (2019).

- 181 Zhang, A. & Lieber, C. M. Nano-Bioelectronics. *Chemical Reviews* **116**, 215-257, doi:10.1021/acs.chemrev.5b00608 (2016).
- 182 Wang, J., Lin, M.-F., Park, S. & Lee, P. S. Deformable conductors for human-machine interface. *Materials Today* **21**, 508-526, doi:10.1016/j.mattod.2017.12.006 (2018).
- 183 Liu, Y., He, K., Chen, G., Leow, W. R. & Chen, X. Nature-Inspired Structural Materials for Flexible Electronic Devices. *Chemical Reviews* **117**, 12893-12941, doi:10.1021/acs.chemrev.7b00291 (2017).
- 184 Ray, T. R. *et al.* Bio-Integrated Wearable Systems: A Comprehensive Review. *Chemical Reviews* **119**, 5461-5533, doi:10.1021/acs.chemrev.8b00573 (2019).
- 185 Yang, C. & Suo, Z. Hydrogel ionotronics. *Nature Reviews Materials* **3**, 125-142, doi:10.1038/s41578-018-0018-7 (2018).
- 186 Chortos, A., Liu, J. & Bao, Z. Pursuing prosthetic electronic skin. *Nature Materials* **15**, 937-950, doi:10.1038/nmat4671 (2016).
- 187 Shi, L. *et al.* Highly stretchable and transparent ionic conducting elastomers. *Nature Communications* **9**, 2630, doi:10.1038/s41467-018-05165-w (2018).
- 188 Kim, C.-C., Lee, H.-H., Oh Kyu, H. & Sun, J.-Y. Highly stretchable, transparent ionic touch panel. *Sci* **353**, 682-687, doi:10.1126/science.aaf8810 (2016).
- 189 Yiming, B. *et al.* A Mechanically Robust and Versatile Liquid-Free Ionic Conductive Elastomer. *Advanced Materials* **33**, 2006111, doi:10.1002/adma.202006111 (2021).
- 190 Wang, M. *et al.* Multifunctional Liquid-Free Ionic Conductive Elastomer Fabricated by Liquid Metal Induced Polymerization. *Advanced Functional Materials* **31**, 2101957, doi:10.1002/adfm.202101957 (2021).
- 191 Zhou, Y. *et al.* Highly Stretchable, Elastic, and Ionic Conductive Hydrogel for Artificial Soft Electronics. *Advanced Functional Materials* **29**, 1806220, doi:10.1002/adfm.201806220 (2019).
- 192 Lei, Z. & Wu, P. Bioinspired Quasi-Solid Ionic Conductors: Materials, Processing, and Applications. *Accounts of Materials Research*, doi:10.1021/accountsmr.1c00165 (2021).
- 193 Zhang, P. *et al.* Dynamically Crosslinked Dry Ion-Conducting Elastomers for Soft Ionotronics. *Advanced Materials* **33**, 2101396, doi:10.1002/adma.202101396 (2021).
- 194 Manuel Stephan, A. & Nahm, K. S. Review on composite polymer electrolytes for lithium batteries. *Polymer* **47**, 5952-5964, doi:10.1016/j.polymer.2006.05.069 (2006).
- 195 Manthiram, A., Yu, X. & Wang, S. Lithium battery chemistries enabled by solid-state electrolytes. *Nature Reviews Materials* **2**, 16103, doi:10.1038/natrevmats.2016.103 (2017).

- 196 Tian, M. *et al.* Largely improved actuation strain at low electric field of dielectric elastomer by combining disrupting hydrogen bonds with ionic conductivity. *Journal of Materials Chemistry C* **2**, 8388-8397, doi:10.1039/C4TC01140F (2014).
- 197 Di Noto, V., Longo, D. & Münchow, V. Ion–Oligomer Interactions in Poly(ethylene glycol)400/(LiCl)<sub>x</sub> Electrolyte Complexes. *The Journal of Physical Chemistry B* **103**, 2636-2646, doi:10.1021/jp983764y (1999).
- 198 Gupta, S., Shahi, K., Binesh, N. & Bhat, S. Investigation of the (PEG)<sub>x</sub>LiCl system using conductivity, DSC and NMR techniques. *Solid State Ionics* **67**, 97-105, doi:10.1016/0167-2738(93)90314-s (1993).
- 199 Sun, B. *et al.* Fabrication of curled conducting polymer microfibrillar arrays via a novel electrospinning method for stretchable strain sensors. *Nanoscale* **5**, 7041-7045, doi:10.1039/C3NR01832F (2013).
- 200 Chen, B. *et al.* Highly Stretchable and Transparent Ionogels as Nonvolatile Conductors for Dielectric Elastomer Transducers. *ACS Applied Materials & Interfaces* **6**, 7840-7845, doi:10.1021/am501130t (2014).
- 201 Keplinger, C. *et al.* Stretchable, Transparent, Ionic Conductors. *Science* **341**, 984-987, doi:10.1126/science.1240228 (2013).
- 202 Ritchie, R. O. The conflicts between strength and toughness. *Nature Materials* **10**, 817-822, doi:10.1038/nmat3115 (2011).
- 203 Gabriel, C., Peyman, A. & Grant, E. H. Electrical conductivity of tissue at frequencies below 1 MHz. *Physics in Medicine and Biology* **54**, 4863-4878, doi:10.1088/0031-9155/54/16/002 (2009).
- 204 Das, D., Chandrasekaran, A., Venkatram, S. & Ramprasad, R. Effect of Crystallinity on Li Adsorption in Polyethylene Oxide. *Chemistry of Materials* **30**, 8804-8810, doi:10.1021/acs.chemmater.8b03434 (2018).
- 205 Wendler, K., Thar, J., Zahn, S. & Kirchner, B. Estimating the Hydrogen Bond Energy. *The Journal of Physical Chemistry A* **114**, 9529-9536, doi:10.1021/jp103470e (2010).
- 206 Han, L. *et al.* A Mussel-Inspired Conductive, Self-Adhesive, and Self-Healable Tough Hydrogel as Cell Stimulators and Implantable Bioelectronics. *Small* **13**, 1601916, doi:10.1002/smll.201601916 (2017).
- 207 Hua, Q. *et al.* Skin-inspired highly stretchable and conformable matrix networks for multifunctional sensing. *Nature Communications* **9**, 244, doi:10.1038/s41467-017-02685-9 (2018).
- 208 Harada, S., Honda, W., Arie, T., Akita, S. & Takei, K. Fully Printed, Highly Sensitive Multifunctional Artificial Electronic Whisker Arrays Integrated with Strain and Temperature Sensors. *ACS Nano* **8**, 3921-3927, doi:10.1021/nn500845a (2014).



- 209 Trung, T. Q., Ramasundaram, S., Hwang, B.-U. & Lee, N.-E. An All-Elastomeric Transparent and Stretchable Temperature Sensor for Body-Attachable Wearable Electronics. *Advanced Materials* **28**, 502-509, doi: 10.1002/adma.201504441 (2016).
- 210 Bang, J. *et al.* Highly Sensitive Temperature Sensor: Ligand-Treated Ag Nanocrystal Thin Films on PDMS with Thermal Expansion Strategy. *Advanced Functional Materials* **29**, 1903047, doi: 10.1002/adfm.201903047 (2019).
- 211 Dang, C. *et al.* Transparent, Highly Stretchable, Rehealable, Sensing, and Fully Recyclable Ionic Conductors Fabricated by One-Step Polymerization Based on a Small Biological Molecule. *Advanced Functional Materials* **29**, 1902467, doi:10.1002/adfm.201902467 (2019).
- 212 Zhang, P. *et al.* Stretchable, Transparent, and Thermally Stable Triboelectric Nanogenerators Based on Solvent-Free Ion-Conducting Elastomer Electrodes. *Advanced Functional Materials* **30**, 1909252, doi: 10.1002/adfm.201909252 (2020).
- 213 Zhang, B. *et al.* Hierarchical Response Network Boosts Solvent-Free Ionic Conductive Elastomers with Extreme Stretchability, Healability, and Recyclability for Ionic Sensors. *ACS Applied Materials & Interfaces* **14**, 8404-8416, doi:10.1021/acsami.1c22602 (2022).
- 214 Wang, L. *et al.* Solvent-free adhesive ionic elastomer for multifunctional stretchable electronics. *Nano Energy* **91**, 106611, doi: 10.1016/j.nanoen.2021.106611 (2022).
- 215 Tao, X. *et al.* An Intrinsically Conductive Elastomer for Thromboembolism Diagnosis. *Advanced Materials Technologies* **6**, 2001076, doi: 10.1002/admt.202001076 (2021).
- 216 Senda, N. Development of molecular calculation support system “Winmostar”. *Idemitsu Tech. Rep.* **49**, 106-111 (2006).
- 217 Martínez, L., Andrade, R., Birgin, E. G. & Martínez, J. M. PACKMOL: a package for building initial configurations for molecular dynamics simulations. *Journal of computational chemistry* **30**, 2157-2164 (2009).
- 218 Wang, J., Wolf, R. M., Caldwell, J. W., Kollman, P. A. & Case, D. A. Development and testing of a general amber force field. *Journal of computational chemistry* **25**, 1157-1174 (2004).
- 219 Brambilla, D. *et al.* PEGylated nanoparticles bind to and alter amyloid-beta peptide conformation: toward engineering of functional nanomedicines for Alzheimer’s disease. *ACS nano* **6**, 5897-5908 (2012).
- 220 Aryafard, M., Abbasi, M., Řeha, D., Harifi-Mood, A. R. & Minofar, B. Experimental and theoretical investigation of solvatochromic properties and ion solvation structure in DESs of reline, glyceline, ethaline and their mixtures with PEG 400. *Journal of Molecular Liquids* **284**, 59-67 (2019).
- 221 Buscaglia, R. *et al.* Polyethylene glycol binding alters human telomere G-quadruplex structure by conformational selection. *Nucleic acids research* **41**, 7934-7946 (2013).

- 222 Mollazadeh, S., Sahebkar, A., Shahlaei, M. & Moradi, S. Nano drug delivery systems: Molecular dynamic simulation. *Journal of Molecular Liquids*, 115823 (2021).
- 223 Nagumo, R., Shimizu, A., Iwata, S. & Mori, H. Molecular dynamics study of the molecular mobilities and side-chain terminal affinities of 2-methoxyethyl acrylate and 2-hydroxyethyl methacrylate. *Polymer Journal* **51**, 365-370 (2019).
- 224 Nagumo, R., Matsuoka, T. & Iwata, S. Interactions between Acrylate/Methacrylate Biomaterials and Organic Foulants Evaluated by Molecular Dynamics Simulations of Simplified Binary Mixtures. *ACS Biomaterials Science & Engineering* **7**, 3709-3717 (2021).
- 225 Hockney, R. W. & Eastwood, J. W. *Computer simulation using particles*. (crc Press, 2021).
- 226 Wang, J., Wang, W., Kollman, P. A. & Case, D. A. Automatic atom type and bond type perception in molecular mechanical calculations. *Journal of molecular graphics and modelling* **25**, 247-260 (2006).
- 227 Jakalian, A., Bush, B. L., Jack, D. B. & Bayly, C. I. Fast, efficient generation of high - quality atomic charges. AM1 - BCC model: I. Method. *Journal of computational chemistry* **21**, 132-146 (2000).
- 228 Jakalian, A., Jack, D. B. & Bayly, C. I. Fast, efficient generation of high-quality atomic charges. AM1-BCC model: II. Parameterization and validation. *Journal of computational chemistry* **23**, 1623-1641 (2002).
- 229 Kasimova, A. O. *et al.* Validation of a novel molecular dynamics simulation approach for lipophilic drug incorporation into polymer micelles. *The Journal of Physical Chemistry B* **116**, 4338-4345 (2012).
- 230 Shivakumar, D. *et al.* Prediction of absolute solvation free energies using molecular dynamics free energy perturbation and the OPLS force field. *Journal of chemical theory and computation* **6**, 1509-1519 (2010).
- 231 Chowdhury, S. C., Elder, R. M., Sirk, T. W. & Gillespie Jr, J. W. Epoxy resin thermo-mechanics and failure modes: Effects of cure and cross-linker length. *Composites Part B: Engineering* **186**, 107814 (2020).
- 232 Dallochio, R. *et al.* Enantioseparations of polyhalogenated 4, 4'-bipyridines on polysaccharide-based chiral stationary phases and molecular dynamics simulations of selector-selectand interactions. *Electrophoresis* (2021).
- 233 Plimpton, S. Fast parallel algorithms for short-range molecular dynamics. *Journal of computational physics* **117**, 1-19 (1995).
- 234 Humphrey, W., Dalke, A. & Schulten, K. VMD: visual molecular dynamics. *Journal of molecular graphics* **14**, 33-38 (1996).
- 235 Rubinstein, M. & Colby, R. H. *Polymer physics*. Vol. 23 (Oxford university press New York, 2003).

- 236 Fixman, M. Radius of gyration of polymer chains. *The Journal of Chemical Physics* **36**, 306-310 (1962).
- 237 Jeffrey, G. A. & Jeffrey, G. A. *An introduction to hydrogen bonding*. Vol. 12 (Oxford university press New York, 1997).
- 238 Shannon, R. D. Revised effective ionic radii and systematic studies of interatomic distances in halides and chalcogenides. *Acta crystallographica section A: crystal physics, diffraction, theoretical and general crystallography* **32**, 751-767 (1976).
- 239 Lan, J. *et al.* Transparent Stretchable Dual-Network Ionogel with Temperature Tolerance for High-Performance Flexible Strain Sensors. *ACS Applied Materials & Interfaces* **12**, 37597-37606, doi:10.1021/acsami.0c10495 (2020).
- 240 Sun, J. *et al.* A transparent, stretchable, stable, self-adhesive ionogel-based strain sensor for human motion monitoring. *Journal of Materials Chemistry C* **7**, 11244-11250, doi:10.1039/C9TC03797G (2019).
- 241 Sun, J. *et al.* A facile strategy for fabricating multifunctional ionogel based electronic skin. *Journal of Materials Chemistry C* **8**, 8368-8373, doi:10.1039/D0TC01057J (2020).
- 242 Zhang, L. M. *et al.* Self-Healing, Adhesive, and Highly Stretchable Ionogel as a Strain Sensor for Extremely Large Deformation. *Small* **15**, 1804651, doi: 10.1002/sml.201804651 (2019).
- 243 Li, T., Wang, Y., Li, S., Liu, X. & Sun, J. Mechanically Robust, Elastic, and Healable Ionogels for Highly Sensitive Ultra-Durable Ionic Skins. *Advanced Materials* **32**, 2002706, doi: 10.1002/adma.202002706 (2020).
- 244 Sun, J. *et al.* Robust Physically Linked Double-Network Ionogel as a Flexible Bimodal Sensor. *ACS Applied Materials & Interfaces* **12**, 14272-14279, doi:10.1021/acsami.0c01472 (2020).
- 245 Wang, Z. *et al.* 3D Printable, Highly Stretchable, Superior Stable Ionogels Based on Poly(ionic liquid) with Hyperbranched Polymers as Macro-cross-linkers for High-Performance Strain Sensors. *ACS Applied Materials & Interfaces* **13**, 5614-5624, doi:10.1021/acsami.0c21121 (2021).
- 246 Lai, J. *et al.* Highly Stretchable, Fatigue-Resistant, Electrically Conductive, and Temperature-Tolerant Ionogels for High-Performance Flexible Sensors. *ACS Applied Materials & Interfaces* **11**, 26412-26420, doi:10.1021/acsami.9b10146 (2019).
- 247 Jiang, N. *et al.* Flexible, transparent, and antibacterial ionogels toward highly sensitive strain and temperature sensors. *Chemical Engineering Journal* **424**, 130418, doi: 10.1016/j.cej.2021.130418 (2021).
- 248 Kim, Y. M. & Moon, H. C. Ionoskins: Nonvolatile, Highly Transparent, Ultrastretchable Ionic Sensory Platforms for Wearable Electronics. *Advanced Functional Materials* **30**, 1907290, doi: 10.1002/adfm.201907290 (2020).

- 249 Kim, J. H., Cho, K. G., Cho, D. H., Hong, K. & Lee, K. H. Ultra-Sensitive and Stretchable Ionic Skins for High-Precision Motion Monitoring. *Advanced Functional Materials* **31**, 2010199, doi: 10.1002/adfm.202010199 (2021).
- 250 Wang, Y., Sun, S. & Wu, P. Adaptive Ionogel Paint from Room-Temperature Autonomous Polymerization of  $\alpha$ -Thioctic Acid for Stretchable and Healable Electronics. *Advanced Functional Materials* **31**, 2101494, doi: 10.1002/adfm.202101494 (2021).
- 251 Wang, Y. *et al.* Highly Stretchable and Reconfigurable Ionogels with Unprecedented Thermoplasticity and Ultrafast Self-Healability Enabled by Gradient-Responsive Networks. *Macromolecules* **54**, 3832-3844, doi:10.1021/acs.macromol.1c00443 (2021).
- 252 Gao, Y. *et al.* Highly Stretchable Organogel Ionic Conductors with Extreme-Temperature Tolerance. *Chemistry of Materials* **31**, 3257-3264, doi:10.1021/acs.chemmater.9b00170 (2019).
- 253 Chen, L. & Guo, M. Highly Transparent, Stretchable, and Conductive Supramolecular Ionogels Integrated with Three-Dimensional Printable, Adhesive, Healable, and Recyclable Character. *ACS Applied Materials & Interfaces* **13**, 25365-25373, doi:10.1021/acsami.1c04255 (2021).
- 254 Wang, S. *et al.* Self-Adhesive, Stretchable, Biocompatible, and Conductive Nonvolatile Eutectogels as Wearable Conformal Strain and Pressure Sensors and Biopotential Electrodes for Precise Health Monitoring. *ACS Applied Materials & Interfaces* **13**, 20735-20745, doi:10.1021/acsami.1c04671 (2021).
- 255 Yuan, Y., Zhou, J., Lu, G., Sun, J. & Tang, L. Highly Stretchable, Transparent, and Self-Adhesive Ionic Conductor for High-Performance Flexible Sensors. *ACS Applied Polymer Materials* **3**, 1610-1617, doi:10.1021/acsapm.0c01442 (2021).
- 256 Hao, S., Zhang, J., Yang, X., Li, T. & Song, H. A novel strategy for fabricating highly stretchable and highly conductive photoluminescent ionogels via an in situ self-catalytic cross-linking reaction in ionic liquids. *Journal of Materials Chemistry C* **9**, 5789-5799, doi:10.1039/D1TC00598G (2021).
- 257 Qin, H., Oweyung, R. E., Sonkusale, S. R. & Panzer, M. J. Highly stretchable and nonvolatile gelatin-supported deep eutectic solvent gel electrolyte-based ionic skins for strain and pressure sensing. *Journal of Materials Chemistry C* **7**, 601-608, doi:10.1039/C8TC05918G (2019).
- 258 Xu, J. *et al.* Self-healing, anti-freezing and highly stretchable polyurethane ionogel as ionic skin for wireless strain sensing. *Chemical Engineering Journal* **426**, 130724, doi: 10.1016/j.cej.2021.130724 (2021).
- 259 Weng, D. *et al.* Polymeric Complex-Based Transparent and Healable Ionogels with High Mechanical Strength and Ionic Conductivity as Reliable Strain Sensors. *ACS Applied Materials & Interfaces* **12**, 57477-57485, doi:10.1021/acsami.0c18832 (2020).

- 260 Zhao, G. *et al.* Transparent and stretchable triboelectric nanogenerator for self-powered tactile sensing. *Nano Energy* **59**, 302-310, doi:10.1016/j.nanoen.2019.02.054 (2019).
- 261 Lai, C.-W. & Yu, S.-S. 3D Printable Strain Sensors from Deep Eutectic Solvents and Cellulose Nanocrystals. *ACS Applied Materials & Interfaces* **12**, 34235-34244, doi:10.1021/acsami.0c11152 (2020).
- 262 Chen, X.-C., Sun, P.-R. & Liu, H.-L. Hierarchically Crosslinked Gels Containing Hydrophobic Ionic Liquids towards Reliable Sensing Applications. *Chinese Journal of Polymer Science* **38**, 332-341, doi:10.1007/s10118-020-2357-2 (2020).
- 263 Yu, Z. & Wu, P. Underwater Communication and Optical Camouflage Ionogels. *Advanced Materials* **33**, 2008479, doi: 10.1002/adma.202008479 (2021).
- 264 Cho, K. G. *et al.* Block Copolymer-Based Supramolecular Ionogels for Accurate On-Skin Motion Monitoring. *Advanced Functional Materials* **31**, 2102386, doi:10.1002/adfm.202102386 (2021).
- 265 Zhang, H., Niu, W. & Zhang, S. Extremely Stretchable, Stable, and Durable Strain Sensors Based on Double-Network Organogels. *ACS Applied Materials & Interfaces* **10**, 32640-32648, doi:10.1021/acsami.8b08873 (2018).
- 266 Lin, M., Hu, H., Zhou, S. & Xu, S. Soft wearable devices for deep-tissue sensing. *Nature Reviews Materials*, doi:10.1038/s41578-022-00427-y (2022).
- 267 Li, M., Pal, A., Aghakhani, A., Pena-Francesch, A. & Sitti, M. Soft actuators for real-world applications. *Nature Reviews Materials* **7**, 235-249, doi:10.1038/s41578-021-00389-7 (2022).
- 268 Herbert, K. M. *et al.* Synthesis and alignment of liquid crystalline elastomers. *Nature Reviews Materials* **7**, 23-38, doi:10.1038/s41578-021-00359-z (2022).
- 269 Allen, M. E., Hindley, J. W., Baxani, D. K., Ces, O. & Elani, Y. Hydrogels as functional components in artificial cell systems. *Nature Reviews Chemistry*, doi:10.1038/s41570-022-00404-7 (2022).
- 270 Fang, Y. *et al.* Dissecting Biological and Synthetic Soft–Hard Interfaces for Tissue-Like Systems. *Chemical Reviews* **122**, 5233-5276, doi:10.1021/acs.chemrev.1c00365 (2022).
- 271 Zhu, Z., Ng, D. W. H., Park, H. S. & McAlpine, M. C. 3D-printed multifunctional materials enabled by artificial-intelligence-assisted fabrication technologies. *Nature Reviews Materials* **6**, 27-47, doi:10.1038/s41578-020-00235-2 (2021).
- 272 Wang, C., Yokota, T. & Someya, T. Natural Biopolymer-Based Biocompatible Conductors for Stretchable Bioelectronics. *Chemical Reviews* **121**, 2109-2146, doi:10.1021/acs.chemrev.0c00897 (2021).
- 273 Hart, L. F. *et al.* Material properties and applications of mechanically interlocked polymers. *Nature Reviews Materials* **6**, 508-530, doi:10.1038/s41578-021-00278-z (2021).

- 274 Xiang, C. *et al.* Stretchable and fatigue-resistant materials. *Materials Today* **34**, 7-16, doi: 10.1016/j.mattod.2019.08.009 (2020).
- 275 Zhao, X. EML webinar overview: Extreme mechanics of soft materials for merging human-machine intelligence. *Extreme Mechanics Letters* **39**, 100784, doi: 10.1016/j.eml.2020.100784 (2020).
- 276 Su, G. *et al.* Human-tissue-inspired anti-fatigue-fracture hydrogel for a sensitive wide-range human-machine interface. *Journal of Materials Chemistry A* **8**, 2074-2082, doi:10.1039/C9TA08111A (2020).
- 277 Shin, M. K., Spinks, G. M., Shin, S. R., Kim, S. I. & Kim, S. J. Nanocomposite Hydrogel with High Toughness for Bioactuators. *Advanced Materials* **21**, 1712-1715, doi: 10.1002/adma.200802205 (2009).
- 278 Kong, B. *et al.* Fiber reinforced GelMA hydrogel to induce the regeneration of corneal stroma. *Nature Communications* **11**, 1435, doi:10.1038/s41467-020-14887-9 (2020).
- 279 Addadi, L. & Weiner, S. Control and Design Principles in Biological Mineralization. *Angewandte Chemie International Edition in English* **31**, 153-169, doi: 10.1002/anie.199201531 (1992).
- 280 Cui, K. *et al.* Phase Separation Behavior in Tough and Self-Healing Polyampholyte Hydrogels. *Macromolecules* **53**, 5116-5126, doi:10.1021/acs.macromol.0c00577 (2020).
- 281 Guo, K. & Buehler, M. J. Nature's Way: Hierarchical Strengthening through Weakness. *Matter* **1**, 302-303, doi: 10.1016/j.matt.2019.07.011 (2019).
- 282 Sato, K. *et al.* Phase-Separation-Induced Anomalous Stiffening, Toughening, and Self-Healing of Polyacrylamide Gels. *Advanced Materials* **27**, 6990-6998, doi: 10.1002/adma.201502967 (2015).
- 283 Tamate, R. *et al.* Self-Healing Micellar Ion Gels Based on Multiple Hydrogen Bonding. *Advanced Materials* **30**, 1802792, doi: 10.1002/adma.201802792 (2018).
- 284 Liang, X. *et al.* Bioinspired 2D Isotropically Fatigue-Resistant Hydrogels. *Advanced Materials* **34**, 2107106, doi: 10.1002/adma.202107106 (2022).